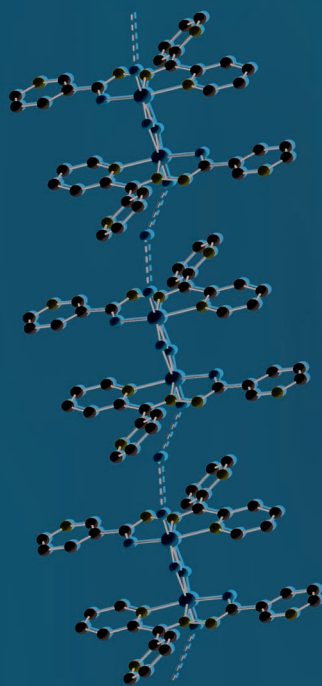


Ph.D. Thesis
December 2010

**Chelating behavior of acylhydrazones towards transition metals:
Spectral and structural aspects**

Chelating behavior of acylhydrazones towards transition metals:
Spectral and structural aspects



Neema Ani Mangalam



Department of Applied Chemistry
Cochin University of Science and Technology
Kochi 682 022

Department of Applied Chemistry
Cochin University of Science and Technology
Kochi 682 022

December 2010

Neema Ani Mangalam

Chelating behavior of acylhydrazones towards transition metals: Spectral and structural aspects

*Thesis submitted to
Cochin University of Science and Technology
in partial fulfillment of the requirements for the award
of the degree of*

DOCTOR OF PHILOSOPHY

*in
CHEMISTRY*

By

Neema Ani Mangalam



Department of Applied Chemistry
Cochin University of Science and Technology
Kochi 682 022

December 2010

**Chelating behavior of acylhydrazones towards transition metals:
Spectral and structural aspects**

Ph.D. Thesis under the faculty of Science

Author:

Neema Ani Mangalam

Research Fellow, Department of Applied Chemistry
Cochin University of Science and Technology
Kochi, India 682 022
Email: neemaani@gmail.com

Research Advisor:

Dr. M.R. Prathapachandra Kurup

Professor
Department of Applied Chemistry
Cochin University of Science and Technology
Kochi, India 682 022
Email: mrp@cusat.ac.in

Department of Applied Chemistry
Cochin University of Science and Technology
Kochi, India 682 022

December 2010

Front cover: Supramolecular chain mediated by $-\text{O}\cdots\text{H}-\text{O}-\text{H}\cdots\text{O}-$
hydrogen bonding in $[\text{VO}(\text{DKN})(\mu_2-\text{O})]_2\cdot\frac{1}{2}\text{H}_2\text{O}$

*“The Lord is my strength and shield; my
heart trusted in Him, and I am helped.”*

(Psalms 28:7)

******to my very dearest
Daddy & Mummy



DEPARTMENT OF APPLIED CHEMISTRY
COCHIN UNIVERSITY OF SCIENCE AND
TECHNOLOGY
KOCHI - 682 022, INDIA

Phone Off. 0484-2575804
Phone Res. 0484-2576904
Telex: 885-5019 CUIN
Fax: 0484-2577595
Email: mrp@cusat.ac.in
mrp_k@yahoo.com

Dr. M.R. Prathapachandra Kurup
Professor

28th December 2010

Certificate

This is to certify that the thesis entitled "Chelating behavior of acylhydrazones towards transition metals: Spectral and structural aspects" submitted by Miss. Neema Ani Mangalam, in partial fulfillment of the requirements for the degree of Doctor of Philosophy, to the Cochin University of Science and Technology, is an authentic record of the original research work carried out by her under my supervision at the Department of Applied Chemistry. Further, the results embodied in this thesis, in full or in part, have not been submitted previously for the award of any other degree.

M. R. Prathapachandra Kurup
(Supervisor)

Declaration

I hereby declare that the work presented in this thesis entitled **“Chelating behavior of acylhydrazones towards transition metals: Spectral and structural aspects”** is entirely original and was carried out independently under the supervision of Prof. M.R. Prathapachandra Kurup, Department of Applied Chemistry, Cochin University of Science and Technology and has not been included in any other thesis submitted previously for the award of any other degree.

28-12-2010

Kochi 22

Neema Ani Mangalam

Acknowledgement.....

A piece of work to become perfect, one needs the blessings and help of many. For the completion of this research work, I'm indebted to many for their generous contributions, be it in the form of a piece of advice or suggestions for improvement.

First of all, let me bow my head in reverent gratitude to God Almighty for the manifold blessings showered on me and for the undeserving grace shown to me for the successful completion of this work,

Let me place on record my profound gratitude to my supervising guide Prof. M.R. Prathapachandra Kurup for admitting me into the program. In my concept, the most important factor in research is to get a right person as the guide. His scholarly assistance, inspiring guidance and his friendly and amiable demeanor really helped me to complete the work in the stipulated time. Apart from the subject of my research, I learnt a lot from him, which I am sure, will be useful in different stages of my life. His simplicity, moral ethics, behavior towards colleagues and students inspired me a lot. Especially I was very inspired in the interest and eagerness shown by him to study how to solve crystal structure for long time eventhough we get bored and tired. Sir, I consider it as a blessing to work under you. In this occasion I thank God for giving me an opportunity to work under him and I shall always cherish this association.

I would like to acknowledge my deep gratitude to Prof. K.K. Mohammed Yusuff, the doctoral committee member, who taught me the group theoretical concepts during my M.Phil which proved to be of great use in my research field also.

But without the whole hearted support and co-operation of Prof. K. Sreekumar, Head of the Department, this work would have been a Herculean task for me. I remember with gratitude the encouragement and support of Prof. K. Girish Kumar, Former Head, who instilled confidence in me during the initial stages of my work,

I sincerely thank all other faculty members and non-teaching staff for the assistance to conduct this research.

Let me place on record my gratitude to all my former teachers who made me what I am today especially to Dr. A. Maria Starwin and my teachers of Mar Thoma College, Tiruvalla.

I wish to express my sincere gratitude to the staff of Indu Photos, Kalamassery for the help provided in the final documentation and printing.

I would like to extend my gratitude to Cochin University of Science and Technology for the financial support offered. I am indebted to the head of the institutions of SAIK Kochi, IIT Madras, IIT Bombay and for the services rendered in sample analyses. Special thanks to Dr. N. Chitrapriya, Bharathiar University, Coimbatore and Dr. C. Jayabalakrishnan, Sri Ramakrishna Mission Vidyalaya College of Arts and Science, Coimbatore for helping me to record cyclic voltammograms of the compounds. I convey special acknowledgement to Prof. Edward R.T. Tiekink, The University of Texas, USA and Dr. E. Suresh, CSMCRI, Bhavanagar for being our collaborators.

I am truly grateful to my seniors Dr. Manoj E., Dr. Leji Latheef, Dr. Suja Krishnan, Dr. Binu Varghese, Dr. Sreesh Sasi and Dr. Bessy Raj and my colleagues Reena chechi, Laly miss, Renjusha chechi, Roji, Eesan sir, Jayakumar sir, Jinsa, Bibitha and Nisha for their whole-hearted support, assistance, and suggestive criticisms during my research work. Special word of gratitude to Nancy and Sheeja for providing me with a good ambiance to do the work and for clarifying my doubts. It is a pleasure to pay tribute for the motherly care and prayers given by Annie miss and Jessy miss when I was very much tensed. Special thanks go to Dr. Seena E.B., who gave an idea to write research papers, in familiarising crystallographic programmes, and installing confidence in me to reduce stress. I am also grateful to all my friends working in various Universities abroad, especially Saino to collect research papers which we could not access here.

Athulya Hostel has been my home for the last four years where I got lot of friends. My room 54 was the perfect place of comfort and serenity which helped me in preparing for the NET exam and for writing research papers. I thank God to have a friend like Digna to share tons of fond memories and we had a lot of enjoyable moments during the evenings which made my CUSAT life so memorable. I am grateful to recall a lot of splendid memories I had with Anju, Manju, Seema and Lorna chechi in the hostel. Those days are so memorable and I would not like to miss them. I don't believe in goodbyes, only a long "I'll see you later". I will surely miss all our crazy and exciting times together but I know that someday our paths will cross again.

Where would I be without my family? My Daddy and Mummy deserve special mention for their unconditional support and prayers, for giving life in the first place, for educating me and my sister with all the opportunities they could provide to explore my potentials and pursue my dreams ever since I was a child. As typical parents in a middle class family, they worked industriously to support the family and did not spare any effort to provide the best possible environment for educating me and my sister. My Mummy, is the one who sincerely raised me with her caring and constant prayers and she never failed to remind me to seek God's will in all things so that He will show which path to take. Hence, this thesis is dedicated to them. I thank God Almighty for blessing me with such caring parents. Thanks of course is due to my younger sister Nivya, for her immense care and support.

Thank you all, who has directly and indirectly extended a helping hand in this endeavor of mine.

Neema

Preface

Interest in the coordination properties of hydrazone ligands towards transition metal ions and in the biological properties of their metal complexes has been growing in recent years. The coordination chemistry of transition metals with ligands from the hydrazone family has been of interest due to different bonding modes shown by these ligands. We have been interested in the chemistry of pyridyl containing ligands, and we have selected 2-benzoylpyridine benzhydrazone and di-2-pyridyl ketone nicotinoylhydrazone as ligands to synthesize and characterize some transition metal complexes which throw a light into their coordination behavior. Di-2-pyridyl ketone nicotinoylhydrazone is an interesting synthon in the class of chelating agents. The choice of di-2-pyridyl ketone is mainly due to the fact that this heteroaromatic moiety can provide a further binding site for metal cations. It is rigid, and provides two aromatic nitrogens whose unshared electron pairs are beautifully placed to act cooperatively in binding cations.

The current work deals with the synthesis and characterization of metal complexes derived from some substituted acylhydrazones. The hydrazones under investigation were characterized by IR, UV, NMR spectral studies and the molecular structure of one of the hydrazones was solved by single crystal XRD studies. In the present work dioxovanadium(V), manganese(II), cobalt(II/III), nickel(II), copper(II), zinc(II) and cadmium(II) complexes were synthesized and characterized by various spectroscopic techniques, molar conductance measurements, magnetic susceptibility measurements and cyclic voltammetry. Single crystals of some of the complexes were isolated and characterized by single crystal X-ray diffraction.

The thesis is divided into eight chapters. Chapter 1 gives an introduction on hydrazones, diversity in their chelating behavior and their application in various fields. This chapter also describes different analytical techniques employed for the characterization of hydrazones and their metal complexes. Chapter 2 includes the synthesis and characterization of two substituted acylhydrazones. This chapter also discusses how the coordination behavior of hydrazones under investigation is interesting. Chapters 3-8 discuss the synthesis and characterization of some transition metal complexes derived from the acylhydrazones under study.

The hydrazones synthesized were found to exist in the amido form. Various characterization techniques were carried out to explore the structure of the synthesized complexes. The results indicate that both the hydrazones coordinate through the pyridyl and azomethine nitrogens and amide oxygen either in enolate or neutral form. Out of synthesized complexes V(V), Zn/Cd(II) and one of the cobalt complex was found to be diamagnetic. We could not isolate single crystals of some of the complexes and most of the complexes crystallized were found to have a distorted octahedral geometry. Thus X-ray crystallographic study which was used as a major tool in the structure determination revealed that the hydrazones undergo a rotation about the azomethine bond on complexation. We hope the work presented in the thesis would be helpful for those who are working in the field of metal complexes and can further they can be utilized for various applications.

Abbreviations

HBPB	2-Benzoylpyridine benzhydrazone
HDKN	Di-2-pyridyl ketone nicotinoylhydrazone
Complex 1	$[\text{VO}(\text{BPB})(\mu_2\text{-O})_2]$
Complex 2	$[\text{VO}(\text{DKN})(\mu_2\text{-O})_2] \cdot 2\text{H}_2\text{O}$
Complex 3	$[\text{Mn}(\text{BPB})_2]$
Complex 4	$[\text{Mn}(\text{DKN})_2]$
Complex 5	$[\text{Co}(\text{BPB})_2]\text{Br}$
Complex 6	$[\text{Co}(\text{BPB})_2]$
Complex 7	$[\text{Co}(\text{BPB})\text{NCS}]$
Complex 8	$[\text{Co}(\text{DKN})\text{Cl}]$
Complex 9	$[\text{Co}(\text{DKN})\text{NCS}] \cdot \text{H}_2\text{O}$
Complex 10	$[\text{Ni}(\text{BPB})_2]$
Complex 11	$[\text{Ni}(\text{HBPB})(\text{BPB})]\text{ClO}_4$
Complex 12	$[\text{Ni}(\text{DKN})_2]$
Complex 13	$[\text{Ni}(\text{DKN})\text{NCS}] \cdot \text{H}_2\text{O}$
Complex 14	$[\text{Cu}(\text{BPB})\text{Br}]$
Complex 15	$[\text{Cu}_2(\text{BPB})_2(\mu\text{-SO}_4)]$
Complex 16	$[\text{Cu}(\text{BPB})_2]$
Complex 17	$[\text{Cu}(\text{DKN})\text{Br}]$
Complex 18	$[\text{Cu}(\text{HDKN})\text{Cl}_2]$
Complex 19	$[\text{Cu}(\text{DKN})_2]$
Complex 20	$[\text{Cu}_2(\text{DKN})_2(\mu\text{-N}_3)_2]$
Complex 21	$[\text{Cu}_2(\text{DKN})_2(\mu\text{-NCS})_2]$
Complex 22	$[\text{Cu}_2(\text{DKN})_2](\text{ClO}_4)_2 \cdot 2\text{H}_2\text{O}$
Complex 23	$[\text{Cd}(\text{BPB})_2]$
Complex 24	$[\text{Cd}(\text{BPB})\text{Cl}]$
Complex 25	$[\text{Cd}(\text{HBPB})\text{Br}_2]$
Complex 26	$[\text{Zn}(\text{DKN})\text{NCS}]$
Complex 27	$[\text{Cd}(\text{DKN})\text{OAc}] \cdot \text{H}_2\text{O}$
Complex 28	$[\text{Cd}(\text{HDKN})\text{Cl}_2]$

Contents

.....

Page No

Chapter 1

A brief outline on acylhydrazones	1-19
1.1 Introduction	1
1.2 Acylhydrazones	2
1.3 Diversity in the chelating behavior of hydrazones	5
1.4 Applications of hydrazones	8
1.4.1 Hydrazones in Non-Linear Optics	8
1.4.2 Hydrazones and magnetochemistry	9
1.4.3 Hydrazones as iron-chelating agents	10
1.4.4 Biological activities of hydrazones	11
1.4.5 Hydrazones as molecular sensors	11
1.5 Objectives of present work	12
1.6 Physical measurements	14
1.6.1 Elemental analyses	14
1.6.2 Conductivity measurements	14
1.6.3 Magnetic susceptibility measurements	14
1.6.4 Infrared spectroscopy	15
1.6.5 Electronic spectroscopy	15
1.6.6 NMR spectroscopy	15
1.6.7 EPR spectroscopy	15
1.6.8 Cyclic voltammetry	15
1.6.9 Thermogravimetric analyses	16
1.6.10 X-ray crystallography	16
References	17

Chapter 2

Spectral and structural characterization of some acylhydrazones	20-33
2.1 Introduction	20
2.2 Experimental	21
2.3 Results and discussion	23
2.3.1 Elemental analyses	23
2.3.2 Infrared spectra	24

2.3.3	Electronic spectra	25
2.3.4	NMR spectra	26
2.3.5	X-ray crystallography	28
2.3.5.1	Crystal structure of HBPB	28
	References	32

Chapter 3

Syntheses, spectral and structural characterization of dioxygen bridged vanadium(V) complexes incorporating tridentate acylhydrazones		34-52
3.1	Introduction	34
3.2	Experimental	36
3.3	Results and discussion	37
3.3.1	Elemental analyses	37
3.3.2	Molar conductivity and magnetic susceptibility measurements	37
3.3.3	Infrared spectra	37
3.3.4	Electronic spectra	40
3.3.5	X-ray crystallography	41
3.3.5.1	Crystal structures of [VO(BPB)(μ_2 -O)] ₂ (1) and [VO(DKN)(μ_2 -O)] ₂ · ½H ₂ O (2)	43
	References	50

Chapter 4

Syntheses, spectral and structural characterization of manganese(II) complexes incorporating tridentate acylhydrazones		53-74
4.1	Introduction	53
4.2	Experimental	54
4.3	Results and discussion	56
4.3.1	Elemental analyses	56
4.3.2	Molar conductivity and magnetic susceptibility measurements	56
4.3.3	Infrared spectra	56
4.3.4	Electronic spectra	58
4.3.5	Cyclic voltammetric studies	59

4.3.6	Electron paramagnetic resonance spectra	60
4.3.7	X-ray crystallography	64
4.3.7.1	Crystal structures of [Mn(BPB) ₂] (3) and [Mn(DKN) ₂] (4)	65
	References	73

Chapter 5

Syntheses, spectral and structural characterization of cobalt(II/III) complexes incorporating tridentate acylhydrazones 75-96

5.1	Introduction	75
5.2	Experimental	76
5.3	Results and discussion	79
5.3.1	Elemental analyses	79
5.3.2	Molar conductivity and magnetic susceptibility measurements	79
5.3.3	Infrared spectra	80
5.3.4	Electronic spectra	84
5.3.5	Cyclic voltammetric studies	87
5.3.6	Thermal analyses	89
5.3.7	X-ray crystallography	89
5.3.7.1	Crystal structure of [Co(BPB) ₂] (6)	91
	References	94

Chapter 6

Syntheses, spectral and structural characterization of nickel(II) complexes incorporating tridentate acylhydrazones 97-116

6.1	Introduction	97
6.2	Experimental	98
6.3	Results and discussion	100
6.3.1	Elemental analyses	100
6.3.2	Molar conductivity and magnetic susceptibility measurements	101
6.3.3	Infrared spectra	101
6.3.4	Electronic spectra	105
6.3.5	Thermal analyses	107

6.3.6	X-ray crystallography	108
6.3.6.1	Crystal structure of [Ni(DKN) ₂]·H ₂ O (12)	109
	References	114

Chapter 7

Syntheses, spectral and structural characterization of copper(II) complexes incorporating tridentate acylhydrazones 117-165

7.1	Introduction	117
7.2	Experimental	119
7.3	Results and discussion	124
7.3.1	Elemental analyses	124
7.3.2	Molar conductivity and magnetic susceptibility measurements	124
7.3.3	Infrared spectra	124
7.3.4	Electronic spectra	132
7.3.5	Thermal analyses	137
7.3.6	Electron paramagnetic resonance spectra	138
7.3.7	X-ray crystallography	153
7.3.7.1	Crystal structures of [Cu(BPB) ₂] (16) and [Cu((DKN) ₂)]·H ₂ O (19)	155
	References	161

Chapter 8

Syntheses, spectral and structural characterization of zinc/cadmium(II) complexes incorporating tridentate acylhydrazones 166-178

8.1	Introduction	166
8.2	Experimental	167
8.3	Results and discussion	170
8.3.1	Elemental analyses and molar conductivity studies	170
8.3.2	Infrared spectra	170
8.3.3	Electronic spectra	175
8.3.4	Thermal analyses	176
	References	177
	Summary & Conclusion	179

****❁****

Chapter 1

A brief outline on acylhydrazones

Contents

- 1.1 Introduction
 - 1.2 Acylhydrazones
 - 1.3 Diversity in the chelating behavior of hydrazones
 - 1.4 Applications of hydrazones
 - 1.5 Objectives of present work
 - 1.6 Physical measurements
- References
-

1.1. Introduction

Coordination compounds have been a challenge to the inorganic chemist since they were identified in the nineteenth century. In the early days they seemed unusual because they appeared to defy the usual rules of valence. Today they comprise a large body of current inorganic research. Although the usual bonding theories can be extended to accommodate these compounds, they still present stimulating theoretical problems and in the laboratory they continue to provide synthetic challenges. Werner's coordination theory in 1893 was the first attempt to explain the bonding in coordination complexes. This theory and his painstaking work over the next 20 years won Alfred Werner the Nobel Prize for

Chemistry in 1913. There has been much work done in attempting to formulate theories to describe the bonding in coordination compounds and to rationalize and predict their properties.

Metal complexes have played an important role since the early days of coordination chemistry. Indeed, a great deal of work has been carried out on the synthesis and characterization of transition metal compounds, mainly due to their applications in various fields. However, the ability of the metal ion to participate in bonding to all possible coordination sites depends in part on its preferences for the donor atoms of the coordinated ligand, the flexibility and conformational adaptability of the ligand used, as well as on the competition from other Lewis acids and different entities capable of occupying a coordination pocket.

1.2. Acylhydrazones

The architectural beauty of coordination complexes arises due to the interesting ligand systems containing different donor sites in heterocyclic rings eg: NNO or NNS. Among the ligand systems, hydrazide and hydrazone occupy special place because transition metal complexes of these compounds are nowadays extensively used for the treatment of several diseases, in synthetic and analytical chemistry as novel heterogeneous catalysts in oxido-reduction processes and various chemical and photochemical reactions as well as numerous industrial applications of science and technology [1-5].

Hydrazones are compounds obtained by the condensation of hydrazides with aldehydes or ketones. Substituted hydrazones can be obtained by introducing substituted hydrazides and carbonyl compounds. General formula for a substituted acylhydrazone is shown in Fig. 1.1.

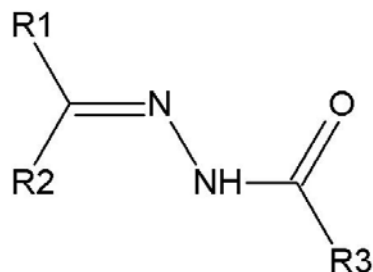


Fig. 1.1. General formula for a substituted acylhydrazone.

Amide oxygen and azomethine nitrogen are the available donor sites in hydrazone compounds. Further, the number of coordination sites can be increased by suitable substitution on the hydrazone framework. If a hetero ring is attached to the hydrazone framework, the hetero atom can also coordinate to the metal center thus increasing the denticity [6] (Fig. 1.2).

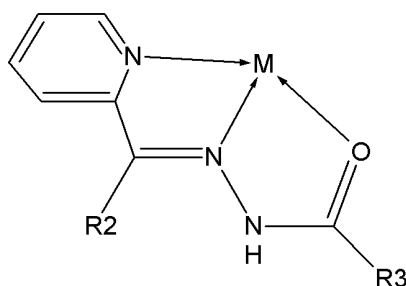


Fig. 1.2. An example for a tridentate acylhydrazone.

In hydrazones, it is well known that a proton transfer can occur between the hydrazinic-N and keto group of hydrazone part. Therefore tautomerization equilibrium exists between amido form and iminol form through intramolecular proton transfer. This proton transfer causes a change in the π -electron configuration and thus increases conjugation. Thus coordination compounds derived from hydrazones contain either neutral amido form or deprotonated form. In solid state, hydrazones predominantly exist in amido form (I), whereas in

solution iminol form (II) predominates (Fig 1.3). This is well established from crystal structures and IR spectral studies.

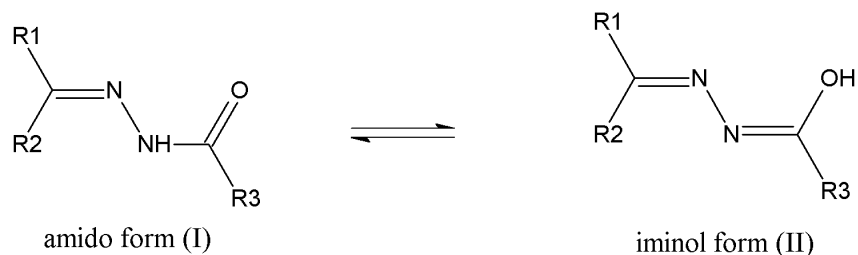


Fig 1.3. Tautomerism in acylhydrazones.

The amido form itself exists in *syn* or *anti* form depending on the azomethine bond (Fig. 1.4). In the *syn* form, as far as the azomethine bond is concerned two bulkier groups are on the same side, while in *anti* form the bulkier groups are on opposite side ($R2 > R1$).

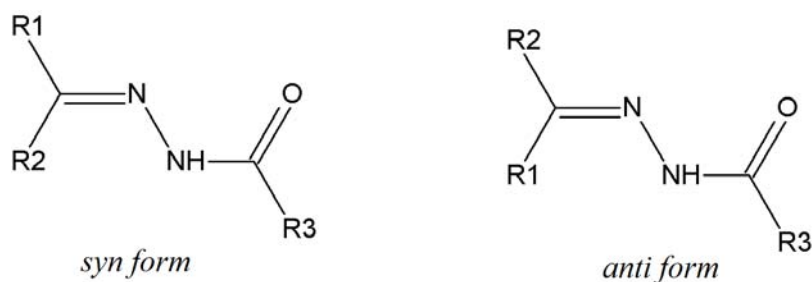


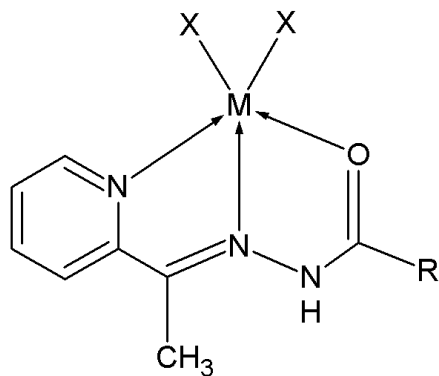
Fig. 1.4. Geometric isomers of acylhydrazones.

Stereochemistry of the hydrazone is much decided by the steric effects of the various substituents in the hydrazone moiety and also favored by additional interactions such as intramolecular hydrogen bonding. It is observed that the *syn* nature of the bond usually transforms to *anti* geometry, while coordinating to metal ions [7,8]. This phenomenon is assumed to be due to chelate effect, which results in an increased stability due to better electron delocalization in chelated ring system consisting of metal ions.

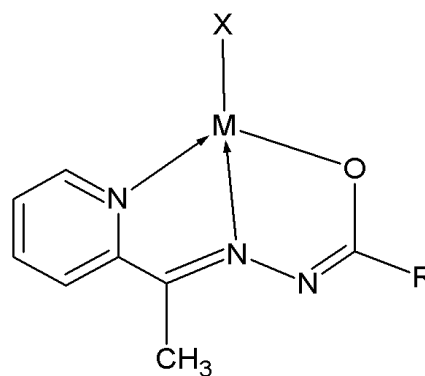
1.3. Diversity in the chelating behavior of hydrazones

The chelating behavior depends on their amido-iminol tautomerism and in addition to this, the number and type of the substituents attached to the hydrazone framework also influences the coordination mode.

As discussed earlier, the expected donor sites in simple hydrazones are the amide oxygen and azomethine nitrogen. In addition to this, if the carbonyl part contains a ring with a hetero atom, hetero atom can coordinate to metal centre thus behaving as a tridentate ligand. Due to tautomerism in hydrazones the amide oxygen can be in neutral *keto* form (Structure I) or enolic form (Structure II). The actual ionization state is dependent upon the condition (pH of the medium) and the metal salts employed. In basic solution amide oxygen get deprotonated and coordinates to the metal center in the enolic form whereas strongly acidic condition favor compounds formulated with a neutral ligand [9,10].

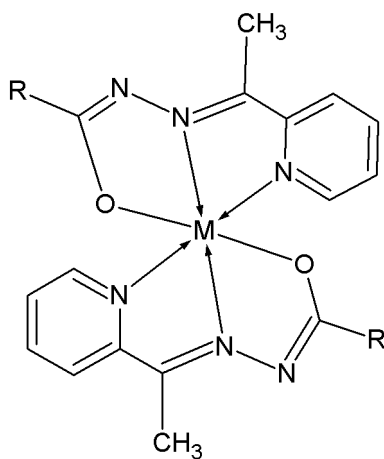


Structure I



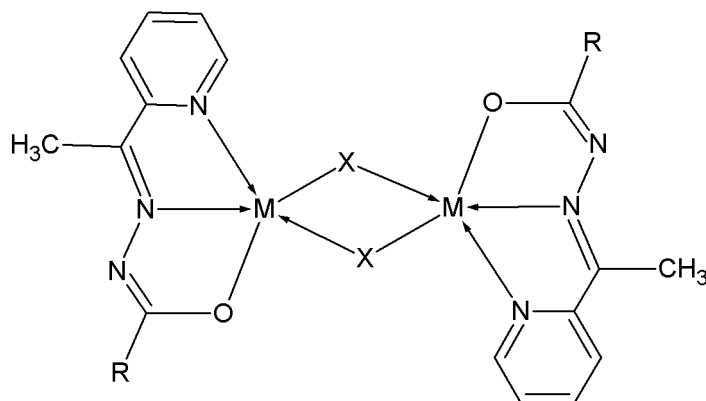
Structure II

In certain cases there is a possibility in which two deprotonated ligand moieties coordinate to the same metal centre giving rise to six coordinate distorted octahedral complexes [11] (Structure III). These types of complexes have increased stability which arises due to chelation.



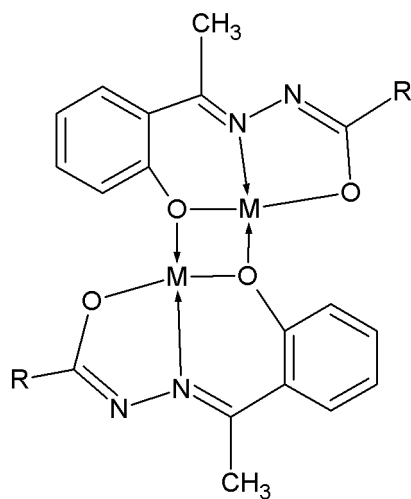
Structure III

There are cases in which hydrazones form bridged complexes. In some cases, an atom or group of atom may act as bridging ligand which results in a dimeric structure (Structure IV). Halogens, azide and thiocyanate ligands can act as these types of bridges [12-14].



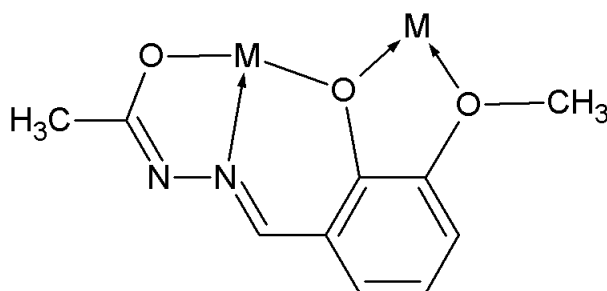
Structure IV

In ONO donor hydrazones containing phenolic group, phenolate oxygen atom can form a bridge between the metal centers thus forming a dimer [15] (Structure V).



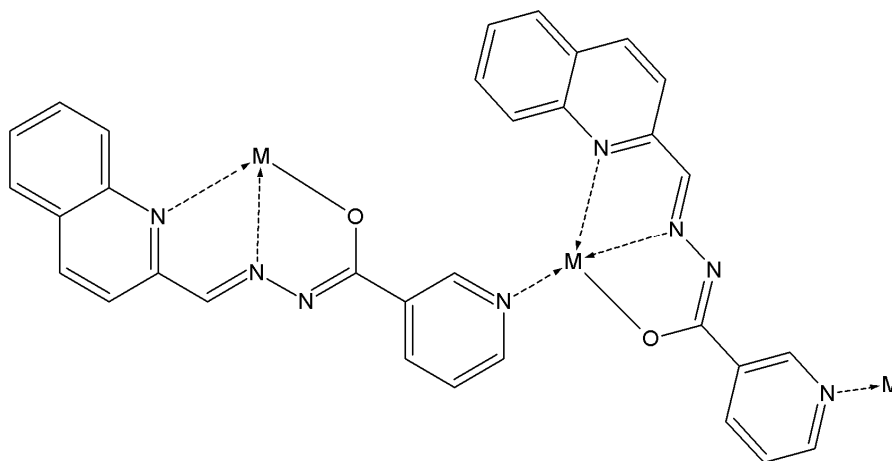
Structure V

Presence of additional donor sites in the ketonic part offers much more coordination possibilities which may result in multinuclear complexes. If $-OMe$ like groups are present in the carbonyl compound, it can utilize both the chelating and bridging capability leading to formation of multinuclear complexes [16] (Structure VI).



Structure VI

Another possibility is that if the hydrazide part of hydrazones contains a hetero atom, it can also involve in bonding (Structure VII). This unusual coordination can evidently change the way the complexes are formed [17].



Structure VII

1.4. Applications of hydrazones

1.4.1. Hydrazones in Non-Linear Optics

Metal coordination has been used in several ways to improve the behaviour of all organic push-pull chromophores for applications in second-order nonlinear optics (NLO). The most common approach is the use of organometallic or metal coordinated fragments attached at the end of organic π conjugated systems. To make the compound of potential interest in second-order NLO, the ligand should be properly functionalized with strong electron donor (CH_3) acceptor groups (NO_2) and it should be non-centrosymmetric.

Hydrazones can exist either in *amido* or *iminol* form. The ligand alone is not expected to show high NLO activity as the electronic structure of the hydrazone is in the amido form with rather low conjugation from donor to acceptor group. Upon coordination to the metal, the electronic structure of the hydrazone changes to the deprotonated form with increase in the conjugation and hence results in NLO activity. The proper choice of the metal, its oxidation state

and the ligand allow the fragment to behave as an electron donor or acceptor group.

The primary role played by the metal is that of generating the actual push-pull chromophore. Furthermore, the use of square planar coordinating metals [Cu(II) or Pd(II)] can force the organic ligand in a planar conformation so as to maximize conjugation. Cariati *et al.* have reported the NLO activity of Cu(II) and Pd(II) complexes of two N-salicylidine-N-arylhyazones containing strong electron donor-acceptor groups with pyridine as an auxiliary ligand [18].

Second, the metal coordinated to the ligand is electrically neutral but coordinatively unsaturated. This means that further coordination with donor atoms is possible (coligands like pyridine *etc.*); this feature which is well-known in this class of complexes, is particularly attractive since the donor atom might belong to a polymer nature, thus allowing automatically the covalent anchorage of the NLO active organometallic fragments to a performed polymer chain.

1.4.2. Hydrazones and magnetochemistry

Investigation of magnetic properties of molecular materials has become a major goal of current research in the fields of condensed matter physics and material chemistry. Among the ligand systems, hydrazones occupy special place due to their well known chelating capability and structural flexibility which can provide rigidity to the skeletal framework of the prepared multinuclear complexes. Considerable efforts have been applied to build and characterize such molecular architectures which can exhibit interesting magnetic properties. The precondition for synthesizing these materials is for the metal ions having unpaired electrons being assembled in a molecule such a way that the said electrons can interact with each other. Coordination complexes possessing metal-metal bridges certainly fulfill this condition and can be achieved by incorporating different terminal and bridging ligands to facilitate ferro- and antiferromagnetic

interactions among the metal centers. Among the bridging ligands, pseudohalides are good choice, because of their versatile coordination behaviour that generates dimeric and multidimensional magnetic materials with diverse magnetic interaction. Azide ion has received much attention for proving super-exchange pathways between paramagnetic centres. Recently many researchers are focussing on this type of work and the magneto-structural correlation of complexes derived from hydrazones is reported [19].

1.4.3. Hydrazones as iron-chelating agents

Initially the search for effective iron chelators was primarily driven by the need to treat Fe overload diseases such as β -thalassemia. However it has become clear that Fe chelators may be useful for the treatment of a wide variety of disease states, including cancer, malaria and free radical mediated tissue damage. Despite the synthesis and biological assessment of a diverse range of ligands, only a few compounds have ever been effective and safe enough to reach clinical trials. At present, the only Fe chelator in widespread clinical use is the desferrioxamine, DFO. Although DFO is a highly effective drug with few side effects, it suffers from a number of serious problems, including its high cost and poor intestinal absorption. Due to its poor intestinal absorption it will take a long time to achieve negative iron balance. This latter disadvantage coupled with the fact that DFO has very short plasma half-life necessitates that the drug be infused subcutaneously. These difficulties with DFO have led to the search for alternative Fe chelators that are economical, orally effective and highly efficient. One group of compounds that satisfies all of these criteria is that of the pyridoxaldehyde isonicotinoylhydrazone [PIH] class [20].

PIH is a ligand that was first identified as an effective Fe chelator in the late 1970's by Ponka *et al.* [21]. Recently the interest in these compounds as clinically useful Fe chelators has increased, and therefore the development of

other orally active Fe chelators should not be excluded in the hope of obtaining a more suitable alternative to DFO. In addition to the potential use of PIH and its analogs as chelators to treat Fe overload, recent studies have shown that these compounds, especially those derived from salicylaldehyde and 2-hydroxy-1-naphthylaldehyde, are effective anti-proliferative agents. Bernhardt *et al.* have designed and patented a novel class of ligands based on 2-pyridinecarbaldehyde.

1.4.4. Biological activities of hydrazones

Hydrazones have been intensively investigated mostly because of their potential application as anticancer, antiviral, antibacterial and antifungal agents. These compounds display a versatile behavior in metal coordination and the biological activity is often increased by bonding to transition metals. It is reported that the biological activity of *d*-metal complexes of *N*-heteroaromatic hydrazones of 2-pyridinecarboxaldehyde is often greater in comparison to the corresponding free ligand, with copper(II) complexes being the most active among all tested complexes [22]. The activity of some hydrazone complexes is very significant against Gram positive bacteria *in vitro*. These hydrazone chelate derivatives act as good potential oral drugs to treat the genetic disorders like thalassemia and are several folds more potent than the metal free chelate, leading to the conclusion that the metal complexes are biologically active species. The antibacterial and antifungal properties of 2,6-diacetylpyridine bis(acylhydrazones) and a series of metal complexes were investigated by Carcelli *et al.* [23]. Recently Affan *et al.* have reported the cytotoxicity and anti-termite property of thiophene-2-carboxaldehyde benzhydrazone and its tin complexes [24].

1.4.5. Hydrazones as molecular sensors

The development of molecular sensors has attracted a lot of research activities in recent years for their use in processes that include food, clinical and environmental analysis. Bistability, *ie.* the ability of the system (substrate plus

surrounding molecules) to exist in two states (electronic or conformational) is essential for molecular recognition as the interconversion between states allows exploring their structural relaxation and interactions with their environment. Optical and thermodynamic measurements on di-2-pyridyl ketone hydrazones in polar non-aqueous solvents revealed reversible interconversion between two interlocked electronic states due to intermolecular interaction between these species and their surroundings. The high values for their extinction coefficients and low values for their activation parameters allowed for these systems as molecular sensors for a variety of chemical and physical stimuli that include metal ions and biomolecules. Bakir *et al.* have also reported rhenium carbonyl compounds of di-2-pyridyl ketone as electrochemical sensors and spectroscopic and electrochemical measurements show the metal complex to undergo faster electron transfer than the free ligand [25].

1.5. Objectives of the present work

An attractive aspect of hydrazones is that they are capable of exhibiting amido-iminol tautomerism and can coordinate in tridentate neutral NNO donor mode, monoanionic NNO donor mode, dianionic tridentate ONO form, tetraanionic form and bidentate neutral NO forms to the metal ions generating mononuclear, dinuclear or polynuclear species. However, it depends on the reaction conditions, such as metal ion, its concentration, the pH of the medium and the nature of the hydrazone used. These interesting properties of the transition metal hydrazone complexes promoted us to synthesize and characterize transition metal complexes derived from NNO donor acylhydrazones thereby investigating their coordinating behavior.

Having all these facts in mind, we undertook the present work with the following objectives:

The current work deals with the synthesis and characterization of metal complexes derived from 2-benzoylpyridine benzoylhydrazone and di-2-pyridyl ketone nicotinoylhydrazone. Di-2-pyridyl ketone was selected as the carbonyl part in one of the hydrazone since it can provide a further binding site for metal cation and can thus increase the denticity. The choice of nicotinoylhydrazide as the hydrazide part was based on the fact that the nitrogen present in the ring can coordinate to metal center and is capable of forming polymeric structures, even though this type of complexes are not reported in this thesis.

The hydrazones under investigation were characterized by IR, UV, NMR spectral studies and the molecular structure of one of the hydrazones was solved by single crystal XRD studies. In the present work dioxovanadium(V), manganese(II), cobalt(II/III), nickel(II), copper(II), zinc(II) and cadmium(II) complexes were synthesized and characterized by various spectroscopic techniques, molar conductance measurements, magnetic susceptibility measurements and cyclic voltammetry. Single crystals of some of the complexes were isolated and characterized by single crystal X-ray diffraction measurements.

Chapter 1 entitled 'A brief outline on acylhydrazones' gives an introduction on hydrazones, diversity in their chelating behavior and their application in various fields. This chapter also describes different analytical techniques employed for the characterization of hydrazones and their metal complexes.

Chapter 2 discusses how the coordination behavior of hydrazones under investigation is interesting and also describes their synthesis and characterization.

Chapters 3-8 discuss the synthesis and characterization of dioxovanadium(V), manganese(II), cobalt(II/III), nickel(II),

copper(II) and zinc/cadmium(II) complexes respectively using various physicochemical techniques.

1.6. Physical measurements

The physicochemical techniques carried out for the present investigation are discussed below:

1.6.1. Elemental analyses

C, H and N analyses of the ligand and the complexes were performed on a Vario EL III CHNS analyzer at SAIF, Kochi, India. The metal content of the complexes were determined by AAS after digestion with con. HNO₃. The analysis were done using Thermo Electron Corporation, M series Atomic Absorption Spectrophotometer at the Department of Applied Chemistry, CUSAT, Kochi, India.

1.6.2. Conductivity measurements

The molar conductances of the complexes in DMF (10⁻³ M) solutions were measured at 298 K with a Systronic model 303 direct-reading conductivity bridge at the Department of Applied Chemistry, CUSAT, Kochi, India.

1.6.3. Magnetic susceptibility measurements

The magnetic susceptibility measurements were performed on powdered samples at 298 K using a Sherwood Scientific Magnetic Susceptibility Balance (M.S.B) MK1 using HgCo(SCN)₄ as calibrant at the Department of Applied Chemistry, CUSAT, Kochi, India and the diamagnetic contribution to the susceptibility was estimated through Pascal's constants.

1.6.4. Infrared spectroscopy

The IR spectra were recorded on a JASCO FT/IR-4100 Fourier Transform Infrared spectrometer using KBr pellets in the range 4000-400 cm^{-1} at the Department of Applied Chemistry, CUSAT, Kochi, India and also on a Thermo Nicolet AVATAR 370 DTGS model FT-IR Spectrophotometer with KBr pellets and ATR technique at the SAIF, Kochi, India.

1.6.5. Electronic spectroscopy

Electronic spectra were recorded in acetonitrile solution on a Spectro UV-vis Double Beam UVD-3500 spectrometer in the 200-900 nm range at the Department of Applied Chemistry, CUSAT, Kochi, India.

1.6.6. NMR spectroscopy

^1H NMR of the synthesized hydrazones was recorded in $\text{CHCl}_3\text{-d}_6$ as solvent on a Bruker Avance DPX-300 MHz NMR Spectrometer at NIIST, Trivandrum. Chemical shifts are reported in $\delta(\text{ppm})$ relative to TMS as the internal standard.

1.6.7. EPR spectroscopy

EPR spectra of complexes were recorded in polycrystalline state at 298 K and in frozen DMF at 77 K on a Varian E-112 spectrometer at X-band, using TCNE as standard ($g = 2.00277$) with 100 kHz modulation frequency and 9.1 GHz microwave frequency at SAIF, IIT Bombay, India.

1.6.8. Cyclic voltammetry

Cyclic voltammograms were recorded on a CHI II20A electrochemical analyzer at Bharathiar University, Coimbatore, India. Electrochemical properties of complexes were studied in DMF medium with tetrabutylammonium phosphate

as supporting electrolyte at a scan rate of 100 mV s⁻¹ with platinum wires as working and counter electrodes and Ag/Ag⁺ as a reference electrode.

1.6.9. Thermogravimetric analyses

TG-DTA-DTG analyses of the the complexes were carried out under nitrogen at a heating rate of 10 °C min⁻¹ in the range 50-800 °C using a Perkin Elmer Pyris Diamond TG/DTA analyzer at the Department of Applied Chemistry, CUSAT, Kochi, India.

1.6.10. X-ray crystallography

Single crystal X-ray diffraction data for HBPB and complex **1** were collected on CrysAlis CCD diffractometer and for **12** [26] data was obtained on CrysAlis CCD diffractometer, equipped with graphite-monochromated Mo K α (λ = 0.71073 Å) radiation at the National Single Crystal X-ray Facility, IIT Bombay, India. The intensity data were collected at 150(2) K and the structures were solved by direct-methods using SHELXS-97 [27] and each refinement was carried out by full-matrix least-squares on F^2 (SHELXL-97) [27] with anisotropic displacement parameters for non-hydrogen atoms and remainder of the hydrogen atoms were placed in calculated positions and allowed to ride on the parent atoms.

Intensity data for complex **2** were collected at 93 K on a Rigaku AFC12/Saturn724 CCD fitted with Mo K α radiation at the University of Texas, San Antonio, Texas, U.S.A. The data set was corrected for absorption based on multiple scans and reduced using standard methods. The structure was solved and refined using SHELXL-97 [27], as described above.

X-ray diffraction experiments for complexes **6** and **16** were performed at 273(2) K using a Bruker SMART CCD area diffractometer with graphite monochromated Mo K α radiation (λ = 0.71073 Å) using ϕ/ω scan technique at the Analytical Science Discipline, Central Salt and Marine Chemicals Research

Institute (CSMCRI), Bhavnagar, Gujarat, India. The Bruker SAINT software was used for data reduction and Bruker SMART for cell refinement. The trial structure was solved and refined as described above.

The crystal data for complexes **4** and **19** were collected out on a Bruker P4 X-ray diffractometer using graphite monochromated Mo K α radiation ($\lambda = 0.71073 \text{ \AA}$) at the School of Chemistry, University of Hyderabad, Hyderabad. The data were solved using Bruker SHELXL by direct method and refined by the full matrix least squares method on F^2 using Bruker SHELXL. The Bruker SAINT software was used for data reduction and Bruker SMART for cell refinement.

The X-ray diffraction experiments of complex **3** were performed on a Bruker axs kappa apex2 CCD Diffractometer with graphite monochromated Mo K α radiation ($\lambda = 0.71073 \text{ \AA}$) at the SAIF, IIT Madras. The APEX2/SAINT and SAINT/XPREP softwares were used for cell refinement and data reduction respectively. The structure was solved using SIR92 by direct method and refinement were carried out by the full matrix least squares method on F^2 using SHELXL-97.

References

- [1] M.M. Heravi, L. Ranjbar, F. Derikvand, H.A. Oskooie, F.F. Bamoharram, *J. Mol. Catal. A: Chem.* 265 (2007) 186.
- [2] R.C. Maurya, S. Rajput, *J. Mol. Struct.* 833 (2007) 133.
- [3] U.O. Ozmen, G. Olgun, *Spectrochim. Acta Part A* 70 (2008) 641.
- [4] N. Ozbek, G. Kavak, Y. Ozcan, S. Ide, N. Karacan, *J. Mol. Struct.* 919 (2009) 154.
- [5] O. Pouralimardan, A.-C. Chamayou, C. Janiak, H.H. –Monfared, *Inorg. Chim. Acta* 360 (2007) 1599.

- [6] A. Ray, S. Banerjee, S. Sen, R.J. Butcher, G.M. Rosair, M.T. Garland, S. Mitra, *Struct. Chem.* 19 (2008) 209.
- [7] N.A. Mangalam, S. Sivakumar, S.R. Sheeja, M.R.P Kurup, E.R.T. Tiekink, *Inorg. Chim. Acta* 362 (2009) 4191.
- [8] A.A.R. Despaigne, J.G. Da Silva, A.C.M. Do Carmo, O.E. Piro, E.E. Castellano, H. Beraldo, *J. Mol. Struct.* 920 (2009) 97.
- [9] M.F. Iskander, T.E. Khalil, R. Werner, W. Haase, I. Svoboda, H. Fuess, *Polyhedron* 19 (2000) 949.
- [10] B. Samanta, J. Chakraborty, S. Shit, S.R. Batten, P. Jensen, J.D. Masuda, S. Mitra, *Inorg. Chim. Acta* 360 (2007) 2471.
- [11] S. Naskar, D. Mishra, R.J. Butcher, S.K. Chattopadhyay, *Polyhedron* 26 (2007) 3703.
- [12] E. Vinuelas-Zahinos, M.A. Maldonado-Rogado, F. Luna-Giles, F.J. Barros-Garcia, *Polyhedron* 27 (2008) 879.
- [13] A. Ray, S. Banerjee, R.J. Butcher, C. Desplanches, S. Mitra, *Polyhedron* 27 (2008) 2409.
- [14] S. Sen, S. Mitra, D.L. Hughes, G. Rosair, C. Desplanches, *Polyhedron* 26 (2007) 1740.
- [15] H. Yin, *Acta Cryst. C* 64 (2008) 324.
- [16] A. Ray, C. Rizzoli, G. Pilet, C. Desplanches, E. Garriga, E. Rentschler, S. Mitra, *Eur. J. Inorg. Chem.* (2009) 2915.
- [17] C.M. Armstrong, P.V. Bernhardt, P. Chin, Des R. Richardson, *Eur. J. Inorg. Chem.* (2003) 1145.
- [18] F. Cariati, U. Caruso, R. Centore, W. Marcolli, A. De Maria, B. Panunzi, M.A. Roviello, A. Tuzi, *Inorg. Chem.* 41 (2002) 6599.

- [19] S. Banerjee, S. Sen, S. Basak, S. Mitra, D.L. Hughes, C. Desplanches, *Inorg. Chim. Acta* 361 (2008) 2707.
- [20] D.S. Kalinowski, P.C. Sharpe, P.V. Bernhardt, Des R. Richardson, *J. Med. Chem.* 51 (2008) 331.
- [21] Des R. Richardson, P. Ponka, *J. Lab. Clin. Med.* 131 (1997) 306.
- [22] N. Filipovic, H. Borrmann, T. Todorovic, M. Borna, V. Spasojevic, D. Sladic, I. Novakovic, K. Andjelkovic, *Inorg. Chim. Acta* 362 (2009) 2000.
- [23] M. Carcelli, P. Mazza, C. Pelizzi, G. Pelizzi, F. Zani, *J. Inorg. Biochem* 57 (1995) 43.
- [24] Md.A. Affan, S.W. Foo, I. Jusoh, S. Hanapi, E.R.T. Tiekink, *Inorg. Chim. Acta* 362 (2009) 5031.
- [25] M. Bakir, O. Brown, *Inorg. Chim. Acta* 353 (2003) 89.
- [26] CrysAlis CCD and CrysAlis RED Versions 1.171.29.2 (CrysAlis NET), Oxford Diffraction Ltd, Abingdon, Oxfordshire, England, 2006.
- [27] G.M. Sheldrick, *Acta Crystallogr. A* 64 (2008) 211.

Chapter 2

Spectral and structural characterization of some acylhydrazones

Contents

- 2.1 Introduction
- 2.2 Experimental
- 2.3 Results and discussion
- References

2.1. Introduction

Interest in the coordination properties of hydrazone ligands towards transition metal ions and in the biological properties of their metal complexes has been growing in recent years [1,2]. The coordination chemistry of transition metals with ligands from the hydrazone family has been of interest due to different bonding modes shown by these ligands. Generally the possible donor sites in acylhydrazones are amide oxygen and azomethine nitrogen. However, there remains the possibility of generating complexes with new molecular architectures by suitable substitution in carbonyl and hydrazide part [3].

This chapter involves the synthesis and characterization of two acylhydrazones. The ligand systems of our interest include

- 1) 2-Benzoylpyridine benzhydrazone (HBPB)
- 2) Di-2-pyridyl ketone nicotinoylhydrazone (HDKN)

We have been interested in the chemistry of pyridyl containing ligands, and we have selected 2-benzoylpyridine benzhydrazone and di-2-pyridyl ketone nicotinoylhydrazone as ligands to synthesize and characterize some transition metal complexes which throw a light into their coordination behavior. Di-2-pyridyl ketone nicotinoylhydrazone is an interesting synthon in the class of chelating agents. The choice of di-2-pyridyl ketone is mainly due to the fact that this heteroaromatic moiety can provide a further binding site for metal cations [4]. It is rigid, and provides two aromatic nitrogens whose unshared electron pairs are beautifully placed to act co-operatively in binding cations. These acylhydrazones of this HL type (H represents dissociable amide proton) can coordinate a given metal ion *via* pyridine-N, the imine-N and amide-O centers.

2.2. Experimental

2.2.1. Materials

Di-2-pyridyl ketone (Aldrich), 2-benzoylpyridine (Aldrich), benzhydrazide (Aldrich), and nicotinic hydrazide (Aldrich) were used as received. Solvents were purified by standard procedures before use.

2.2.2. Syntheses of acylhydrazones

The hydrazones were synthesized by adapting the earlier reported procedure [5], namely *via* condensation between appropriate aldehyde/ketone with the respective acid hydrazide as described below. The chemical structures and abbreviations for the hydrazones are given in Fig. 2.1.

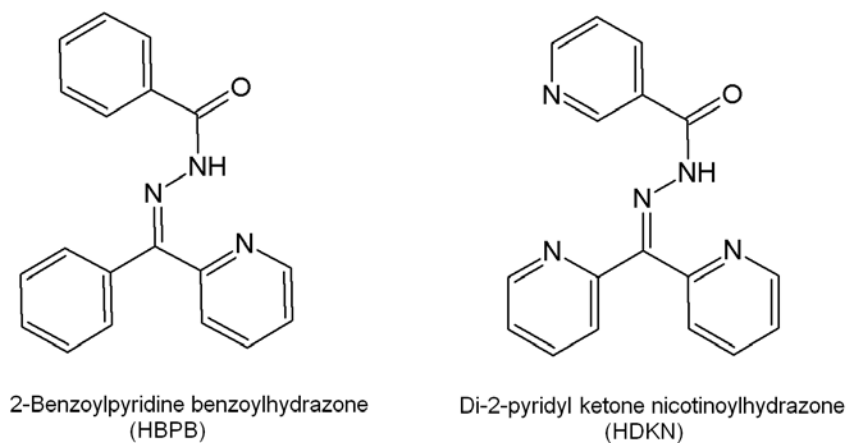
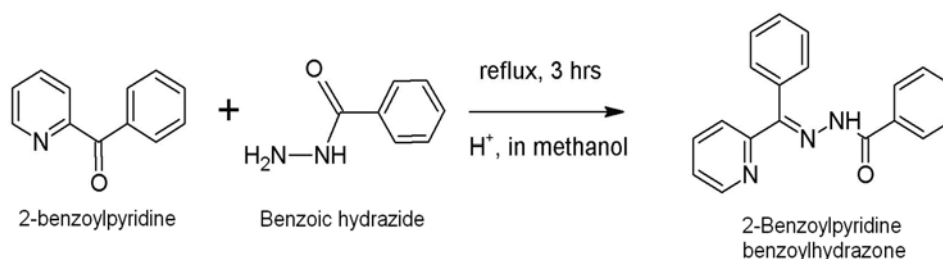


Fig. 2.1. Chemical structures of hydrazones and their abbreviations.

2.2.2.1. Synthesis of 2-benzoylpyridine benzoylhydrazone (HBPB)

A methanolic solution of benzoic hydrazide (0.136 g, 1 mmol) was refluxed with 2-benzoylpyridine (0.183 g, 1 mmol) continuously for 4 h. after adding a few drops of glacial acetic acid. There was no immediate formation of the product. Then the reaction mixture was kept aside for slow evaporation at room temperature. After 3-4 days, colorless block-shaped crystals suitable for single crystal analyses were formed and carefully separated. The scheme for the reaction is shown below (Scheme 1).

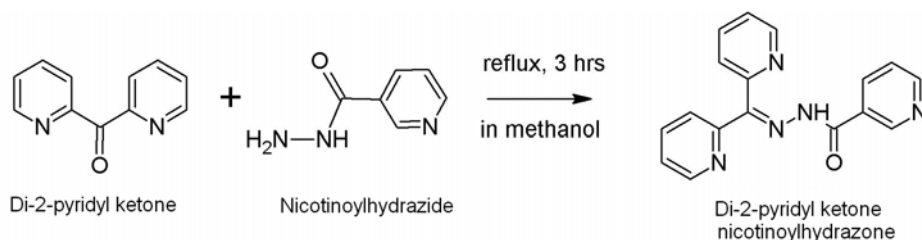


Scheme 1. Synthesis of 2-benzoylpyridine benzoylhydrazone.

Yield: 79%, M. P.: 129 °C. Elemental Anal. Found (Calcd.) (%): C: 75.46 (75.73), H: 5.23 (5.02), N: 13.98 (13.94).

2.2.2.2. *Synthesis of di-2-pyridyl ketone nicotinoylhydrazone hemihydrate (HDKN·0.5H₂O)*

To a methanolic solution of nicotinoyl hydrazide (0.137 g, 1 mmol), di-2-pyridyl ketone (0.184 g, 1 mmol) in methanol was added to it. The reaction mixture was refluxed for 5 h. and the reaction mixture was kept at room temperature for slow evaporation. After a week, white compound was separated, filtered and washed with ether and dried over P₄O₁₀ *in vacuo*. Reaction scheme for the synthesis of HDKN is shown below (Scheme 2).



Scheme 2. Synthesis of di-2-pyridyl ketone nicotinoylhydrazone.

Yield: 84%, Color: colorless, M.P.: 159 °C, Elemental Anal. Found (Calcd.) (%): C: 65.94 (65.37), H: 4.26 (4.52), N: 22.47 (22.42) for HDKN·0.5H₂O.

2.3. Results and discussion

2.3.1. Elemental analyses

C, H, N analyses of the synthesized hydrazones are given in Section 2.2 and were consistent with that of the formulae suggested.

2.3.2. Infrared spectra

The IR spectra of the hydrazones HBPB and HDKN have been analyzed in the region 4000-400 cm^{-1} using the KBr discs. The bands of diagnostic importance and their tentative assignments are listed in Table 2.1. Strong bands due to the $\nu(\text{NH})$ and $\nu(\text{C}=\text{O})$ modes at 3063 and 1678 cm^{-1} are observed in the spectrum of HBPB (Fig. 2.2) which suggests that the hydrazone exists in the amido form in the solid state [6]. A prominent band at 1571 cm^{-1} due to azomethine $\nu(\text{C}=\text{N})$ linkage is observed in the spectrum [7] indicating that condensation between ketone moiety of carbonyl compound and that of the hydrazide has taken place resulting into the formation of desired ligand HBPB.

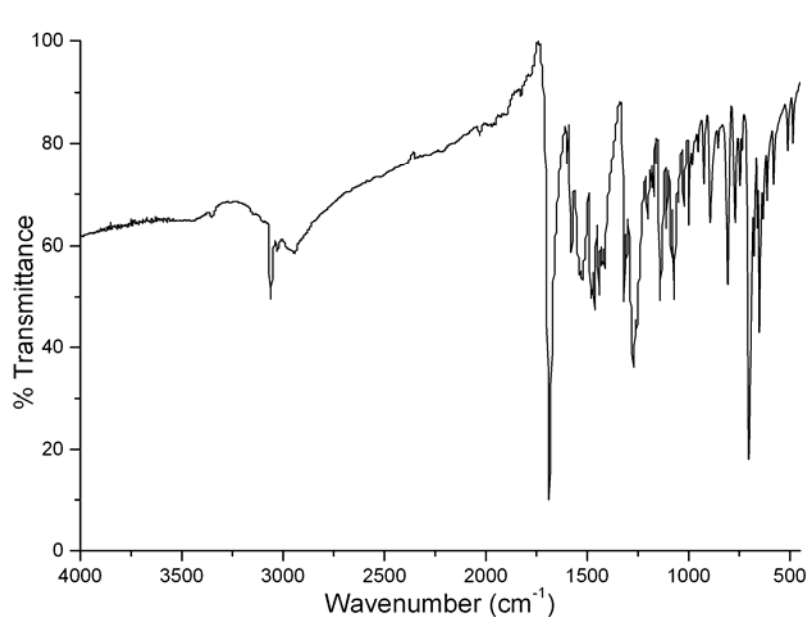


Fig. 2.2. IR spectrum of HBPB.

Hydrazones can exist in the amido or in iminol form or an equilibrium mixture of two since it has an amide group. In the IR spectrum of HDKN (Fig. 2.3), the $\nu(\text{N-H})$ and $\nu(\text{C}=\text{O})$ stretching bands are observed at 2928 and 1689 cm^{-1} respectively [8]. These two observations suggest that HBPB and HDKN exist in

amido form in the solid state. It is worthy mentioning that the spectrum of HDKN exhibits a strong band at 1579 cm^{-1} . This band can be assigned to the stretching mode for (C=N) group [9] formed from the reaction between the keto group of the carbonyl compound and corresponding hydrazide.

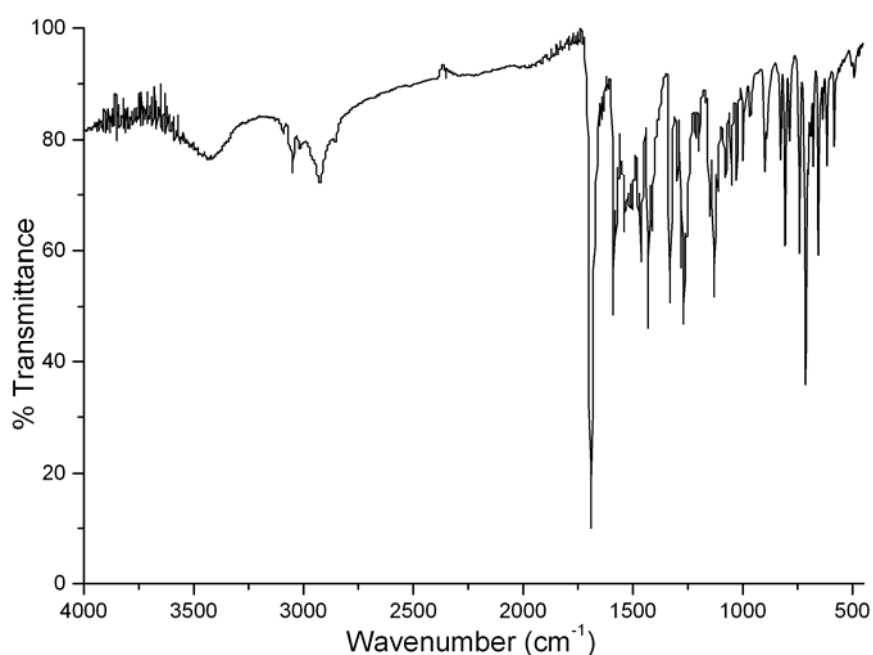


Fig. 2.3. IR spectrum of HDKN.

Table 2.1. Selected infrared spectral data (cm^{-1}) of the hydrazones.

Compound	$\nu(\text{N-H})$	$\nu(\text{C=O})$	$\nu(\text{C=N})$
HBPB	3063	1678	1571
HDKN	2928	1689	1579

2.3.3. Electronic spectra

The electronic spectra of the hydrazones were recorded in acetonitrile solutions (10^{-4} M) and the absorption bands are summarized in Table 2.2. The

UV spectra of HBPB and HDKN display three bands which corresponds to the $n-\pi^*$ and $\pi-\pi^*$ transitions associated with azomethine chromophore and the pyridyl rings of the hydrazones [10,11] (Fig. 2.4).

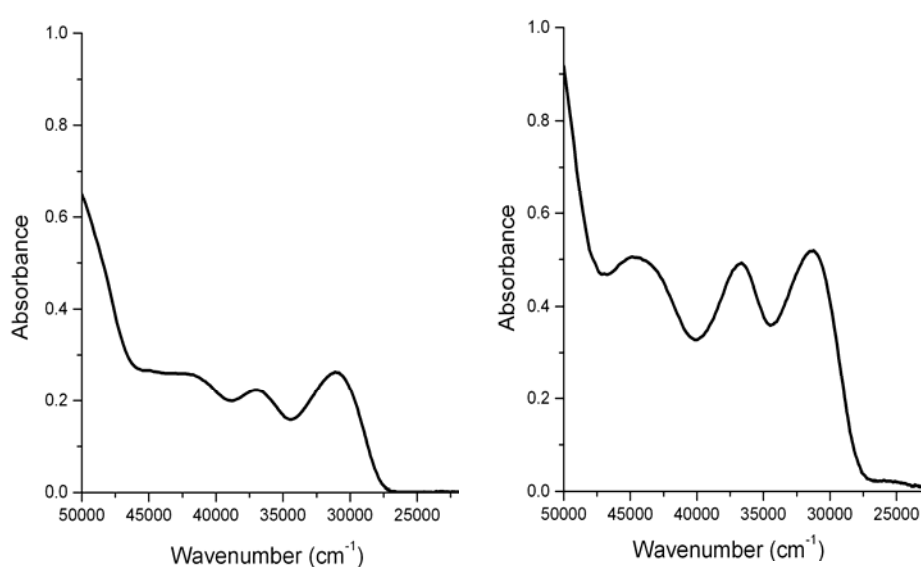


Fig. 2.4. Electronic spectra of HBPB (left) and HDKN (right) in acetonitrile solution.

Table 2.2. Electronic spectral data of the hydrazones.

Compound	UV absorption bands (cm^{-1})
HBPB	42920, 36900, 31050
HDKN	44400, 36700, 31270

2.3.4. NMR spectra

The ^1H NMR spectra of HBPB and HDKN are recorded in CDCl_3 and are shown in Figs. 2.5 and 2.6. The sharp signal at $\delta = 15.2$ ppm is due to the existence of the compound in iminol form. On D_2O exchange the intensity of this signal is found to be considerably decreased. Aromatic protons appear as multiplets at 7.2-8.8 ppm range.

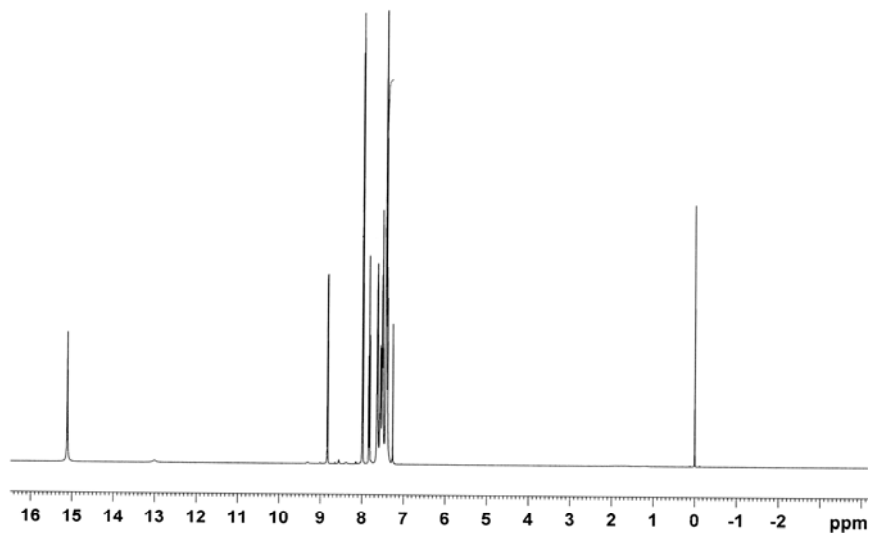


Fig. 2.5. ¹H NMR spectrum of HBPB.

The sharp signal at $\delta = 15.7$ ppm in the spectrum of HDKN suggest the existence of the hydrazone in iminol form. On D₂O exchange, as for HBPB, the intensity of this signal is found to be considerably decreased. Aromatic protons appear as a multiplet at $\delta = 7.2$ -8.2 ppm range.

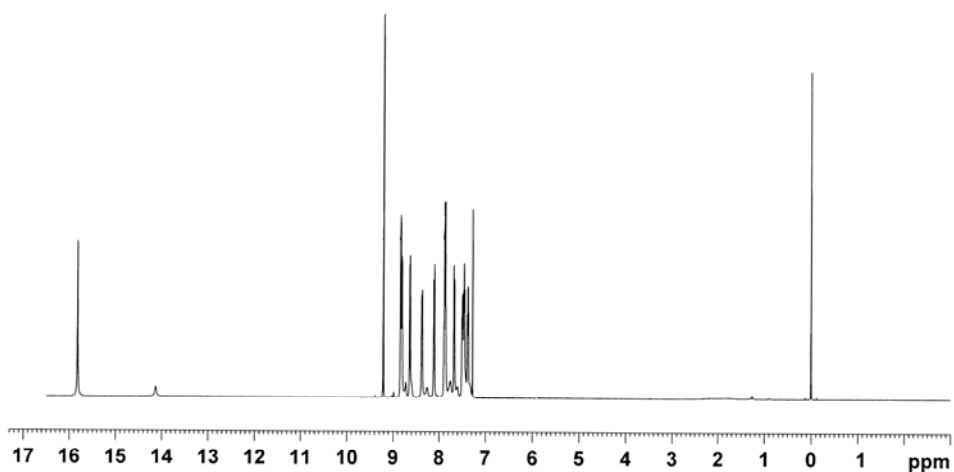


Fig. 2.6. ¹H NMR spectrum of HDKN.

2.3.5. X-ray crystallography

Single crystal X-ray diffraction data for colorless HBPB was performed on a CrysAlis CCD diffractometer with graphite monochromated Mo K α radiation ($\lambda = 0.71073 \text{ \AA}$). The CrysAlis RED software was used for cell refinement and data reduction [12]. The structure was solved by direct-methods using SHELXS-97 [13] and each refinement was carried out by full-matrix least-squares on F^2 (SHELXL-97) [13] with anisotropic displacement parameters for non-hydrogen atoms and a weighting scheme of the form $w = 1/[\sigma^2(F_o^2) + (0.aP)^2 + bP]$ where $P = (F_o^2 + 2F_c^2)/3$. The nitrogen-bound hydrogen atom was located from a difference Fourier map and refined. The remaining hydrogen atoms were placed in their calculated positions in the riding model approximation.

Crystal data and refinement details of HBPB are given in Table 2.3. The figures representing the molecular structure of HBPB and supramolecular chain mediated by C–H \cdots N and C–H \cdots O contacts were drawn using ORTEP with 50% displacement ellipsoids [14] and DIAMOND respectively [15].

2.3.5.1. Crystal structure of HBPB

The colorless block-shaped crystals suitable for X-ray diffraction were grown by slow evaporation from a methanolic solution of the HBPB. A perspective view of the compound showing the numbering scheme is shown in Fig. 2.7; selected geometric parameters are collected in Table 2.4. The central part of the molecule is essentially planar due to the presence of an intramolecular N–H \cdots N_{pyridine} hydrogen bond. The maximum deviation from the least-squares plane calculated for the hydrazone moiety, i.e. C6–N2–N3–C13–O1, is 0.0189(12) \AA for the N2 atom. The terminal aromatic rings are twisted out of this plane as seen in the values of the N2–C6–C7–C8 and N3–C13–C14–C15 torsion angles of $-47.93(18)$ and $159.25(12)^\circ$, respectively. The dihedral angle formed between the terminal rings is $66.67(7)^\circ$.

Table 2.3. Crystallographic and refinement details of HBPB.

Parameters	HBPB
Empirical Formula	C ₁₉ H ₁₅ N ₃ O
Formula weight (M)	301.34
Temperature (T) K	150 K
Wavelength (Mo K α) (Å)	0.71073
Crystal system	Triclinic
Space group	$P\bar{1}$
Lattice constants	
<i>a</i> (Å)	8.0330(5)
<i>b</i> (Å)	8.6486(5)
<i>c</i> (Å)	11.3168(8)
α (°)	89.329(5)
β (°)	84.857(5)
γ (°)	72.332(5)
Volume V (Å ³)	746.03(8)
<i>Z</i>	2
Calculated density (ρ) (Mg m ⁻³)	1.341
Absorption coefficient, μ (mm ⁻¹)	0.086
<i>F</i> (000)	316
Crystal size (mm ³)	0.36 x 0.32 x 0.28
θ Range for data collection	3.0 – 25.0°
Limiting Indices	-9 ≤ <i>h</i> ≤ 9 -10 ≤ <i>k</i> ≤ 10 -11 ≤ <i>l</i> ≤ 11
Reflections collected	6500
Unique Reflections	2625
Refinement method	Full-matrix least-squares on <i>F</i> ²
Data / restraints / parameters	2625 / 0 / 212
Goodness-of-fit on <i>F</i> ²	1.032
Final <i>R</i> indices [<i>I</i> > 2 σ (<i>I</i>)]	<i>R</i> ₁ = 0.035, <i>wR</i> ₂ = 0.079
<i>R</i> indices (all data)	<i>R</i> ₁ = 0.052, <i>wR</i> ₂ = 0.084

$$wR_2 = [\sum w(F_o^2 - F_c^2)^2 / \sum w(F_o^2)^2]^{1/2}; R_1 = \sum ||F_o| - |F_c|| / \sum |F_o|$$

The C13–O1 bond distance of 1.2213(14) Å indicates the molecule exists in the amido form in the solid-state [16]. The N2–C6 bond length is 1.2955(16) Å, with significant double-bond character, is comparable to those previously reported analogous of hydrazone structures [17-19]. The above notwithstanding, the values of the N2–N3 and N3–C13 bond distances of 1.3682(15) and 1.3610(16) Å, respectively, indicate significant delocalization of π -electron density over the hydrazone portion of the molecule. The configuration about the N2–C6 bond is *Z* [20]. The torsional angles observed C(5)–C(6)–N(2)–N(3), 2.9(2)° and N(2)–N(3)–C(13)–O(1), 1.3(2)° supports the *cis* configuration of C(6)–N(2) bond and *cis* configuration of the C(13)–N(3) bond in the ligand.

Table 2.4. Selected bond lengths (Å) and bond angles (°) for HBPB.

Bond lengths		Bond angles	
C13–O1	1.2213(14)	O1–C13–N3	124.67(12)
N2–N3	1.3682(15)	N3–N2–C6	117.38(10)
N2–C6	1.2955(16)	N2–C6–C5	127.69(12)
N3–C13	1.3610(16)	N2–C6–C7	114.35(10)
C5–C6	1.4945(17)	N2–N3–C13	121.33(10)
C6–C7	1.4960(18)	N3–C13–C14	112.84(10)

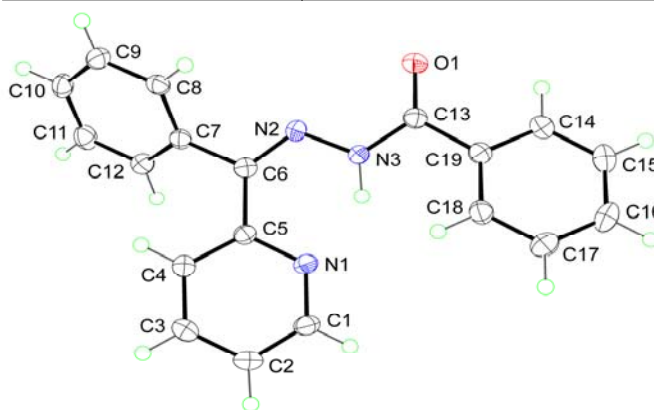


Fig. 2.7. The molecular structure of HBPB along with the atom numbering scheme (Displacement ellipsoids are drawn at the 50% probability level and hydrogen atoms are shown as small spheres of arbitrary radii).

The principal feature of the crystal packing is the formation of a supramolecular chain mediated by cooperative C–H⋯N and C–H⋯O contacts; the formation of a chain mediated by amide ⋯O=C–N–H hydrogen bonds is precluded owing to the presence of the intramolecular N–H⋯N_{pyridine} contact. The supramolecular chains, illustrated in Fig. 2.8 are oriented along the *b*-direction and stacked side by side with neighbouring chains to form layers approximately in the (2 0 $\bar{1}$) plane. The primary connections between layers are of the type C–H⋯ π (Table 2.5).

Table 2.5. H-bonding, π - π and C–H⋯ π interaction parameters of HBPB.

H-bonding				
Donor–H⋯A (Å)	D–H	H⋯A	D⋯A	D–H⋯A
N3–H(3)⋯N(1)	0.913	1.847	2.6101	139.6
C2–H(2)⋯N(2) ^a	0.95	2.62	3.5693	174
π - π interactions				
Cg(I)⋯Cg(J)	Cg–Cg (Å)	α (°)	β (°)	
Cg(1)⋯Cg(3) ^b	3.7264	11.07	25.28	
Cg(3)⋯Cg(1) ^b	3.7266	11.07	16.13	
C–H⋯ π interaction				
X–H(I)⋯Cg(J)	H⋯Cg (Å)	XH⋯Cg (°)	X⋯Cg (Å)	
C(11)–H(11)⋯Cg(3) ^c	2.86	139	3.6300	
Equivalent position codes				
a = x, -1+y, z ; b = 1-x, -y, 1-z; c = x, y, 1 + z.				
Cg(1) = N(1), C(1), C(2), C(3), C(4), C(5) ; Cg(3) = C(14), C(15), C(16), C(17), C(18), C(19) ; Cg(6) = C(7), C(8), C(9), C(10), C(11), C(12)				

D, donor; A, acceptor; Cg, centroid; α , dihedral angles between planes I and J; β , angle Cg(I) – Cg(J) vector normal to plane I

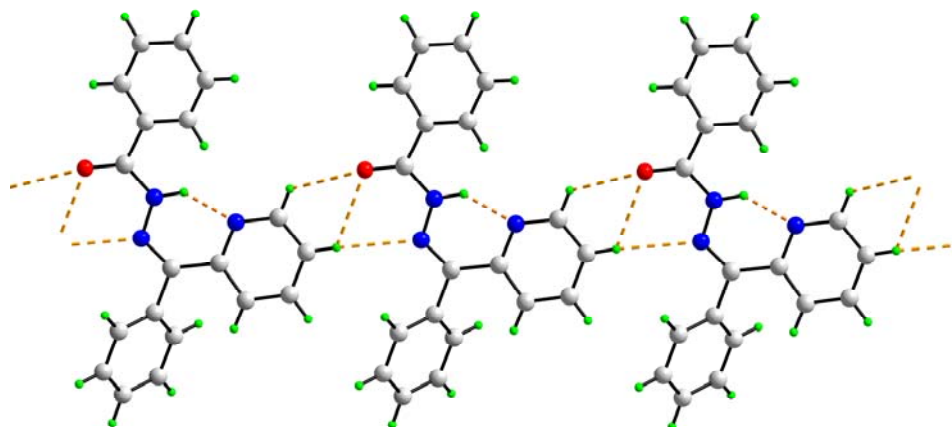


Fig. 2.8. Supramolecular chain mediated by C–H···N and C–H···O contacts. These contacts and the intramolecular N–H···N hydrogen bonds are shown as orange dashed lines.

References

- [1] D.S. Kalinowski, P.C. Sharpe, P.V. Bernhardt, Des R. Richardson, *J. Med Chem.* 51 (2008) 331.
- [2] R.C. Maurya, S. Rajput, *J. Mol. Struct.* 833 (2007) 133.
- [3] C.M. Armstrong, P.V. Bernhardt, P. Chin, Des R. Richardson, *Eur. J. Inorg. Chem.* (2003) 1145.
- [4] T.A. Reena, E.B. Seena, M.R.P. Kurup, *Polyhedron* 27 (2008) 1825.
- [5] P.V. Bernhardt, G.J. Wilson, P.C. Sharpe, D.S. Kalinowski, Des R. Richardson, *J. Biol. Inorg. Chem.* 13 (2008) 107.
- [6] N. Mathew, M. Kuriakose, E.B. Seena, M.R.P. Kurup, *Acta Cryst. E* 63 (2007) 2190.
- [7] M. Carcelli, P. Cozzini, T. Maccagni, C. Pelizzi, L. Righi, *Inorg. Chim. Acta* 303 (2000) 238.

- [8] F. Hueso-Urena, N.A. Illan-Cabeza, M.N. Moreno-Carretero, A.L. Penas-Chamorro, R. Faure, *Polyhedron* 19 (2000) 689.
- [9] F.B. Tamboura, P.M. Haba, M. Gaye, A.S. Sall, A.H. Barry, T. Jouini, *Polyhedron* 23 (2004) 1191.
- [10] W. Kemp, *Organic Spectroscopy*, 3rd edn., Macmillan, Hampshire (1996).
- [11] D.L. Pavia, G.M. Lapman, G.S. Kriz, J.R. Vyvyan, 3rd edn., *Introduction to Spectroscopy*, Harcourt College Publishers, Orlando (2004).
- [12] CrysAlis CCD and CrysAlis RED Versions 1.171.29.2 (CrysAlis 171.NET), Oxford Diffraction Ltd, Abingdon, Oxfordshire, England, 2006.
- [13] G.M. Sheldrick, *Acta Crystallogr. A* 64 (2008) 211.
- [14] L.J. Farrugia, *J. Appl. Cryst.* 30 (1997) 565.
- [15] K. Brandenburg, DIAMOND Version 3.1, Visual Crystal Structure Information System, CRYSTAL IMPACT, Postfach 1251, D- 53002 Bonn, Germany (2006), Germany.
- [16] M. Bakir, O. Brown, *J. Mol. Struct.* 609 (2002) 129.
- [17] H.-K. Fun, P.S. Patil, S.R. Jebas, K.V. Sujith, B. Kalluraya, *Acta. Cryst. E* 64 (2008) 1594.
- [18] D.S. Kalinowski, P.C. Sharpe, P.V. Bernhardt, Des R. Richardson, *J. Med. Chem.* 51 (2008) 331.
- [19] M. Bakir, C. Gyles, *J. Mol. Struct.* 649 (2003) 133.
- [20] A.A.R. Despaigne, J.G. Da Silva, A.C.M. Do Carmo, O.E. Piro, E.E. Castellano, H. Beraldo, *J. Mol. Struct.* 920 (2009) 97.

*****CQ*****

Chapter 3

Syntheses, spectral and structural characterization of dioxygen bridged vanadium(V) complexes incorporating tridentate acylhydrazones

Contents

- 3.1 Introduction
 - 3.2 Experimental
 - 3.3 Results and discussion
 - References
-

3.1. Introduction

Vanadium exists in a plethora of oxidation states and its coordination compounds play an important role in nitrogen activation and fixation and other biologically important reactions. This revelation has stimulated interest in the stereochemistry and reactivity of its coordination compounds that contain the diazo and hydrazido group because they may provide some understanding of the mechanism of metalloenzymatic reduction of nitrogen. Substituted arylhydrazones possessing a suitably disposed amino group, whilst often bind directly to the metal; they may also interact with compounds containing carbonyl groups, for *eg.* salicylaldehydes and β -diketones. Such reactions have been exploited adroitly to form Schiff bases that are capable of confining metal atoms and controlling their properties and functionality.

Coordination chemistry of vanadium received a shot in the arm in recent times because of (a) discovery of the presence of vanadium in some sea squirts, mushrooms, and vanadium-dependant enzymes nitrogenases and haloperoxidases, (b) the involvement of vanadium in the inhibition of phosphate metabolizing enzymes and stimulation of phosphomutases, (c) anticancer activity, (d) insulin mimetic activity of some vanadium(IV) and (V) complexes [1], and (e) use of vanadium(IV) complexes of Schiff base ligands as oxidation catalysts [2]. Recent reports on insulin-mimetic activity by vanadium(V) complexes in some dianionic tridentate ONO ligands [3,4] makes us optimistic about the possible insulin-mimetic behavior of our complexes, eventhough vanadyl ion is known to be less toxic than vanadate ion.

Vanadium has an extremely complex chemistry. It forms large array of compounds in which the most important oxidation states are +3, +4 and +5. Very pure vanadium is very rare because it is quite reactive towards oxygen, nitrogen and carbon at elevated temperatures. The oxophilic nature of V(IV) causes the overwhelming majority of V(IV) compound to contain the vanadyl ion (*ie.* VO^{2+}) which is considered to be the most stable oxo cation of the first row transition metal ions. Vanadyl complexes, typically adopt 5-coordinate square pyramidal or 6-coordinated distorted octahedral geometries, with the vanadium–oxo distance being shorter than the distance from the metal to the ligand trans to the oxo [5,6]. Vanadium easily switches between the oxidation states V and IV. It is known that the coordination complexes of aroylhydrazones act as enzyme inhibitors and are useful due to their pharmacological applications.

3.2. Experimental

3.2.1. Materials

Di-2-pyridylketone (Aldrich), 2-benzoylpyridine (Aldrich), benzhydrazide (Aldrich), and nicotinic hydrazide (Aldrich), vanadyl sulfate (Aldrich) and VO(acac)₂ (E-Merck) were used as received. Solvents were purified by standard procedures before use.

3.2.2. Syntheses of the acylhydrazones

The syntheses of hydrazones HBPB and HDKN are discussed already in Chapter 2.

3.2.3. Syntheses of the complexes

3.2.3.1. Synthesis of [VO(BPB)(μ₂-O)]₂ (1)

Complex **1** was prepared by refluxing methanolic solutions of HBPB (0.301 g, 1 mmol) and vanadyl sulfate (0.163 g, 1 mmol) for 5 h. The resulting solution was allowed to stand at room temperature and after slow evaporation, yellow crystals of complex **1** were separated, filtered and washed with ether and dried over P₄O₁₀ *in vacuo*.

[VO(BPB)(μ₂-O)]₂: Yield: 63%, λ_m (DMF): 6 ohm⁻¹cm² mol⁻¹, Elemental Anal. Found (Calcd.) (%): C: 59.86 (59.70), H: 4.28 (4.37), N: 11.31 (10.71).

3.2.3.2. Synthesis of [VO(DKN)(μ₂-O)]₂·2H₂O (2)

To a solution of HDKN (0.312 g, 1 mmol) in methanol, a DMF-methanol mixture of VO(acac)₂ (0.265 g, 1 mmol) was added. The resulting solution was refluxed for 5 h. and then kept at room temperature. The pale-yellow crystals of **2** that separated out were filtered, washed with ether and dried over P₄O₁₀ *in vacuo*.

[VO(DKN)(μ_2 -O)]₂·2H₂O: Yield: 83%, λ_m (DMF): 8 ohm⁻¹cm² mol⁻¹, Elemental Anal. Found (Calcd.) (%): C: 51.65 (51.23), H: 3.23 (3.69), N: 17.71 (17.07) for [VO(DKN)(μ_2 -O)]₂·2H₂O.

3.3. Results and discussion

3.3.1. Elemental analyses

The analytical data indicate that the complexes have the formula given in Section 3.2 and was also supported by their crystal structures. The observed C, H, N values were in close agreement with that of the formulae suggested.

3.3.2. Molar conductivity and magnetic susceptibility measurements

The molar conductivity measurements in 10⁻³ M DMF solutions indicate that both complexes are non-electrolytic in nature. Both the complexes contain the VO²⁺ unit in which vanadium is in +5 oxidation state (*d⁰*). Due to the absence of unpaired electrons both of them were found to be diamagnetic.

3.3.3. Infrared spectra

The comparison of the main vibrational bands of the acylhydrazones with those of the complexes helps to establish their ligating behavior to the metal center. Selected IR bands of the complexes are represented in Table 3.1. The IR spectra of HBPB and HDKN exhibit bands at 3063 and 2928 cm⁻¹ due to ν (N–H) stretching and 1678 and 1689 cm⁻¹ due to ν (C=O) stretching, which are indicative of their amido nature in the solid-state [7,8]. These bands disappear on complexation and a new band appearing in the region 1360-1385 cm⁻¹ is assigned to ν (C–O) indicating the involvement of the original carbonyl-oxygen in bonding as an enolate. The existence of HBPB in the amido tautomeric form was confirmed from its crystal structure, which was discussed in second chapter. Each of the acylhydrazones under discussion display a strong and sharp band in

the region $1570\text{--}1595\text{ cm}^{-1}$ ascribed to $\nu(\text{C}=\text{N})$ of the azomethine group [9,10]. These bands undergo shifts to the lower wavenumbers upon complexation which suggest the coordination of the azomethine nitrogen to vanadium. The presence of new bands in the region at *ca.* 1593 cm^{-1} , which may be due to the newly formed $\nu(\text{C}=\text{N})$ bond, confirms the coordination *via* azomethine nitrogen [11]. The out-of-plane bending modes of vibrations of the free ligands at 622 cm^{-1} are found to be shifted to higher energies in the spectra of complexes indicating the coordination *via* pyridyl nitrogen [12]. Further, the intense band observed at 945 cm^{-1} in both the complexes corresponds to the terminal $\text{V}=\text{O}$ stretching [13,14]. In addition to this, these dimeric complexes **1** and **2** exhibit bands at *ca.* 853 cm^{-1} due to the $\text{V}\text{--}\text{O}\text{--}\text{V}$ bridging vibrations [15,16].

IR spectra of the complexes **1** and **2** are presented in Figs. 3.1. and 3.2. respectively.

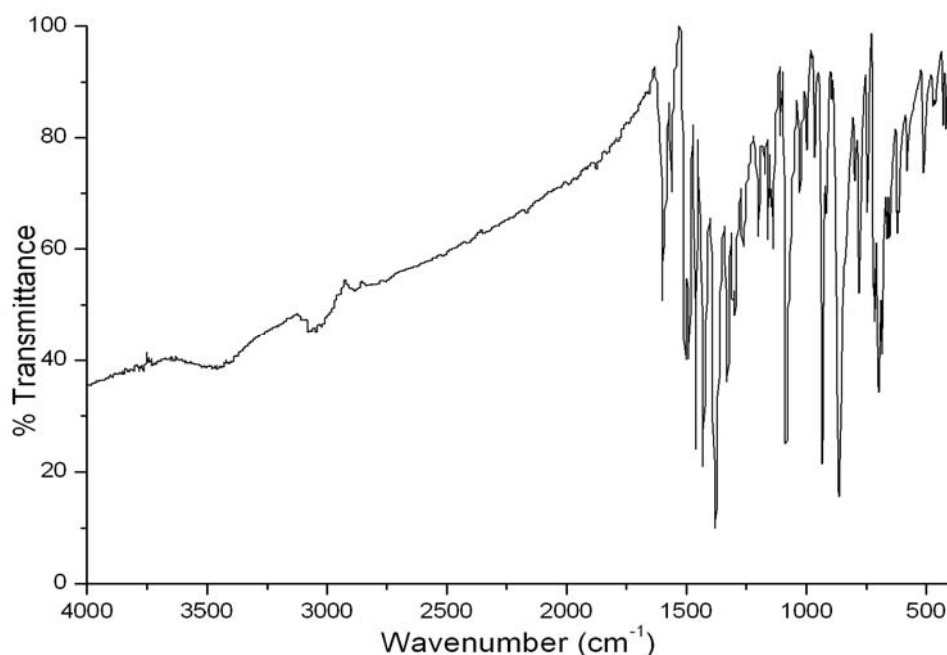


Fig. 3.1. IR spectrum of $[\text{VO}(\text{BPB})(\mu_2\text{-O})_2]$ (**1**).

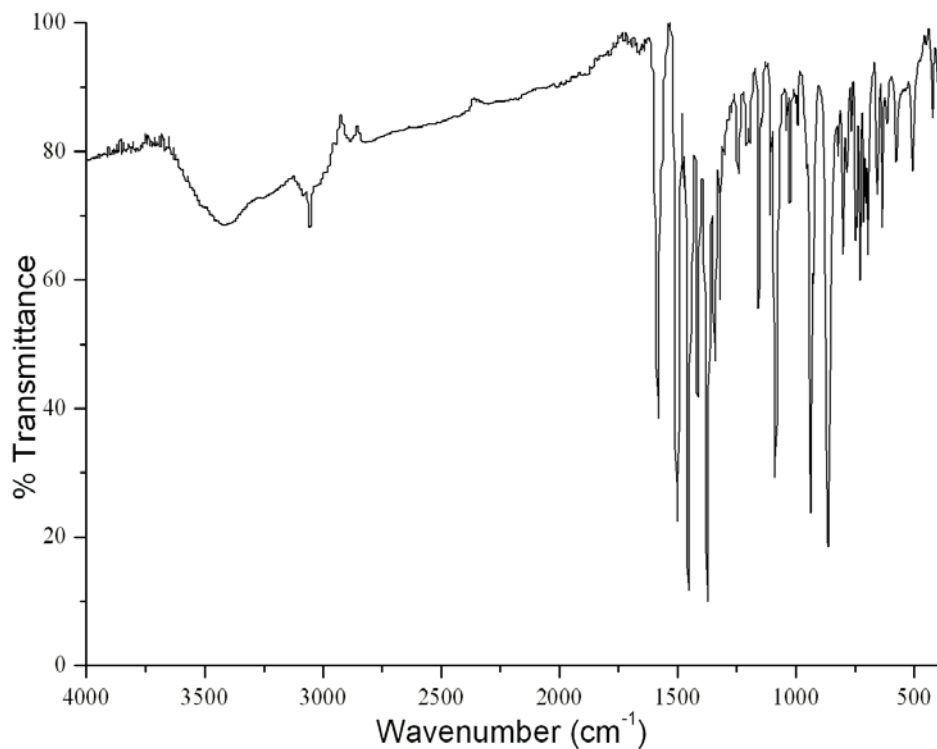


Fig. 3.2. IR spectrum of $[\text{VO}(\text{DKN})(\mu_2\text{-O})]_2 \cdot 2\text{H}_2\text{O}$ (2).

Table 3.1. Infrared spectral data (cm^{-1}) of vanadium(V) complexes.

Compound	$\nu(\text{N-H})$	$\nu(\text{C=O})/\nu(\text{C-O})$	$\nu(\text{C=N})$	$\nu(\text{C=N})^a$	$\nu(\text{V=O})$	$\nu(\text{V-O-V})$
HBPB	3063	1678	1571
$[\text{VO}(\text{BPB})(\mu_2\text{-O})]_2$ (1)	...	1368	1509	1599	946	853
HDKN	2928	1689	1579
$[\text{VO}(\text{DKN})(\mu_2\text{-O})]_2 \cdot 2\text{H}_2\text{O}$ (2)	...	1373	1509	1588	945	853

^a Newly formed C=N

3.3.4. Electronic spectra

The electronic absorption bands of the complexes (10^{-5} M) are recorded in acetonitrile solution and all data are summarized in Table 3.2. The bands at *ca.* 31250, 36360 and 42550 cm^{-1} , attributed to the $n-\pi^*$ and $\pi-\pi^*$ transitions of the uncomplexed hydrazones are slightly shifted upon complexation. For complexes **1** and **2**, high energy bands at 24630 and 24930 cm^{-1} respectively are assigned to the ligand to metal charge transfer (LMCT) transitions arising from phenolate oxygen of the hydrazone to an empty d orbital of the vanadium(V) ion [17,18] (Fig. 3.3). These dioxovanadium(V) complexes have a d^0 configuration, and $d-d$ bands are therefore not expected.

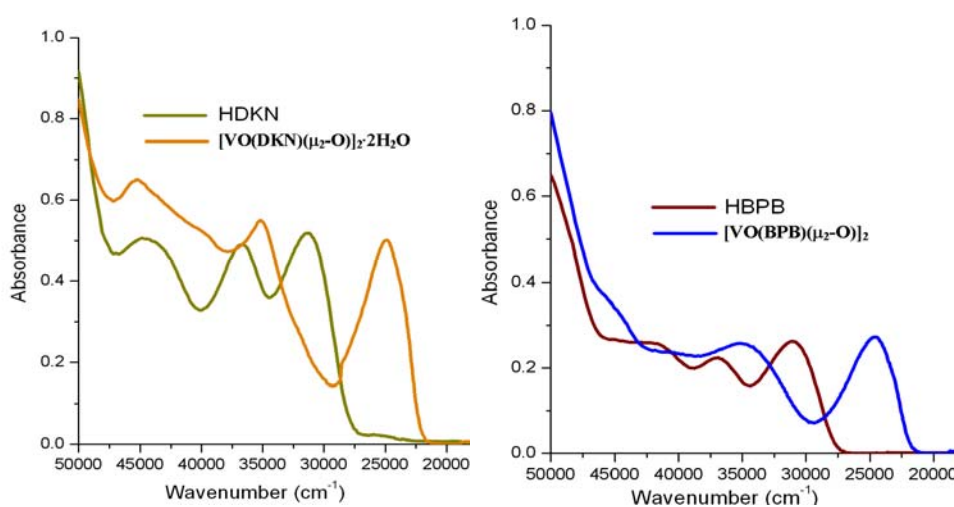


Fig. 3.3. Electronic spectra of the complex **1** (left) and **2** (right).

Table 3.2. Electronic spectral data of the vanadium complexes.

Compound	Uv-vis absorption bands (cm^{-1})
$[\text{VO}(\text{BPB})(\mu_2\text{-O})]_2$ (1)	24630, 34870, 44810
$[\text{VO}(\text{DKN})(\mu_2\text{-O})]_2 \cdot 2\text{H}_2\text{O}$ (2)	24930, 35165, 45200

3.3.5. X-ray crystallography

Single crystal X-ray diffraction data for yellow $[\text{VO}(\text{BPB})(\mu_2\text{-O})]_2$ were collected on an CrysAlis CCD diffractometer with graphite monochromated Mo $K\alpha$ radiation ($\lambda = 0.71073 \text{ \AA}$). The CrysAlis RED software was used for cell refinement and data reduction [19]. The structures were solved by direct-methods using SHELXS-97 [20] and each refinement was carried out by full-matrix least-squares on F^2 (SHELXL-97) [20] with anisotropic displacement parameters for non-hydrogen atoms and a weighting scheme of the form $w = 1/[\sigma^2(F_o^2) + (0.aP)^2 + bP]$ where $P = (F_o^2 + 2F_c^2)/3$. All non-hydrogen atoms were refined anisotropically. The hydrogen atoms of the nitrogen atoms were located from difference fourier maps and refined isotropically and remainder of the hydrogen atoms were placed in calculated positions and allowed to ride on the parent atoms.

Intensity data for a pale-yellow prism of $[\text{VO}(\text{DKN})(\mu_2\text{-O})]_2 \cdot 2\text{H}_2\text{O}$ were collected at 93 K on a Rigaku AFC12/Saturn724 CCD fitted with Mo $K\alpha$ radiation. The data set was corrected for absorption based on multiple scans [21] and reduced using standard methods [22]. The structure was solved and refined using SHELXL-97 [20], as described above. A residual electron density peak, consistent with the presence of a disordered solvent water molecule was evident towards the end of the refinement. This was modelled as 0.25 of a water molecule proximate, over a centre of inversion (1.651(12) \AA), to a centrosymmetric mate so that the crystal chosen for analysis is formulated as $[\text{VO}(\text{DKN})(\mu_2\text{-O})]_2 \cdot \frac{1}{2}\text{H}_2\text{O}$; hydrogen atoms were not included for the water molecule.

Crystal data and refinement details of complexes **1** and **2** are given in Table 3.3. Figs. 3.4 and 3.6, showing the atom labeling schemes were drawn with 50% displacement ellipsoids [23], and the remaining crystallographic figures (Figs. 3.5 and 3.7) were drawn with MERCURY [24] and DIAMOND [25] softwares respectively.

Table 3.3. Crystallographic and refinement details of **1** and **2**.

Parameters	1	2
Empirical Formula	C ₃₈ H ₂₈ N ₆ O ₆ V ₂	C ₃₄ H ₂₅ N ₁₀ O _{6.5} V ₂
Formula weight (M)	766.54	779.52
Temperature (T) K	150	98
Wavelength (Mo K α) (Å)	0.611	0.639
Crystal system	Monoclinic	Triclinic
Space group	<i>P2₁/n</i>	<i>P</i> $\bar{1}$
Lattice constants		
<i>a</i> (Å)	9.9435(1)	8.0494(12)
<i>b</i> (Å)	9.9285(2)	9.750(2)
<i>c</i> (Å)	17.1187(2)	10.7678(19)
α (°)	90	89.291(9)
β (°)	90.464(1)	77.852(8)
γ (°)	90	81.034(9)
Volume <i>V</i> (Å ³)	1689.97(4)	815.8(3)
<i>Z</i>	2	1
Calculated density (ρ) (Mg m ⁻³)	1.506	1.587
Absorption coefficient, μ (mm ⁻¹)	0.611	0.639
<i>F</i> (000)	784	397
θ Range for data collection	3.1 – 25.0°	2.8 – 26.5°
Limiting Indices	-9 ≤ <i>h</i> ≤ 9 -11 ≤ <i>k</i> ≤ 11 -20 ≤ <i>l</i> ≤ 20	-10 ≤ <i>h</i> ≤ 10 -12 ≤ <i>k</i> ≤ 11 -13 ≤ <i>l</i> ≤ 13
Reflections collected	13940	12219
Unique Reflections	2992	3325
Refinement method	Full-matrix least-squares on <i>F</i> ²	Full-matrix least-squares on <i>F</i> ²
Data / restraints / parameters	2992 / 0 / 235	3325 / 0 / 239
Goodness-of-fit on <i>F</i> ²	1.07	1.06
Final <i>R</i> indices [<i>I</i> > 2 σ (<i>I</i>)]	<i>R</i> ₁ = 0.036, <i>wR</i> ₂ = 0.091	<i>R</i> ₁ = 0.043, <i>wR</i> ₂ = 0.103
<i>R</i> indices (all data)	<i>R</i> ₁ = 0.047, <i>wR</i> ₂ = 0.095	<i>R</i> ₁ = 0.045, <i>wR</i> ₂ = 0.104

$$wR_2 = [\sum w(F_o^2 - F_c^2)^2 / \sum w(F_o^2)^2]^{1/2}; R_1 = \sum ||F_o| - |F_c|| / \sum |F_o|$$

3.3.5.1. Crystal structures of $[VO(BPB)(\mu_2-O)]_2$ (**1**) and $[VO(DKN)(\mu_2-O)]_2 \cdot \frac{1}{2}H_2O$ (**2**)

Yellow diamond-shaped crystals of **1** were obtained by slow evaporation from a methanolic solution of **1**. The molecular structure and numbering scheme is illustrated in Fig. 3.4 and relevant bond lengths and angles are listed in Tables 3.4 and 3.5 (vanadium coordination geometry). The binuclear complex is centrosymmetric, being disposed about a crystallographic centre of inversion. Each VO_2^+ is coordinated by the tridentate BPB anion *via* the pyridyl-N1, azomethine-N2 and enolic-O1 atoms. The final position in the hexacoordinated geometry is completed by a bridging oxo-O2ⁱ atom [26]. The coordination geometry is based on an octahedron with one triangular face defined by three oxygen atoms, *i.e.* O1, O2 and O3, and the other by the N1, N2 and O2ⁱ atoms; the major distortions from the ideal geometry are ascribed to the acute chelate angles, Table 3.5.

Table 3.4. Selected bond lengths (Å) and bond angles (°) for HBPB and $[VO(BPB)(\mu_2-O)]_2$ (**1**).

	HBPB	1
C13–O1	1.2213(14)	1.300(3)
N2–N3	1.3682(15)	1.372(3)
N2–C6	1.2955(16)	1.291(3)
N3–C13	1.3610(16)	1.313(3)
O1–C13–N3	124.67(12)	124.3(2)
N3–N2–C6	117.38(10)	121.72(18)
N2–C6–C5	127.69(12)	112.6(2)
N2–C6–C7	114.35(10)	125.1(2)
N2–N3–C13	121.33(10)	107.09(17)
N3–C13–C14	112.84(10)	118.25(19)

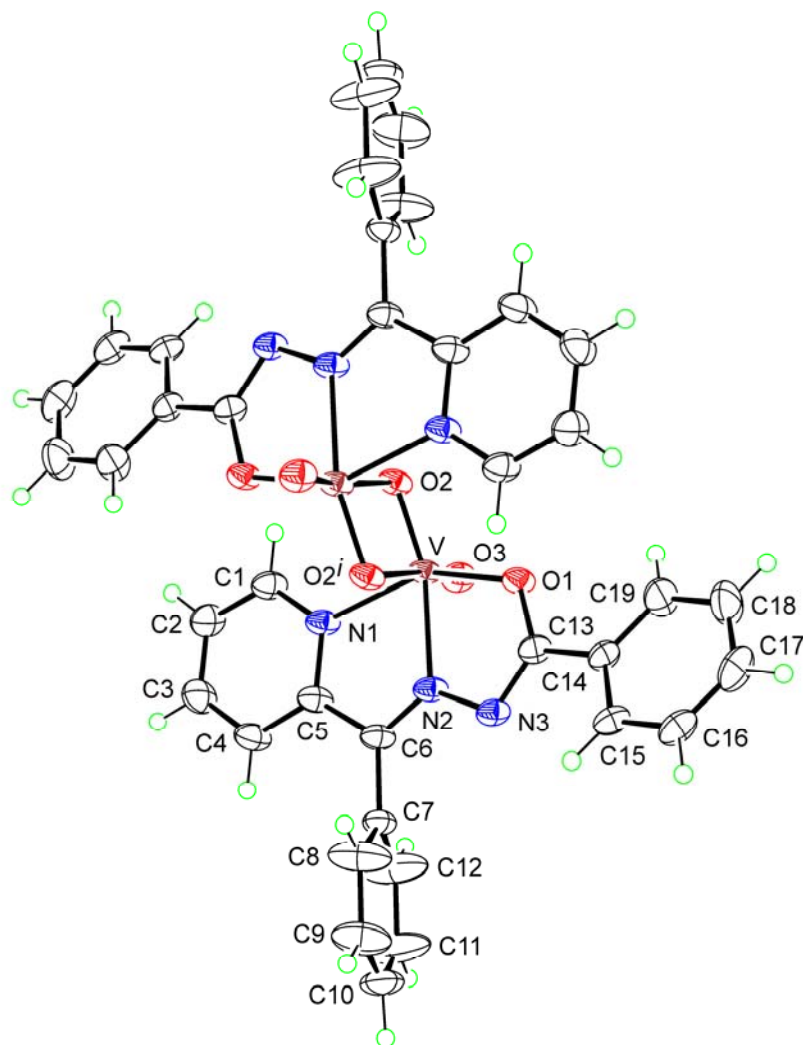


Fig. 3.4. The molecular structure of centrosymmetric $[\text{VO}(\text{BPB})(\mu_2\text{-O})]_2$ (**1**) along with the atom numbering scheme (Displacement ellipsoids are drawn at the 50% probability level and hydrogen atoms are shown as small spheres of arbitrary radii).

From the data collected in Table 3.4, it is evident that there is significant elongation of the C13–O1 bond distance with a concomitant reduction in the N3–C13 bond upon coordination of BPB. These changes indicate BPB is functioning

as an enolate ligand. The changes in bond distances are accompanied by some significant changes in the bond angles in BPB when the five-membered chelate rings are formed in the complex. Most notably, the N2–N3–C13 angle contracts by about 14° and the N2–C6–C7 angle widens by about 11°.

Selected bond distances and angles describing the vanadium atom geometry in **1** are summarized in Table 3.5. The V₂O₂ core is a parallelogram (1.66 x 2.35 Å) owing to the significant disparity of about 0.7 Å in the V–O₂ and V–O₂ⁱ bond distances; the terminal vanadyl-oxygen atoms, from symmetry, lie above and below this plane. The influence of the asymmetric bridging on the V=O bond distances is apparent so that the V–O₂ distance, i.e. involving the bridging–O₂ atom, of 1.6589(16) Å is longer than the V=O₃ distance of 1.6092(18) Å [27]. The disparity in the bridging distances is partly ascribed to the observation that the longer V–O₂ⁱ bond is *trans* to the terminal vanadyl–O₃ atom. The V–N1 bond distance of 2.110(2) Å is marginally shorter than the V–N2 bond distance of 2.1256(18) Å. The intramolecular V···V bond distance is 3.1463(7) Å, which falls within the range of known V···V distances in doubly-bridged vanadium polynuclear systems [28,29].

The molecular packing of **1** is shown in Fig. 3.5. The crystal structure of **1** is consolidated into a three-dimensional network by a C–H···O, C–H···N and π ··· π contacts. The unit cell is viewed along the *c* axis in which each molecule is stacked one above the other. The centroid Cg(2) is involved in π – π interaction with Cg(1) of the neighboring unit at a distance of 2.5928(10) Å which contribute stability to the unit cell packing as depicted in Table 3.6. However no significant C–H··· π interactions are found in the packing of this complex. Two weak intermolecular hydrogen bonding interactions are observed between C(16)–H(16) and O(2) and between C(17)–H(17) and N(3) with angles 135 and 155°. No classic hydrogen bonds are found in this complex.

Table 3.5. Selected bond lengths (Å) and bond angles (°) of [VO(BPB)(μ₂-O)]₂ (**1**) and [VO(DKN)(μ₂-O)]₂·½H₂O (**2**).

	1		2
V-01	1.9563(16)	V-01	1.9704(15)
V-02	1.6589(16)	V-03	1.6679(15)
V-02 ⁱ	2.3475(17)	V-03 ⁱ	2.3013(16)
V-03	1.6092(18)	V-02	1.6136(17)
V-N1	2.110(2)	V-N1	2.3013(16)
V-N2	2.1256(18)	V-N3	2.1298(18)
O2-V-O2 ⁱ	77.87(7)	O3-V-O3 ⁱ	77.91(7)
O2 ⁱ -V-O3	173.93(7)	O2-V-O3 ⁱ	175.08(8)
O1-V-N1	146.80(7)	O1-V-N1	146.97(7)
O1-V-N2	74.05(7)	O1-V-N3	74.72(6)
O2-V-N2	151.59(8)	O3-V-N3	152.32(7)
N1-V-N2	73.56(7)	N1-V-N3	72.92(7)
V-02-V ⁱ	102.13(7)	V-03-V ⁱ	102.09(7)

Table 3.6. H-bonding and π-π interaction parameters of the compound [VO(BPB)(μ₂-O)]₂ (**1**).

H-bonding				
D-H...A (Å)	D-H	H...A	D...A	D-H...A
C(16)-H(16)...O(2) ^a	0.95	2.55	3.286	135
C(17)-H(17)...N(3) ^b	0.95	2.56	3.447	155
π-π interactions				
Cg(I)...Cg(J)	Cg...Cg (Å)	α (°)	β (°)	
Cg(2)...Cg(1) ^c	2.5928	86.66	54.19	

Equivalent position codes

a = ½+x, ½-y, -½+z; b = ½-x, ½+y, ¾-z, c = x, y, z

Cg(2) = V(1), O(1), C(13), N(3), N(2); Cg(1) = V(1), O(2), V(1a), O(2a)

D, donor; A, acceptor; Cg, centroid; α, dihedral angles between planes I and J; β, angle Cg(I) – Cg(J) vector normal to plane I

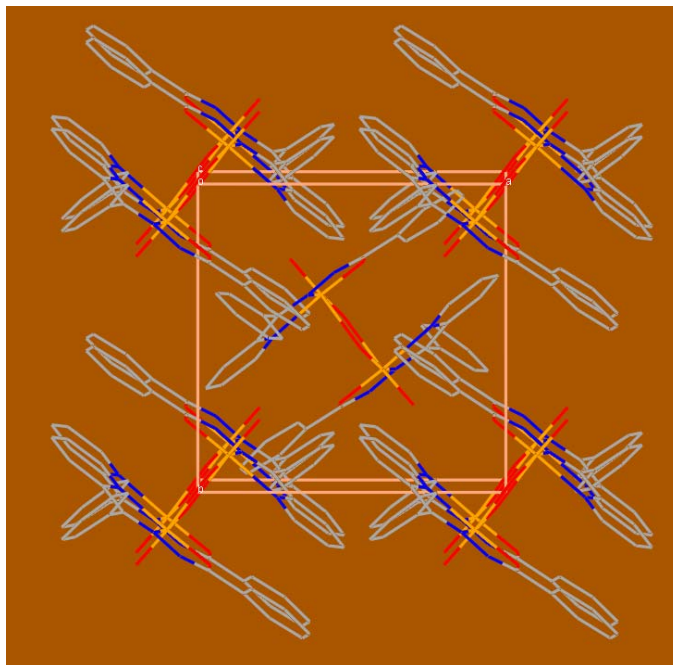


Fig. 3.5. Packing diagram of complex **1** viewed along crystallographic 'c' axis.

To a first approximation, the molecular structure of the complex $[\text{VO}(\text{DKN})(\mu_2\text{-O})_2] \cdot \frac{1}{2}\text{H}_2\text{O}$ (**2**) resembles that just described (Fig. 3.6 and Table 3.5.) In this case, the pyridine-N1 atom forms a significantly longer V–N1 bond, i.e. 2.3013(16) Å, compared with the V–N3 bond, i.e. 2.1298(18) Å, formed by the azomethine-nitrogen atom. Significant differences in the V–O bond distances are also evident between **1** and **2**. Thus, in **2**, each of V–O1, V–O2 and V–O3 are shorter but the bridging V–O3ⁱ distance is longer. It is noted that with the exception of the elongation of the C5–C6 bond distance in **2** to 1.485(3) Å, compared with 1.460(3) Å in **1**, the bond distances defining the N1–C2–N2–C12–O1 backbones of the tridentate ligands in each of **1** and **2** are indistinguishable. In the absence of any obvious electronic influence exerted by the pendant pyridine residue in **2**, compared to phenyl in **1**, this reorganization of electron density giving rise to disparate bond distances in the structures is ascribed to participation of solvent water in the (supramolecular) structure of **2**, see Fig. 3.7.

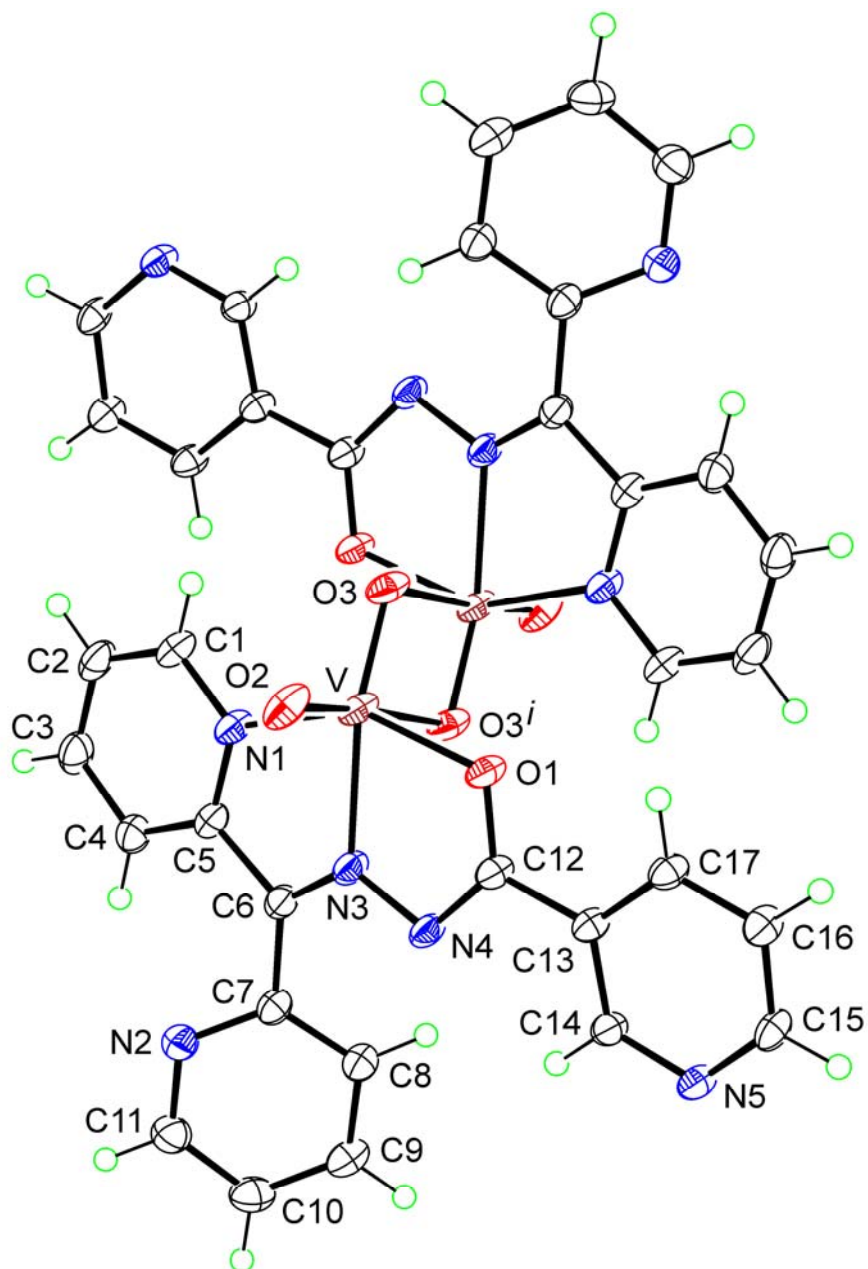
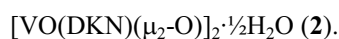


Fig. 3.6. The molecular structure of centrosymmetric $[\text{VO}(\text{DKN})(\mu_2\text{-O})]_2 \cdot \frac{1}{2}\text{H}_2\text{O}$ (**2**) along with the atom numbering scheme. The solvent water molecule has been omitted for reasons of clarity (Displacement ellipsoids are drawn at the 50% probability level and hydrogen atoms are shown as small spheres of arbitrary radii).

The intervention of solvent water in the crystal structure of **2**, Fig. 3.7, leads to the formation of a supramolecular chain along the *c*-direction. While the solvent water molecule is only partially occupied and disordered across a centre of inversion, see Experimental, it forms significant alternating O···O interactions of 2.834(9) and 3.2923(9) Å with the vanadyl-O2 atom, Fig. 3.7. Chains are consolidated into the crystal structure by a large number of C–H···O, C–H···N and π ··· π contacts (Table 3.7).

Table 3.7. H-bonding, π - π and C–H··· π interaction parameters of



H-bonding				
D–H···A	D–H	H···A	D···A	D–H···A
C9–H(9)···O(2) ^a	0.95	2.35	3.2933	172
C1–H(1)···N(5) ^b	0.95	2.53	3.3313	143
C16–H(16)···O(3) ^c	0.95	2.41	3.0503	125
C3–H(3)···O(2) ^d	0.95	2.57	3.1873	123
π - π interactions				
Cg(I)···Cg(J)	Cg···Cg (Å)	α (°)	β (°)	
Cg(3)···Cg(1) ^e	2.6151	85.80	55.35	
C–H··· π interaction				
X–H(I)···Cg(J)		Y–X···Cg (°)	X···Cg (Å)	
O(4)b–O(4)···Cg(3) ^f		81.24	3.3779	
Equivalent position codes				
a = x, 1+y, z, b = 1+x, -1+y, z, c = -x, -y, 2-z, d = 1+x, y, z, e = 1-x, -y, 2-z, f = 1-x, -x, 1-z				
Cg(1) = V, O(3), V(a), O(3a); Cg(3) = V, N(1), C(5), C(6), N(3)				

D, donor; A, acceptor; Cg, centroid; α , dihedral angles between planes I and J; β , angle Cg(I) – Cg(J) vector normal to plane I

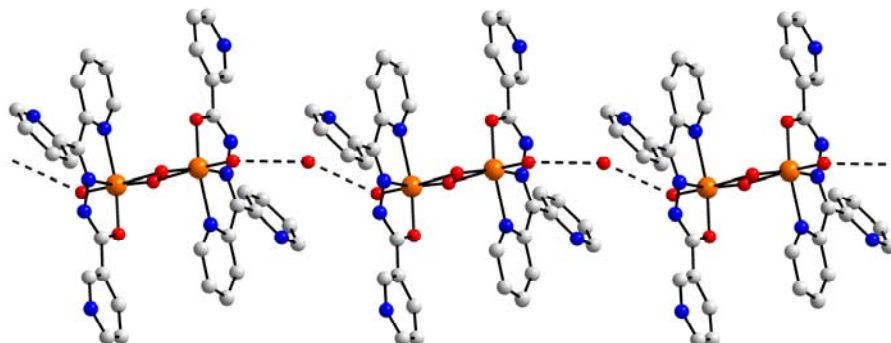


Fig. 3.7. Supramolecular chain mediated by $-O\cdots H-O-H\cdots O-$ hydrogen bonding (black dashed lines) in **2**. Hydrogen atoms have been omitted for clarity.

References

- [1] M. Hiroma, Y. Adachi, M. Machida, M. Hattori, H. Sakurai, *Metallomics*, 1 (2009) 92.
- [2] S. Bunce, R.J. Cross, L.J. Farrugia, S. Kunchandy, L.L. Meason, K.W. Muir, M.O. Donnell, R.D. Peacock, D. Stirling, S.J. Teat, *Polyhedron* 17 (1998) 4179.
- [3] D.C. Trans, Y. Yang, T. Jakusch, T. Kiss, *Inorg. Chem.* 39 (2000) 4409.
- [4] P. Noblia, E.J. Baran, L. Otero, P. Draper, H. Cerecetto, M. Gonzalez, O.E. Piro, E.E. Castellano, T. Inohara, Y. Adachi, H. Sakurai, D. Gambino, *Eur. J. Inorg. Chem.* (2004) 322.
- [5] E.B. Seena, N. Mathew, M. Kuriakose, M.R.P. Kurup, *Polyhedron* 27 (2008) 1455.
- [6] Y. Dong, R.K. Narla, E. Sudbeck, F.M. Uckun, *J. Inorg. Biochem.* 78 (2000) 321.
- [7] A. Ray, S. Banerjee, S. Sen, R.J. Butcher, G.M. Rosair, M.T. Garland, S. Mitra, *Struct. Chem.* 19 (2008) 209.

- [8] A.A.R. Despaigne, J.G. Da Sila, A.C.M. do Carmo, O.E. Piro, E.E. Castellano, H. Beraldo, *Inorg. Chim. Acta* 362 (2009) 2117.
- [9] A. Syamal, K.S. Kale, *Ind. J. Chem.* 16A (1978) 46.
- [10] S. Naskar, D. Mishra, R.J. Butcher, S.K. Chattopadhyay, *Polyhedron* 26 (2007) 3703.
- [11] S.N. Rao, D.D. Mishra, R.C. Maurya, N.N. Rao, *Polyhedron* 16 (1996) 1825.
- [12] P.F. Raphael, E. Manoj, M.R.P. Kurup, *Polyhedron* 26 (2007) 5088.
- [13] N.A. Mangalam, M.R.P. Kurup, *Spectrochim. Acta Part A* 71 (2009) 2040.
- [14] T. Ghosh, S. Bhattacharya, A. Das, G. Mukherjee, M.G.B. Drew, *Inorg. Chim. Acta* 358 (2005) 989.
- [15] M. Kuriakose, M.R.P. Kurup, E. Suresh, *Polyhedron* 26 (2007) 2713.
- [16] R. Dinda, P. Sengupta, S. Ghosh, T.C.W. Mak, *Inorg. Chem.* 41 (2002) 1684.
- [17] R.C. Maurya, S. Rajput, *J. Mol. Struct.* 833 (2007) 133.
- [18] D.U. Ward, C.D. Satish, V.H. Kulkarni, C.S. Bajpur, *Ind. J. Chem.* 39A (2000) 415.
- [19] CrysAlis CCD and CrysAlis RED Versions 1.171.29.2 (CrysAlis 171.NET), Oxford Diffraction Ltd, Abingdon, Oxfordshire, England, 2006.
- [20] G.M. Sheldrick, *Acta Crystallogr. A* 64 (2008) 211.
- [21] T. Higashi, ABSCOR. Rigaku Corporation, Tokyo, Japan (1995).
- [22] CrystalClear User Manual. Rigaku/MSI Inc., Rigaku Corporation, The Woodlands, TX (2005).
- [23] L.J. Farrugia, *J. Appl. Cryst.* 30 (1997) 565.

- [24] C.F. Macrac, P.R. Edington, P. McCabe, E. Pidcock, G.P. Shields, R. Taylor, M. Towler, J. Van de Streek, *J. Appl. Cryst.* 39 (2006) 453.
- [25] K. Brandenburg, DIAMOND. Visual Crystal Structure Information System, Version 3.1, CRYSTAL IMPACT, Postfach 1251, D- 53002 Bonn, Germany 2006.
- [26] S. Rayati, A. Wojtczak, A. Kozakiewicz, *Inorg. Chim. Acta* 361 (2008) 1530.
- [27] B. Mondal, M.G.B. Drew, R. Banerjee, T. Ghosh, *Polyhedron* 27 (2008) 3197.
- [28] A. Sreekanth, H.-K. Fun, M.R.P. Kurup, *J. Mol. Struct.* 737 (2005) 61.
- [29] C. Tsiamis, B. Voulgaropoulos, D. Charistos, G.P. Voutsas, C.A. Kavounis, *Polyhedron* 19 (2000) 2003.

Chapter 4

Syntheses, spectral and structural characterization of manganese(II) complexes incorporating tridentate acylhydrazones

Contents

- 4.1 Introduction
 - 4.2 Experimental
 - 4.3 Results and discussion
 - References
-

4.1. Introduction

Manganese, with seven valence electrons, shows the widest variety of oxidation states in the first transition series. A number of metalloproteins containing manganese are known and their active sites have been increasingly identified. Many of the manganese-protein compounds are enzymes dealing with the control of dioxygen species in the organism especially in protecting against damage by peroxide or superoxide radicals. Human superoxide dismutase has been shown to contain four separate Mn atoms, each in an identical protein subunit. Among the larger units is the active site in “photosystem II” which is involved in the oxidation of H₂O to O₂ driven by visible light. Manganese and its compounds find very historical importance in medicine and play a significant role in enzyme activation. It is well known that Mn plays an important role in many

biological redox processes including disproportionation of H_2O_2 (catalase activity) [1] in microorganisms, decomposition of O_2^- radicals catalyzed by superoxide dismutases (SODs) and water oxidation by photosynthetic enzymes (photosystem II) [2,3]. In contrast to all oxidation states, Mn(II) is very stable and widely represented. It is in the d^5 state and all the compounds contain five unpaired electrons.

Manganese is involved in essential processes of life such as photosynthesis, synthesis of DNA or the urea cycle. High spin mononuclear Mn(II) complexes are largely investigated since they are of importance in several fields such as material chemistry, catalysis or biochemistry [4-6]. The Mn(II) ion is often used as a building element in nanomagnets as well as for the development of catalysts especially for oxidation reactions [7]. Mononuclear Mn(II) complexes are also found in a number of metalloenzymes as active sites. The reactivity of the Mn(II) complexes is correlated with their geometry and thus their electronic structure.

4.2. Experimental

4.2.1. Materials

2-Benzoylpyridine (Aldrich), di-2-pyridyl ketone (Aldrich), benzhydrazide (Aldrich), and nicotinic hydrazide (Aldrich), manganese(II) acetate tetrahydrate (E-Merck) were used as received. Solvents were purified by standard procedures before use.

4.2.2. Syntheses of the acylhydrazones

The syntheses of hydrazones HBPB and HDKN are discussed already in Chapter 2.

4.2.3. Syntheses of the complexes

4.2.3.1. Synthesis of $[Mn(BPB)_2]$ (3)

To a solution of the acylhydrazone HBPB (0.301 g, 1 mmol) in methanol one drop of triethylamine was added. To this, methanolic solution of $Mn(CH_3COO)_2 \cdot 4H_2O$ (0.245 g, 1 mmol) was added and the reaction mixture was refluxed for 4 h. The resulting solution was allowed to stand at room temperature and after slow evaporation, brown crystalline product was separated, filtered and washed with ether and dried over P_4O_{10} *in vacuo*.

$[Mn(BPB)_2]$ (3): Yield: 85%, λ_m (DMF): 4 $ohm^{-1}cm^2 mol^{-1}$, μ_{eff} (B.M.): 5.48, Elemental Anal. Found (Calcd.) (%): C: 69.56 (69.62), H: 4.22 (4.30), N: 12.48 (12.82), Mn: 8.93 (8.38).

4.2.3.2. Synthesis of $[Mn(DKN)_2]$ (4)

To a methanolic solution of HDKN (0.312 g, 1 mmol), one drop of triethylamine was added. To this, $Mn(CH_3COO)_2 \cdot 4H_2O$ (0.245 g, 1 mmol) in methanol was added and the reaction mixture was refluxed for 4 h. The resulting solution was allowed to stand at room temperature and after slow evaporation, brown crystalline product was separated, filtered and washed with ether and dried over P_4O_{10} *in vacuo*.

$[Mn(DKN)_2]$ (4): Yield: 75%, λ_m (DMF): 7 $ohm^{-1}cm^2 mol^{-1}$, μ_{eff} (B.M.): 5.73, Elemental Anal. Found (Calcd.) (%): C: 61.65 (61.91), H: 3.61 (3.67), N: 20.94 (21.24), Mn: 8.21 (8.33).

4.3. Results and discussion

4.3.1. Elemental analyses

The analytical data indicate that the observed C, H, N values of the complexes were in close agreement with that of the formula suggested. The metal content % of the complexes was determined by AAS after digestion with con. HNO₃ and was found to be consistent with that of the theoretical results.

4.3.2. Molar conductivity and magnetic susceptibility measurements

The molar conductances of the complexes in DMF (10⁻³ M) solutions were measured at 298 K with a Systronic model 303 direct-reading conductivity bridge. Molar conductivity data reveal that the complexes are non-electrolytes, in accordance with the proposed formulations [8]. Magnetic measurements were recorded at room temperature using diamagnetic corrections for the complexes and their effective magnetic moment (μ_{eff}) values are given in Section 4.2.3. The magnetic moment of the Mn(II) complexes was found to be 5.48 and 5.73 B.M. for **3** and **4** respectively which are indicative of a high spin d^5 system [9].

4.3.3. Infrared spectra

The main stretching frequencies of the IR spectra of the hydrazones and complexes together with their tentative assignments are tabulated in Table 4.1. Comparing the IR spectra of the hydrazone HBPB with that of the complex **3**, we observed that $\nu(\text{N-H})$ and $\nu(\text{C=O})$ stretching vibrations of the hydrazone disappeared in the IR spectra of its complex (Fig. 4.1), which showed that the frame H-N-C=O has transformed to N=C-O-H form coordinating to metal (Mn) in enolate form [10]. Additionally a new C-O absorption band appeared at 1348 cm⁻¹ in [Mn(BPB)₂]. The $\nu(\text{C=N})$ stretching bands are strongly affected by chelation and are shifted to lower wavenumbers which is attributed to the conjugation of the *p*-orbital on the double bond with the *d*-orbital on the metal ion

with the reduction of the force constant [11]. This supports the participation of imine group of the hydrazone in binding to the metal ion. The appearance of a new band due to the new $\nu(\text{C}=\text{N})$ formed as a result of enolization of the ligands at 1583 cm^{-1} may be taken as additional evidence for the participation of the imine nitrogen in coordination [12]. The low energy pyridine ring out-of-plane vibrations observed in the spectrum of the hydrazone at $\sim 650\text{ cm}^{-1}$ is shifted to higher frequencies in the case of complex, which is a good indication of the coordination of the heterocyclic nitrogen atom. The ligand coordination is substantiated by two bands appearing at 481 and 439 cm^{-1} for the complex $[\text{Mn}(\text{BPB})_2]$; these are mainly attributed to $\nu(\text{M}-\text{N})$ and $\nu(\text{M}-\text{O})$ bands respectively.

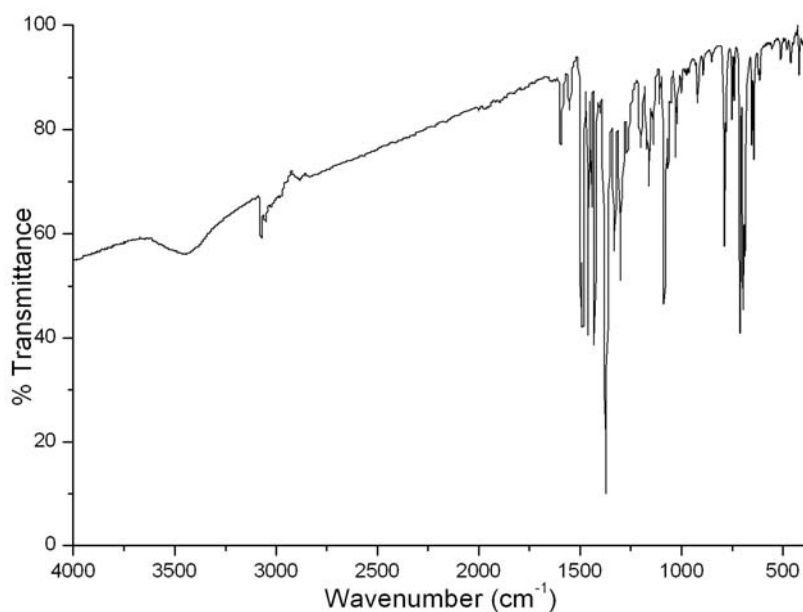


Fig. 4.1. IR spectrum of $[\text{Mn}(\text{BPB})_2]$ (3).

For complex **4**, the $\nu(\text{C}=\text{N})$ stretching band is shifted to 1538 cm^{-1} , which gives an evidence for the coordination of hydrazone through imine nitrogen. Also

the appearance of a new band at 1582 cm^{-1} due to the new $\nu(\text{C}=\text{N})$ formed as a result of enolization is an additional evidence for the participation of imine nitrogen in coordination. From the above observations it was found that in both the complexes the hydrazones coordinate through imine and pyridyl nitrogens and enolate oxygen and was established by their crystal structures.

Table 4.1. Infrared spectral data (cm^{-1}) of the manganese(II) complexes.

Compound	$\nu(\text{N-H})$	$\nu(\text{C=O})$ / $\nu(\text{C-O})$	$\nu(\text{C=N})$	$\nu(\text{C=N})^a$	$\nu(\text{Mn-N}_{\text{azo}})$	$\nu(\text{Mn-O})$
HBPB	3063	1678	1571
[Mn(BPB) ₂] (3)	...	1348	1520	1583	481	439
HDKN	2928	1689	1579
[Mn(DKN) ₂] (4)	...	1361	1538	1582	485	447

^a Newly formed C=N

4.3.4. Electronic spectra

The absorption bands of the complexes were recorded in acetonitrile solution and the spectral data are given in Table 4.2. The ground state of high-spin octahedral Mn(II) complex is ${}^6\text{A}_{1g}$ and as there are no excited terms of sextet spin multiplicity, $d-d$ transitions are doubly forbidden. However, some forbidden transitions occur and consequently, these transitions have an extremely low molar extinction coefficient value. The electronic spectra of the manganese(II) complexes exhibit four weak intensity absorption bands in the ranges 17280-18950; 23,923-28380; 28450-28980; 31055-31600 cm^{-1} , which may be assigned to the transitions: ${}^4\text{T}_{1g} ({}^4\text{G}) \leftarrow {}^6\text{A}_{1g}$, ${}^4\text{A}_{1g} ({}^4\text{G})$, ${}^4\text{E}_g \leftarrow {}^6\text{A}_{1g}$, ${}^4\text{E}_g ({}^4\text{D}) \leftarrow {}^6\text{A}_{1g}$, ${}^4\text{T}_{1g} ({}^4\text{P}) \leftarrow {}^6\text{A}_{1g}$ respectively. For octahedral Mn(II) complexes, electronic spectra normally show two bands *ca.* 18000 and 20000 cm^{-1} , which are assigned to ${}^4\text{T}_{1g} (\text{G}) \leftarrow {}^6\text{A}_{1g}$ and ${}^4\text{T}_{2g} (\text{G}) \leftarrow {}^6\text{A}_{1g}$ respectively (Fig. 4.2) [13,14]. But the high

intense charge transition tailing into the visible region, obscure the very weak *d-d* absorptions of the Mn(II) complexes.

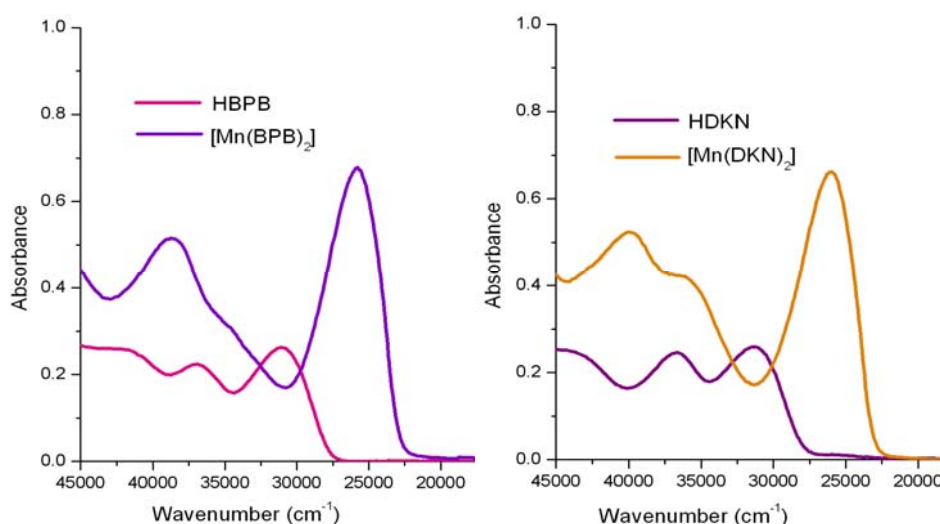


Fig. 4.2. Electronic spectra of the complexes [Mn(BPB)₂] (**3**) (left) and [Mn(DKN)₂] (**4**) (right) in the region 45,000-20,000 cm⁻¹.

Table 4.2. Electronic spectral data of the Mn(II) complexes.

Compound	UV-vis absorption bands (cm ⁻¹)
[Mn(BPB) ₂] (3)	38760, 35460(sh), 25770, 14080
[Mn(DKN) ₂] (4)	40160, 35970 (sh), 26110

4.3.5. Cyclic voltammetric studies

Electrochemical properties of complexes **3** and **4** were studied in DMF medium with tetrabutylammonium phosphate as supporting electrolyte at a scan rate of 100 mV s⁻¹ with platinum wires as working and counter electrodes and Ag/Ag⁺ as a reference electrode. The obtained data from the electrochemical properties of the metal complexes are given in Table 4.3. Complex **3** shows (Fig. 4.3) an oxidative response at 1.03 V *versus* SCE, which is assigned to the Mn(II) to Mn(III) oxidation, and a reductive response at -0.23 V *versus* SCE, assigned to

Mn(III) to Mn(II) change [15] and the process is thus reversible. The voltammogram of **4** (Fig. 4.3) shows a peak at 0.55 V which can be attributed to the oxidation of Mn(II) to Mn(III). Another peak at -1.20 V was assigned to the reduction of Mn(III) to Mn(II) and this process is also reversible.

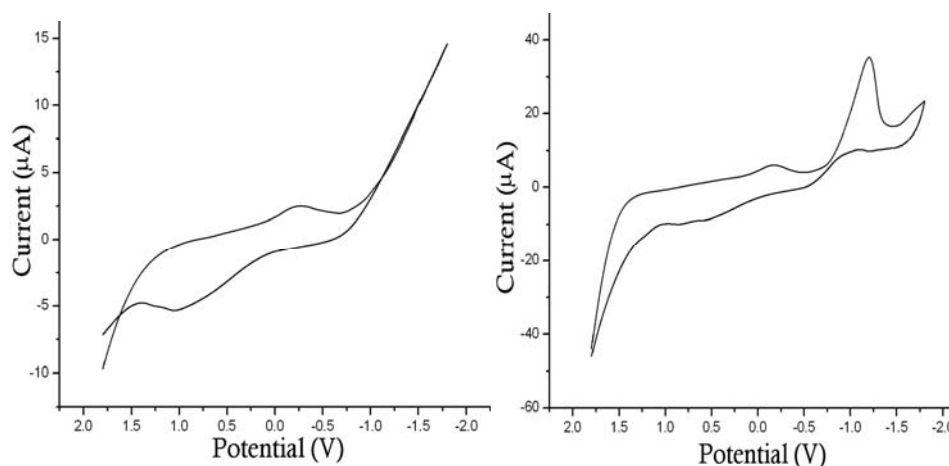


Fig. 4.3. Cyclic voltammograms of Mn(BPB)₂ (**3**) (left) and [Mn(DKN)₂] (**4**) (right) in DMF.

Table 4.3. Electrochemical data of the Mn(II) complexes in DMF.

Compound	E _{pc} (V)	E _{pa} (V)	I _{pc} (μA)	I _{pa} (μA)
[Mn(BPB) ₂] (3)	-0.23	1.03	2.47	-5.37
[Mn(DKN) ₂] (4)	-1.20	0.55	35.04	-9.05

4.3.6. Electron paramagnetic resonance spectra

The electron spin properties of manganese have long been of interest as a spectroscopic probe of manganese centers in manganese proteins and as a spectroscopically active surrogate for other divalent metal ions. The Mn(II) oxidation state possesses Kramers' ground-state doublets and exhibits characteristic spin transitions in the normal mode X-band regime. Its electronic properties are described by the following spin Hamiltonian:

$$\hat{H} = g\beta BS + IAS + D \left[S_z^2 - \frac{S(S+1)}{3} \right] + E(S_x^2 - S_y^2)$$

where B is the magnetic field vector, g is the spectroscopic splitting factor, β is the Bohr magneton, D is the axial zero field splitting parameter, E is rhombic zero field splitting parameter and S is the electron spin vector. The first two terms represent the electronic Zeeman and the electron nuclear hyperfine interactions respectively, whereas the last two terms define the zero-field splitting interaction with D and E gauging the axial and the rhombic parts.

Mn^{2+} (d^5) being an odd electron system, the zero-field splitting produces three doubly degenerate spin states $M_s = \pm 5/2, \pm 3/2, \pm 1/2$ (Kramers' degeneracy). Each of these is split into two singlets by the applied field, producing six levels. As a result of this splitting, five transitions ($-5/2 \rightarrow -3/2, -3/2 \rightarrow -1/2, -1/2 \rightarrow 1/2, 1/2 \rightarrow 3/2, 3/2 \rightarrow 5/2$) are expected. But in practice usually only one signal is observed since they are of equal energy [16]. The spectrum will further be split by the nuclear hyperfine interaction with the ^{55}Mn nucleus ($I = 5/2$) which would give rise to thirty peaks in the spectrum.

The observed g values from the EPR spectra are summarized in the Table 4.4. In polycrystalline state at 298 K, EPR spectrum of $[Mn(BPB)_2]$ gave two broad signals with g values ; $g_1 = 2.091$ having a peak to peak separation of 62 mT and $g_2 = 4.999$ (Fig. 4.4). However when recorded in frozen DMF at 77 K, the spectrum displayed two signals with g values; $g_1 = 2.091$ and $g_2 = 4.999$ in which one signal showed hyperfine sextet with hyperfine coupling constant 7.7 mT (Fig. 4.5). In addition to this, a pair of low intensity lines is found in between each of the two main hyperfine levels. These are the forbidden lines which arise due to the mixing of the nuclear hyperfine levels with the zero field splitting factor of the Hamiltonian (D and E).

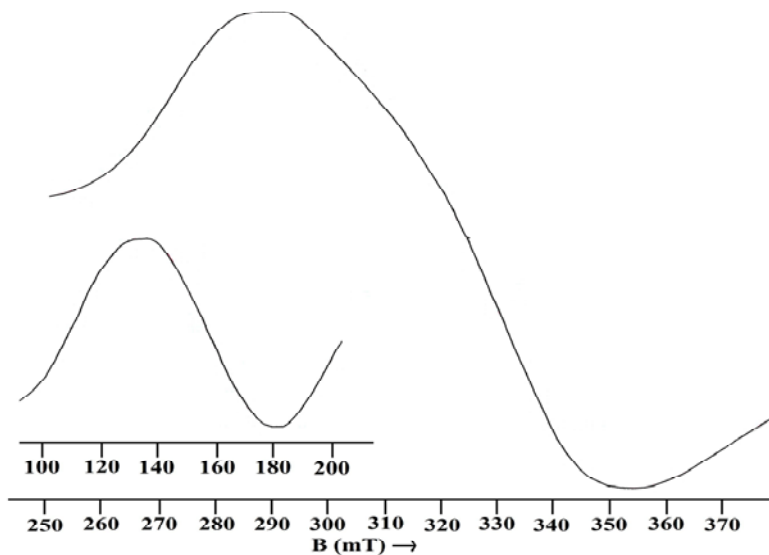


Fig. 4.4. EPR spectrum of $[\text{Mn}(\text{BPB})_2]$ (**3**) in polycrystalline state at 298 K.

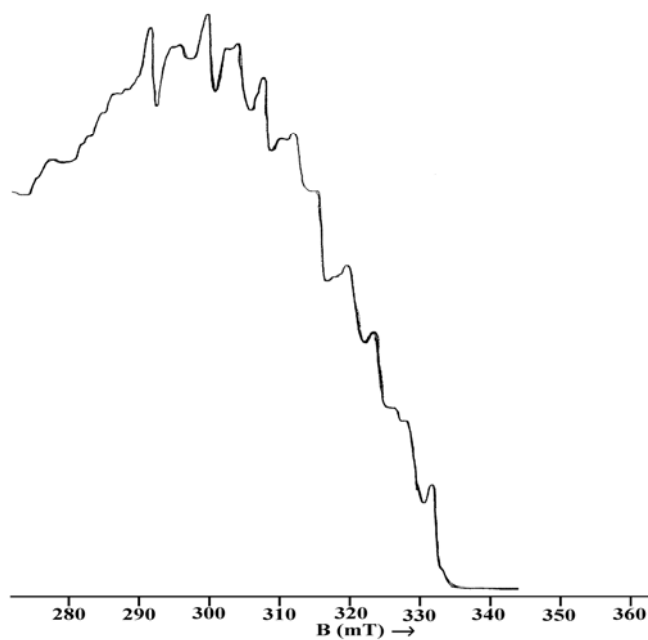


Fig. 4.5. EPR spectrum of $[\text{Mn}(\text{BPB})_2]$ (**3**) in frozen DMF at 77 K.

EPR spectrum of $[\text{Mn}(\text{DKN})_2]$ in polycrystalline state at 298 K gave a broad signal with $g = 2.083$ (peak to peak separation is 84 mT) without any

resolved hyperfine splitting (Fig. 4.6). The broadness of the spectrum may be due to immobilization of Mn(II) ion in the complex or may be due to dipolar interactions and enhanced spin lattice relaxation. The frozen solution spectrum of **4** in DMF at 77 K was simulated using EasySpin [17] (Fig. 4.7) and a hyperfine sextet was observed arising due to the hyperfine interaction between the unpaired electron with the ^{55}Mn nucleus ($I = 5/2$) with hyperfine coupling constant 9.3 mT. The observed g value is very close to the free electron spin value of 2.0023 which is consistent with the typical Mn(II) and also suggestive of the absence of spin orbit coupling in the ground state ${}^6A_{1g}$ without another sextet term of higher energy. The forbidden lines with an average spacing of ~ 2.5 mT corresponds to $\Delta m_l = \pm 1$ transitions arises due to the mixing of the nuclear hyperfine levels with the zero field splitting factor of the Hamiltonian (D and E) in between each of the two main hyperfine levels [18-20]. Axial splitting factor D and the rhombic splitting factor E were calculated for the complex **4** and E/D ratio of this complex is consistent with the reported values of distorted octahedral Mn(II) complexes [21].

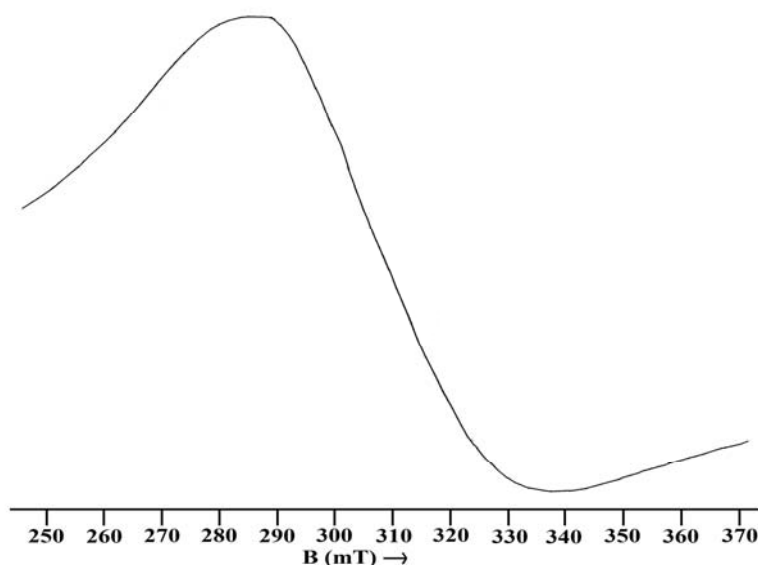


Fig. 4.6. EPR spectrum of $[\text{Mn}(\text{DKN})_2]$ (**4**) in polycrystalline state at 298 K.

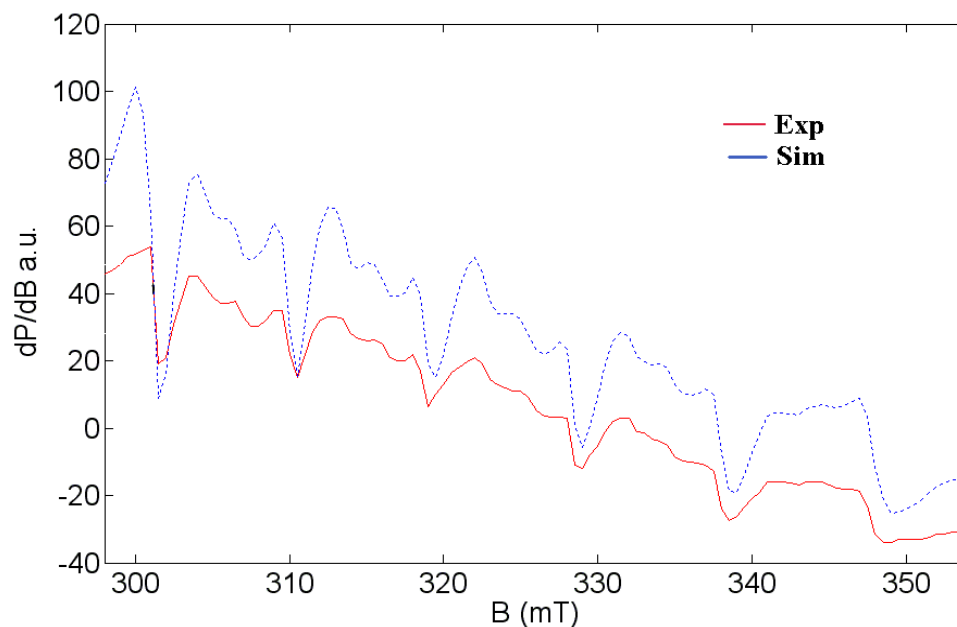


Fig. 4.7. EPR spectrum of [Mn(DKN)₂] (**4**) in frozen DMF at 77 K.

Table 4.4. EPR data for the complexes.

Compound	<i>g</i> values		<i>D</i> (MHz)	<i>E</i> (MHz)	<i>E/D</i>
	Polycrystalline at 298 K	DMF at 77 K			
[Mn(BPB) ₂] (3)	2.091, 4.999	2.091, 4.999	---	---	---
[Mn(DKN) ₂] (4)	2.083	2.001	420	120	0.285

4.3.7. X-ray crystallography

Small brown needle crystals of **3** (0.20x0.20x0.30 mm³) were obtained by slow evaporation from a methanol-acetonitrile solution and the X-ray diffraction data were collected on a Bruker axis kappa apex2 CCD Diffractometer with graphite monochromated Mo K α radiation ($\lambda = 0.71073 \text{ \AA}$) at 293 K. The APEX2/SAINT and SAINT/XPREP softwares were used for cell refinement and data reduction respectively. The structure was solved using SIR92 by direct method and refinement were carried out by the full matrix least squares method

on F^2 using SHELXL-97. All non-hydrogen atoms were refined with anisotropic displacement parameters and the hydrogen atoms were placed at calculated positions and refined as riding atoms using isotropic displacement parameters.

Intensity data for a brown block shaped crystal of $[\text{Mn}(\text{DKN})_2]$ ($0.10 \times 0.22 \times 0.32 \text{ mm}^3$) grown from methanolic solution was collected on a Bruker P4 X-ray diffractometer using graphite monochromated Mo $K\alpha$ radiation ($\lambda = 0.71073 \text{ \AA}$) at 150 K. The data were solved using SHELXS-97 [22] by direct method and each refinement was carried out by full-matrix least-squares on F^2 (SHELXL-97) with anisotropic displacement parameters for non-hydrogen atoms. The Bruker SAINT software was used for data reduction and Bruker SMART for cell refinement.

Crystal data and refinement details are given in Table 4.5 and molecular structures of the compounds (Figs. 4.8, 4.10) were drawn using the program DIAMOND Version 3.1f [23] with 50% displacement ellipsoids, and the remaining crystallographic figures (Figs. 4.9, 4.11) were drawn with MERCURY [24].

4.3.7.1. Crystal structures of $[\text{Mn}(\text{BPB})_2]$ (**3**) and $[\text{Mn}(\text{DKN})_2]$ (**4**)

A perspective view of **3** along with the atom numbering scheme is depicted in Fig. 4.8 and the bond dimensions are listed in Table 4.6. The manganese atom in $[\text{Mn}(\text{BPB})_2]$ is coordinated in a distorted octahedral configuration in a *trans*-N(2,5)-*cis*-N(1,4)-*cis*-O(1,2) configuration. The coordinated ligands form two five membered chelate rings, imposing large distortions on the ideally octahedral coordinate angles. The *trans* angle N2–Mn1–N5 is much farther from 180° , $164.16(5)^\circ$ in **3** compared with similar Cu (178.03°) and Zn (175.23°) complexes, [25] whereas the *trans* N1–Mn1–O1 ($142.04(5)^\circ$) and N4–Mn1–O2 ($143.07(5)^\circ$) angles defined by each meridionally coordinated ligand also deviate markedly from linearity.

Table 4.5. Crystal data and structure refinement parameters for complexes **3** and **4**.

Parameters	[Mn(BPB) ₂] (3)	[Mn(DKN) ₂] (4)
Empirical Formula	C ₃₈ H ₂₈ MnN ₆ O ₂	C ₃₄ H ₂₄ MnN ₁₀ O ₂
Formula weight (M)	655.60	659.57
Temperature (T) K	293(2)	150
Wavelength (Mo K α) (Å)	0.71073	0.71073
Crystal system	triclinic	monoclinic
Space group	<i>P</i> -1	<i>P</i> 2 ₁
Lattice constants		
<i>a</i> (Å)	10.4629(3)	9.5069(7)
<i>c</i> (Å)	12.6639(4)	10.1525(7)
<i>b</i> (Å)	13.2640(4)	16.6511(10)
α (°)	65.9150(10)	90.00
β (°)	84.4190(10)	100.390(7)
γ (°)	84.9730(10)	90.00
Volume <i>V</i> (Å ³)	1594.66(8)	1580.79(19)
<i>Z</i>	2	2
Calculated density (ρ) (Mg m ⁻³)	1.365	1.386
Absorption coefficient μ (mm ⁻¹)	0.459	0.466
Limiting Indices	-15 ≤ <i>h</i> ≤ 15 -18 ≤ <i>k</i> ≤ 18 -19 ≤ <i>l</i> ≤ 19	-11 ≤ <i>h</i> ≤ 11 -11 ≤ <i>k</i> ≤ 11 -19 ≤ <i>l</i> ≤ 19
Reflections collected	44066 [R(int) = 0.0398]	11389 [R(int) = 0.0240]
Unique Reflections	10915	5359
Refinement method	Full-matrix least-squares on <i>F</i> ²	Full-matrix least-squares on <i>F</i> ²
Data / restraints / parameters	10915 / 0 / 425	5359/1/425
Goodness-of-fit on <i>F</i> ²	0.998	1.046
Final <i>R</i> indices [<i>I</i> > 2 σ (<i>I</i>)]	<i>R</i> ₁ = 0.0479, <i>wR</i> ₂ = 0.1207	<i>R</i> ₁ = 0.0438, <i>wR</i> ₂ = 0.1243
<i>R</i> indices (all data)	<i>R</i> ₁ = 0.1092, <i>wR</i> ₂ = 0.1571	<i>R</i> ₁ = 0.0514, <i>wR</i> ₂ = 0.1277

$$wR_2 = [\sum w(F_o^2 - F_c^2)^2 / \sum w(F_o^2)^2]^{1/2}; R_1 = \sum ||F_o| - |F_c|| / \sum |F_o|$$

The intraligand bite angles are correspondingly more acute at 71.49° in **3** when compared to other metal complexes reported with similar ligands. As the coordinate bonds become longer, the inflexible ligand maintains the same conformation, leading to the contraction of the coordinate angles. The crystal structure of HBPB was discussed in the second chapter and although the C6–N2 and N2–N3 bond lengths are less affected by the complexation [*ca.* 1.287 and 1.369 Å in complex compared with 1.295 and 1.368 Å in free ligand respectively], the C13–O1 bond lengthens significantly (by *ca.* 0.04 Å). Relevant bond length and bond angles of HBPB are tabulated in Table 4.6. Overall, these observations are consistent with the enolate resonance form of the hydrazone being dominant in the deprotonated coordinated ligand, and this is supported by the IR spectral data. Both bicyclic chelate rings are close to being perpendicular to each other with a dihedral angle of 86.24° between them. The M–N_(pyridine), M–N_(imine) and M–O bond lengths observed here are within the range reported for other similar complexes of divalent metal ions [26,27].

Table 4.6. Selected bond lengths (Å) and bond angles (°) for HBPB, complexes **3** and **4**.

	HBPB	[Mn(BPB) ₂] (3)	[Mn(DKN) ₂] (4)
<i>Bond lengths</i>	<i>Bond lengths</i>	<i>Bond lengths</i>	<i>Bond lengths</i>
Mn1–N2	-----	2.190(2)	Mn1–N3 2.204(3)
Mn1–N5	-----	2.194(2)	Mn1–N8 2.195(3)
Mn1–O1	-----	2.120(1)	Mn1–O1 2.133(3)
Mn1–O2	-----	2.096(1)	Mn1–O2 2.125(3)
Mn1–N1	-----	2.287(2)	Mn1–N1 2.313(3)
Mn1–N4	-----	2.284(2)	Mn1–N6 2.268(3)
N2–N3	1.3682(2)	1.369(2)	N3–N4 1.375(4)
N5–N6	-----	1.370(2)	N8–N9 1.373(4)
N2–C6	1.2955(2)	1.287(2)	N3–C6 1.280(5)
N5–C25	-----	1.292(2)	N8–C23 1.295(5)
C13–O1	1.2213(1)	1.267(2)	C12–O1 1.261(4)
N3–C13	1.3610(2)	1.332(2)	N4–C12 1.343(5)
N6–C32	-----	1.334(2)	N9–C29 1.326(5)
<i>Bond angles</i>	<i>Bond angles</i>	<i>Bond angles</i>	<i>Bond angles</i>
O1–C13–N3	124.67(1)	125.97(2)	O1–C12–N4 126.80(3)
N2–Mn1–N5	-----	164.16(5)	N3–Mn1–N8 161.95(1)
N2–Mn1–O1	-----	71.75(5)	N3–Mn1–O1 72.41(1)
N1–Mn1–N4	-----	97.76(6)	N1–Mn1–N6 97.38(1)
N5–Mn1–O2	-----	71.75(5)	N8–Mn1–O2 72.15(1)
N1–Mn1–N2	-----	71.14(5)	N1–Mn1–N3 71.23(1)
N4–Mn1–N5	-----	71.33(5)	N6–Mn1–N8 70.85(1)
O1–Mn1–O2	-----	101.40(5)	O1–Mn1–O2 102.48(1)
O1–Mn1–N1	-----	142.04(5)	O1–Mn1–N1 143.59(1)
O2–Mn1–N4	-----	143.07(5)	O2–Mn1–N6 142.15(1)
N2–Mn1–N4	-----	94.19(5)	N3–Mn1–N6 96.48(1)
N5–Mn1–N1	-----	103.69(6)	N8–Mn1–N1 97.08(1)
C6–N2–N3	117.38(1)	120.01(1)	C6–N3–N4 120.20(3)
N2–C6–C5	127.69(1)	114.57(2)	N3–C6–C5 115.10(3)
N2–C6–C7	114.35(1)	125.26(2)	N3–C6–C7 125.50(3)

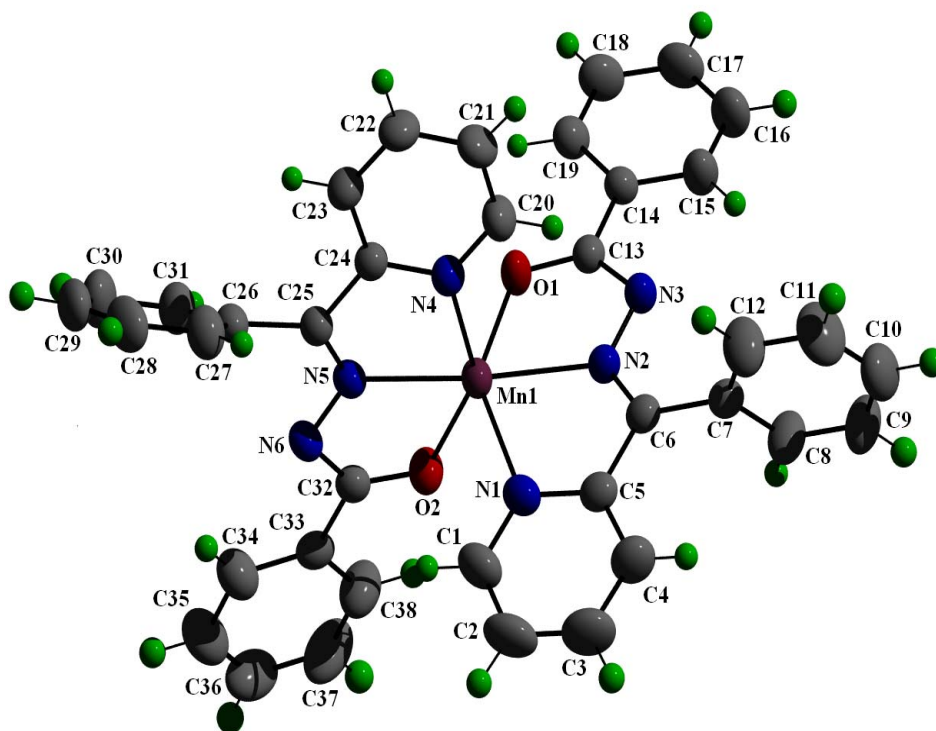


Fig. 4.8. Molecular structure of $[\text{Mn}(\text{BPB})_2]$ (**3**) along with the atom numbering scheme (Displacement ellipsoids are drawn at the 50% probability level and hydrogen atoms are shown as small spheres of arbitrary radii).

No classical hydrogen bond was found in the crystal structure of **3**. A weak intermolecular hydrogen bonding interaction is observed in **3** between the hydrogen atoms on C8 and N3 of the hydrazone moiety and these interactions are illustrated in Fig. 4.9. The crystal packing is determined by intermolecular hydrogen bonds, π - π interactions and C-H \cdots π interactions as depicted in Table 4.7. The centroid Cg(6) is involved in π - π interaction with Cg(6) of the neighboring unit at a distance of 3.731 Å (Table 4.7).

Table 4.7. H-bonding, π - π and C–H $\cdots\pi$ interaction parameters of [Mn(BPB)₂] (**3**).

H-bonding interactions				
D–H \cdots A (Å)	D–H	H \cdots A	D \cdots A	D–H \cdots A
C8–H(8) \cdots N(3) ^a	0.93	2.57	3.332	140
π - π interactions				
Cg(I) \cdots Cg(J)	Cg–Cg (Å)	α (°)	β (°)	
Cg(6) \cdots Cg(6) ^b	3.731	0.03	18.63	
C–H $\cdots\pi$ interaction				
X–H \cdots Cg(J)	H \cdots Cg (Å)	X–H \cdots Cg (°)	X \cdots Cg (Å)	
C(9)–H(9) \cdots Cg(1) ^c	2.74	139	3.492	
Equivalent position codes				
a = 1-x, 1-y, 2-z, b = 2-x, -y, 2-z, c = 1-x, 1-y, 2-z				
Cg(6) = N(4), C(20), C(21), C(22), C(23), C(24); Cg(1) = Mn (1), O(1), C(13), N(3), N(2)				

D, donor; A, acceptor; Cg, centroid; α , dihedral angles between planes I and J; β , angle Cg(I) – Cg(J) vector normal to plane I

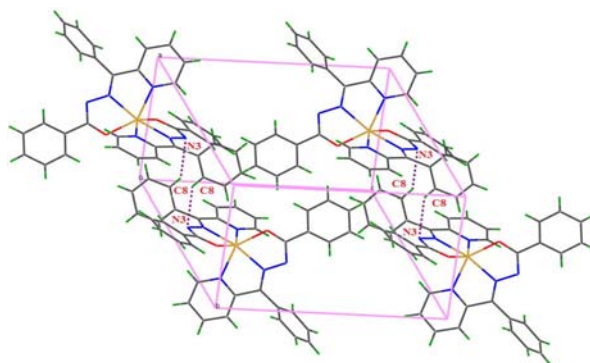


Fig. 4.9. Packing diagram of [Mn(BPB)₂] (**3**) (Intermolecular hydrogen bonds are shown as dotted lines).

The molecular structure along with crystallographic numbering scheme of **4** is illustrated in Fig. 4.10 and relevant bond lengths and angles are listed in Table 4.6. Crystal structure of [Mn(DKN)₂] is very similar to that of **3**, in which each ligand binds as a monoanionic N,N,O chelator in a meridional fashion, leading to an approximately orthogonal arrangement of the two ligands. The bond lengths in

Mn(DKN)₂ are similar to those found in [Mn(BPB)₂] analogue. The N–N, N=C and C–O bond distances in the =N–N=C(O⁻)- fragment of [Mn(DKN)₂] are consistent with the enolate form of the hydrazone functionality. This implies that the coordinated HDKN ligand also exists predominantly in the enolate resonance form with the conjugated C=N–N=C–O⁻ moiety, agreeing with the IR data. The negative charge of the monoanionic ligand is delocalized over the DKN moiety and the C12–O1 bond distance is consistent with increased single bond character. As in **3**, the *trans* angle N3–Mn1–N8 (161.95(11)°) deviate much from linearity and the intraligand bite angles are *ca.* 71.66° which exhibits a highly distorted octahedral geometry. Similar to **3**, the bicyclic chelate rings of **4** make a dihedral angle of 86.13° between them which indicates that they are closely perpendicular to each other.

In the crystal structure of **4**, the asymmetric units are linked by intermolecular interactions (Table 4.8) forming a one-dimensional supramolecular network as shown in Fig. 4.11.

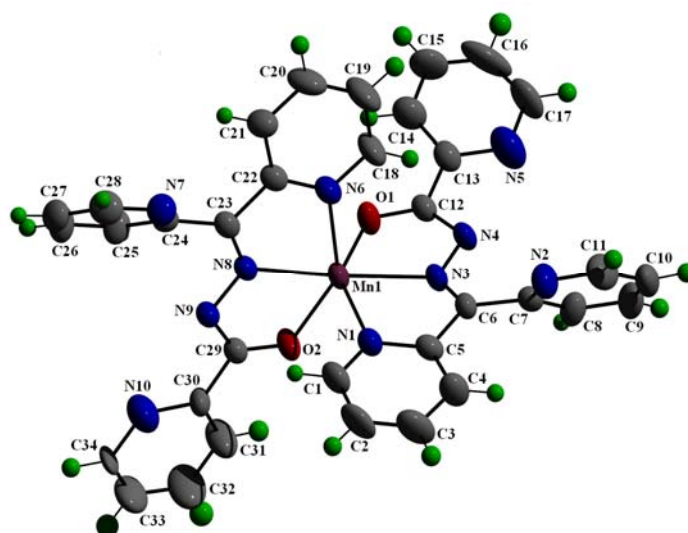


Fig. 4.10. Molecular structure of [Mn(DKN)₂] (**4**) along with the atom numbering scheme (Displacement ellipsoids are drawn at the 50% probability level and hydrogen atoms are shown as small spheres of arbitrary radii).

Table 4.8. H-bonding, π - π and C-H $\cdots\pi$ interaction parameters of [Mn(DKN)₂] (4).

H-bonding interactions				
D-H \cdots A (Å)	D-H	H \cdots A	D \cdots A	D-H \cdots A
C16-H(16) \cdots N(4) ^d	0.93	2.60	3.523	176
π - π interactions				
Cg(I) \cdots Cg(J)	Cg-Cg (Å)	α (°)	β (°)	
Cg(1) \cdots Cg(6) ^e	3.751	17.49	13.44	
C-H $\cdots\pi$ interaction				
X-H \cdots Cg(J)	H \cdots Cg (Å)	X-H \cdots Cg (°)	X \cdots Cg (Å)	
C(28)-H(28) \cdots Cg(2) ^f	2.65	146	3.462	
Equivalent position codes				
d = -x, -1/2+y, -z, e = 1-x, -1/2+y, -z, f = 1-x, 1/2+y, 1-z,				
Cg(1) = N(4), C(20), C(21), C(22), C(23), C(24); Cg(6) = Mn(1), O(1), C(12), N(4), N(3); Cg(2) = Mn(1), O(2), C(29), N(9), N(8)				

D, donor; A, acceptor; Cg, centroid; α , dihedral angles between planes I and J; β , angle Cg(I) - Cg(J) vector normal to plane I

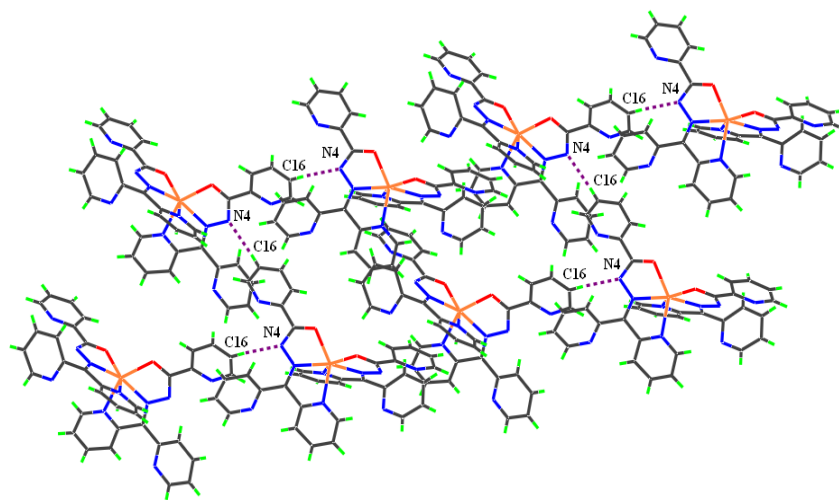


Fig. 4.11. Intermolecular hydrogen bonding interactions in [Mn(DKN)₂] (4) (Only the atoms involved in hydrogen bonding are numbered).

References

- [1] M. Pick, I. Roboni, J. Fridovich, *J. Am. Chem. Soc.* 96 (1974) 7329.
- [2] R.J. Debus, *Biochim. Biophys. Acta* 1102 (1992) 269.
- [3] G. Christou, J.B. Vincent, *Inorg. Chim. Acta* 136 (1987) L41.
- [4] E.C. Sanudo, V.A. Grillo, M.J. Knapp, J.C. Bollinger, J.C. Huffman, D.N. Hendrickson, G. Christou, *Inorg. Chem.* 41 (2002) 2441.
- [5] A. Deroche, I. M.-Baradau, M. Cesario, J. Guilhem, B. Keita, L. Nadjjo, C.H. -Levin, *J. Am. Chem. Soc.* 118 (1996) 4567.
- [6] B.A. Bernat, L.T. Laughlin, R.N. Armstrong, *Biochemistry* 38 (1999) 7462.
- [7] J.-F. Pan, K. Chen, *J. Mol. Catal. A* 176 (2001) 19.
- [8] W.J. Geary, *Coord. Chem. Rev.* 7 (1971) 109.
- [9] A.A.A. Abu-Hussen, A.A.A. Emara, *J. Coord. Chem.* 57 (2004) 973.
- [10] C.-Y. Meng, X.-S. Wan, X.-F. Zheng, L.-Y. Meng, H.-Y. Zhang, R. Yang, H.-W. Hou, *Synth and React. Inorg. Met. Org. and Nano Met. Chem.* 37 (2007) 97.
- [11] M. Aslantas, E. Kendi, N. Demir, A.E. Sabik, M. Tumer, M. Kertmen, *Spectrochim. Acta Part A* 74 (2009) 617.
- [12] X.-H. Chen, Q.-J. Wu, Z.-Y. Liang, C.-R. Zhan, J.-B. Liu, *Acta Cryst. C.* 65 (2009) 190.
- [13] M.S. Refat, S. Chandra, M. Tyagi, *J. Therm. Anal. Calorim.* 100 (2010) 261.
- [14] S. Verma, S. Chandra, U. Dev, N. Joshi, *Spectrochim. Acta Part A* 74 (2009) 370.

- [15] S. Banerjee, A. Ray, S. Sen, S. Mitra, D.L. Hughes, R.J. Butcher, S.R. Batten, D.R. Turner, *Inorg. Chim. Acta* 361 (2008) 2692.
- [16] S. Naskar, D. Mishra, S.K. Chattopadhyay, M. Corbella, A.J. Blake, *Dalton Trans.* (2005) 2428.
- [17] S. Stoll, A. Schweiger, *J. Magn. Reson.* 178 (2006) 42.
- [18] T.H. Bennur, D. Srinivas, P. Ratnasamy, *Microporous and Mesoporous Materials* 48 (2001) 111.
- [19] A. Sreekanth, M. Joseph, H.-K. Fun, M.R.P. Kurup, *Polyhedron* 25 (2006) 1408.
- [20] R. Kumar, S. Chandra, *Spectrochim. Acta Part A* 67 (2007) 188.
- [21] C. Mantel, C. Baffert, I. Romero, A. Deronzier, J. Pecaut, M. Collomb, C. Duboc, *Inorg. Chem. C* 43 (2004) 6455.
- [22] G.M. Sheldrick, *Acta Crystallogr. A* 64 (2008) 211.
- [23] K. Brandenburg, *Diamond Version 3.1f*, Crystal Impact GbR, Bonn, Germany, 2008.
- [24] C.F. Macrac, P.R. Edington, P. McCabe, E. Pidcock, G.P. Shields, R. Taylor, M. Towler, J. Van de Streek, *J. Appl. Cryst.* 39 (2006) 453.
- [25] C.M. Armstrong, P.V. Benhardt, P. Chin, Des R. Richardson, *Eur. J. Inorg. Chem.* (2003) 1145.
- [26] A. Ray, S. Banerjee, S. Sen, R.J. Butcher, G.M. Rosair, M.T. Garland, S. Mitra, *Struct. Chem.* 19 (2008) 209.
- [27] A.R. Stefankiewicz, M.W.-Chorab, H.B. Szczesniak, V. Patroniak, M. Kubicki, Z. Hnatejko, J. Harrowfield, *Polyhedron* 29 (2009) 178.

****๑๐๑****

Chapter 5

Syntheses, spectral and structural characterization of cobalt (II/III) complexes incorporating tridentate acylhydrazones

Contents

- 5.1 Introduction
- 5.2 Experimental
- 5.3 Results and discussion
- References

5.1. Introduction

Hydrazones are a class of compounds very promising in the treatment of many diseases, cancer in particular, and its development is still in progress. Hydrazones bearing an aromatic heterocyclic moiety seem to present an implemented biological activity and are found to act as iron chelators [1]. Co(III) complexes with nitroprusside as a counter ion of pyridoxal thiosemicarbazone was found to have antileukemic activity [2].

Co(II) complexes has a d^7 configuration and are very stable and difficult to oxidise. In contrast, many Co(II) complexes are readily oxidised to Co(III), this happens because the crystal field stabilization energy of Co(III) with a d^6 configuration is higher than for Co(II) with a d^7 configuration. Most Co(II) complexes are low spin octahedral. Tetrahedral complexes are also common and

have more intense colors than octahedral complexes. Only the +2 and +3 states have any stability in water and the +2 state are far more stable than +3 except in the presence of complexing ligands. The highest oxidation state shown by cobalt is IV. In Co(III) octahedral complexes, the metal has a d^6 configuration, and most of the ligands are strong enough to cause spin pairing, giving the electronic arrangement $(t_{2g})^6 (e_g)^0$. This arrangement has very large crystal field stabilization energy and is found to be diamagnetic.

Though Co complexes are not involved in oxygen metabolism in the body, they serve as useful models for metal-oxygen binding in biological system. Coenzyme B₁₂, nature's unique organometallic reagent is also the only well-defined cobalt containing biochemical. It contains a low spin Co(III) atom in the middle of a tetradentate macrocycle, a substituted corrin. The Co is coordinated in a square planar array with four nitrogen atoms from the ring.

5.2. Experimental

5.2.1. Materials

Di-2-pyridyl ketone (Aldrich), 2-benzoylpyridine (Aldrich), benzhydrazide (Aldrich), and nicotinic hydrazide (Aldrich), cobalt(II) chloride dihydrate (E-Merck), cobalt(II) bromide (Aldrich), cobalt(II) acetate tetrahydrate (Nice Chemicals Pvt. Ltd.), potassium thiocyanate (Merck) and ammonium thiocyanate (E-Merck) were used as received. Solvents were purified by standard procedures before use.

5.2.2. Syntheses of the acylhydrazones

The syntheses of hydrazones HBPB and HDKN are discussed already in Chapter 2.

5.2.3. Syntheses of the complexes

5.2.3.1. Synthesis of $[Co(BPB)_2]Br$ (5)

Complex **5** was prepared by refluxing methanolic solutions of HBPB (0.301 g, 1 mmol) and cobalt(II) bromide (0.218 g, 1 mmol) for 3 h. after adding two drops of triethylamine to the methanolic solution of ligand. The dark colored solution was allowed to stand at room temperature and after slow evaporation, brown crystalline product was separated, filtered and washed with ether and dried over P_4O_{10} *in vacuo*.

$[Co(BPB)_2]Br$ (**5**): Yield: 68%, λ_m (DMF): 79 $ohm^{-1}cm^2 mol^{-1}$, μ (B.M.): diamagnetic, Elemental Anal. Found (Calcd.) (%): C: 61.27 (61.72), H: 3.74 (3.82), N: 10.98 (11.36), Co: 7.43 (7.97).

5.2.3.2. Synthesis of $[Co(BPB)_2]$ (6)

Into a solution of HBPB (0.301 g, 1 mmol) in methanol, two drops of triethylamine was added with stirring, after which a methanolic solution of cobalt(II) acetate tetrahydrate (0.249 g, 1 mmol) was added and the resulting mixture was refluxed for 3 h. at 40 °C. The solution was allowed to stand at room temperature and after slow evaporation, the brown crystalline product was separated, filtered and washed with ether and dried over P_4O_{10} *in vacuo*.

$[Co(BPB)_2]$ (**6**): Yield: 73%, λ_m (DMF): 9 $ohm^{-1}cm^2 mol^{-1}$, μ (B.M.): 4.89, Elemental Anal. Found (Calcd.) (%): C: 68.94 (69.19), H: 4.23 (4.28), N: 12.49 (12.74), Co: 8.69 (8.93).

5.2.3.3. Synthesis of $[Co(BPB)NCS]$ (7)

To a methanolic solution of HBPB (0.301 g, 1 mmol), a solution of potassium thiocyanate (0.097 g, 1 mmol) in minimum volume of water was added, followed by the addition, with constant stirring, solution of cobalt(II)

acetate tetrahydrate (0.249 g, 1 mmol) in the methanol was added. The final solution was refluxed for 3 h. and the resulting solution was allowed to stand at room temperature and after slow evaporation, the brown crystalline product was separated, filtered and washed with ether and dried over P_4O_{10} *in vacuo*.

[Co(BPB)NCS] (**7**): Yield: 60%, λ_m (DMF): $10 \text{ ohm}^{-1}\text{cm}^2 \text{ mol}^{-1}$, μ (B.M.): 4.57, Elemental Anal. Found (Calcd.) (%): C: 57.57 (57.56), H: 3.64 (3.38), N: 13.40 (13.42), Co: 14.19 (14.12).

5.2.3.4. Synthesis of [Co(DKN)Cl] (**8**)

The hydrazone HDKN (0.312 g, 1 mmol) was dissolved in methanol and triethylamine was added dropwise. To this, methanolic solution of cobalt(II) chloride dihydrate (0.237 g, 1 mmol) was added and after the addition was complete the solution was refluxed for 3 h. at 40 °C. The green colored solid obtained was filtered and washed several times with methanol followed by ether and dried over P_4O_{10} *in vacuo*.

[Co(DKN)Cl] (**8**): Yield: 69%, λ_m (DMF): $12 \text{ ohm}^{-1}\text{cm}^2 \text{ mol}^{-1}$, μ (B.M.): 4.65, Elemental Anal. Found (Calcd.) (%): C: 50.83 (51.21), H: 3.21 (3.54), N: 17.51 (17.56), Co: 14.39 (14.78).

5.2.3.5. Synthesis of [Co(DKN)NCS]·H₂O (**9**)

To a solution of HDKN (0.312 g, 1 mmol) in methanol, a mixture of ammonium thiocyanate (0.076 g, 1 mmol) and cobalt(II) acetate tetrahydrate (0.249 g, 1 mmol) in methanol was added to it and refluxed for 3 h. The resulting dark colored solution was allowed to stand at room temperature and after slow evaporation, brown solid was separated, filtered and washed with ether and dried over P_4O_{10} *in vacuo*.

[Co(DKN)NCS]·H₂O (**9**): Yield: 73%, λ_m (DMF): 5 ohm⁻¹cm² mol⁻¹, μ (B.M.): 4.58, Elemental Anal. Found (Calcd.) (%): C: 48.97 (49.21), H: 3.34 (3.67), N: 18.74 (19.13), Co: 13.04 (13.41).

5.3. Results and discussion

5.3.1. Elemental analyses

The analytical data indicate that the observed C, H, N values were in close agreement with that of the proposed formula. The metal content % of the complexes was determined by AAS after digestion with con. HNO₃ and was found to be consistent with that of the theoretical results.

5.3.2. Molar conductivity and magnetic susceptibility measurements

The molar conductance values of the complexes (10⁻³ M DMF) except **6** lie in the range 4-12 ohm⁻¹cm² mol⁻¹ range. These low values indicate their non-electrolytic nature while complex **6** is found to be a 1:1 electrolyte [3]. The magnetic susceptibility measurements were performed on powdered samples at 298 K using a Sherwood Scientific Magnetic Susceptibility Balance (M.S.B) MK1 using HgCo(SCN)₄ as calibrant, the diamagnetic contribution to the susceptibility was estimated through Pascal's constants. The complex [Co(BPB)₂]Br was found to be diamagnetic in nature, showing that it has no unpaired electrons with a spin paired octahedral configuration. The observed magnetic moment for the octahedral complex [Co(BPB)₂] is found to be 4.89 B.M. which is higher than calculated by the spin-only formula [4]. This suggests that there is an orbital contribution. In octahedral complexes, Co²⁺ has (t_{2g})⁵(e_g)² configuration and is possible to transform an orbital into an equivalent (degenerate) orbital by rotation. This suggests that complex **6** has a high spin octahedral configuration. The magnetic moment of the other three complexes was found in the range 4.57-4.65 B.M. suggesting a tetrahedral geometry [5].

5.3.3. Infrared spectra

The IR spectrum of HBPB shows strong bands at 3063 and 1678 cm^{-1} which are assigned to $\nu(\text{N-H})$ and $\nu(\text{C=O})$ vibrations, respectively, suggesting that the hydrazone is present in the amido form in solid state [6]. Spectral assignments of the complexes are made compared with that of the hydrazones and are tabulated in Table 5.1. Dramatic changes are observed in the spectrum of $[\text{Co}(\text{BPB})_2]\text{Br}$ (Fig. 5.1) which shows no characteristic bands of the amide and amino groups suggesting that the hydrazone is coordinated in the enolic form [7]. Instead, on complexation a new band at 1368 cm^{-1} assignable to $\nu(\text{C-O})$ stretching vibration is seen [8]. Strong absorption at 1571 cm^{-1} assigned to $\nu(\text{C=N})$ of the azomethine group in the ligand shows a downward shift to 1558 cm^{-1} indicating that the nitrogen of the azomethine group is ligated to the metal atom [9]. A new band appearing at $\sim 1595 \text{ cm}^{-1}$ seems to have its origin in the stretching vibration mode of the conjugate $-\text{C=N-C=N}-$ grouping analogous to that of azines, suggesting the participation azomethine nitrogen in coordination. The pyridyl ring in-plane and out-of-plane ring deformation are found to be shifted to higher frequencies on complexation indicating the coordination through pyridyl nitrogen [10].

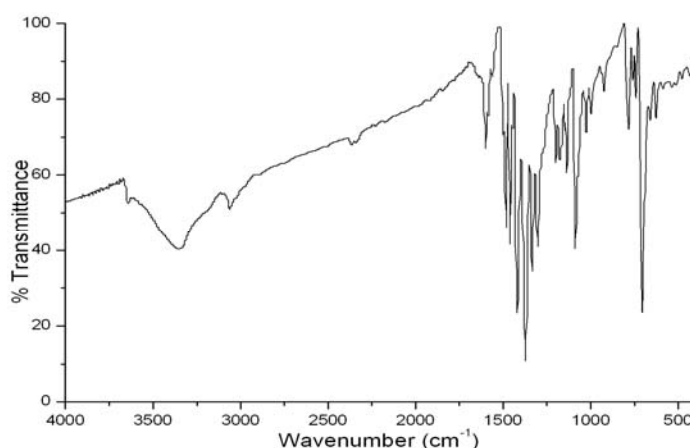


Fig. 5.1. IR spectrum of $[\text{Co}(\text{BPB})_2]\text{Br}$ (5).

Similar to complex **5**, in the IR spectrum of $[\text{Co}(\text{BPB})_2]$ (Fig. 5.2), the bands due to $\nu(\text{N-H})$ and $\nu(\text{C=O})$ vibrations are absent and the presence of a new band at 1360 cm^{-1} ascribed to $\nu(\text{C-O})$ stretching suggests the enolization of the $-\text{C=O}$ of the acyl keto group giving rise to the $-\text{C=N-C=N-}$ moiety [11]. Of the two bands at 1584 and 1541 cm^{-1} , one may be due to the new $\nu(\text{C=N})$ and other may be attributed to the original $\nu(\text{C=N})$ which has undergone shift to lower wavenumber, suggesting the coordination of azomethine nitrogen to the metal center. The coordination of the pyridyl nitrogen is evident from the peaks at 649 and 451 cm^{-1} for the ring in-plane and out-of-plane ring deformation. On the basis of spectral studies, it appears that HBPB is coordinated *via* azomethine, pyridyl nitrogen and enolate oxygen. This is also well established from its crystal structure.

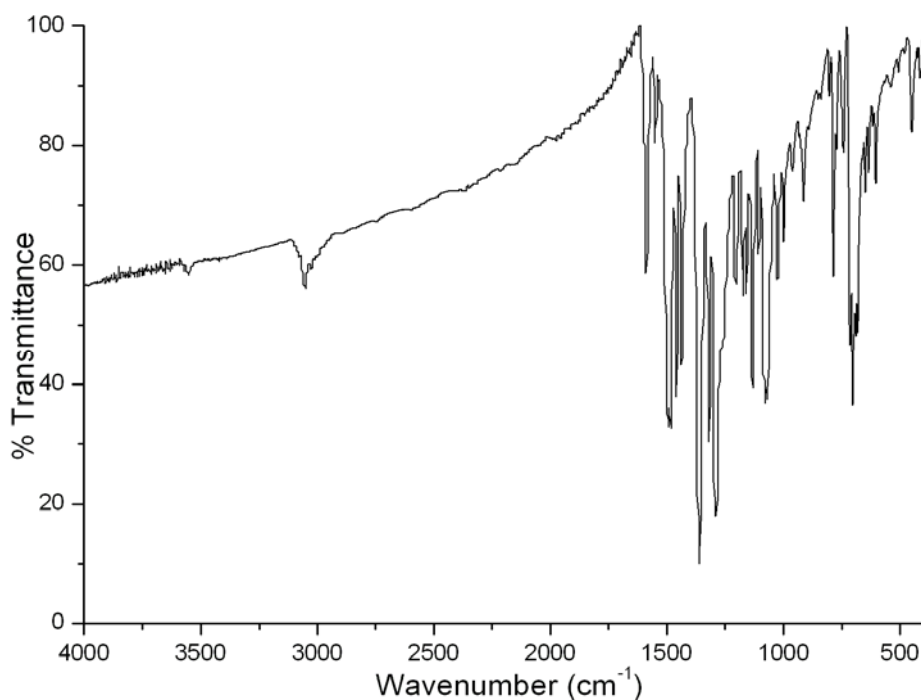


Fig. 5.2. IR spectrum of $[\text{Co}(\text{BPB})_2]$ (**6**).

The IR pattern of [Co(BPB)NCS] (Fig. 5.3) is similar to that of the other complexes discussed above and the major difference lies in the 2100-2000 cm^{-1} region of the spectrum. The azomethine nitrogen coordination is evident from the shifting of $\nu(\text{C}=\text{N})$ stretching to 1551 cm^{-1} and was further confirmed by the appearance of the new band at 1597 cm^{-1} due to new $\nu(\text{C}=\text{N})$ stretching vibration. The most interesting peak in the IR spectrum of this compound is a sharp band at 2062 cm^{-1} which is assignable to the $\nu(\text{CN})$ stretching of the thiocyanate group. The singlet structure of this band indicates the presence of one type of thiocyanate in this complex [12]. The position of the peak and its structure (singlet) points out to the presence of N-bonded terminal thiocyanate group in the complex. The $\nu(\text{CS})$ of the NCS ligand at 774 cm^{-1} indicates the coordination through nitrogen atom of the terminal NCS ligand [13] but the bending vibration of the NCS group which is expected near 480 cm^{-1} which are normally weak tend to be obscured by other bands.

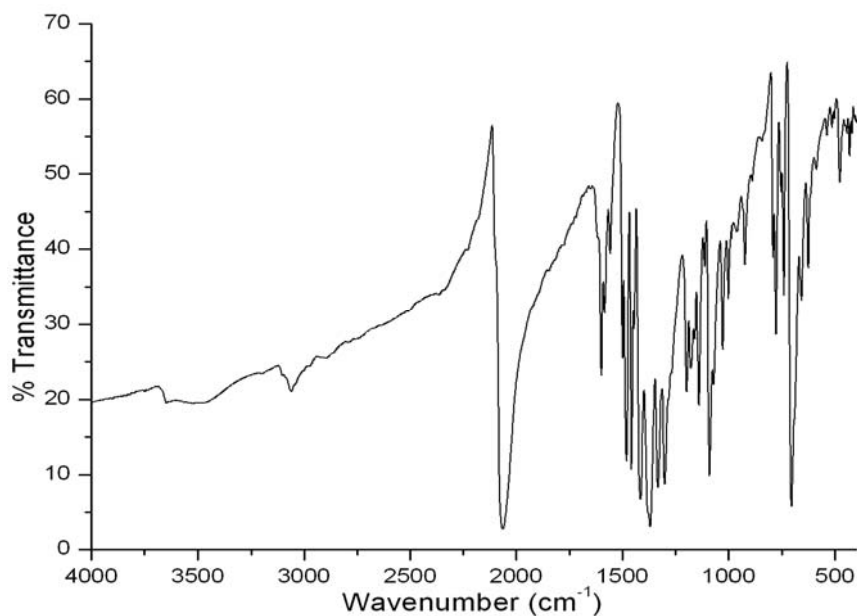


Fig. 5.3. IR spectrum of [Co(BPB)NCS] (7).

In the IR spectrum of $[\text{Co}(\text{DKN})\text{Cl}]$ (Fig. 5.4), the azomethine band undergoes a negative shift and is observed at 1508 cm^{-1} which is further supported by the appearance of a new $\nu(\text{C}=\text{N})$ band at 1589 cm^{-1} .

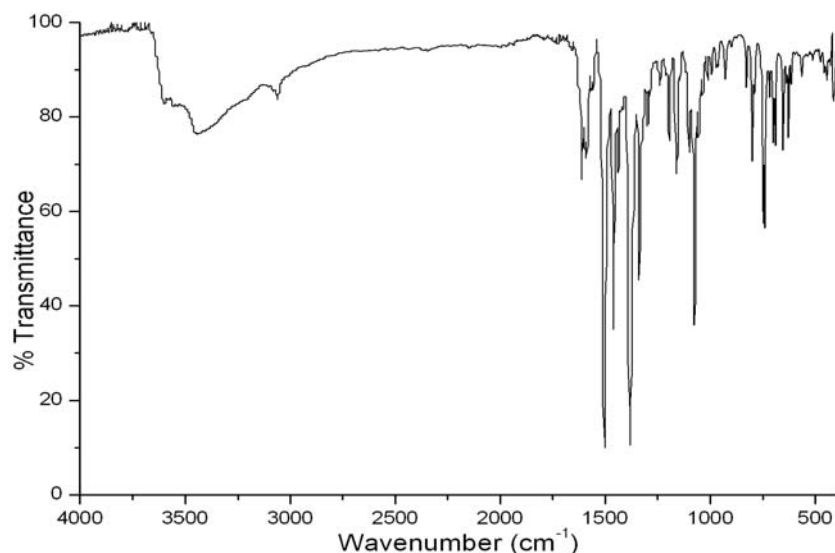


Fig. 5.4. IR spectrum of $[\text{Co}(\text{DKN})\text{Cl}]$ (**8**).

In the thiocyanato complex $[\text{Co}(\text{DKN})\text{NCS}] \cdot \text{H}_2\text{O}$ (Fig. 5.5), the medium intensity band at 1584 cm^{-1} is assigned to the azomethine function. The disappearance of $\nu(\text{N}-\text{H})$ and $\nu(\text{C}=\text{O})$ peaks is an evidence for the coordination of HDKN in the enolate form. The pyridyl in-plane ring deformation and out-of-plane ring deformation are found at higher frequencies compared to that of the ligand, suggesting the coordination of pyridyl nitrogen. The characteristic asymmetric stretching due to the thiocyanate is observed as a strong band at 2070 cm^{-1} , which clearly indicates the presence of one type of non-bridging thiocyanate bonded through nitrogen atom [12]. The $\nu(\text{CS})$ band of the NCS ligand observed at 758 cm^{-1} also suggests the coordination of thiocyanate group through nitrogen atom. A broad band due to the presence of lattice water in the complex was seen at 3420 cm^{-1} which was also evident from the thermogravimetric analysis.

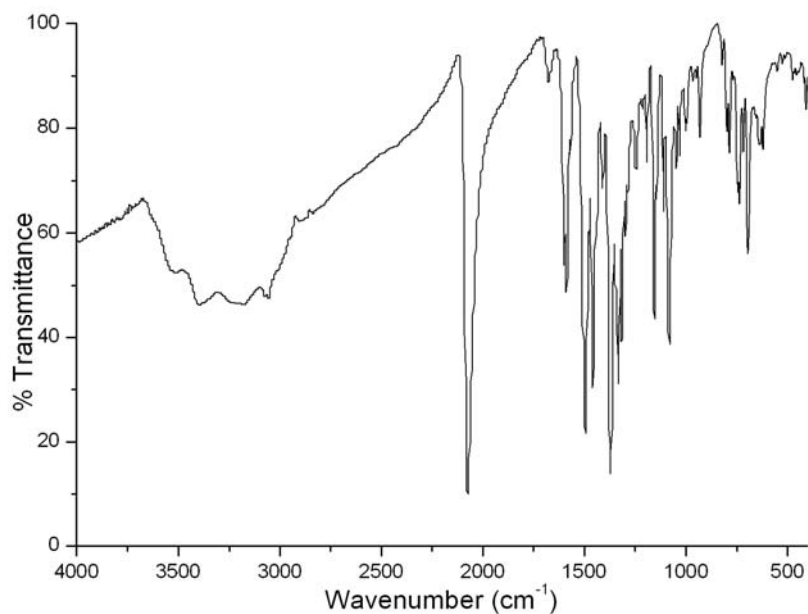


Fig. 5.5. IR spectrum of $[\text{Co}(\text{DKN})\text{NCS}] \cdot \text{H}_2\text{O}$ (**9**).

Table 5.1. Infrared spectral data (cm^{-1}) of Co(II/III) complexes.

Compound	$\nu(\text{N-H})$	$\nu(\text{C=O})/\nu(\text{C-O})$	$\nu(\text{C=N})$	$\nu(\text{C=N})^a$	$\nu(\text{Co-O})$	$\nu(\text{Co-N})$
HBPB	3063	1678	1571
$[\text{Co}(\text{BPB})_2]\text{Br}$ (5)	...	1368	1558	1595	531	475
$[\text{Co}(\text{BPB})_2]$ (6)	...	1360	1541	1584	535	445
$[\text{Co}(\text{BPB})\text{NCS}]$ (7)	...	1373	1551	1597	538	479
HDKN	2928	1689	1579
$[\text{Co}(\text{DKN})\text{Cl}]$ (8)	...	1377	1508	1589	548	470
$[\text{Co}(\text{DKN})\text{NCS}] \cdot \text{H}_2\text{O}$ (9)	...	1364	1509	1584	550	470

^a Newly formed C=N

5.3.4. Electronic spectra

The electronic absorption bands of the complexes (10^{-5} M) were recorded in acetonitrile solution and spectral data are summarized in Table 5.2. On complexation the intraligand transitions of the uncomplexed hydrazones are

slightly shifted upon complexation. The bands in the range 24360-26070 cm^{-1} corresponds to the ligand to metal charge transfer (LMCT) transitions [14] (Fig. 5.6).

The terms arising for a Co^{2+} (d^7 system) are the ground state 3F and the excited states 3P , 1G , 1D , 1S . The transitions from the ground state to the three singlet states (1G , 1D , 1S) are spin forbidden and will be very weak and can be ignored. The two remaining states 3F and 3P can have spin permitted transitions. The F state split into $A_{2g}+T_{1g}+T_{2g}$ and P state is transformed into a T_{1g} state. Hence three peaks should appear in the spectrum corresponding to $^4T_{2g}(F) \leftarrow ^4T_{1g}(F)$, $^4A_{2g}(F) \leftarrow ^4T_{1g}(F)$ and $^4T_{1g}(P) \leftarrow ^4T_{1g}(F)$. There are two T_{1g} states and since they are of same symmetry, they interact one another and this interelectronic repulsion is much more marked in $d^7 T_d$ case. Due to this they may cross each other but it is impossible because states of same symmetry cannot cross each other. But this occurs in O_h case and thus $^4A_{2g} \leftarrow ^4T_{2g}$ transition is very weak.

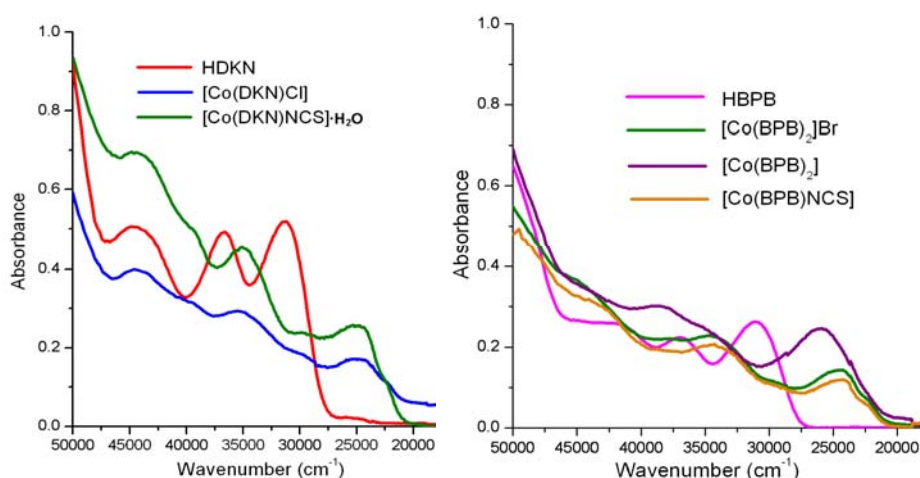


Fig. 5.6. Electronic spectra of the Co(II/III) complexes in the region 50,000-20,000 cm^{-1} .

In tetrahedral complexes of Co^{2+} the electronic arrangement is $(e)^4(t_2)^3$. Three transitions are expected, $^4T_2(F) \leftarrow ^4A_2$, $^4T_1(F) \leftarrow ^4A_2$, $^4T_1(P) \leftarrow ^4A_2$. In the Co(II) complexes except $[\text{Co}(\text{BPB})_2]$, two bands in the range 14910-17100 cm^{-1}

are observed corresponding to ${}^4T_1(F) \leftarrow {}^4A_2$ and ${}^4T_1(P) \leftarrow {}^4A_2$ transitions [15,16] (Figs. 5.7-5.9), but the other transition lies in the near IR region and is not observed as it is out of the range of the used spectrophotometer (200-900 nm). In complex $[Co(BPB)_2]$, a weak band at 18130 cm^{-1} was found which can be assigned to ${}^4T_{1g}(P) \leftarrow {}^4T_{1g}(F)$ transition [17]. In the case of $[Co(BPB)_2]Br$, cobalt is in +3 oxidation state with a d^6 electronic configuration. So only one weak $d-d$ transition is observed at 18200 cm^{-1} .

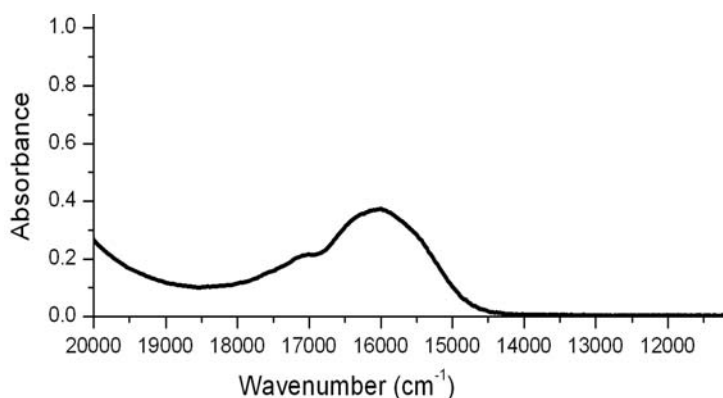


Fig. 5.7. Electronic spectrum of $[Co(BPB)NCS]$ (**7**) in the region $20,000\text{-}12,000\text{ cm}^{-1}$.

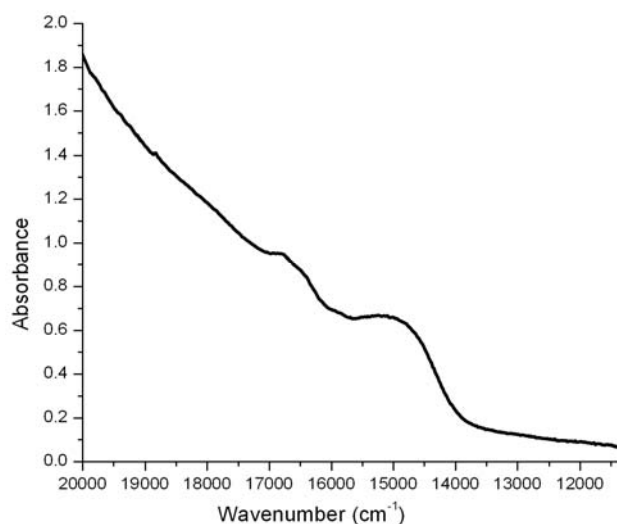


Fig. 5.8. Electronic spectrum of $[Co(DKN)Cl]$ (**8**) in the region $20,000\text{-}12,000\text{ cm}^{-1}$.

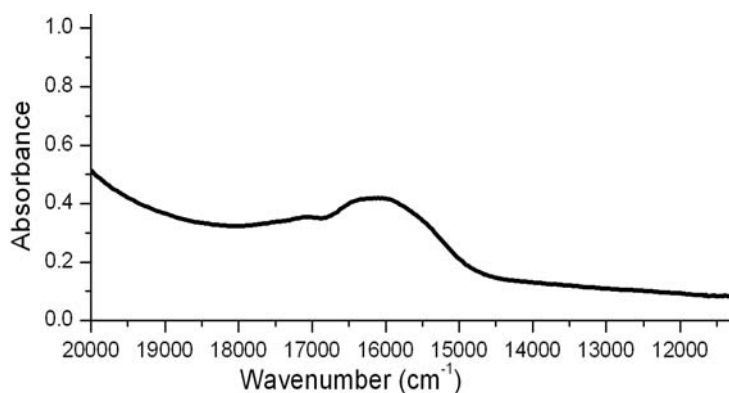


Fig. 5.9. Electronic spectrum of $[\text{Co}(\text{DKN})\text{NCS}] \cdot \text{H}_2\text{O}$ (**9**) in the region 20,000-12,000 cm^{-1} .

Table 5.2. Electronic spectral data of the cobalt(II/III) complexes.

Compound	UV-vis absorption bands (cm^{-1})
$[\text{Co}(\text{BPB})_2]\text{Br}$ (5)	44120, 34580, 24360, 18200
$[\text{Co}(\text{BPB})_2]$ (6)	38350, 34480, 26070, 18130
$[\text{Co}(\text{BPB})\text{NCS}]$ (7)	42695, 34530, 24410, 17100, 16040
$[\text{Co}(\text{DKN})\text{Cl}]$ (8)	44225, 39390, 35240, 30040, 29760, 24750, 16780, 14910
$[\text{Co}(\text{DKN})\text{Cl}]$ (8)	44225, 39390, 35240, 30040, 29760, 24750, 16780, 14910
$[\text{Co}(\text{DKN})\text{NCS}] \cdot \text{H}_2\text{O}$ (9)	43990, 39490, 35020, 24890, 17070, 16100

5.3.5. Cyclic voltammetric studies

Electrochemical studies of the complexes **5-9** were performed using DMF as the solvent, TBAP (tetrabutylammonium phosphate) as the supporting electrolyte at a scan speed of 100 mV s^{-1} with platinum wires as working and counter electrodes and Ag/Ag^+ as reference electrode.

The cyclic voltammograms of metal complexes except **5** consist of one oxidation peak and one reduction peak. The obtained data from the electrochemical properties of the metal complexes are given in Table 5.3. The cyclic voltammogram for the complex **6** is shown in Fig. 5.10. which shows the reduction peak at -0.32 V attributed to $\text{Co}(\text{II})/\text{Co}(\text{I})$ reduction. On the reverse

scan the corresponding oxidation peak at 0.97 V is ascribed to the Co(I)/Co(II) oxidation. On the other hand, complex **5** shows two anodic and two cathodic peak potentials during the forward and reverse scans. As seen from Fig. 5.10, the cyclic voltammogram of complex **5** shows two well defined redox process in which one of them corresponds to the formation of Co(III)/Co(II) couple at $E_{pc} = 0.93$ V and $E_{pa} = 0.92$ V which is found to be reversible. The other one corresponds to the formation of Co(II)/Co(I) couple at $E_{pc} = -0.18$ V and the associated cathodic peak at $E_{pa} = -0.41$ V.

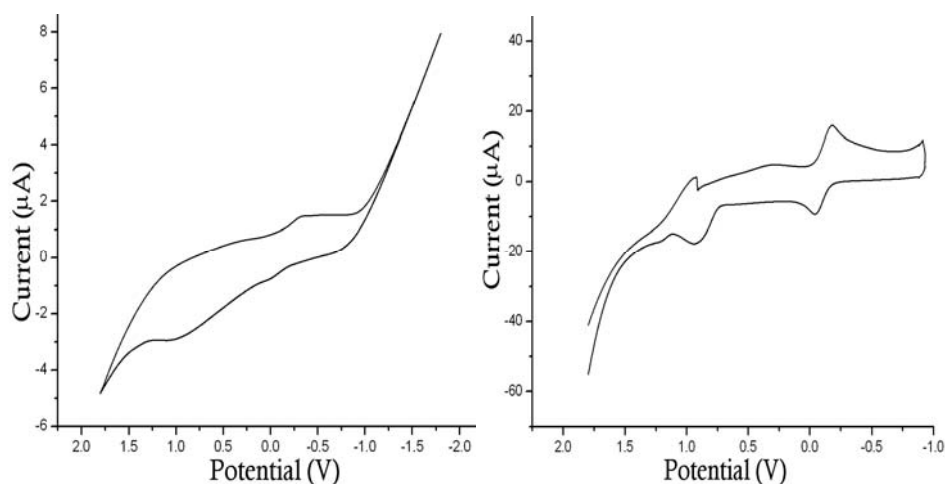


Fig. 5.10. Cyclic voltammograms of $[\text{Co}(\text{BPB})_2]\text{Br}$ (**5**) (left) and $[\text{Co}(\text{BPB})_2]$ (**6**) (right) in DMF at a scan rate of 100 mV s^{-1} .

Table 5.3. Electrochemical data of the Co(II/III) complexes in DMF.

Compound	E_{pc} (V)	E_{pa} (V)	I_{pc} (μA)	I_{pa} (μA)
$[\text{Co}(\text{BPB})_2]\text{Br}$ (5)	0.93, -0.18	0.92, -0.41	1.28, 15.41	-17.45, -8.92
$[\text{Co}(\text{BPB})_2]$ (6)	-0.32	0.97	1.48	-2.91
$[\text{Co}(\text{BPB})\text{NCS}]$ (7)	-0.40	-0.22	0.56	26.10
$[\text{Co}(\text{DKN})\text{Cl}]$ (8)	-0.11	0.12	0.97	-0.71
$[\text{Co}(\text{DKN})\text{NCS}] \cdot \text{H}_2\text{O}$ (9)	-0.73	0.11	5.57	-1.27

5.3.6. Thermal analyses

Thermogravimetric analyses were done to get information concerning the thermal stability of the complexes and to confirm the presence of lattice water. TGA studies were carried out from 50-800 °C in nitrogen atmosphere at a heating rate of 10 °C/min and selected TG-DTG curves are shown in Fig. 5. 11. Thermograms of anhydrous cobalt complexes were observed in the range 50-800 °C. As expected there was no mass loss up to 280 °C indicating the absence of water. The TGA curve for the complex **9** displays the first stage of decomposition in the range 60-110 °C, which is due to the loss of one molecule of water [19] with 3.90 % of the total weight of the complex (Calcd. 4.09%).

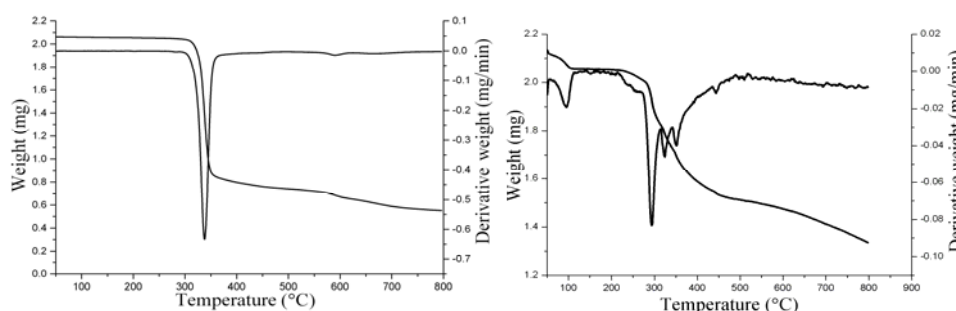


Fig. 5.11. TG-DTG curves of [Co(BPB)₂] (**6**) (left) and [Co(DKN)NCS]·H₂O (**9**) (right).

5.3.7. X-ray crystallography

Plate like brown crystals of [Co(BPB)₂] of dimensions 0.2 x 0.2 x 0.3 mm³ were selected and diffraction data were collected on a Bruker SMART APEX diffractometer equipped with graphite monochromated radiation ($\lambda = 0.71073 \text{ \AA}$) by using the φ/ω scan technique at room temperature. The structure was solved by direct methods and refined by full-matrix least-squares on F^2 using the SHELXTL-97 [20] program package. All non-hydrogen atoms were subjected to anisotropic refinement and all the hydrogen atoms were assigned with common isotropic displacement factors and were included in the final refinement by use of geometrical constraints.

Crystal data and details of the refinement for [Co(BPB)₂] (**6**) are summarized in Table 5.4, selected bond lengths (Å) and angles (°) are presented in Table 5.5. Fig. 5.12 displaying the molecular structure of the complex **6** showing the atom labeling scheme was drawn with 50% displacement ellipsoids with DIAMOND [21] and the remaining crystallographic figure (Fig. 5.13) showing the packing was drawn [22] using MERCURY.

Table 5.4. Crystal data and structure refinement parameters for [Co(BPB)₂] (**6**).

Parameters	[Co(BPB) ₂] (6)
Empirical Formula	C ₃₈ H ₂₈ CoN ₆ O ₂
Formula weight (M)	659.59
Temperature (T) K	273(2)
Wavelength (Mo Kα) (Å)	0.71073
Crystal system	Triclinic
Space group	<i>P</i> -1
Lattice constants	
<i>a</i> (Å)	10.728(2)
<i>b</i> (Å)	12.498(3)
<i>c</i> (Å)	12.883(3)
α (°)	66.802(3)
β (°)	83.614(4)
γ (°)	83.103(4)
Volume <i>V</i> (Å ³)	1572.3(6)
<i>Z</i>	2
Calculated density (ρ) (Mg m ⁻³)	1.393
Absorption coefficient, μ (mm ⁻¹)	0.591
Limiting Indices	-13 ≤ <i>h</i> ≤ 13 -15 ≤ <i>k</i> ≤ 15 -15 ≤ <i>l</i> ≤ 15
Reflections collected	10982
Unique Reflections	6182 [R(int) = 0.0386]
Refinement method	Full-matrix least-squares on <i>F</i> ²
Data / restraints / parameters	6182 / 0 / 424
Goodness-of-fit on <i>F</i> ²	1.070
Final <i>R</i> indices [<i>I</i> > 2σ(<i>I</i>)]	<i>R</i> ₁ = 0.0824, <i>wR</i> ₂ = 0.1602
<i>R</i> indices (all data)	<i>R</i> ₁ = 0.1136, <i>wR</i> ₂ = 0.1889

$$wR_2 = [\sum w(F_o^2 - F_c^2)^2 / \sum w(F_o^2)^2]^{1/2}; R_1 = \sum ||F_o| - |F_c|| / \sum |F_o|$$

5.3.7.1. Crystal structure of [Co(BPB)₂] (**6**)

Brown plate-shaped crystals of **6** were obtained by slow evaporation from a mixture of dichloromethane-methanol (1:1 v/v) solution of [Co(BPB)₂]. The molecular structure of [Co(BPB)₂] along with atom numbering scheme is depicted in Fig. 5.12. The structural refinement parameters and the selected bond lengths and angles are given in Tables 5.4 and 5.5. The bond distances and angles reveal that the independent units of the molecule exist in a distorted octahedral geometry around the metal center. The Co(II) center is coordinated in an N₄O₂ meridional manner in which each of the hydrazone moiety coordinates using *cis* pyridyl nitrogen, *trans* azomethine nitrogen and *cis* enolate oxygen atoms [23,24]. The Co–N_{azo} bond lengths are less compared to Co–N_{py} indicating the higher strength of former bond than the latter. This observation is also seen in Mn complexes of similar ligands [25], but in copper(II) complexes of hydrazones this is little bit different, one of the pyridyl nitrogen and enolate oxygen were slightly longer than the remaining four bond lengths [26]. It is interesting to note that the carbonyl bond distance is increased in complex when compared to the corresponding value in the free ligand 1.2213(14) Å, and this supports coordination through enolate oxygen. A significant amount of metal-to-ligand π back bonding generates a delocalized conjugating effect along the metal-chelate rings which imparts partial single and double bond nature to the C6–N2 and N2–N3 hydrazine bonds in the hydrazone moiety owing to the extensive delocalization over the entire coordination framework.

The metal center is shared by four fused five membered chelate rings. The dihedral angle between the planes constituting Co1, N1, C5, C6, N2 and Co1, N2, N3, C13, O1 with a maximum deviation from the mean plane of 0.0528 Å for C5 and 0.0571 Å for N2 respectively is found to be 3.47°. The *trans* angle N2–Co1–N5 is much farther from 180° compared to Cu(II) complexes reported with HBPB hydrazone [27]. It was found that this deviation was highest for Mn(II)

complexes of similar hydrazones [28]. The intraligand bite angles also become more acute (75.76°-76.95°) in this complex when compared to its Cu(II) complex, but this was more pronounced in the Mn(II) complex (70.85°-72.41°). The two ligand moieties in the present compound are aligned almost perpendicular to each other as revealed from the dihedral angle of 87.95° between the plane containing atoms {N1, C5, C6, N2, N3, C13, O1, Co1} with that to second plane {N4, C24, C25, N5, N6, C32, O2, Co1}.

Table 5.5. Selected bond lengths (Å) and bond angles (°) for [Co(BPB)₂] (6).

Bond lengths		Bond angles	
Co1–N2	2.036(4)	N2–Co1–N5	169.77(18)
Co1–N5	2.028(4)	N2–Co1–O1	76.33(16)
Co1–O1	2.054(4)	N2–Co1–N1	76.95(17)
Co1–O2	2.092(3)	N5–Co1–O2	75.76(14)
Co1–N1	2.141(5)	N5–Co1–N4	76.32(16)
Co1–N4	2.152(4)	O1–Co1–N1	153.13(15)
N2–N3	1.363(5)	O2–Co1–N4	151.09(15)
N5–N6	1.368(5)	N5–Co1–N1	93.98(16)
N2–C6	1.294(7)	N2–Co1–N4	99.81(16)
N5–C25	1.291(6)	N1–Co1–N4	96.80(17)
O1–C13	1.283(6)	N4–Co1–O1	90.42(16)
O2–C32	1.267(6)	N1–Co1–O2	92.47(16)
N3–C13	1.343(6)	N2–Co1–O2	108.97(15)
N6–C32	1.343(6)	O2–Co1–O1	93.56(15)
C13–C14	1.489(7)	C6–N2–N3	122.1(4)
C32–C33	1.496(7)	C25–N5–N6	120.7(4)

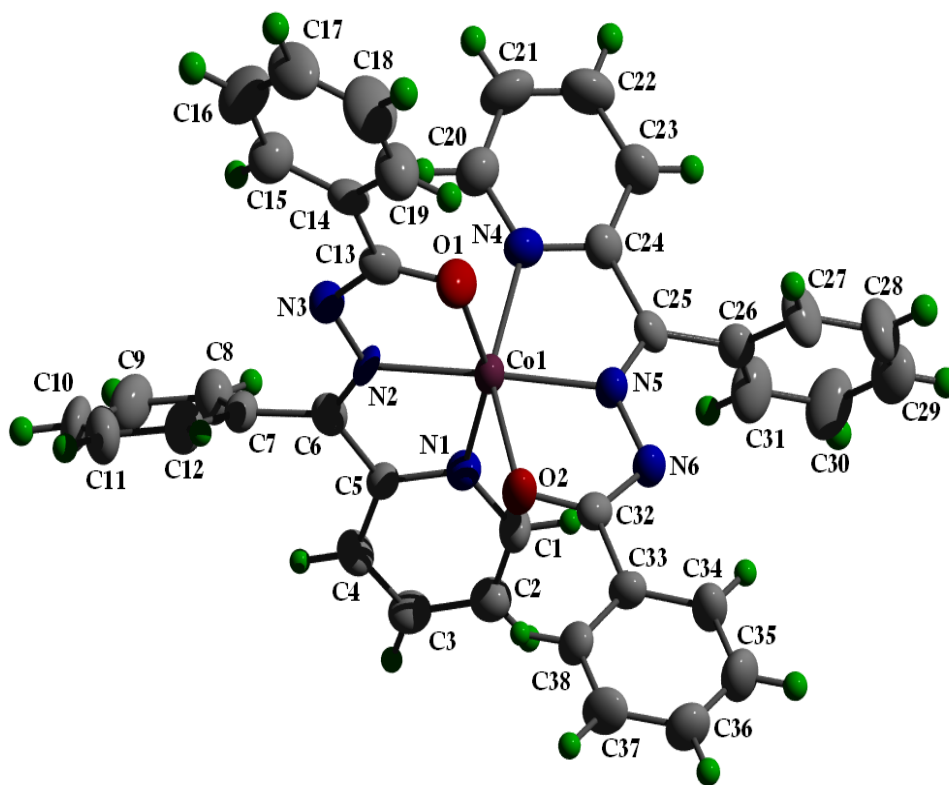


Fig. 5.12. The molecular structure of $[\text{Co}(\text{BPB})_2]$ (**6**) along with the atom numbering scheme (Displacement ellipsoids are drawn at the 50% probability level and hydrogen atoms are shown as small spheres of arbitrary radii).

There are no classic hydrogen bonds seen in the crystal structure. However some weak hydrogen bonding and $\text{C-H}\cdots\pi$ interactions including that between metal containing chelate ring $\text{Cg}(2)$ with the protons on $\text{C}(28)$ are seen in the crystal lattice (Table 5.6). The orientation in the close packing (Fig. 5.13) is in such a way that molecules are interconnected through weak hydrogen bonding interaction.

Table 5.6. H-bonding, π - π and C-H $\cdots\pi$ interaction parameters of [Co(BPB)₂] (6).

H-bonding				
Donor \cdots H \cdots A (Å)	D-H	H \cdots A	D \cdots A	D-H \cdots A
C27-H(27) \cdots N(6) ^a	0.93	2.60	3.3228	139
π - π interactions				
Cg(I) \cdots Cg(J)	Cg-Cg (Å)	α (°)	β (°)	
Cg(5) \cdots Cg(5) ^b	3.8114	0.00	22.40	
C-H $\cdots\pi$ interaction				
X-H(I) \cdots Cg(J)	H \cdots Cg (Å)	X-H \cdots Cg (°)	X \cdots Cg (Å)	
C(28)-H(28) \cdots Cg(2) ^c	2.79	138	3.5378	
Equivalent position codes				
a = 1-x, 1-y, 1-z, b = 2-x, -x, 1-z, c = 1-x, 1-y, 1-z				
Cg(5) = N(1), C(1), C(2), C(3), C(4), C(5), Cg(2) = Co(1), O(2), C(32), N(6), N(5)				

D, donor; A, acceptor; Cg, centroid; α , dihedral angles between planes I and J; β , Cg(I) – Cg(J) vector normal to plane I

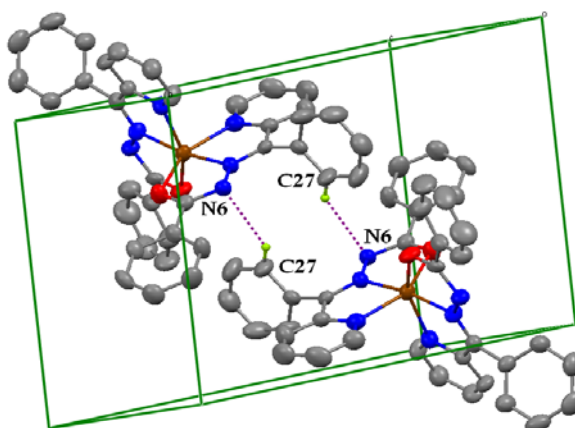


Fig. 5.13. Packing diagram of [Co(BPB)₂] (6) showing the hydrogen bonding interactions.

References

- [1] P.V. Bernhardt, J. Mattsson, Des R. Richardson, *Inorg. Chem.* 45 (2006) 752.
- [2] M.B. Ferrari, F. Bisceglie, C. Casoli, S. Durot, I.M. Badarau, G. Pelosi, E. Pilotti, S. Pinelli, P. Tarasconi, *J. Med. Chem.* 48 (2005) 1671.

- [3] W.J. Geary, *Coord. Chem. Rev.* 7 (1971) 109.
- [4] M.S. Refat, S. Chandra, M. Tyagi, *Therm. Anal. Calorim.* 100 (2009) 261.
- [5] A.A.A. Abu-Hussen, W. Linert, *Spectrochim. Acta Part A* 74 (2009) 214.
- [6] S. Naskar, D. Mishra, R.J. Butcher, S.K. Chattopadhyay, *Polyhedron* 26 (2007) 3703.
- [7] R.M. Issa, A.A. Hassanein, I.M. El-Mehasseb, R.I.A. El-Wadoud, *Spectrochim. Acta Part A* 65 (2006) 206.
- [8] R.C. Maurya, S. Rajput, *J. Mol. Struct.* 833 (2007) 133.
- [9] U.O. Ozmen, G. Olgun, *Spectrochim. Acta Part A* 70 (2008) 641.
- [10] A.A.R. Despaigne, J.G. Da Silva, A.C.M. do Carmo, O.E. Piro, E.E. Castellano, H. Beraldo, *J. Mol. Struct.* 920 (2009) 97.
- [11] X.-H. Chen, Q.-J. Wu, Z.-Y. Liang, C.-R. Zhang, J.-B. Liu, *Acta Cryst.* 65 (2009) 190
- [12] K. Nakamoto, *Infrared and Raman spectra of Inorganic and Coordination compounds*, 5th ed., Wiley, New York, 1997.
- [13] M. Joseph, M. Kuriakose, M.R.P. Kurup, E. Suresh, A. Kishore, S.G. Bhat, *Polyhedron* 25 (2006) 61.
- [14] V. Suni, M.R.P. Kurup, M. Nethaji, *Polyhedron* 26 (2007) 5203.
- [15] S. AbouEl-Enein, F.A. El-Saied, S.M. Emam, M.A. Ell-Salamony, *Spectrochim. Acta Part A* 71 (2008) 421.
- [16] A.B.P. Lever, *Inorganic Electronic Spectroscopy*, 2nd edition, Elsevier, Amsterdam, 1984.
- [17] K.A. Ketcham, J.K. Swearingen, A. Castineiras, I. Garcia, E. Bermejo, D.X. West, *Polyhedron* 20 (2001) 3265.
- [18] A. Panja, D.M. Eichhorn, *J. Coord. Chem.* 62 (2009) 2600.
- [19] M. Sonmez, M.R. Bayram, M. Celebi, *J. Coord. Chem.* 62 (2009) 2728.

- [20] G.M. Sheldrick, SHELXTL98, Version 5.1, Bruker AXS, Inc., Madison, Wisconsin, USA (1999).
- [21] K. Brandenburg, Diamond Version 3.1f, Crystal Impact GbR, Bonn, Germany, 2008.
- [22] C.F. Macrac, P.R. Edington, P. McCabe, E. Pidcock, G.P. Shields, R. Taylor, M. Towler, J. Van de Streek, *J. Appl. Cryst.* 39 (2006) 453.
- [23] C.M. Armstrong, P.V. Bernhardt, P. Chin, Des R. Richardson, *Eur. J. Inorg. Chem.* (2003) 1145.
- [24] N. Bouslimani, N. Clement, G. Rogez, P. Turek, S. Choua, S. Dagorne, R. Welter, *Inorg. Chim. Acta* 363 (2010) 213.
- [25] A. Ray, S. Banerjee, S. Sen, R.J. Butcher, G.M. Rosair, M.T. Garland, S. Mitra, *Struct. Chem.* 19 (2008) 209.
- [26] A.S. Pedrares, N. Camina, J. Romero, M.L. Duran, J.A.G. Vazquez, A. Sousa, *Polyhedron* 27 (2008) 3391.
- [27] N.A. Mangalam, S. Sivakumar, M.R.P. Kurup, E. Suresh, *Spectrochim. Acta A* 75 (2010) 686.
- [28] S. Banerjee, A. Ray, S. Sen, S. Mitra, D.L. Hughes, R.J. Butcher, S.R. Batten, D.R. Turner, *Inorg. Chim. Acta* 361 (2008) 2692.

Chapter 6

Syntheses, spectral and structural characterization of nickel(II) complexes incorporating tridentate acylhydrazones

Contents

- 6.1 Introduction
 - 6.2 Experimental
 - 6.3 Results and discussion
 - References
-

6.1. Introduction

The chemistry of nickel is much simpler than that of other first row transition elements. The only oxidation state of importance is Ni(II) and these compounds are stable. Ni(II) is the d^8 ion and is able to form square planar complexes as well as octahedral ones. Ligands with large crystal field favor square planar coordination, because of the more favorable CFSE.

Coordination polymers are presently playing a prominent role in material science and their potential as functional materials is clearly recognized. Supramolecular architectures of the coordination complexes through hydrazone ligand-based hydrogen-bonding interactions are very rare and yet not explored. Earlier many authors reported several coordination complexes derived by acylhydrazones for their pharmacological activity and

magnetic properties but such complexes were devoid of any hydrogen bonding interactions that could generate supramolecular architectures with intriguing structures [1,2]. Recently Chattopadhyay and his group have shown how the supramolecular architectures of Mn(II) acylhydrazone complexes can be controlled by slight modification of the substituents attached to the ligand framework [3]. The self assembly of multimetallic assemblies held together by intermolecular forces (hydrogen bonds, van der Waals forces *etc.*) is greatly dependent on the metal ions. The interactions of hydrogen bonds play vital roles for molecular recognition in a wide variety of biological systems and have also been applied in the synthesis of molecular magnetic materials. The ligand based hydrogen bonding interactions with solvent molecules are also responsible for generating 3 D supramolecular architectures in these types of complexes.

6.2. Experimental

6.2.1. Materials

Di-2-pyridylketone (Aldrich), 2-benzoylpyridine (Aldrich), benzhydrazide (Aldrich), and nicotinic hydrazide (Aldrich), nickel(II) perchlorate hexahydrate (Fluka), nickel(II) acetate tetrahydrate (C.D.H. Chemicals) and potassium thiocyanate (Merck) were used as received. Solvents were purified by standard procedures before use.

6.2.2. Syntheses of the acylhydrazones

The syntheses of hydrazones HBPB and HDKN are discussed already in Chapter 2.

6.2.3. Syntheses of the complexes

6.2.3.1. Synthesis of $[Ni(BPB)_2]$ (**10**)

To a methanolic solution of HBPB (0.301 g, 1 mmol), nickel(II) acetate tetrahydrate (0.248 g, 1 mmol) in methanol was added. The reaction mixture was refluxed for 3 h. The dark colored solution was allowed to stand at room temperature and after slow evaporation, dark crystalline product was separated, filtered and washed with ether and dried over P_4O_{10} *in vacuo*.

$[Ni(BPB)_2]$ (**10**): Yield: 71%, λ_m (DMF): 13 $\text{ohm}^{-1}\text{cm}^2 \text{mol}^{-1}$, μ (B.M.): 2.74, Elemental Anal. Found (Calcd.) (%): C: 69.02 (69.22), H: 4.12 (4.28), N: 12.43 (12.75), Ni: 8.38 (8.90).

6.2.3.2. Synthesis of $[Ni(HBPB)(BPB)]ClO_4$ (**11**)

Nickel(II) perchlorate hexahydrate (0.365 g, 1 mmol) is dissolved in 10 ml methanol and the metal salt solution was added dropwise to a 20 ml methanolic solution HBPB (0.301 g, 1 mmol) with stirring. The reaction mixture was refluxed for 3 h. at 40 °C. The resulting deep colored solution was left undisturbed at room temperature and after slow evaporation, the brown crystalline product was separated, filtered and washed with ether and dried over P_4O_{10} *in vacuo*.

$[Ni(HBPB)(BPB)]ClO_4$ (**11**): Yield: 61%, λ_m (DMF): 83 $\text{ohm}^{-1}\text{cm}^2 \text{mol}^{-1}$, μ (B.M.): 2.88, Elemental Anal. Found (Calcd.) (%): C: 59.56 (60.07), H: 3.66 (3.85), N: 10.91 (11.06), Ni: 7.77 (7.72).

6.2.3.3. Synthesis of $[Ni(DKN)_2]$ (**12**)

The ligand HDKN (0.312 g, 1 mmol) was dissolved in methanol and to this nickel(II) acetate tetrahydrate (0.248 g, 1 mmol) dissolved in the same solvent was added dropwise. The resulting solution was refluxed for 3 h. and was

allowed to stand at room temperature and after slow evaporation, brown crystalline product was separated within 2-3 days, which was filtered and washed with ether and dried over P_4O_{10} *in vacuo*.

[Ni(DKN)₂] (**12**): Yield: 74%, λ_m (DMF): 6 $\text{ohm}^{-1}\text{cm}^2 \text{mol}^{-1}$, μ (B.M.): 2.77, Elemental Anal. Found (Calcd.) (%): C: 61.02 (61.56), H: 3.54 (3.65), N: 20.84 (21.12), Ni: 8.57 (8.85).

6.2.3.4. Synthesis of [Ni(DKN)NCS]·H₂O (**13**)

To a methanolic solution of HDKN (0.312 g, 1 mmol), an aqueous solution of KSCN (0.097 g, 1 mmol) was added and stirred for half an hour. To this solution, nickel(II) acetate tetrahydrate (0.248 g, 1 mmol) in the same solvent was added and the reaction mixture was refluxed for 3 h. The resulting green colored solution was allowed to stand at room temperature and after slow evaporation, a green product was separated, filtered and washed with ether and dried over P_4O_{10} *in vacuo*.

[Ni(DKN)NCS]·H₂O (**13**): Yield: 65%, λ_m (DMF): 19 $\text{ohm}^{-1}\text{cm}^2 \text{mol}^{-1}$, μ (B.M.): 3.30, Elemental Anal. Found (Calcd.) (%): C: 49.22 (49.46), H: 3.18 (3.23), N: 18.91 (19.23), Ni: 13.20 (13.43).

Caution! Although [Ni(HBPB)(BPB)]ClO₄ has not yet proved to be mechanistically sensitive, such perchlorates are potentially explosive and should be handled with due caution.

6.3. Results and discussion

6.3.1. Elemental analyses

The analytical data indicate that the observed C, H, N values are consistent with the formulae suggested for the complexes. The metal content % of the

complexes was determined by AAS after digestion with con. HNO_3 and is found to be in good agreement with that of the theoretical results.

6.3.2. Molar conductivity and magnetic susceptibility measurements

The molar conductances of the complexes **10**, **12**, **13** in DMF are in the range 6-19 $\text{ohm}^{-1}\text{cm}^2 \text{mol}^{-1}$, which are well below the range (65-90 $\text{ohm}^{-1}\text{cm}^2 \text{mol}^{-1}$) observed for uni-univalent electrolytes in this solvent, indicating that the hydrazones are coordinated to the Ni(II) ion as a uninegatively charged chelating agent and that the thiocyanate ion is also coordinated to the Ni(II) ion in the thiocyanato complex. The complex $[\text{Ni}(\text{HBPB})(\text{BPB})]\text{ClO}_4$ has a molar conductivity of 83 $\text{ohm}^{-1}\text{cm}^2 \text{mol}^{-1}$ indicating a 1:1 electrolyte [4]. Effective magnetic moments of the complexes were calculated from molar magnetic susceptibilities. All the nickel complexes were found to be paramagnetic which excludes the possibility of a square planar configuration. Complexes **10-12** have magnetic moments in the range 2.74-2.88 B.M. as predicted for a high spin d^8 system with two unpaired electrons [5,6]. These values provide evidence for a six coordinated Ni(II) ion with octahedral geometries. For complex **13**, magnetic moment was found to be 3.30 B.M. which was slightly greater than the spin only value which may be due to the orbital contribution. This suggest a tetrahedral geometry which was similar to that reported in other Ni(II) tetrahedral complexes [7].

6.3.3. Infrared spectra

The IR bands that are considered most useful in ascertaining the mode of coordination of the hydrazones to the Ni(II) ion are summarized in Table 6.1. The IR spectrum of HBPB in the solid state, exhibits bands corresponding to $\nu(\text{NH})$ and $\nu(\text{C}=\text{O})$ stretches indicating that in the solid state, it remains mainly in the amido form [8]. However in solution and in the presence of metal salts, it readily converts to the iminol tautomeric form with the concomitant formation of

Ni(II) complex of the deprotonated *enolate* form of the ligand [9]. On the other hand, the band corresponding to the stretching vibration of the azomethine group of the hydrazone is shifted to 1547 cm^{-1} in the IR spectrum of $[\text{Ni}(\text{BPB})_2]$ (Fig. 6.1), indicating the coordination of the azomethine nitrogen to the central metal ion [10]. The increase in the frequency of the $\nu(\text{N-N})$ band in the spectrum of the complex, due to the increase in the bond strength, again confirms coordination *via* azomethine nitrogen. IR spectrum of the complex showed a sharp band at 1580 cm^{-1} due to the newly formed $\nu(\text{C=N})$ bond, indicating the coordination of oxygen in enolate form rather than the amido form [11]. A medium band at 650 cm^{-1} , indicating pyridyl in-plane and out-of-plane ring deformation in the uncomplexed hydrazone, shifts to higher frequencies on complexation which confirms the coordination of the hydrazone to the metal ion *via* the pyridyl nitrogen [12].

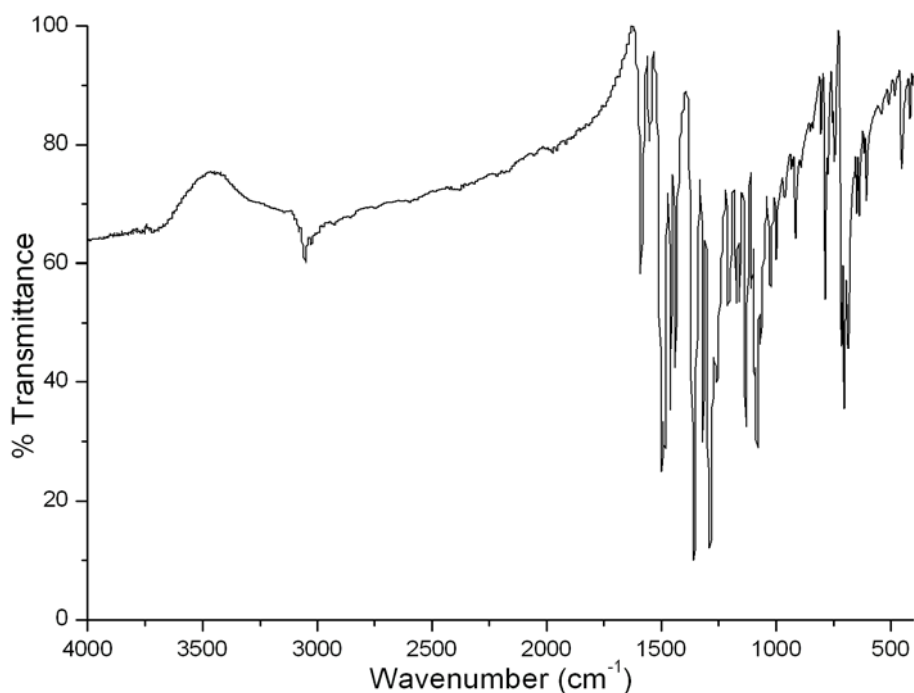


Fig. 6.1. IR spectrum of $[\text{Ni}(\text{BPB})_2]$ (10).

Unlike in other complexes, in complex **11** the $\nu(\text{C}=\text{O})$ band is only slightly shifted to lower wavenumber, this could be attributed to the fact that one of the coordinated ligand is not deprotonated. Also the strong bands at 1087 and 620 cm^{-1} (Fig. 6.2), assignable to $\nu_3(\text{ClO}_4)$ and $\nu_4(\text{ClO}_4)$ respectively indicates the presence of ionic perchlorate [13,14]. The perchlorate anion exists as counteranion to neutralize the positive charge of the central metal ion. The presence of ClO_4^- as counteranion was also supported by its molar conductivity value of $83 \text{ ohm}^{-1}\text{cm}^2 \text{ mol}^{-1}$.

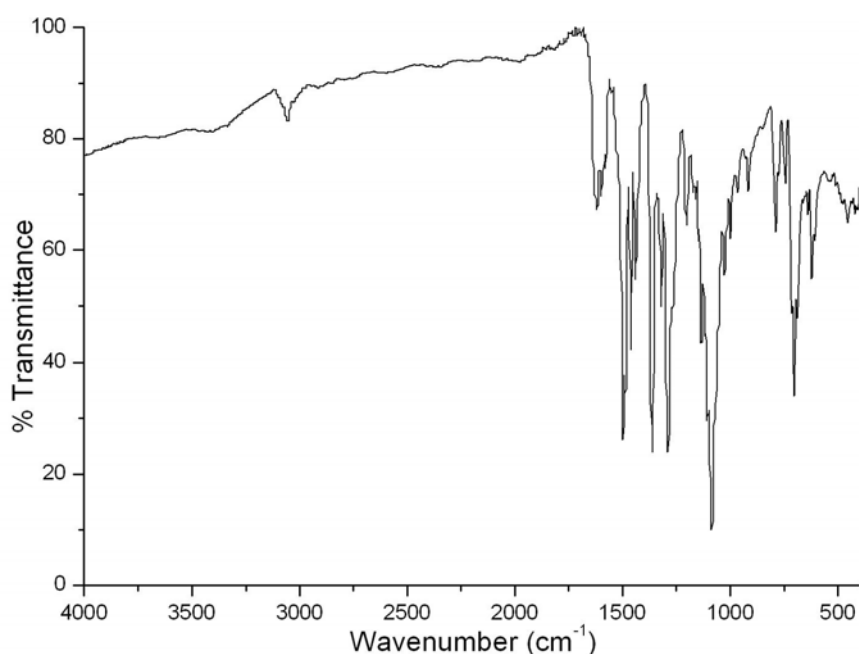


Fig. 6.2. IR spectrum of $[\text{Ni}(\text{HBPB})(\text{BPB})]\text{ClO}_4$ (**11**).

The coordination in $[\text{Ni}(\text{DKN})_2]$ is similar to that in $[\text{Ni}(\text{BPB})_2]$, IR data support coordination of HDKN to the Ni(II) ion *via* the azomethine nitrogen atom (shift of the $\nu(\text{C}=\text{N})$ from 1579 cm^{-1} in the ligand to 1557 cm^{-1} in the complex) (Fig. 6.3) and the pyridine nitrogen atom (shift of the pyridine ring deformation mode from 650 to 690 cm^{-1}).

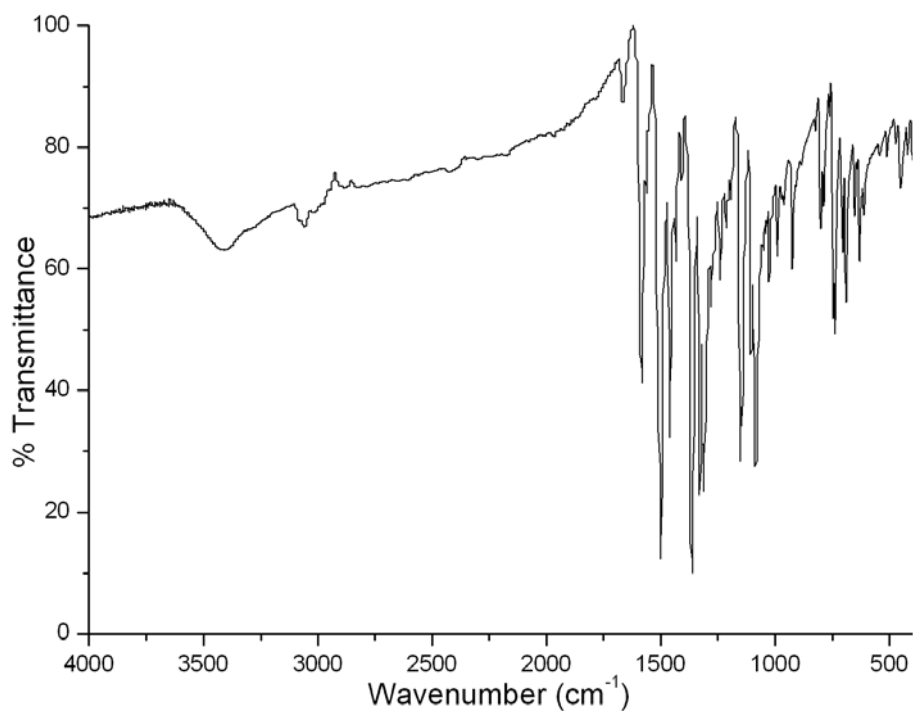


Fig. 6.3. IR spectrum of [Ni(DKN)₂] (12).

In the IR spectrum of the thiocyanato complex, the most important part lies in the 2000-2100 cm^{-1} region. The characteristic CN stretching frequency of NCS group is observed at 2081 cm^{-1} (Fig. 6.4) which reveals the coordination through the nitrogen atom of the -NCS group [15]. The N-bonded nature of the thiocyanate group is further supported by several low intensity bands around 480 cm^{-1} . However, these bands are weak and tend to be obscured by other bands. The broad band at 3380 cm^{-1} may be due to the presence of lattice water in the complex, which was also evident from the thermogravimetric analysis.

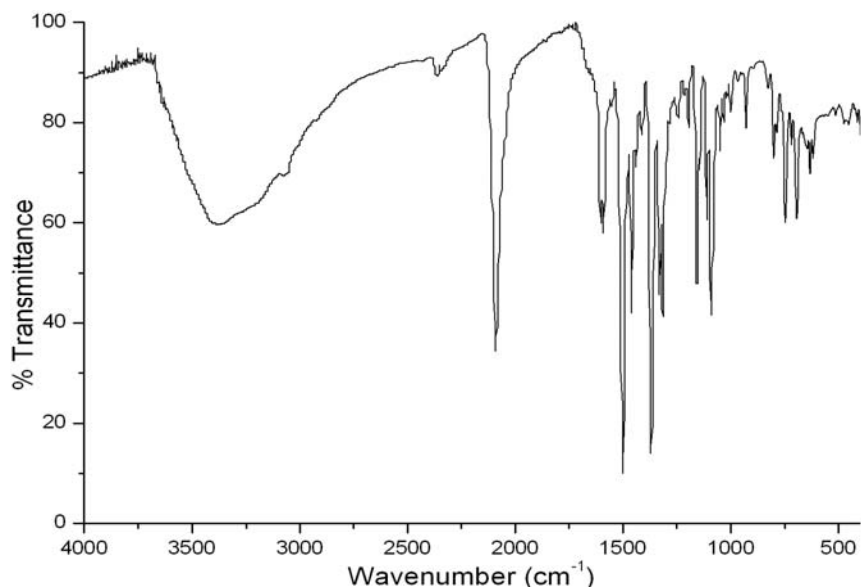


Fig. 6.4. IR spectrum of $[\text{Ni}(\text{DKN})\text{NCS}] \cdot \text{H}_2\text{O}$ (**13**).

Table 6.1. Infrared spectral data (cm^{-1}) of Ni(II) complexes.

Compound	$\nu(\text{N-H})$	$\frac{\nu(\text{C=O})}{\nu(\text{C-O})}$	$\nu(\text{C=N})$	$\nu(\text{C=N})^a$	$\nu(\text{Ni-O})$	$\nu(\text{Ni-N})$
HBPB	3063	1678	1571
$\text{Ni}(\text{BPB})_2$ (10)	...	1353	1547	1580	542	452
$[\text{Ni}(\text{HBPB})(\text{BPB})]\text{ClO}_4$ (11)	...	1620, 1365	1503	1585	540	454
HDKN	2928	1689	1579
$[\text{Ni}(\text{DKN})_2]$ (12)	...	1361	1557	1581	520	451
$[\text{Ni}(\text{DKN})\text{NCS}] \cdot \text{H}_2\text{O}$ (13)	...	1367	1507	1594	510	452

^aNewly formed C=N

6.3.4. Electronic spectra

The electronic absorption spectra of the complexes were recorded in 10^{-4} M acetonitrile solution and data are gathered in Table 6.2. The spectra of the complexes **10-13** in the region $45,000\text{-}20,000 \text{ cm}^{-1}$ are shown in Fig. 6.5. The higher energy bands in the region $30970\text{-}41030 \text{ cm}^{-1}$ can be assigned to the intraligand transitions. The strong absorption bands *ca.* 25130 cm^{-1} can be

assigned for the charge transfer transition [16] from the coordinated unsaturated ligand to the metal ion (enolate O → Ni(II)).

Three spin allowed transitions ${}^3T_{2g}(F) \leftarrow {}^3A_{2g}(F)$, ${}^3T_{1g}(F) \leftarrow {}^3A_{2g}(F)$, ${}^3T_{1g}(P) \leftarrow {}^3A_{2g}(F)$ are expected for Ni(II) octahedral complexes. The ${}^3T_{2g}(F) \leftarrow {}^3A_{2g}(F)$ band is expected in the near IR region and the higher energy band ${}^3T_{1g}(P) \leftarrow {}^3A_{2g}(F)$ is usually obscured by strong charge transfer transitions. In addition, two spin forbidden bands are usually quite prominent, one ${}^1E_g \leftarrow {}^3A_{2g}$ near the second spin allowed transition and the second, primarily to ${}^1T_{2g}$ between the second and third spin allowed band. Indeed the 1E_g state lies so close to ${}^3T_{1g}$ that extensive mixing takes place leading to observation of a doublet band where the spin forbidden transition has stolen intensity from the spin allowed transition. It is not properly correct to assign one component of the doublet to 1E_g and other to ${}^3T_{1g}$, they are scrambled, by the mechanism of spin orbit coupling [17,18]. In Ni(II) complexes with tetrahedral stereochemistry also three transitions are expected ${}^3T_2(F) \leftarrow {}^3T_1(F)$, ${}^3A_2(F) \leftarrow {}^3T_1(F)$, ${}^3T_1(P) \leftarrow {}^3T_1(F)$; but unfortunately the *d-d* bands are obscured by the high intense charge transfer transitions in these complexes [19].

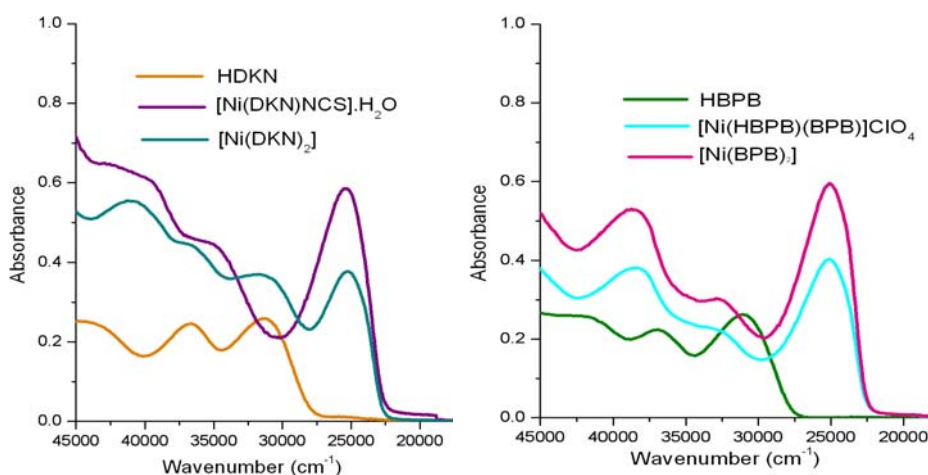


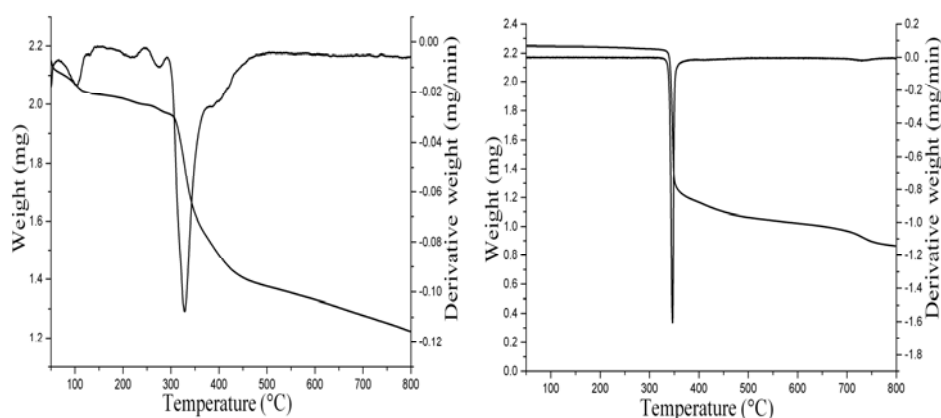
Fig. 6.5. Electronic spectra of the Ni(II) complexes in the region 45,000-20,000 cm^{-1} .

Table 6.2. Electronic spectral data of Ni(II) complexes.

Compound	UV-vis absorption bands (cm ⁻¹)
[Ni(BPB) ₂] (10)	38520, 32610, 24950
[Ni(HBPB)(BPB)]ClO ₄ (11)	38520, 32600, 25070
[Ni(DKN) ₂] (12)	41030, 36500, 30970, 25190
[Ni(DKN)NCS]·H ₂ O (13)	40900, 34750, 25320

6.3.5. Thermal analyses

The presence of lattice water in the hydrated complex was confirmed from thermogravimetric analyses. TGA studies for all the complexes except **11** were carried out from 50-800 °C in nitrogen atmosphere at a heating rate of 10 °C/min and selected TG-DTG curves are shown in Fig. 6.6. The TGA profiles of the complexes **10** and **12** show that they are stable up to 320 °C but decompose on further increasing the temperature. The TGA curve for the hydrated complex **13** displays two stages of decomposition in which first stage of decomposition occurs in the range 55-115 °C, which corresponds to the loss of a water molecule with 3.67 % of the total weight of the complex (Calcd. 4.11%).

**Fig. 6.6.** TG-DTG curves of [Ni(BPB)₂] (**10**) (left) and [Ni(DKN)NCS]·H₂O (**13**) (right).

6.3.6. X-ray crystallography

Reddish-brown block shaped crystal of $[\text{Ni}(\text{DKN})_2]\cdot\text{H}_2\text{O}$ ($0.32 \times 0.28 \times 0.25 \text{ mm}^3$) obtained by slow evaporation from its methanolic solution were selected and structure diffraction intensities were collected at 150 K on a CrysAlis CCD diffractometer using multi scan technique with graphite monochromated $\text{Mo K}\alpha$ ($\lambda = 0.71073 \text{ \AA}$) radiation. The structure was solved with direct methods and refined with full-matrix least-squares technique using the SHELXS-97 and SHELXL-97 programs [20], respectively. Anisotropic displacement parameters were applied to all non-hydrogen atoms. The hydrogen atoms were generated geometrically, and refined with isotropic displacement parameters. The hydrogen atoms of the lattice water could not located by difference Fourier map. Crystal data as well as details of data collection and refinement for the complex are summarized in Table 6.3.

The molecular structure of $[\text{Ni}(\text{DKN})_2]\cdot\text{H}_2\text{O}$ showing the atom labelling scheme (Fig. 6.7) was drawn with 50% displacement ellipsoids using DIAMOND [21] and the remaining figures (Figs. 6.8, 6.9) showing the packing were drawn using MERCURY [22].

Table 6.3. Crystal data and structure refinement parameters for [Ni(DKN)₂] \cdot H₂O (**12**).

Parameters	[Ni(DKN) ₂] \cdot H ₂ O (12)
Empirical Formula	C ₃₄ H ₂₄ NiN ₁₀ O ₃
Formula weight (M)	1342.64
Temperature (T) K	150(2)
Wavelength (Mo K α) (Å)	0.71073
Crystal system	Monoclinic
Space group	<i>P</i> 2 ₁
Lattice constants	
<i>a</i> (Å)	9.2909(8)
<i>b</i> (Å)	10.0192(6)
<i>c</i> (Å)	16.5802(19)
α (°)	90.00
β (°)	100.993(9)
γ (°)	90.00
Volume <i>V</i> (Å ³)	1515.1(2)
<i>Z</i>	1
Calculated density (ρ) (Mg m ⁻³)	1.472
Absorption coefficient, μ (mm ⁻¹)	0.693
Limiting Indices	-11 \leq h \leq 7 -11 \leq k \leq 8 -19 \leq l \leq 19
Reflections collected	7787
Unique Reflections	4211 [R(int) = 0.0416]
Refinement method	Full-matrix least-squares on <i>F</i> ²
Data / restraints / parameters	4211 / 1 / 433
Goodness-of-fit on <i>F</i> ²	1.070
Final <i>R</i> indices [<i>I</i> > 2 σ (<i>I</i>)]	<i>R</i> ₁ = 0.0375, <i>wR</i> ₂ = 0.0913
<i>R</i> indices (all data)	<i>R</i> ₁ = 0.0455, <i>wR</i> ₂ = 0.0958

$$wR_2 = [\sum w(F_o^2 - F_c^2)^2 / \sum w(F_o^2)^2]^{1/2}; R_1 = \sum ||F_o| - |F_c|| / \sum |F_o|$$

6.3.6.1. Crystal structure of [Ni(DKN)₂] \cdot H₂O (**12**)

The molecular structure of the bis-ligand complex, [Ni(DKN)₂] \cdot H₂O (Fig. 6.7) shows that it is monomeric, with each ligand coordinating to the Ni(II) ion in a tridentate manner in a monodeprotonated enolate form, giving a six-coordinate environment for the Ni(II) complex. The selected bond lengths and angles are

given in Table 6.4. The disposition of the two ligands in the complex is such that the meridional isomer is obtained (N_{py} and $O_{enolate}$ atoms *cis* to each other and N_{azo} atoms *trans*), probably due to the rigidity of the tridentate ligand. The coordination sphere around Ni(II) ion in the complex may be described as a distorted octahedron. All the angles subtended at the Ni(II) ion by donor atoms show marked deviation from that expected for an ideal octahedral geometry. These angles are the main cause of distortion from a regular octahedral geometry. In this way the complex has two *cis* O–Ni–N bond angles $155.05(12)^\circ$ and $155.11(11)^\circ$, where donor atoms from the same ligand are involved, and a *trans* N–Ni–N bond angle $172.42(14)^\circ$, which involves donor atoms from two different ligands. A comparison of bond angles of $[Ni(DKN)_2]$ with those of the related six-coordinate complexes of similar ligands shows that, the angles compare well with each other [23], but were far from those expected for an ideal octahedral geometry. The *trans* angle N3–Ni1–N8 is $172.42(14)^\circ$ gives clear evidence for the deviation from perfect octahedron. The intraligand bite angles are in the range $76.97(13)$ – $78.16(13)^\circ$, but was more acute in its Mn(II) complex (70.85° – 72.41°) which was already discussed in Chapter 4.

Coordination of the ligand to the metal gives rise to the formation of two five-membered rings with O–Ni–N chelate angles $76.97(13)$ and $77.52(11)^\circ$ and N–Ni–N chelate angles $78.12(13)$ and $78.16(13)^\circ$, in both case these values are low and outside the theoretical value expected for a regular geometry. Each bicyclic chelate system, $\{N1, C5, C6, N3, N4, C12, O1, Ni1\}$ and $\{N6, C22, C23, N8, N9, C29, O2, Ni1\}$ is approximately planar as evidenced by the maximum deviation of 0.0834 \AA for N3 and 0.0818 \AA for Ni1 respectively. They are placed nearly perpendicular to each other with a dihedral angle of 85.78° . Three different types of bond distances can be found in the complex and these correspond to the three types of donor atoms that exist in the ligand. In general, all of the bond distances between metal and the donor atoms in question can be

considered normal and are similar to those found in other compounds that contain similar monoanionic tridentate hydrazone ligands with the metal in an octahedral environment [23,24]. In this complex, the Ni–N(iminic) bond distances are smaller compared to Ni–O and Ni–N(pyridyl) bond distances.

As far as the structural parameters of the complex are concerned, it is worthy to highlight the variation observed in some of the bond distances in comparison to those found in the free ligand. Although the crystal structure of the free ligand HDKN is not available, structural data for similar ligands are known. In these compounds the C–O bond lengths are in the range 1.217–1.232 Å and C–N(amide) bond lengths are in the range 1.265–1.302 Å [25–27]. Comparison of these values with those found in this complex shows that the corresponding C–O distance 1.268 Å, is slightly longer whereas the C–N(amide) distance 1.288 Å, is shorter even though this bond length is less affected. These data are consistent with the increased conjugation experienced by the hydrazone in its deprotonated form.

There is one lattice water per molecule and the water molecule forms hydrogen bonds with one of the pyridyl nitrogen (N2) of one of the molecule and to the nicotinic nitrogen (N3) of other molecule. Thus adjacent molecules are thus linked into chains by these interactions as shown in Fig. 6.8. These chains form 2 D sheets and results in a two dimensional polymeric structure parallel to [010] plane (Fig. 6.9). In addition, the packing is stabilized by C–H \cdots π interaction (Table 6.5).

Table 6.4. Selected bond lengths (Å) and bond angles (°) for [Ni(DKN)₂] \cdot H₂O.

Bond lengths		Bond angles	
Ni1–N3	1.996(3)	O1–C12–N4	127.0(4)
Ni1–N8	1.988(3)	N3–Ni1–N8	172.42(14)
Ni1–O1	2.107(3)	N3–Ni1–O1	76.97(13)
Ni1–O2	2.083(3)	N1–Ni1–N6	96.86(14)
Ni1–N1	2.104(4)	N8–Ni1–O2	77.52(11)
Ni1–N6	2.090(3)	N1–Ni1–N3	78.12(13)
N3–N4	1.372(5)	N6–Ni1–N8	78.12(13)
N8–N9	1.377(4)	O1–Ni1–O2	94.92(11)
N3–C6	1.288(6)	O1–Ni1–N1	155.05(12)
N8–C23	1.285(5)	O2–Ni1–N6	155.11(11)
C12–O1	1.268(5)	N3–Ni1–N6	97.53(13)
N4–C12	1.343(6)	N8–Ni1–N1	96.09(13)
N9–C29	1.322(5)	C6–N3–N4	120.8(3)

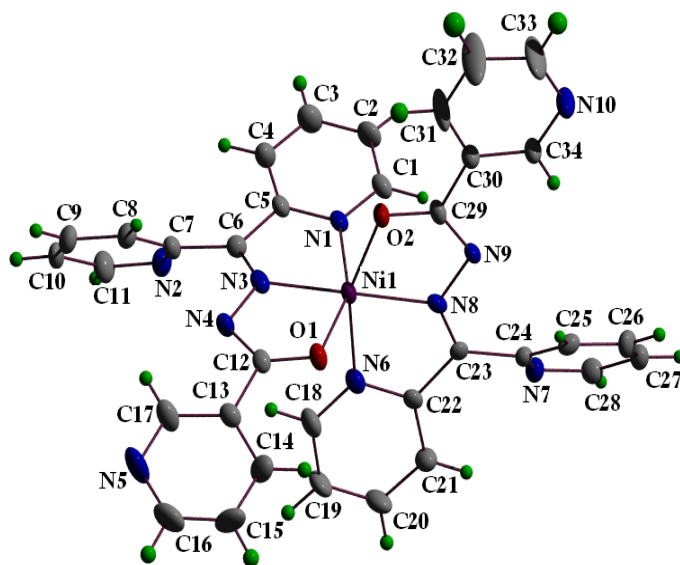


Fig. 6.7. The molecular structure of [Ni(DKN)₂] \cdot H₂O (**12**) along with the atom numbering scheme. The solvent water molecule has been omitted for reasons of clarity. (Displacement ellipsoids are drawn at the 50% probability level and hydrogen atoms are shown as small spheres of arbitrary radii).

Table 6.5. H-bonding, π - π and C-H $\cdots\pi$ interaction parameters of [Ni(DKN)₂] \cdot H₂O.

H-bonding				
Donor-H \cdots A (Å)	D-H	H \cdots A	D \cdots A	D-H \cdots A
C16-H(16) \cdots N(4) ^a	0.95	2.55	3.4856	169
C25-H(25) \cdots N(7) ^b	0.95	2.59	3.4805	156
C20-H(20) \cdots N(10) ^c	0.95	2.57	3.3796	144
C1-H(1) \cdots N(10) ^d	0.95	2.62	3.2985	129
C10-H(10) \cdots O(2) ^e	0.95	2.42	3.0794	126
π - π interactions				
Cg(I) \cdots Cg(J)	Cg-Cg (Å)		α (°)	β (°)
Cg(8) \cdots Cg(10) ^f	3.7353		7.65	26.57
C-H $\cdots\pi$ interaction				
X-H \cdots Cg(J)	H \cdots Cg (Å)		XH \cdots Cg (°)	X \cdots Cg (Å)
C(28)-H(28) \cdots Cg(2) ^g	2.59		151	3.4445

Equivalent position codes

a = 3-x, 1/2+y, 1-z, b = 2-x, 1/2+y, -z, c = 2-x, -1/2+y, -z, d = 1-x, -1/2+y, -z, e = 2-x, -1/2+y, 1-z, f = 1+x, y, z, g = 2-x, -1/2+y, -z

Cg(8) = N(6), C(18), C(19), C(20), C(21), C(22); Cg(10) = N(10), C(30), C(31), C(32), C(33), (34); Cg(2) = Ni(1), O(2), C(29), N(9), N(8)

D, donor; A, acceptor; Cg, centroid; α , dihedral angles between planes I and J; β , angle Cg(I) - Cg(J) vector normal to plane I

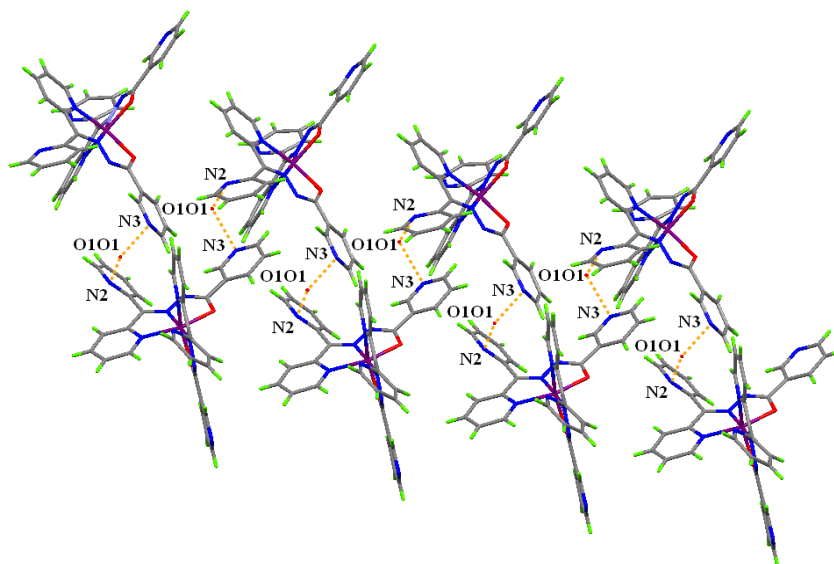


Fig. 6.8. Supramolecular chain mediated by intermolecular hydrogen bonding (orange dashed lines).

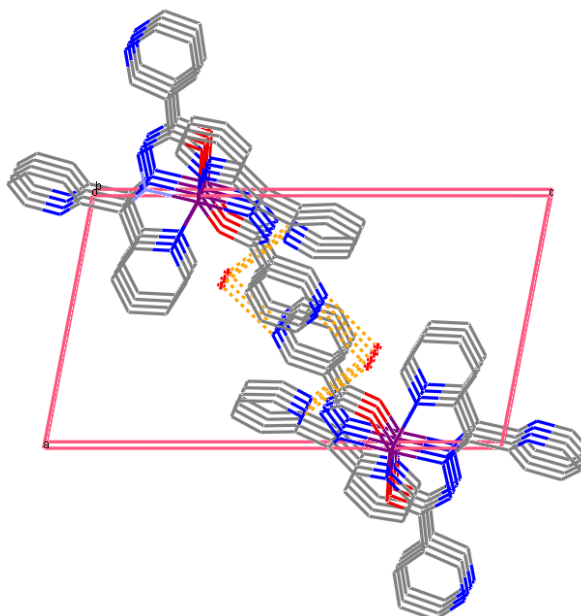


Fig. 6.9. Packing diagram showing two dimensional polymeric chain along crystallographic 'b' axis (hydrogen atoms are omitted for clarity).

References

- [1] E.W. Ainscough, A.M. Brodie, W.A. Denny, G.J. Finlay, S.A. Gothe, J.D. Ranford, *J. Inorg. Biochem.* 77 (1999) 125.
- [2] N. Bouslimani, N. Clement, G. Rogez, P. Turek, M. Bernard, S. Dagorne, D. Martel, H.N. Cong, R. Welter, *Inorg. Chem.* 47 (2008) 7623.
- [3] S. Naskar, M. Corbella, A.J. Blake, S.K. Chattopadhyay, *Daton Trans.* (2007) 1150.
- [4] W.J. Geary, *Coord. Chem. Rev.* 7 (1971) 109.
- [5] Y. Wang, Z.-Y. Yang, *J. Lumin.* 128 (2008) 373.

- [6] N.C. Kasuga, K. Sekino, C. Koumo, N. Shimada, M. Ishikawa, K. Nomiya, *J. Inorg. Biochem.* 84 (2001) 55.
- [7] A.A.A. Abu-Hussen, A.A.A. Emara, *J. Coord. Chem.* 57 (2004) 973.
- [8] T. Ghosh, S. Bhattacharya, A. Das, G. Mukherjee, M.G.B. Drew, *Inorg. Chim. Acta* 358 (2005) 989.
- [9] W. Luo, X.-Gao Meng, G.-Zheng Cheng, Z.-Ping Ji, *Inorg. Chim. Acta* 362 (2009) 551.
- [10] Md. A. Affan, S.W. Foo, I. Jusoh, S. Hanapi, E.R.T. Tiekink, *Inorg. Chim. Acta* 362 (2009) 5031.
- [11] J. Patole, U. Sandbhor, S. Padhye, D.N. Deobagkar, C.E. Anson, A. Powell, *Biorg. Med. Chem. Let.* 13 (2003) 51.
- [12] P.F. Rapheal, E. Manoj, M.R.P. Kurup, E. Suresh, *Polyhedron* 26 (2007) 607.
- [13] F. Hueso-Urena, A.L. Penas-Chamorro, M.N. Moreno-Carretero, J.M. Amigo, V. Esteve, T. Debaerdemaeker, *Polyhedron* 18 (1999) 2205.
- [14] K. Nakamoto, *Infrared and Raman spectra of Inorganic and Coordination compounds*, 5th ed., Wiley, New York, 1997.
- [15] S. Sen, S. Mitra, D.L. Hughes, G. Rosair, C. Desplanches, *Polyhedron* 26 (2007) 1740.
- [16] M. Asadi, K. Mohammadi, S. Esmailzadeh, B. Etemadi, H.-K. Fun, *Polyhedron* 28 (2009) 1409.
- [17] A.B.P. Lever, *Inorganic Electronic Spectroscopy*, 2nd edition, Elsevier, Amsterdam, 1984.
- [18] S.K. Dey, N. Mondal, M.S. El Fallah, R. Vicente, A. Escuer, X. Solans, M. Font-Bardia, T. Matsushita, V. Gramlich, S. Mitra, *Inorg. Chem.* 43 (2004) 2427.

- [19] P. Mukherjee, M.G.B. Drew, C.J. Gomez-Garc, A. Ghosh, *Inorg. Chem.* 48 (2009) 5848.
- [20] G.M. Sheldrick, *Acta Crystallogr. A* 64 (2008) 211.
- [21] K. Brandenburg, Diamond Version 3.1f, Crystal Impact GbR, Bonn, Germany, 2008.
- [22] C.F. Macrac, P.R. Edington, P. McCabe, E. Pidcock, G.P. Shields, R. Taylor, M. Towler, J. Van de Streek, *J. Appl. Cryst.* 39 (2006) 453.
- [23] B. Samanta, J. Chakraborty, S. Shit, S.R. Batten, P. Jensen, J.D. Masuda, S. Mitra, *Inorg. Chim. Acta* 360 (2007) 2471.
- [24] P.V. Bernhardt, J. Mattsson, Des R. Richardson, *Inorg. Chem.* 45 (2006) 752.
- [25] M. Bakir, O. Brown, *J. Mol. Struct.* 609 (2002) 129.
- [26] M. Kuriakose, M.R.P. Kurup, E. Suresh, *Spectrochim. Acta Part A* 66 (2007) 353.
- [27] M. Bakir, C. Gyles, *J. Mol. Struct.* 649 (2003) 133.

****ଝଞ****

Chapter 7

Syntheses, spectral and structural characterization of copper(II) complexes incorporating tridentate acylhydrazones

Contents

- 7.1 Introduction
 - 7.2 Experimental
 - 7.3 Results and discussion
 - References
-

7.1. Introduction

Copper ions as biologically essential substances have important roles such as oxygen carrier and charge transfer reactions. Copper(II) is an essential and spectroscopically well investigated metal ion in biological systems. The Jahn-Teller active ground state leads to structural properties which are not in a priori predictable by the classical molecular mechanics approach. Importantly copper is a center in the enzyme cytochrome c oxidase and superoxide dismutase. Both of these enzymes are thought to be determinants in diabetes by their roles in regulating oxidant status.

Cisplatin is a widely used and metal based drug for cancer therapy, but it possesses inherent limitations such as side effects and low administration dosage. Therefore attempts are being made to replace this drug with suitable

alternatives, and numerous transition metal complexes are synthesized and screened for their anticancer activities. Next to Ru(II) complexes, Cu(II) complexes are regarded as the most promising alternatives to cisplatin as anticancer substances. Copper(II) is known to play a significant role in biological systems and also as pharmacological agents. Synthetic Cu(II) complexes have been reported to act as potential anticancer and cancer inhibiting agents [1] and a number of copper complexes have been found to be active both *in vitro* and *in vivo* [2]. Recently it was reported that mixed ligand Cu(II) complexes of diimines could bind and cleave DNA and exhibit anticancer activity that is more efficient than that of cisplatin [3].

This chapter discuss the versatility of the coordination behavior of the acylhydrazones by incorporating different anions and pseudohalogens into copper precursor complexes by treating with various Cu(II) salts and coligands. The contemporary challenge to the synthetic inorganic chemists is to produce new compounds with preassigned magnetic properties and, for this, the rational synthetic design for the tuning of the solid state structure is important. Thus pseudohalide bridged complexes have drawn attention of many authors because of their diverse structural types and fascinating magnetic properties [4,5]. Among the larger number of bridging ligands, the azide anions are good choice as they can act as an efficient and versatile magnetic coupler owing to its different bridging modes, especially in $\mu_{1,1}$ (end-on, EO) or in $\mu_{1,3}$ (end-to-end, EE) (Chart 1) [6,7]. Great efforts have been devoted to the study of bridged polynuclear and dinuclear transition metal azides complexes. The literature survey indicates that a considerable number of works have been reported concerning the versatility of the azide ion [8,9]. Less literature is available for magneto-structural studies on copper(II) complexes containing bridged thiocyanate groups as this co-ligand is less efficient as a transmitter of magnetic interactions than

azide. From the magnetic point of view, the coordination modes of the azide and thiocyanate ligands greatly affect the nature and magnitude of the magnetic exchange interaction in these polynuclear pseudohalide complexes [10,11]. It is well established that the complexes with double symmetric EE bridges produce antiferromagnetic coupling, whereas symmetric EO bridges usually exhibit ferromagnetic coupling [12]. Furthermore, EE and EO bridging modes may simultaneously exist in the same species, leading to different topologies and magnetic properties [13]. The studies concerning magneto-structural correlation including theoretical calculations of this type of complexes have been done by several groups of researchers [14].

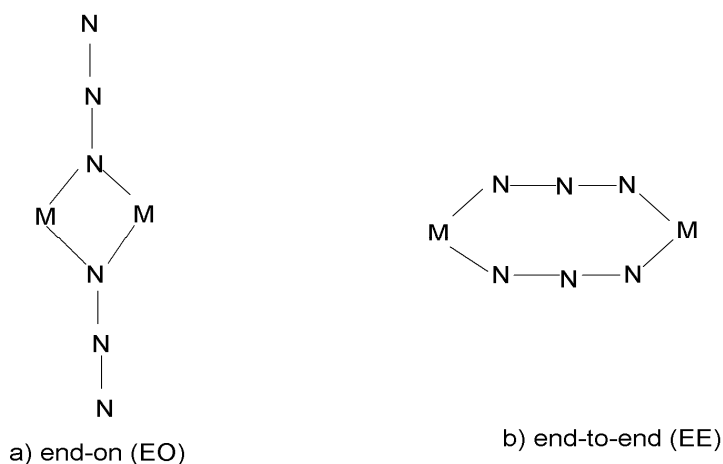


Chart 1. Different types of bridging modes of azide ion

7.2. Experimental

7.2.1. Materials

2-Benzoylpyridine (Aldrich), di-2-pyridyl ketone (Aldrich), benzhydrazide (Aldrich), nicotinic hydrazide (Aldrich), copper(II) acetate monohydrate (E-Merck), copper(II) chloride dihydrate (E-Merck), copper(II) bromide (Aldrich), copper(II) perchlorate hexahydrate (Aldrich), copper(II) sulfate pentahydrate (E-

Merck), sodium azide (Reidel-De Haen) and potassium thiocyanate (E-Merck) were used as received. Solvents were purified by standard procedures before use.

7.2.2. Syntheses of the acylhydrazones

The syntheses of hydrazones HBPB and HDKN are discussed already in Chapter 2.

7.2.3. Syntheses of the complexes

7.2.3.1. Synthesis of $[Cu(BPB)Br]$ (14)

To a methanolic solution of HBPB (0.301 g, 1 mmol), methanolic solution of $CuBr_2$ (0.218 g, 1 mmol) was added and the reaction mixture was refluxed for 3 h. The resulting solution was allowed to stand at room temperature and after slow evaporation, green product was separated, filtered and washed with ether and dried over P_4O_{10} *in vacuo*.

$[Cu(BPB)Br]$ (14): Yield: 68%, λ_m (DMF): $8 \text{ ohm}^{-1}\text{cm}^2 \text{ mol}^{-1}$, μ_{eff} (B.M.): 1.59, Elemental Anal. Found (Calcd.) (%): C: 52.01 (51.42), H: 3.62 (3.18), N: 9.50 (9.47), Cu: 13.92 (14.32).

7.2.3.2. Synthesis of $[Cu_2(BPB)_2(\mu-SO_4)]$ (15)

To a methanolic solution of $CuSO_4 \cdot 5H_2O$ (0.249 g, 1 mmol), methanolic solution of the hydrazone HBPB (0.301 g, 1 mmol) was added dropwise while the mixture was stirred. The final solution was refluxed for 4 h. and on slow evaporation green crystalline compound was separated after two days which was washed with methanol followed by ether and dried over P_4O_{10} *in vacuo*.

$[Cu_2(BPB)_2(\mu-SO_4)]$ (15): Yield: 73%, λ_m (DMF): $11 \text{ ohm}^{-1}\text{cm}^2 \text{ mol}^{-1}$, μ_{eff} (B.M.): 1.27, Elemental Anal. Found (Calcd.) (%): C: 54.96 (55.40), H: 3.22 (3.43), N: 9.89 (10.20), Cu: 15.42 (15.43).

7.2.3.3. Synthesis of [Cu(BPB)₂] (16)

Complex **16** was prepared by refluxing a mixture of methanolic solution of HBPB (0.301 g, 1 mmol) and Cu(CH₃COO)₂·H₂O (0.199 g, 1 mmol) for 5 hrs. The resulting solution was allowed to stand at room temperature and after slow evaporation, green crystalline compound was separated, filtered and washed with ether and dried over P₄O₁₀ *in vacuo*. Green block shaped crystals suitable for single crystal X-ray diffraction studies were obtained by the slow evaporation of its solution in methanol.

[Cu(BPB)₂] (**16**): Yield: 88%, λ_m (DMF): 6 ohm⁻¹cm² mol⁻¹, μ_{eff} (B.M.): 1.63, Elemental Anal. Found (Calcd.) (%): C: 69.32 (68.71), H: 4.28 (4.25), N: 12.05 (12.65), Cu: 10.15 (9.57).

7.2.3.4. Synthesis of [Cu(DKN)Br] (17)

A solution of CuBr₂ (0.218 g, 1 mmol) in methanol was mixed with a solution of the hydrazone HDKN (0.312 g, 1 mmol) in the same solvent and the resulting mixture was refluxed for 3 h. The resulting green solid was filtered, washed several times with methanol and ether and dried over P₄O₁₀ *in vacuo*.

[Cu(DKN)Br] (**17**): Yield: 78%, λ_m (DMF): 12 ohm⁻¹cm² mol⁻¹, μ_{eff} (B.M.): 1.86, Elemental Anal. Found (Calcd.) (%): C: 45.26 (45.81), H: 2.96 (2.71), N: 15.20 (15.71), Cu: 14.63 (14.26).

7.2.3.5. Synthesis of [Cu(HDKN)Cl₂] (18)

To a methanolic solution of HDKN (0.312 g, 1 mmol), CuCl₂·2H₂O (0.170 g, 1 mmol) in methanol was added dropwise. The green colored solution was refluxed for 3 h. The green product separated out was collected, washed with methanol followed by ether and dried over P₄O₁₀ *in vacuo*.

[Cu(HDKN)Cl₂] (**18**): Yield: 75%, λ_m (DMF): 9 ohm⁻¹cm² mol⁻¹, μ_{eff} (B.M.): 1.89, Elemental Anal. Found (Calcd.) (%): C: 46.56 (46.64), H: 2.67 (2.99), N: 15.56 (16.00), Cu: 14.23 (14.52).

7.2.3.6. Synthesis of [Cu(DKN)₂] (**19**)

An aqueous solution of Cu(CH₃COO)₂·H₂O (0.199, g 1 mmol) was added gradually to a solution of HDKN (0.312 g, 1 mmol) in methanol. The reaction mixture was heated to reflux for 3 h. The resulting solution was kept at room temperature for slow evaporation and after 2-3 days, green crystalline compound was separated out and was washed with methanol followed by ether and dried over P₄O₁₀ *in vacuo*.

[Cu(DKN)₂] (**19**): Yield: 81%, λ_m (DMF): 5 ohm⁻¹cm² mol⁻¹, μ_{eff} (B.M.): 1.72, Elemental Anal. Found (Calcd.) (%): C: 60.86 (61.12), H: 3.58 (3.62), N: 20.36 (20.96), Cu: 9.83 (9.51).

7.2.3.7. Synthesis of [Cu₂(DKN)₂(μ -N₃)₂] (**20**)

To a methanolic solution of HDKN (0.312 g, 1 mmol), a solution of NaN₃ (0.065 g, 1 mmol) in minimum volume of water-methanol mixture was added dropwise and stirred for half an hour. To this, aqueous solution of Cu(CH₃COO)₂·H₂O (0.199 g, 1 mmol) was added and again stirred for 2 h. Green precipitate obtained was filtered, washed with methanol and dried over P₄O₁₀ *in vacuo*.

[Cu₂(DKN)₂(μ -N₃)₂] (**20**): Yield: 85%, Color: green, λ_m (DMF): 8 ohm⁻¹cm² mol⁻¹, μ_{eff} (B.M.): 1.24, Elemental Anal. Found (Calcd.) (%): C: 49.73 (50.06), H: 2.40 (2.97), N: 27.68 (27.47), Cu: 15.07 (15.58).

7.2.3.8. *Synthesis of [Cu₂(DKN)₂(μ-NCS)₂] (21)*

The hydrazone HDKN (0.312 g, 1 mmol) was dissolved in methanol; to this an aqueous solution of KSCN (0.097 g, 1 mmol) was added dropwise and stirred for half an hour. This was followed by the addition of aqueous solution of Cu(CH₃COO)₂·H₂O (0.199 g, 1 mmol) and again stirred for 2 h. The final solution was kept at room temperature and green crystalline compound separated out was filtered, washed with methanol and dried over P₄O₁₀ *in vacuo*.

[Cu₂(DKN)₂(μ-NCS)₂] (**21**): Yield: 70%, λ_m (DMF): 3 ohm⁻¹cm² mol⁻¹, μ_{eff} (B.M.): 1.42, Elemental Anal. Found (Calcd.) (%): C: 50.55 (51.00), H: 2.31 (2.85), N: 19.82 (19.82), Cu: 14.29 (14.99).

7.2.3.9. *Synthesis of [Cu₂(DKN)₂](ClO₄)₂·2H₂O (22)*

A methanolic solution of Cu(ClO₄)₂·6H₂O (0.370 g, 1 mmol) was added to a solution of HDKN (0.312 g, 1 mmol) in methanol. The green colored solution was refluxed for 3 h and the green product obtained was separated out, filtered, washed with methanol and dried over P₄O₁₀ *in vacuo*.

[Cu₂(DKN)₂](ClO₄)₂·2H₂O (**22**): Yield: 90%, λ_m (DMF): 165 ohm⁻¹cm² mol⁻¹, μ_{eff} (B.M.): 1.26, Elemental Anal. Found (Calcd.) (%): C: 42.38 (42.25), H: 2.99 (2.92), N: 14.61 (14.49), Cu: 13.47 (13.15).

Caution! Although no problems were encountered during this research, azide and perchlorate salts of metal complexes with organic ligands are potentially explosive. So they should be prepared in small quantities and handled with care.

7.3. Results and discussion

7.3.1. Elemental analyses

The observed C, H, N values of the complexes are in close agreement with that of the proposed formulae. The metal content % of the complexes was determined by AAS after digestion with con. HNO₃ and was compatible with that of the theoretical values.

7.3.2. Molar conductivity and magnetic susceptibility measurements

The molar conductances of the complexes in DMF (10⁻³ M) solutions were measured at 298 K with a Systronic model 303 direct-reading conductivity bridge. The molar conductance values of all the Cu(II) complexes except **22** are in the range 3-12 ohm⁻¹cm² mol⁻¹. These low values indicate their non-electrolytic nature, but **22** is found to be a 2:1 electrolyte [15]. Magnetic moments for the complexes were calculated from magnetic susceptibility measurements at 298 K using diamagnetic corrections. The effective magnetic moment (μ_{eff}) value for the mononuclear Cu(II) complexes (*d*⁹ system) were found to be close to the spin only value, which corresponds to a single unpaired electron. The low magnetic moment for the dinuclear complexes may be attributed to the coupling of two magnetic centers [16].

7.3.3. Infrared spectra

Exhaustive comparisons of the selected vibrational bands of the free hydrazones with its copper complexes give information about the ligating mode of the ligand upon complexation. The important infrared spectral bands of the hydrazones and complexes along with their tentative assignments are given in Table 7.1. In complex **14** (Fig. 7.1), it was found that the characteristic spectral bands for $\nu(\text{NH})$ and $\nu(\text{C}=\text{O})$ stretches of the hydrazone appearing at 3063 and 1678 cm⁻¹ respectively disappear on complexation, which supports the

coordination *via* enolate form instead of amido form during the tautomerization process [17,18]. A new band appears at 1296 cm^{-1} due to the coordination of the $\nu(\text{C}-\text{O})$ enolic mode [19]. The strong absorption band at 1571 cm^{-1} ascribed to the imine stretching frequency of the uncoordinated ligand, shifts towards lower frequency on complexation with the metal, suggesting coordination to the metal through imine nitrogen [20,21]. A characteristic band of the ligand at 1071 cm^{-1} due to $\nu(\text{N}-\text{N})$ stretching undergoes a shift to higher wavenumber in complexes due to the increase in the double bond character of $\text{N}-\text{N}$, offsetting the loss of electron density *via* donation to the metal ion which gives further evidence of coordination of the ligand through the imine nitrogen atom [22]. On complexation a new band due to $\nu(\text{C}=\text{N})$ is resolved at 1594 cm^{-1} , which confirms the coordination of the ligand through imine nitrogen [23,24]. The out-of-plane bending modes of vibrations of the free ligands at 622 cm^{-1} are found to be shifted to higher energies in the spectra of complexes indicating the coordination *via* pyridine nitrogen [25].

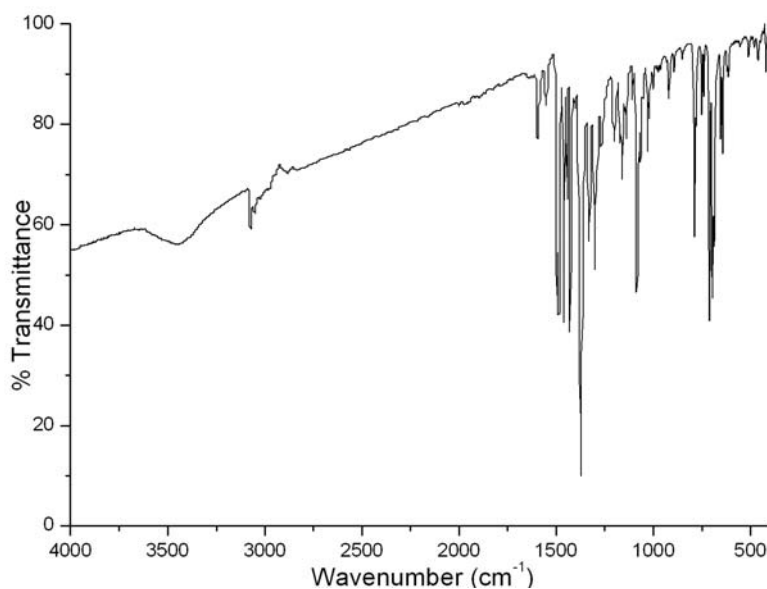


Fig. 7.1. IR spectrum of $[\text{Cu}(\text{BPB})\text{Br}]$ (14).

In the sulfato complex (Fig. 7.2), the ν_1 and ν_2 vibrations observed as weak bands at 1002 and 459 cm^{-1} , suggest the bridged bidentate nature of the sulfato anion in the complex. The ν_3 vibration is observed at 1084 cm^{-1} while the ν_4 vibrations are observed near 615 cm^{-1} , similar to the corresponding values of other complexes where the sulfato anion exists in the bridged bidentate form [26,27].

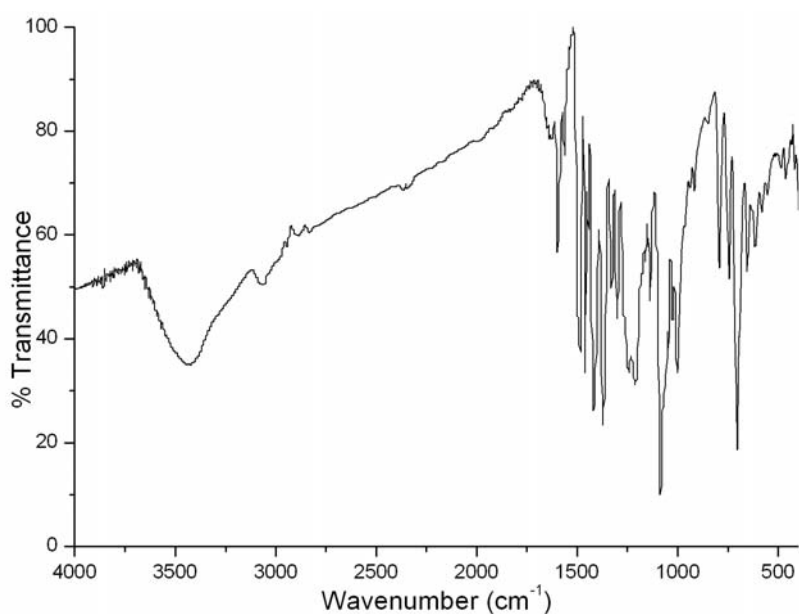


Fig. 7.2. IR spectrum of $[\text{Cu}_2(\text{BPB})_2(\mu\text{-SO}_4)]$ (**15**).

For complex **16** (Fig. 7.3), the azomethine stretching frequency is shifted to 1530 cm^{-1} and the appearance of a new $\nu(\text{C}=\text{N})$ band at 1585 cm^{-1} gives evidence for the coordination of the hydrazone through imine nitrogen. Both $\nu(\text{NH})$ and $\nu(\text{C}=\text{O})$ stretches disappear and the ligand coordinates in the enolate form and the coordination through pyridyl nitrogen was evident from the shifting of out-of-plane bending modes of vibrations of the free ligand to higher frequency. The crystal structure also supports these findings.

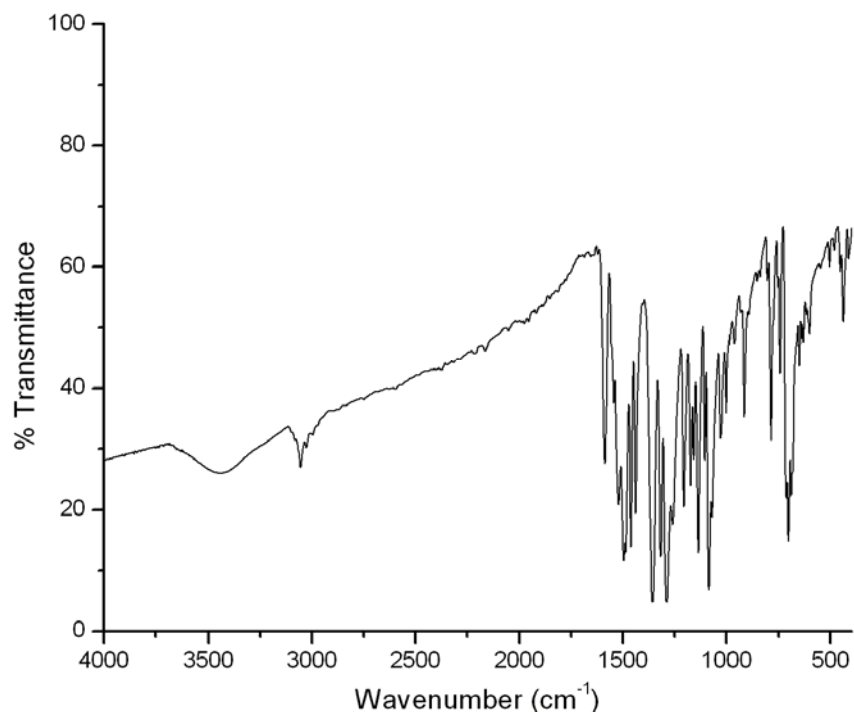


Fig. 7.3. IR spectrum of the compound $[\text{Cu}(\text{BPB})_2]$ (16).

Bonding of the hydrazone HDKN to Cu(II) centre has been suggested by a careful comparison of the infrared spectra of the complexes with that of the free ligand. The $\nu(\text{N-H})$ and $\nu(\text{C=O})$ stretching bands at 2928 and 1689 cm^{-1} respectively, corresponding to the free HDKN are not observed in the spectra of its complexes except $[\text{Cu}(\text{HDKN})\text{Cl}_2]$. This fact, along with the presence of a medium intensity band at *ca.* 1369 cm^{-1} assignable to $\nu(\text{C-O})$, indicates that the hydrogen atoms of the amide group are lost during the synthesis and the deprotonated ligand is predominantly in the enolate form in the complexes. In the spectrum of $[\text{Cu}(\text{DKN})\text{Br}]$, the $\nu(\text{C=N})$ band of HDKN is shifted to 1501 cm^{-1} (Fig. 7.4), which supports the participation of azomethine group of the ligand in binding to the Cu(II) ion. A shift to the higher frequency of the $\nu(\text{N-N})$ band and the appearance of a new band due to $\nu(\text{C=N})$ at 1583 cm^{-1} may be taken as additional evidence for the participation of the imine nitrogen. The low energy

pyridine ring in-plane and out-of-plane vibrations observed in the spectrum of the HDKN at 615 cm^{-1} , are shifted to higher frequencies in the case of complexes, which is a good indication of the coordination of the heterocyclic nitrogen to the metal center.

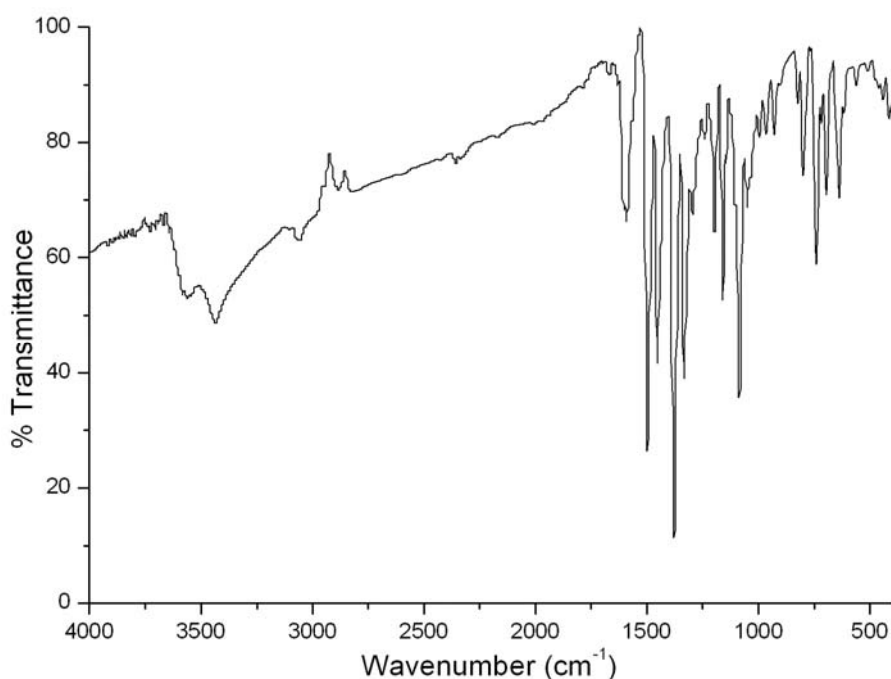


Fig. 7.4. IR spectrum of $[\text{Cu}(\text{DKN})\text{Br}]$ (**17**).

Unlike others, in complex **18** (Fig. 7.5), the carbonyl ($\text{C}=\text{O}$) stretching signal was retained, but was shifted towards lower frequencies (1604 cm^{-1}) indicating that the hydrazone has not undergone enolization and is coordinated to the metal center in neutral form [28]. The band due to azomethine stretching vibrations is shifted to lower wavenumber suggesting the coordination through azomethine nitrogen but a band due to the formation of new $\text{C}=\text{N}$ bond is absent in complex **18**, since the ligand is coordinated in the neutral form.

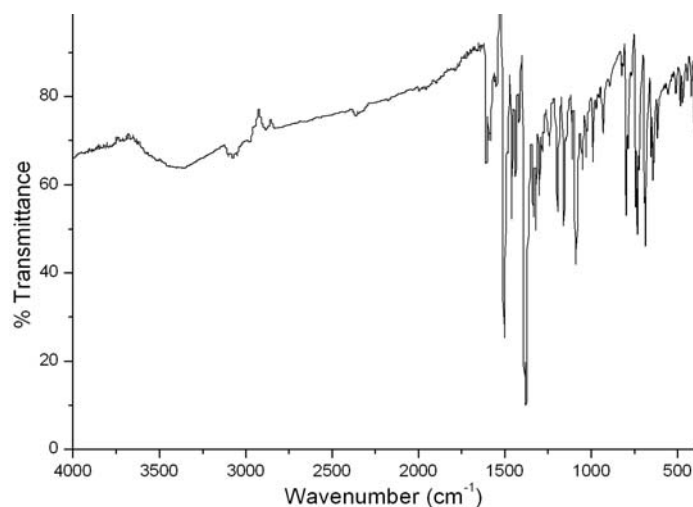


Fig. 7.5. IR spectrum of $[\text{Cu}(\text{HDKN})\text{Cl}_2]$ (**18**).

In the spectrum of complex $[\text{Cu}(\text{DKN})_2]$ (Fig. 7.6), it was found that the ligand HDKN is coordinating through the azomethine and pyridyl nitrogens and enolate oxygen which is evident from the shifting in azomethine stretching vibrations, disappearance of $\nu(\text{N-H})$ and $\nu(\text{C=O})$ stretches. The information regarding the coordination of the ligand in complex **19** is consistent with its X-ray diffraction studies.

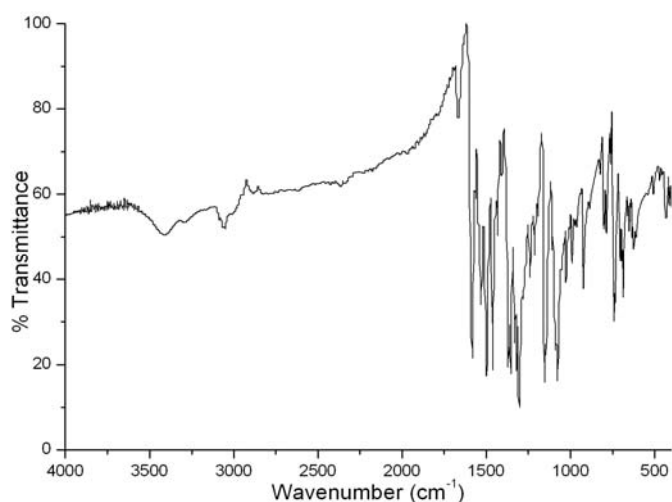


Fig. 7.6. IR spectrum of $[\text{Cu}(\text{DKN})_2]$ (**19**).

The most interesting part of the spectrum in complex **20** is the 2000-2100 cm^{-1} region where the strong absorption band due to the azide group is visible (Fig. 7.7). The azido bridges in the complex take the end-on structure with the $\nu_a(\text{N}_3)$ at 2057 cm^{-1} [26,29].

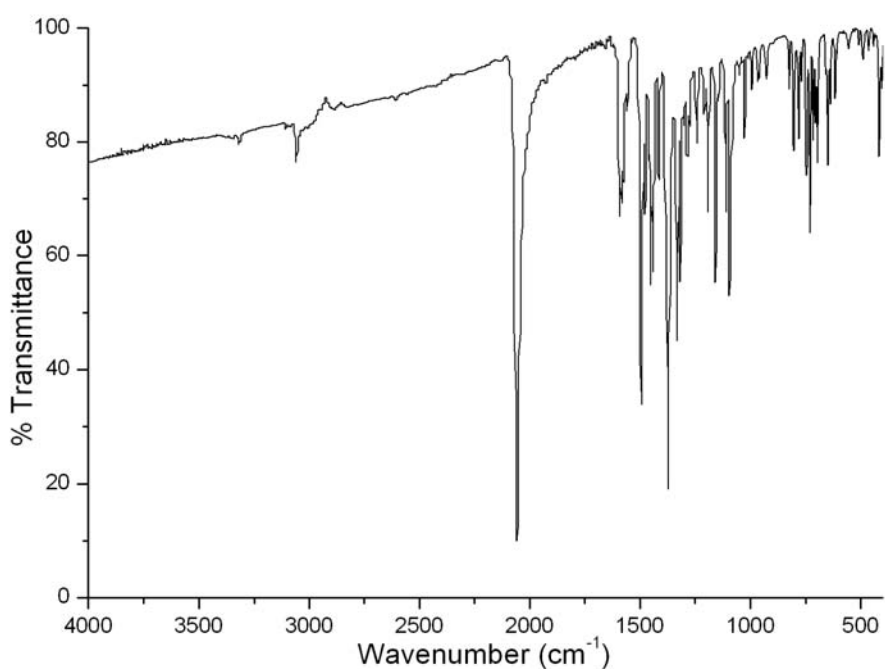


Fig. 7.7. IR spectrum of $[\text{Cu}_2(\text{DKN})_2(\mu\text{-N}_3)_2]$ (**20**).

In the thiocyanato complex (Fig. 7.8), a single strong and sharp peak at 2078 cm^{-1} , assignable to $\nu(\text{CN})$ stretching mode of a thiocyanate group is observed which corresponds to the bridging CN stretching [26,30]. The intensity and band position indicate the coordination of the thiocyanate through the nitrogen atom.

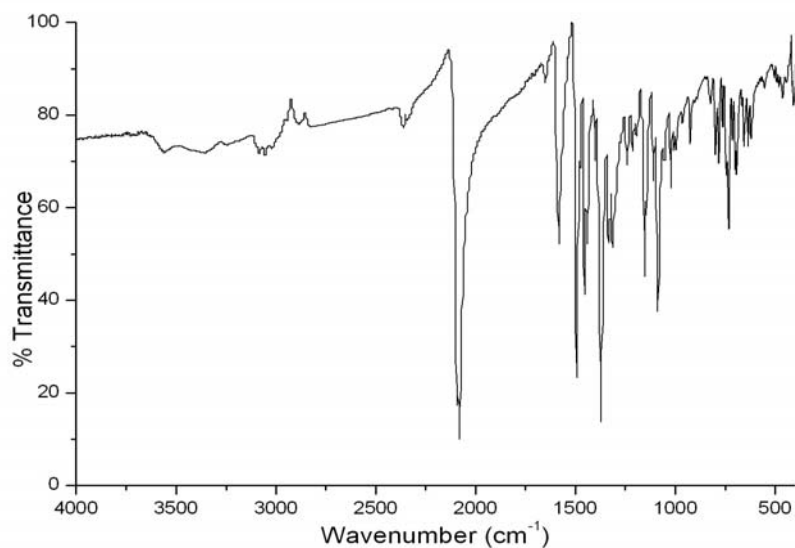


Fig. 7.8. IR spectrum of $[\text{Cu}_2(\text{DKN})_2(\mu\text{-NCS})_2]$ (**21**).

The perchlorate complex shows a strong absorption at 1091 cm^{-1} (Fig. 7.9) and an unsplit band at 623 cm^{-1} , indicating the presence of ionic perchlorate [31].

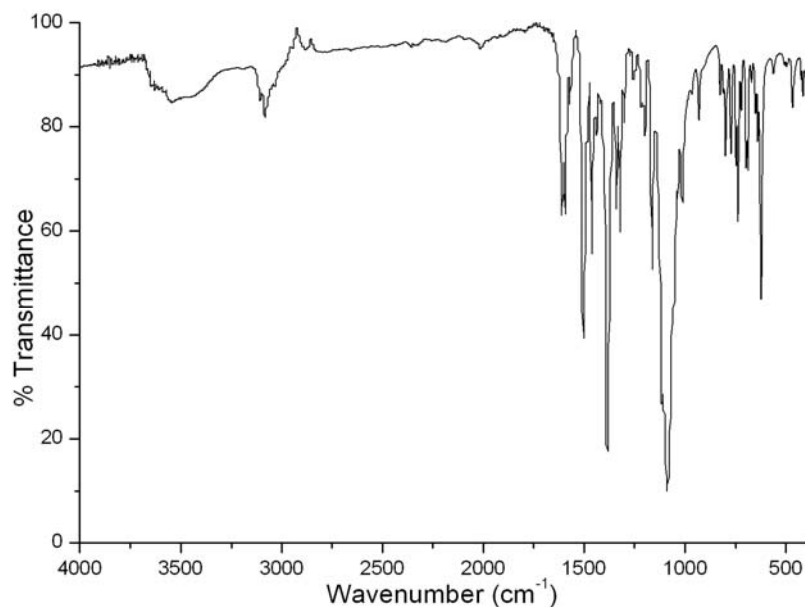


Fig. 7.9. IR spectrum of $[\text{Cu}_2(\text{DKN})_2](\text{ClO}_4)_2 \cdot 2\text{H}_2\text{O}$ (**22**).

Table 7.1. IR spectral data (cm⁻¹) of copper(II) complexes.

Compound	$\nu(\text{N-H})$	$\nu(\text{C=O})$ / $\nu(\text{C-O})$	$\nu(\text{C=N})$	$\nu(\text{C=N})^a$	$\nu(\text{Cu-N}_{\text{azo}})$	$\nu(\text{Cu-O})$
HBPB	3063	1678	1571
[Cu(BPB)Br] (14)	...	1296	1547	1594	459	425
[Cu ₂ (BPB) ₂ (μ -SO ₄)] (15)	...	1370	1560	1596	463	420
[Cu(BPB) ₂] (16)	...	1297	1530	1585	471	433
HDKN	2928	1689	1579
[Cu(DKN)Br] (17)	...	1371	1501	1583	477	447
[Cu(HDKN)Cl ₂] (18)	1509	...	483	443
[Cu(DKN) ₂] (19)	...	1351	1521	1585	471	433
[Cu ₂ (DKN) ₂ (μ -N ₃) ₂] (20)	...	1375	1506	1585	464	442
[Cu ₂ (DKN) ₂ (μ -NCS) ₂] (21)	...	1368	1503	1582	463	441
[Cu ₂ (DKN) ₂](ClO ₄) ₂ ·2H ₂ O (22)	...	1382	1505	1590	467	430

7.3.4. Electronic spectra

The electronic absorption bands of the complexes (Figs. 7.10-7.18) are summarized in Table 7.2. The Cu(II) complexes with d^9 configuration is expected to experience Jahn-Teller distortion which leads to further splitting of the 2E_g and ${}^2T_{2g}$ levels and give rise to three spin allowed transitions *viz.* ${}^2A_{1g} \leftarrow {}^2B_{1g}$, ${}^2B_{2g} \leftarrow {}^2B_{1g}$, ${}^2E_g \leftarrow {}^2B_{1g}$ which occur in the ranges 11760-18180, 15500-18010 and 17240-20000 cm⁻¹ respectively. But often these theoretical expectations are unseen in practice and these bands usually appear overlapped and become difficult to resolve into separate bands due to the very small energy difference between the d levels. The presence of a broad band in all the complexes in the range 15060-14180 cm⁻¹ can be assigned to the envelope of ${}^2A_{1g} \leftarrow {}^2B_{1g}$, ${}^2B_{2g} \leftarrow {}^2B_{1g}$, ${}^2E_g \leftarrow$

$^2B_{1g}$ transitions. The intense bands observed in the range 21180-25770 cm^{-1} in all Cu(II) complexes are mainly due to the phenoxy $O \rightarrow \text{Cu(II)}$ charge transfer transitions [32-34]. The remaining bands of the complexes correspond to the intraligand transitions which suffered marginal shifts on complexation.

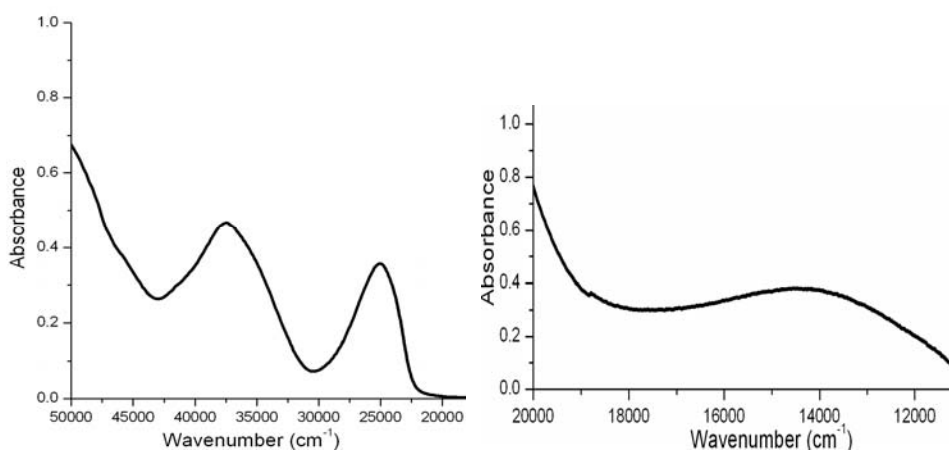


Fig. 7.10. Electronic spectra of [Cu(BPB)Br] (**14**).

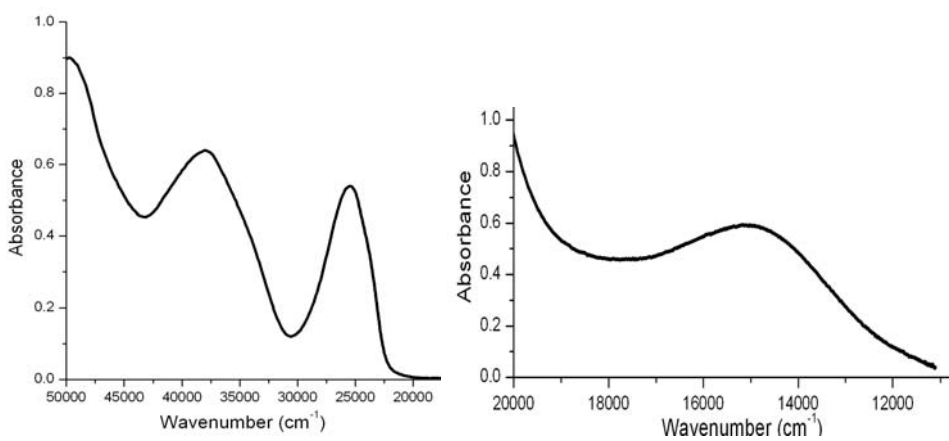


Fig. 7.11. Electronic spectra of [Cu₂(BPB)₂(μ-SO₄)] (**15**).

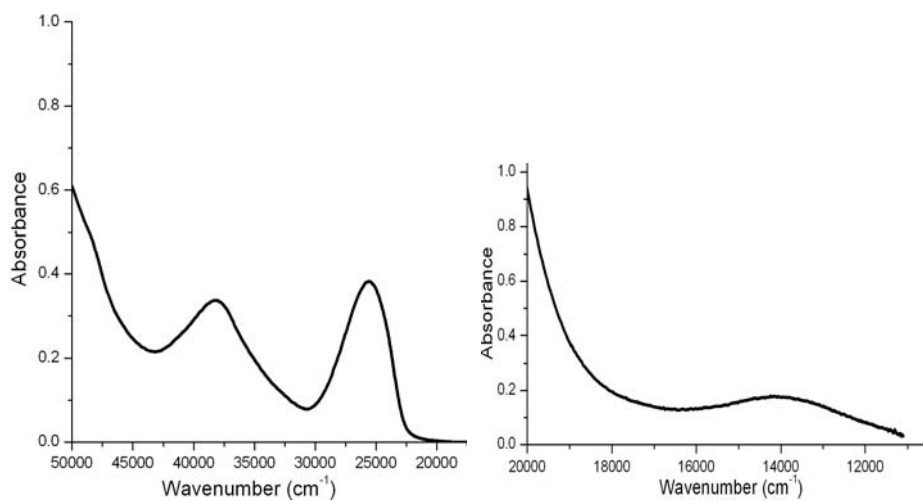


Fig. 7.12. Electronic spectra of [Cu(BPB)₂] (16).

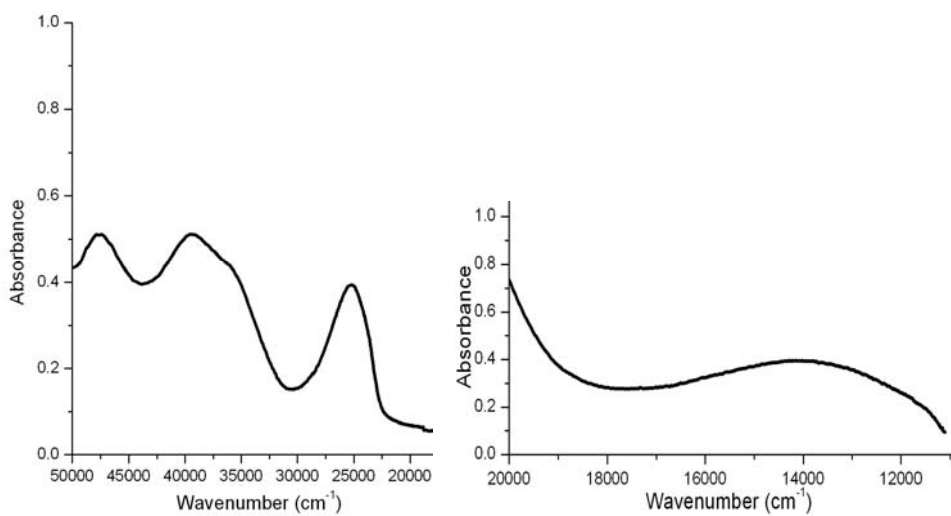


Fig. 7.13. Electronic spectra of [Cu(DKN)Br] (17).

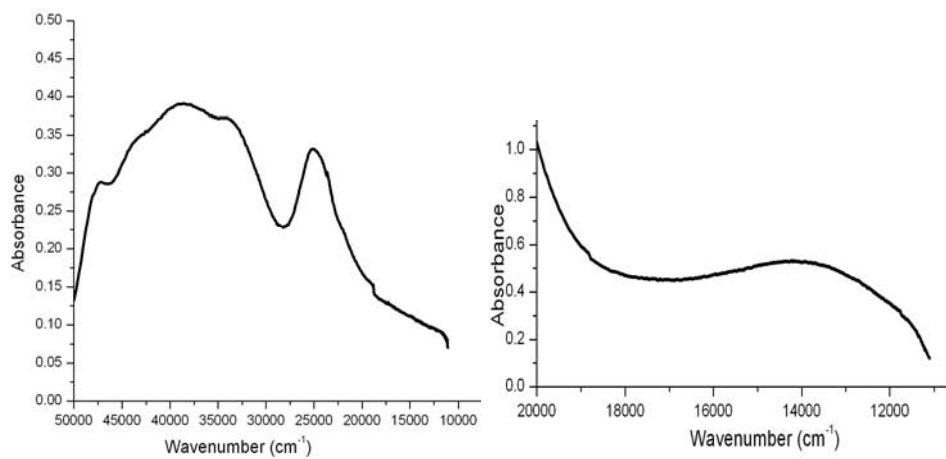


Fig. 7.14. Electronic spectra of [Cu(HDKN)Cl₂] (18).

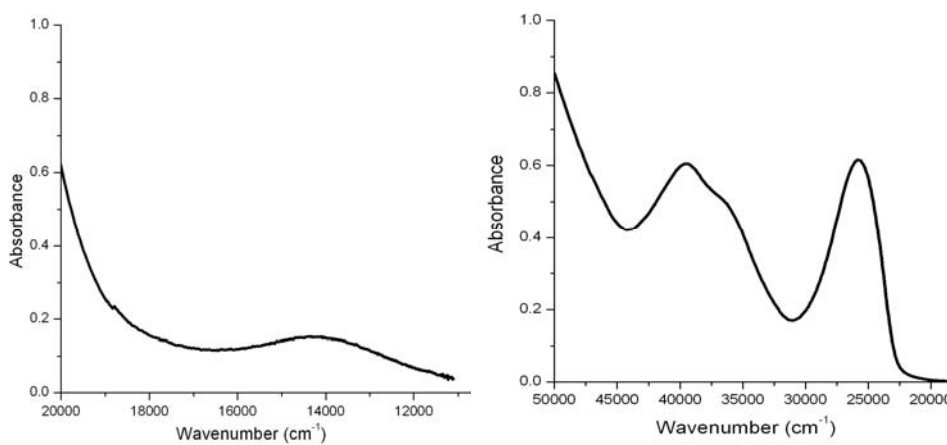


Fig. 7.15. Electronic spectra of [Cu(DKN)₂] (19).

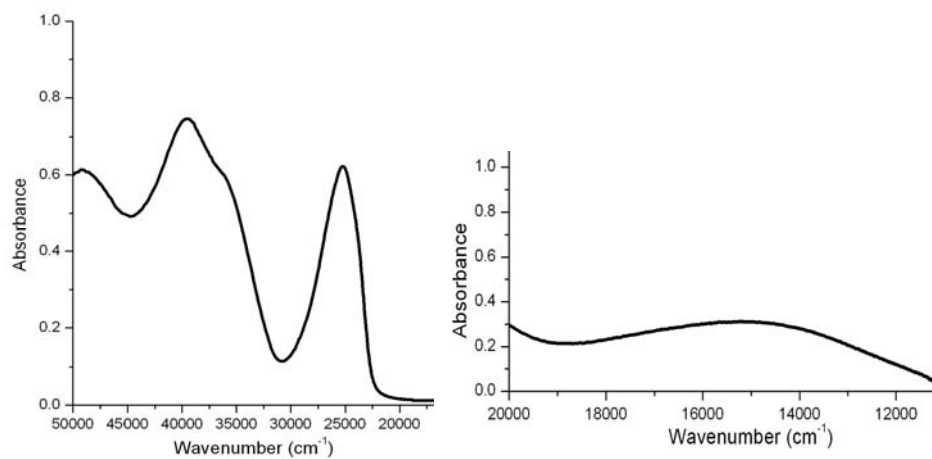


Fig. 7.16. Electronic spectra of [Cu₂(DKN)₂(μ-N₃)₂] (20).

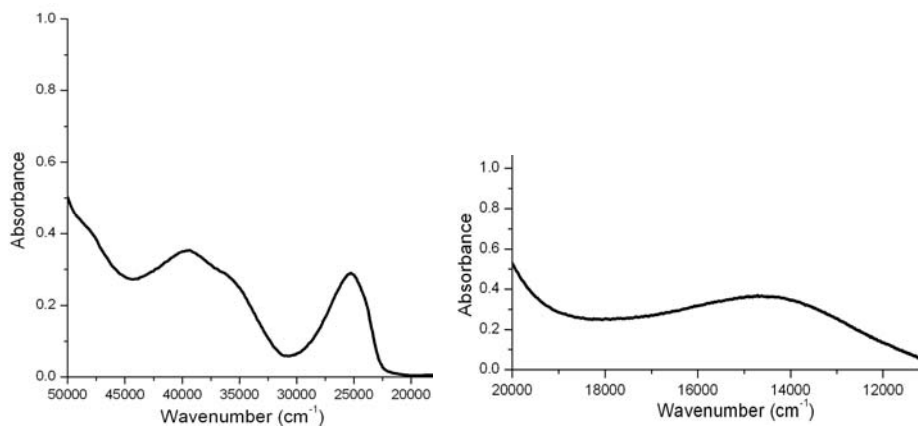


Fig. 7.17. Electronic spectra of [Cu₂(DKN)₂(μ-NCS)₂] (21).

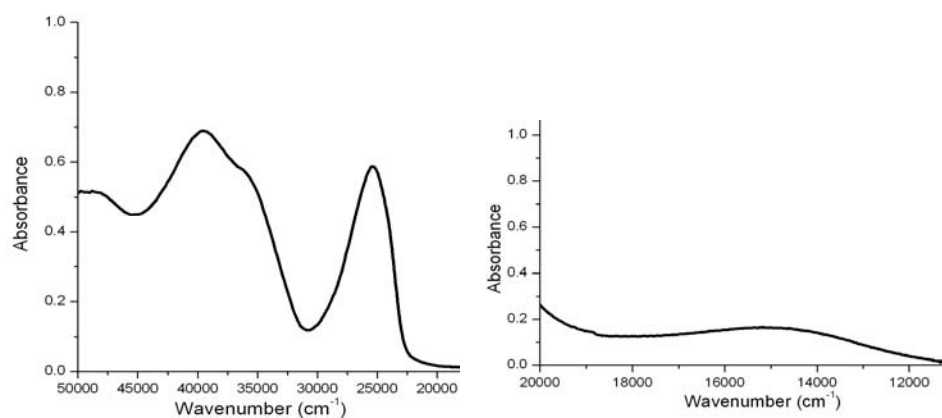


Fig. 7.18. Electronic spectra of $[\text{Cu}_2(\text{DKN})_2](\text{ClO}_4)_2 \cdot 2\text{H}_2\text{O}$ (**22**).

Table 7.2. Electronic spectral data of the copper(II) complexes.

Compound	UV-vis absorption bands (cm^{-1})
$[\text{Cu}(\text{BPB})\text{Br}]$ (14)	37450, 25250, 14180
$[\text{Cu}_2(\text{BPB})_2(\mu\text{-SO}_4)]$ (15)	37950, 33980, 25430, 15030
$[\text{Cu}(\text{BPB})_2]$ (16)	38310, 25570, 14220
$[\text{Cu}(\text{DKN})\text{Br}]$ (17)	39520, 35970 (sh), 25180, 14640
$[\text{Cu}(\text{HDKN})\text{Cl}_2]$ (18)	38750, 33780 (sh), 25060, 15060
$[\text{Cu}(\text{DKN})_2]$ (19)	39520, 36630 (sh), 25770, 14300
$[\text{Cu}_2(\text{DKN})_2(\mu\text{-N}_3)_2]$ (20)	39840, 36630 (sh), 21180, 15060
$[\text{Cu}_2(\text{DKN})_2(\mu\text{-NCS})_2]$ (21)	39520, 36635 (sh), 25310, 14570
$[\text{Cu}_2(\text{DKN})_2](\text{ClO}_4)_2 \cdot 2\text{H}_2\text{O}$ (22)	39520, 36230 (sh), 25440, 14940

7.3.5. Thermal analyses

TGA was performed for all complexes except for azido and perchlorate complexes from 50-800 °C in N_2 atmosphere at the heating rate of 10 °C/min and selected TG--DTG curves are presented in Fig. 7.19. TG curves are drawn as weight (mg) versus temperature (°C). All the reported complexes are stable up to 260 °C above which they undergo decomposition in between 260-290 °C. Since the TGA curves of the complexes do not show any weight loss up to 250 °C, the complexes are suggested to be unhydrated ones.

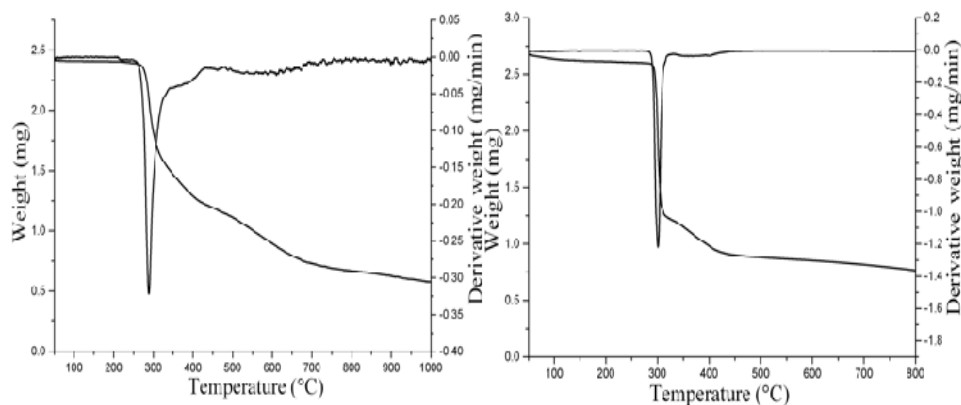


Fig. 7.19. TG-DTG curves of the Cu(II) complexes [Cu(DKN)Br] (left) and [Cu(DKN)₂] (right).

7.3.6. Electron paramagnetic resonance spectra

The copper(II) ion, with a d^9 configuration, has an effective spin of $s = \frac{1}{2}$ and associated spin angular momentum $m_s = \frac{1}{2}$, leading to a doubly degenerate spin state in the absence of magnetic field. In a magnetic field this degeneracy is removed and the energy difference between these two states is given by $E = h\nu = g\beta B$, where h is Planck's constant, ν is the frequency, g is the Lande splitting factor, β is the electronic Bohr magneton and B is the magnetic field. For the free copper(II) ion there is also an interaction with the magnetic field due to the orbital angular momentum L of the electron, and the total interaction becomes $E = (2.0023S + L)H$. The orbital degeneracy is removed by the crystal field and the orbital angular momentum is said to be quenched for the ground states of copper(II) complexes. Spin-orbit coupling mixes into the ground state some orbital angular momentum from certain excited states, the extent of which is reflected in the modifications of Lande splitting factor g . For the case of a $3d^9$ copper(II) ion, the appropriate spin Hamiltonian assuming a B_{1g} ground state is given by

$$\hat{H} = \beta [g_{\parallel} B_z S_z + g_{\perp} (B_x S_x + B_y S_y)] + A_{\parallel} I_z S_z + A_{\perp} (I_x S_x + I_y S_y)$$

The copper(II) ion having a d^9 configuration with an effective spin of $S = 1/2$ couples with nuclear spin of ^{63}Cu ($I = 3/2$) and give rise to four ($2nI+1=4$) hyperfine lines. The EPR spectra of all the complexes were recorded in polycrystalline state at 298 K and in frozen DMF at 77 K in the X band frequency using TCNE as standard ($g = 2.00277$) with 100 kHz modulation frequency and 9.1 GHz microwave frequency and various magnetic induction parameters are summarized in the Table 7.3. But the spectra for complexes **17**, **18** and **22** in DMF were of poor quality and were taken in DMSO. Some of the EPR spectra are simulated and the experimental (green) and simulated (pink) best fits are included [35]. In polycrystalline state, since it is magnetically concentrated the anisotropy may be lost. Dilution of the solid isolates the electron spin of the given complex from that of another paramagnetic molecule. The EPR spectrum of complex **14** is isotropic in nature, which is attributable to enhanced spin lattice relaxation and dipolar interaction (Fig. 7.20), while it showed a well-resolved axial spectrum with four hyperfine lines in the parallel region in frozen DMF at 77 K with $g_{\parallel} > g_{\perp} > 2.0023$ relationship, consistent with a $d_{x^2-y^2}$ ground state in a square planar geometry [36,37]. In addition to the hyperfine lines in the parallel region, five splitting are also observed in the perpendicular region (Fig. 7.21) with an average spacing of $13.15 \times 10^{-4} \text{ cm}^{-1}$ due to the coupling of electron spin with the nuclear spin of nitrogen which is an evidence for the participation of pyridyl and azomethine nitrogens in bonding.

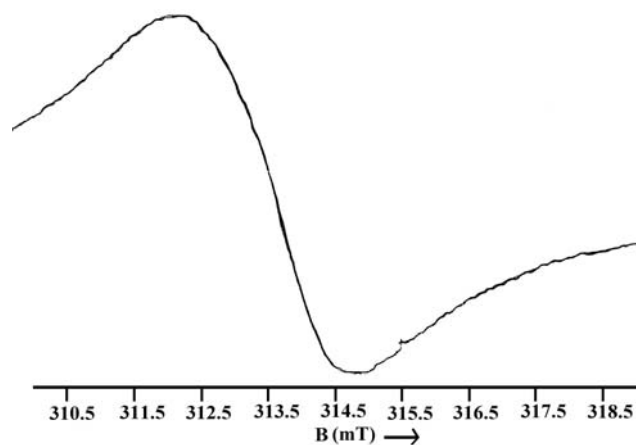


Fig. 7.20. EPR spectrum of [Cu(BPB)Br] (**14**) in polycrystalline state in 298 K.

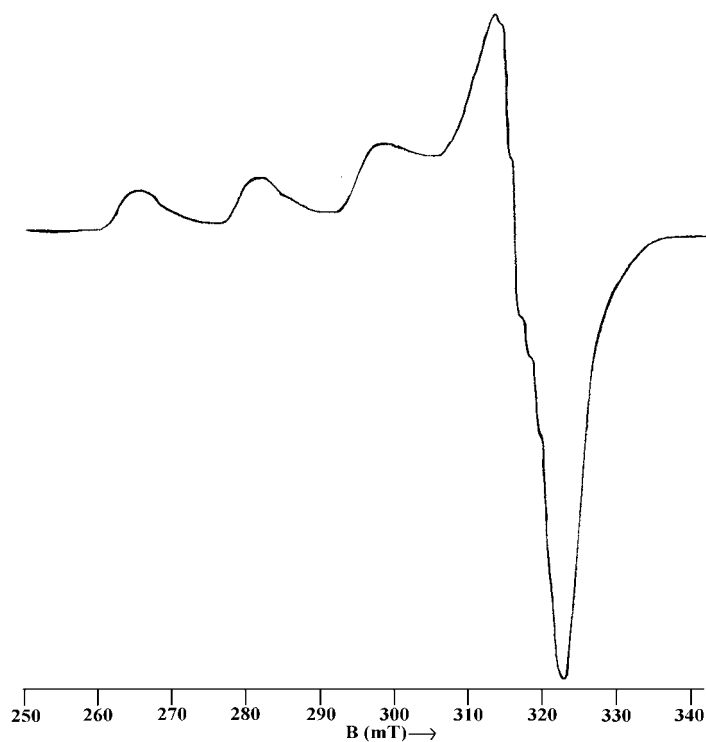


Fig. 7.21. EPR spectrum of [Cu(BPB)Br] (**14**) in DMF at 77 K.

The complex **15**, in polycrystalline state at 298 K showed only one broad signal with $g_{\text{iso}} = 2.099$. Such isotropic spectra consisting of only one broad signal and hence only one g value (g_{iso}), arise from extensive exchange coupling

through misalignment of the local molecular axes between the different molecules in the unit cell (dipolar broadening) and enhanced spin lattice relaxation. This type of spectra unfortunately give no information on the electronic ground state of the Cu(II) ions present in the complex. But a half field signal at $g = 4.618$, indicates the presence of dimeric species which arises due to the $\Delta M_s = \pm 2$ transitions (Fig. 7.22). However in frozen DMF at 77 K, an axial spectrum was observed with four hyperfine splittings. Moreover in the perpendicular region five splittings are seen with an average spacing of $15.67 \times 10^{-4} \text{ cm}^{-1}$ which corresponds due to the interaction of the electron with nuclear spin of two nitrogens ($2 \times 2 \times 1 + 1 = 5$), which gives an evidence for the coordination of pyridyl and azomethine nitrogens. The most important aspect found in the spectrum is the presence of a half field signal at $g = 4.475$ with seven hyperfine splittings (Fig. 7.23) due to the coupling of the electron spin with the nuclear spin of the two Cu centers ($2nI + 1 = 2 \times 2 \times 3/2 + 1$). This aspect is rarely found and is a good evidence for the dimeric species.

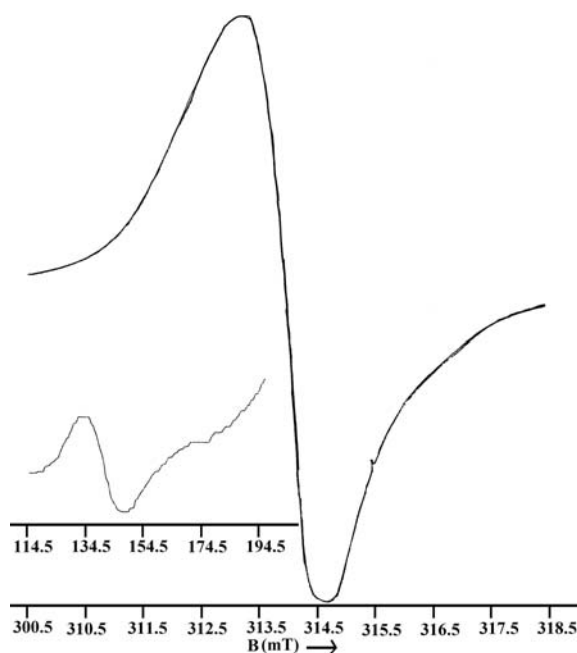


Fig. 7.22. EPR spectrum of $[\text{Cu}_2(\text{BPB})_2(\mu\text{-SO}_4)]$ (15) in polycrystalline state in 298 K.

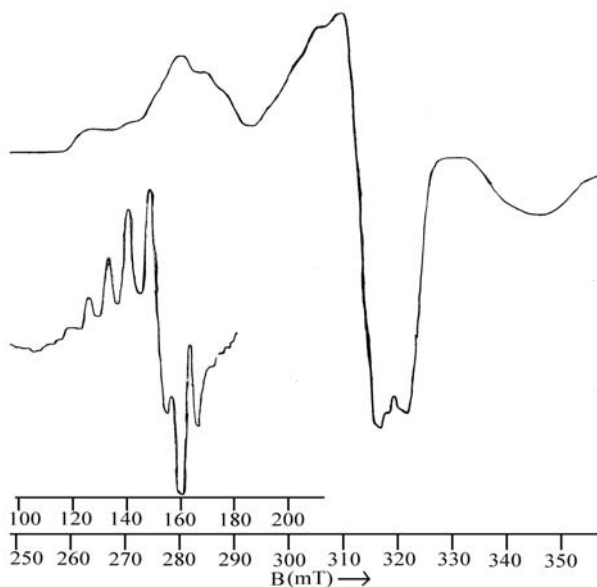


Fig. 7.23. EPR spectrum of $[\text{Cu}_2(\text{BPB})_2(\mu\text{-SO}_4)]$ (**15**) in DMF at 77 K.

In polycrystalline state at 298 K, the EPR spectrum of compound **16** is found to be axial in nature (Fig. 7.24) with $g_{\parallel} = 2.352$ and $g_{\perp} = 2.092$. In frozen DMF, the complex $[\text{Cu}(\text{BPB})_2]$ displayed well-resolved axial anisotropy with four hyperfine splittings (Fig. 7.25) resulting from coupling of the electron spin with the spin of the ^{63}Cu nucleus ($I = 3/2$).

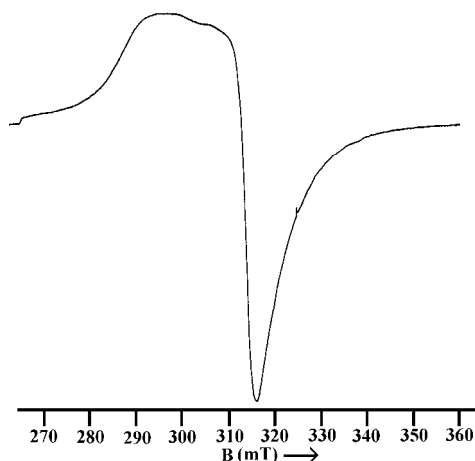


Fig. 7.24. EPR spectrum of $[\text{Cu}(\text{BPB})_2]$ (**16**) in polycrystalline state at 298 K.

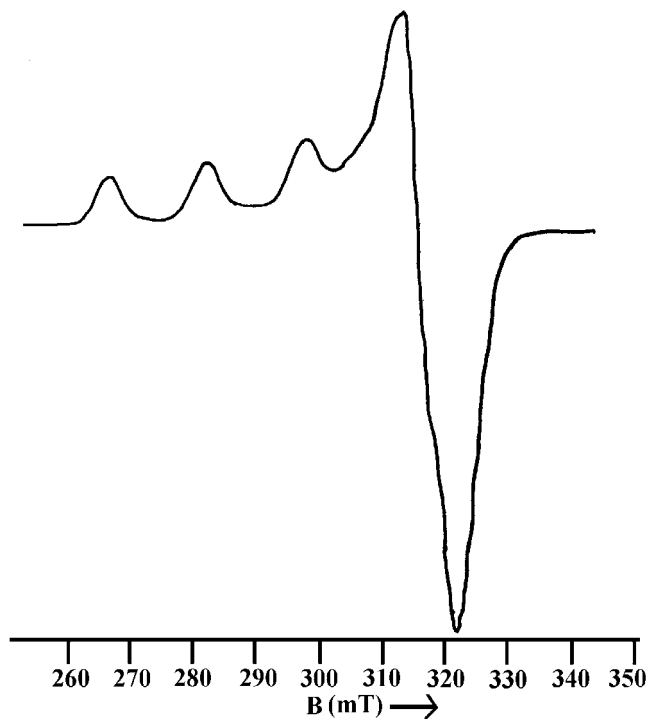


Fig. 7.25. EPR spectrum of $[\text{Cu}(\text{BPB})_2]$ (**16**) in DMF at 77 K.

In the case of complex **17** even more dramatic changes occur in the powder ESR spectrum from an axial spectrum at room temperature to a reverse axial spectrum in DMSO at 77 K (Figs. 7.26, 7.27). These changes correspond with the variations of stereochemistry from square planar to trigonal bipyramidal structure which may be due to the coordination of the solvent with $g_{\perp} > g_{\parallel} > 2.0023$ relationship with a d_z^2 ground state [38]. DMSO is an aggressive solvent, so solvolysis of the complex and a change in coordination geometry in that solvent is not unreasonable.

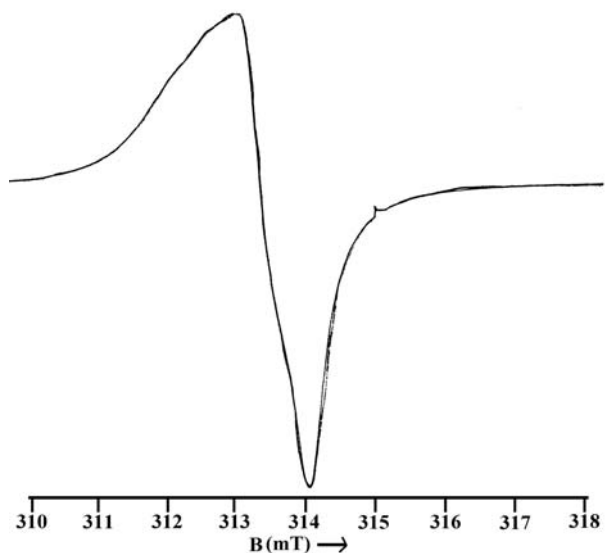


Fig. 7.26. EPR spectrum of [Cu(DKN)Br] (**17**) in polycrystalline state in 298 K.

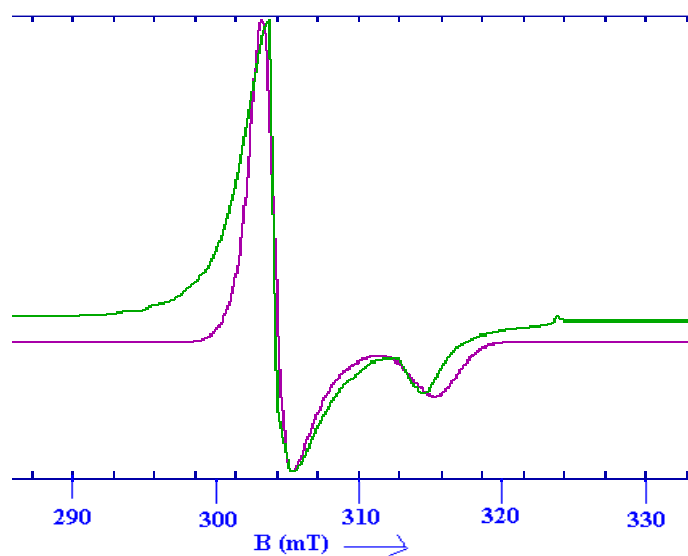


Fig. 7.27. EPR spectrum of [Cu(DKN)Br] (**17**) in DMSO at 77 K.

In polycrystalline state the EPR spectrum of complex **18** is axial in nature even though the hyperfine splittings were not very clear since it is magnetically concentrated (Fig. 7.28). In frozen DMSO the spectrum of [Cu(HDKN)Cl₂] is broad but not isotropic in nature and does not give much information (Fig. 7.29).

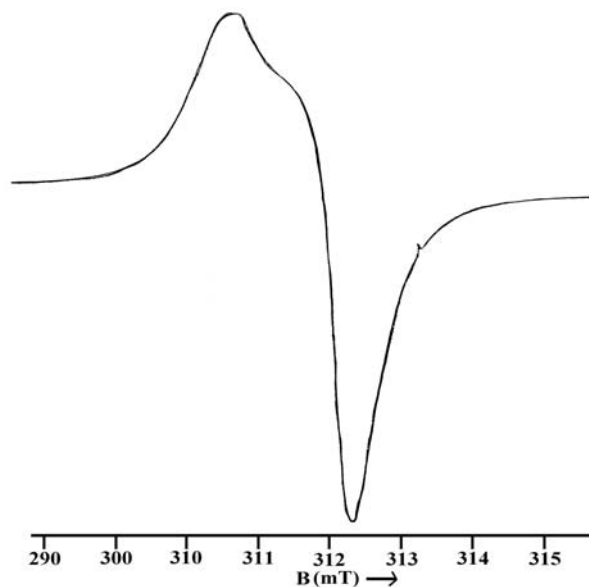


Fig. 7.28. EPR spectrum of $[\text{Cu}(\text{HDKN})\text{Cl}_2]$ (**18**) in polycrystalline state in 298 K.

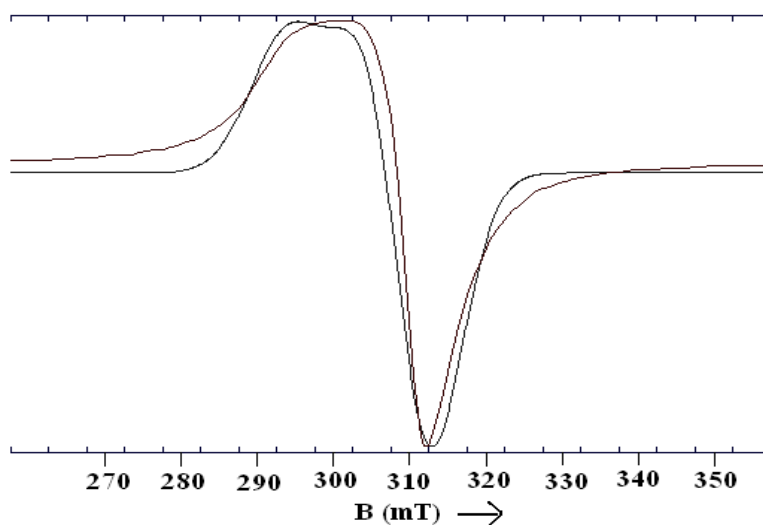


Fig. 7.29. EPR spectrum of $[\text{Cu}(\text{HDKN})\text{Cl}_2]$ (**18**) in DMSO at 77 K.

The EPR spectrum of $[\text{Cu}(\text{DKN})_2]$ in polycrystalline state was found to be axial in nature with $g_{\parallel} = 2.352$ and $g_{\perp} = 2.108$ (Fig. 7.30). However in frozen DMF at 77 K, the spectrum of compound **19** is found to be rhombic in nature with

three g values g_1, g_2, g_3 , where $g_3 > g_2 > g_1$, where g_3 is split into four hyperfine lines (Fig. 7.31).

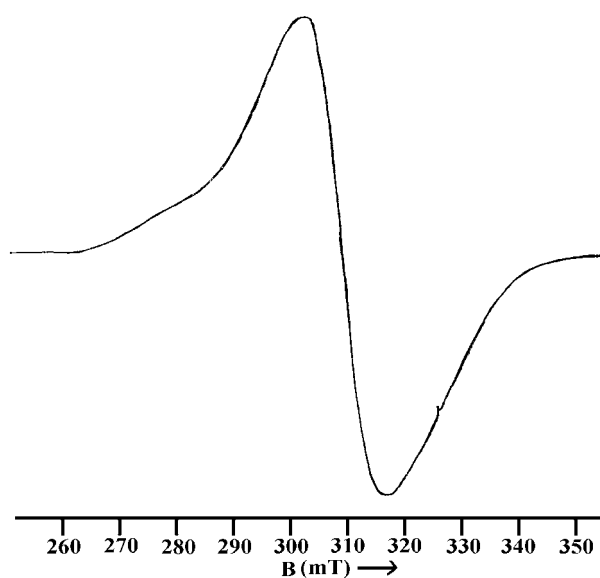


Fig. 7.30. EPR spectrum of $[\text{Cu}(\text{DKN})_2]$ (19) in polycrystalline state in 298 K.

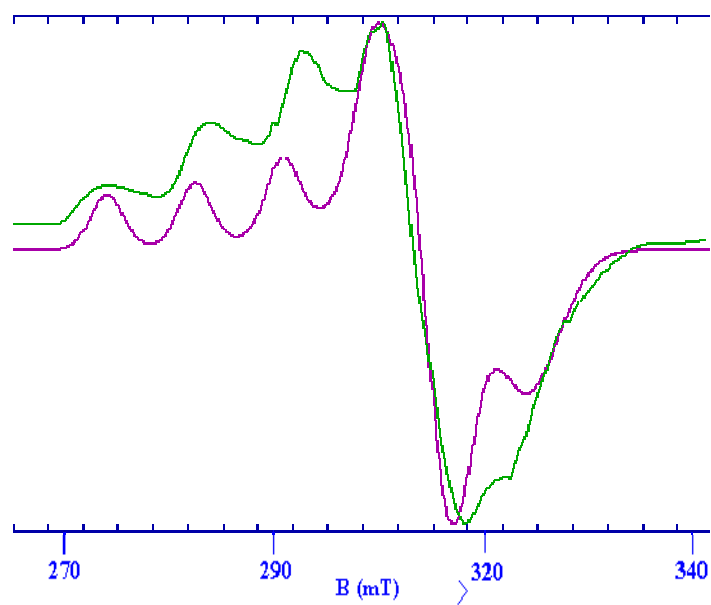


Fig. 7.31. EPR spectrum of $[\text{Cu}(\text{DKN})_2]$ (19) in DMF at 77 K.

In polycrystalline state the azido complex displayed an axial spectrum (Fig. 7.32) at 298 K while in frozen DMF an axial spectrum with four hyperfine splittings is observed due to the coupling of the electron spin with the nuclear spin of ^{63}Cu ($I = 3/2$) with different g_{\parallel} and g_{\perp} values consistent with a $d_{x^2-y^2}$ ground state with an elongated octahedral geometry [39] (Fig. 7.33). However the thiocyanate derivative undergoes distortion around the metal center and the lower symmetry is reflected in the rhombic spectrum (Fig. 7.34). Three g values g_1 , g_2 , g_3 are observed and the large anisotropy in these values is indicative of a geometry distorted from regular octahedron in the solid state. In polynuclear Cu(II) complexes the most important application of the measurement of the ESR spectra is in the identification of Cu-Cu dipolar interaction. Additional transitions arise associated with the $\Delta M_s = \pm 2$ values, compared with the $\Delta M_s = \pm 1$ values in mononuclear complexes. In the X-band spectra, $\Delta M_s = \pm 1$ transitions are associated with fields of *ca.* 300 mT, while the $\Delta M_s = \pm 2$ generate an absorption at the half field value of *ca.* 150 mT and the presence of this half field band is a useful criterion for dipolar interaction for the presence of some dinuclear or polynuclear complex formation [40]. The EPR spectra of compounds **20** and **21** in polycrystalline state suggest a dimeric structure as they exhibited a half field signal at 146.5 and 158 mT with g values of 4.436 and 4.119 respectively, which indicate that indeed a weak interaction between two Cu(II) ions is present. In DMF at 77 K the EPR spectrum of complex **21** was found to be axial in nature with hyperfine splittings (Fig. 7.35).

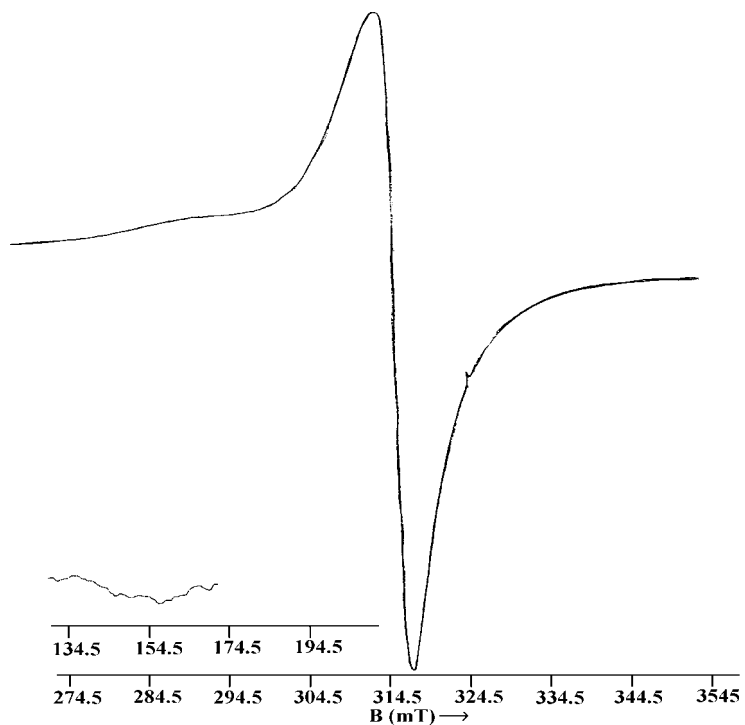


Fig. 7.32. EPR spectrum of $[\text{Cu}_2(\text{DKN})_2(\mu\text{-N}_3)_2]$ (**20**) in polycrystalline state at 298 K.

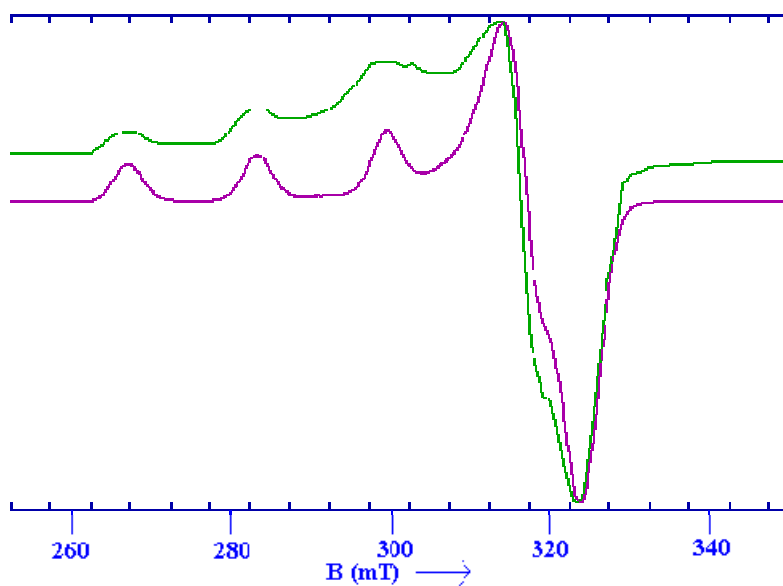


Fig. 7.33. EPR spectrum of $[\text{Cu}_2(\text{DKN})_2(\mu\text{-N}_3)_2]$ (**20**) in DMF at 77 K.

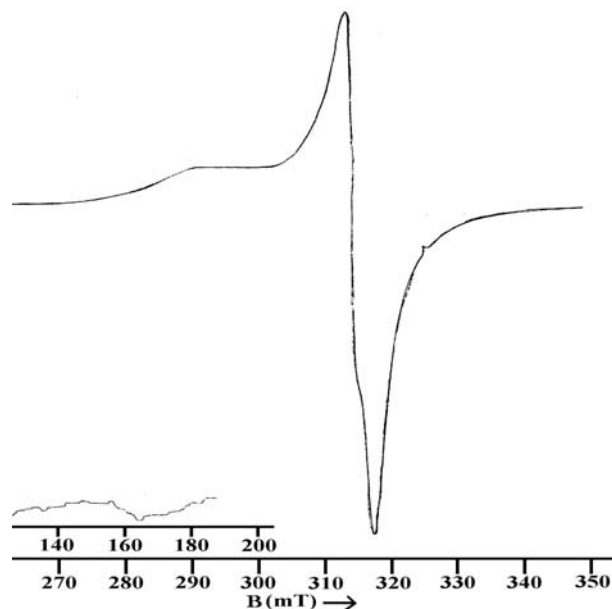


Fig. 7.34. EPR spectrum of $[\text{Cu}_2(\text{DKN})_2(\mu\text{-NCS})_2]$ (**21**) in polycrystalline state at 298 K.

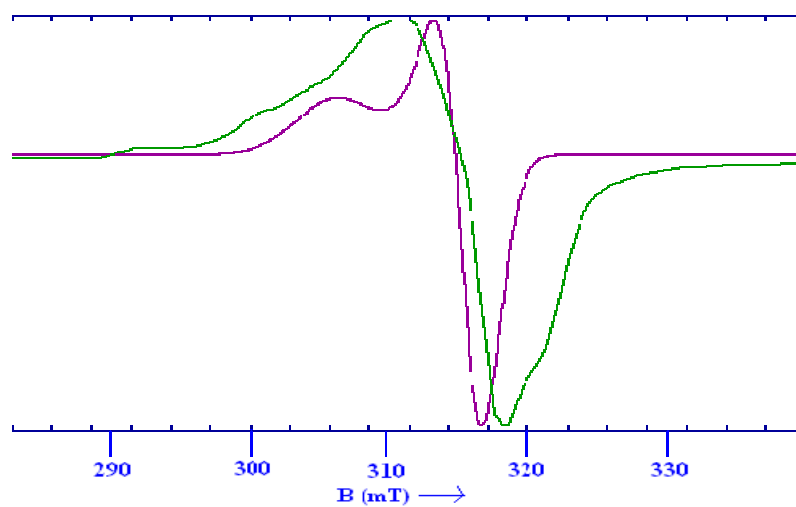


Fig. 7.35. EPR spectrum of $[\text{Cu}_2(\text{DKN})_2(\mu\text{-NCS})_2]$ (**21**) in DMF at 77 K.

The perchlorate complex in polycrystalline state displayed a typical rhombic spectrum (Fig. 7.36) with three g values which shows that the complex has undergone distortion around the metal center from regular octahedron in the

solid state. But unfortunately it did not show any anisotropic feature and hyperfine splittings in frozen DMSO, which may be due to poor glass formation (Fig. 7.37).

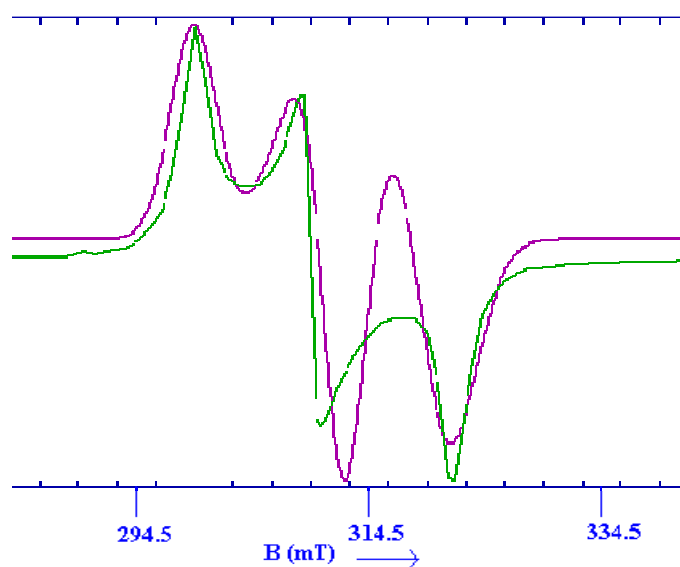


Fig. 7.36. EPR spectrum of $[\text{Cu}_2(\text{DKN})_2](\text{ClO}_4)_2 \cdot 2\text{H}_2\text{O}$ (**22**) in polycrystalline state at 298 K.

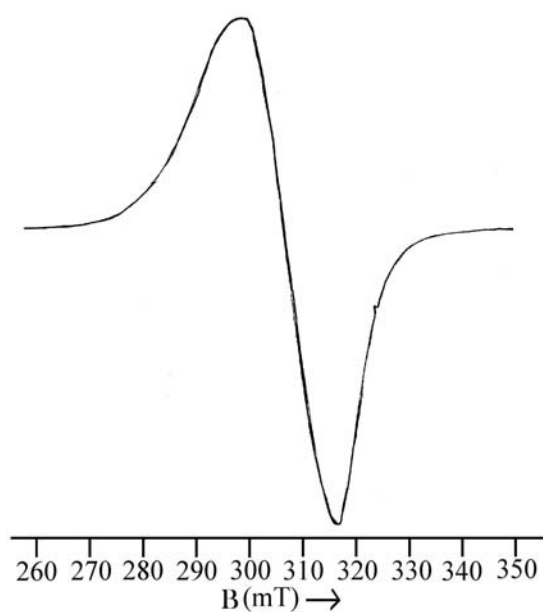


Fig. 7.37. EPR spectrum of $[\text{Cu}_2(\text{DKN})_2](\text{ClO}_4)_2 \cdot 2\text{H}_2\text{O}$ (**22**) in DMSO at 77 K.

For axial spectra, G which is a measure of the exchange interactions between the copper centers, is calculated using the equation: $G = (g_{\parallel} - 2.0023)/(g_{\perp} - 2.0023)$. If $G < 4.0$ considerable exchange interaction is indicated in the solid complex [41]. The value of in-plane sigma bonding parameter α^2 was estimated for each species, from the expression [42],

$$\alpha^2 = -A_{\parallel}/0.036 + (g_{\parallel} - 2.0023) + {}^3/7 (g_{\perp} - 2.0023) + 0.04.$$

The orbital reduction factors K_{\parallel} and K_{\perp} were estimated from the expression

$$K_{\parallel} = (g_{\parallel} - 2.0023)E_{d-d}/8\lambda_o$$

$$K_{\perp} = (g_{\perp} - 2.0023)E_{d-d}/2\lambda_o$$

where $K_{\parallel} = \alpha^2\beta^2$, $K_{\perp} = \alpha^2\gamma^2$ and λ_o represents the one electron spin-orbit coupling constant for the free ion, equal to -828 cm^{-1} . Significant information about the nature of bonding in the copper(II) complexes can be derived from the magnitude of K_{\parallel} and K_{\perp} . In case of pure σ bonding $K_{\parallel} \approx K_{\perp} \approx 0.77$ whereas $K_{\parallel} < K_{\perp}$ implies considerable in-plane bonding, while for out-of-plane bonding, $K_{\parallel} > K_{\perp}$.

The EPR parameters g_{\parallel} , g_{\perp} , $A_{\parallel}(\text{Cu})$ and energies of $d-d$ transitions were used to evaluate the bonding parameters α^2 , β^2 and γ^2 , which may be regarded as measures of covalency of the in-plane σ -bonds, in-plane π -bonds and out-of-plane π -bonds respectively [43]. Since α^2 values decrease with increasing covalency and obtained values lie above 0.5 and below 1.0, it is inferred that the complexes have significant covalent character in the ligand environment.

Table 7.3. EPR spectral parameters of copper(II) complexes in the polycrystalline state at 298 K and in DMF/DMSO at 77 K.

	14	15	16	17	18	19	20	21	22
Polycrystalline									
(298 K)									
g_{\parallel}/g_{\perp}	-	-	2.352	2.138	2.198	2.352	2.244	2.053	2.044
$g_{\perp}/g_2, g_3$	-	-	2.092	2.110	2.106	2.108	2.059	2.069,	2.110,
								2.244	2.198
$g_{\text{iso}}/g_{\text{av}}$	2.139	2.099	2.178	2.119	2.136	2.189	2.120	-	-
G	-	-	2.025	1.259	1.887	3.308	4.262	-	-
DMF/									
DMSO (77 K)									
g_{\parallel}/g_{\perp}	2.205	2.125	2.184	2.060	2.192	2.015	2.225	2.270	-
$g_{\perp}/g_2, g_3$	2.050	2.066	2.092	2.142	2.079	2.086,	2.055	2.040	-
						2.248			
$g_{\text{av}}/g_{\text{iso}}$	2.101	-	2.122	2.114	2.116	-	2.111	2.116	2.110
A_{\parallel}	197.29	269.50	176.72	-	-	111.36	165.50	166.02	-
α^2	0.809	0.972	0.7482	-	-	-	0.742	0.784	-
β^2	0.812	0.541	0.8334	-	-	-	0.940	0.975	-
γ^2	0.785	0.778	1.1698	-	-	-	0.911	0.728	-
K_{\parallel}	0.657	0.526	0.6236	-	-	-	0.698	0.765	-
K_{\perp}	0.635	0.757	0.8753	-	-	-	0.677	0.571	-

^a Expressed in units of cm^{-1} multiplied by a factor of 10^{-4}

7.3.7. X-ray crystallography

Suitable green block shaped crystals of [Cu(BPB)₂] were obtained by the slow evaporation of its solution in methanol and single crystal X-ray diffraction data were collected at 273(2) K using a Bruker SMART CCD area diffractometer with graphite monochromated Mo K α radiation ($\lambda = 0.71073 \text{ \AA}$). The Bruker SAINT software was used for data reduction and Bruker SMART for cell refinement. The trial structure was solved using SHELXL-97 by direct methods and refinement was carried out by full-matrix least squares procedures on F^2 using SHELXL-97 programs [44]. Anisotropic displacement parameters were defined for all non-hydrogen atoms. Positions of hydrogen atoms were derived from Fourier difference maps which were placed geometrically and refined with a riding model.

X-ray quality crystals of **19** were grown from its methanol-acetonitrile mixture and the crystal chosen for analysis is formulated as [Cu(DKN)₂] \cdot H₂O; hydrogen atoms of the lattice water could not be located using difference Fourier map and are not included in the model. The determination of the crystal structure was carried out on a Bruker P4 X-ray diffractometer using graphite monochromated Mo K α radiation ($\lambda = 0.71073 \text{ \AA}$) at 153 K. The data was solved using Bruker SHELXTL by direct method and refined by the full matrix least squares method on F^2 using Bruker SHELXTL [44]. The Bruker SAINT software was used for data reduction and Bruker SMART for cell refinement. The atoms C(32) and C(33) of a pyridine ring are disordered over two sites with relative occupancies of 58 and 42% for A and B components respectively. All non-hydrogen atoms were refined with anisotropic displacement parameters. The hydrogen atoms attached to carbon were placed in calculated positions with C–H = 0.93 \AA (aromatic protons) and $U(\text{H}) = 1.2 U_{\text{eq}}(\text{C})$ and refined isotropically in the riding model approximation. Pertinent crystallographic data and structure refinement parameters for the structures are given in Table 7.4. The molecular

structures of the complexes **16** and **19** were plotted using DIAMOND Version 3.1f [45] and ORTEP respectively [46] and the remaining figures were drawn using MERCURY [47].

Table 7.4. Crystallographic and refinement details of complexes [Cu(BPB)₂] (**16**) and [Cu((DKN)₂)]·H₂O (**19**).

Parameters	[Cu(BPB) ₂] (16)	[Cu((DKN) ₂)]·H ₂ O (19)
Empirical Formula	C ₃₈ H ₂₈ CuN ₆ O ₂	C ₃₄ H ₂₄ CuN ₁₀ O ₃
Formula weight (M)	664.21	684.18
Temperature (T) K	273(2)	153(2) K
Wavelength (Mo K α) (Å)	0.71073	0.71073
Crystal system	Triclinic	Monoclinic
Space group	<i>P</i> -1	<i>P</i> 2 ₁
Lattice constants		
<i>a</i> (Å)	10.6493(13)	9.3770(19)
<i>b</i> (Å)	12.4467(15)	10.111(2)
<i>c</i> (Å)	12.9613(15)	16.763(3)
α (°)	67.641(2)	90
β (°)	83.979 (2)	101.33(3)
γ (°)	83.907(2)	90
Volume <i>V</i> (Å ³)	1576.0(3)	1557.2(5)
<i>Z</i>	2	2
Calculated density (ρ) (Mg m ⁻³)	1.400	1.459
Absorption coefficient, μ (mm ⁻¹)	0.738	0.755
<i>F</i> (000)	686	702.0
θ Range for data collection	2.48-22.63°	2.22-25.00°
Limiting Indices	-13 \leq h \leq 13, -15 \leq k \leq 15 -15 \leq l \leq 15	-11 \leq h \leq 11, -12 \leq k \leq 12 -19 \leq l \leq 19
Reflections collected	12215	14918
Unique Reflections	6189 [R(int) = .0441]	5466
Refinement method	Full-matrix least-squares on <i>F</i> ²	Full-matrix least-squares on <i>F</i> ²
Data / restraints / parameters	6189 / 0 / 424	5086 / 17 / 453
Goodness-of-fit on <i>F</i> ²	1.239	1.055
Final <i>R</i> indices [<i>I</i> > 2 σ (<i>I</i>)]	R ₁ = 0.0968, wR ₂ = 0.1859	R ₁ = 0.0356, wR ₂ = 0.086
<i>R</i> indices (all data)	R ₁ = 0.1194, wR ₂ = 0.1960	R ₁ = 0.0387, wR ₂ = 0.0875

$$wR_2 = [\sum w(F_o^2 - F_c^2)^2 / \sum w(F_o^2)^2]^{1/2}; R_1 = \sum ||F_o| - |F_c|| / \sum |F_o|$$

7.3.7.1. Crystal structures of [Cu(BPB)₂] (16) and [Cu((DKN)₂)]·H₂O (19)

Green plate-shaped crystals of [Cu(BPB)₂] were obtained by slow evaporation from its methanolic solution. Molecular structure of [Cu(BPB)₂] together with the atom labeling scheme is depicted in Fig. 7.38. Selected bond lengths and bond angles are listed in Table 7.5. Compound crystallizes in triclinic space group *P*-1 and the Cu(II) center exhibits a distorted octahedral geometry comprising of two equivalent monoanionic ligands coordinated in a meridional fashion using *cis* pyridyl, *trans* azomethine nitrogen and *cis* enolate oxygen atoms. The ligand has undergone keto-enol tautomerism and the torsional angle C9–C8–N2–N1, 176.34° observed supports the *E* conformation of the ligand on coordination [48]. The Cu(II) complex bears a tetragonally elongated structure with *trans* pair of bonds, Cu1–N3 and Cu1–O1, being longer than the remaining four bond lengths (Cu1–N6, Cu1–N5, Cu1–O2, Cu1–N2). This is a consequence of the Jahn Teller effect that operates on the *d*⁹ electronic ground state of the six coordinate complex which elongates one *trans* pair of coordinate bonds while shortening the remaining four. From the bond angles O1–Cu1–N2, 75.25(16)°; N2–Cu1–N3, 75.61(17)°; N5–Cu1–N6, 79.37(18)°; N5–Cu1–O2, 78.21(17)°; it is observed that the coordination geometry is quite far from a perfect octahedron [49]. The Cu(II) center is shared by four fused five membered chelate rings and the bicyclic chelate system {Cu1,O1,C7,N1,N2,C8,C9,N3} making a dihedral angle of 86.47° with its counter part {Cu1,O2,C26,N4,N5,C27,C28,N6} is approximately planar with a maximum mean plane deviation of 0.1517 Å for N3 and 0.0933 Å for C28 [50]. The Cu–N(py), Cu–N(imine) and Cu–O bond lengths observed here are within the range reported for other similar complexes of divalent metal ions. In general, the shortest coordinate bonds are to the central imine N donors, while those to the distal pyridyl and carbonyl groups are significantly weaker. This can be attributed to greater π-back bonding in the Cu–

N(imine) bond than in the Cu–N(py) bond and also to the steric requirements of the meridionally coordinated ligand [51].

Table 7.5. Selected bond lengths (Å) and bond angles (°) for [Cu(BPB)₂] (**16**) and [Cu(DKN)₂]·H₂O (**19**).

[Cu(BPB) ₂] (16)		[Cu(DKN) ₂]·H ₂ O (19)	
<i>Bond lengths</i>		<i>Bond lengths</i>	
Cu1–N5	1.953(4)	Cu1–N2	1.986(2)
Cu1–N2	2.012(4)	Cu1–N7	1.947(2)
Cu1–O1	2.202(4)	Cu1–O1	2.253(2)
Cu1–O2	2.048(4)	Cu1–O2	2.066(2)
Cu1–N3	2.290(5)	Cu1–N1	2.276(3)
Cu1–N6	2.083(4)	Cu1–N6	2.069(2)
N2–N1	1.366(6)	N2–N3	1.378(3)
N5–N4	1.378(6)	N7–N8	1.357(3)
N2–C8	1.298(6)	N2–C6	1.299(4)
N5–C27	1.290(6)	N7–C23	1.297(3)
O1–C7	1.254(6)	O1–C12	1.253(3)
O2–C26	1.253(6)	O2–C29	1.264(3)
N1–C7	1.346(7)	N3–C12	1.338(4)
N4–C26	1.349(7)	N8–C29	1.338(4)
<i>Bond angles</i>		<i>Bond angles</i>	
N5–Cu1–N2	172.06(19)	N2–Cu1–N7	171.7(3)
N2–Cu1–O1	75.25(16)	N2–Cu1–O1	74.8 (6)
N2–Cu1–N3	75.61(17)	N2–Cu1–N1	76.3 (9)
N5–Cu1–O2	78.21(17)	N7–Cu1–O2	78.2 (5)
N5–Cu1–N6	79.37(18)	N7–Cu1–N6	79.0 (0)
O1–Cu1–N3	149.91(15)	O1–Cu1–N1	150.9(8)
O2–Cu1–N6	157.36(16)	O2–Cu1–N6	156.1(9)
N5–Cu1–N3	100.19(17)	N7–Cu1–N1	96.7(9)
N2–Cu1–N6	94.47(17)	N2–Cu1–N6	97.2(9)
N6–Cu1–N3	98.51(17)	N6–Cu1–N1	99.2(2)
O1–Cu1–N3	149.91(15)	O2–Cu1–N1	90.3(4)
N6–Cu1–O1	91.07(16)	N6–Cu1–O1	88.2(8)
N2–Cu1–O2	108.14(16)	N2–Cu1–O2	106.1(7)
O2–Cu1–N3	88.56(16)	O2–Cu1–O1	93.8(7)
O2–Cu1–O1	93.45(15)	C6–N2–N3	118.1(2)
C8–N2–N1	119.2(4)	C23–N7–N8	122.3(2)

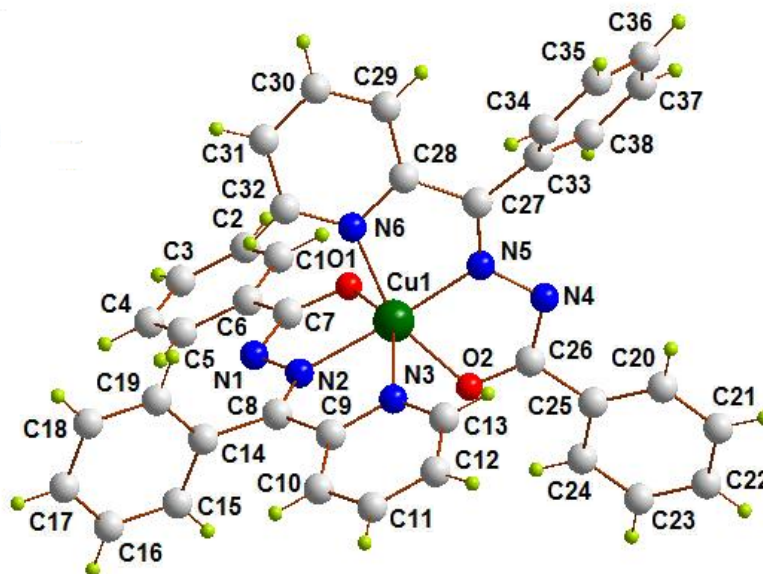


Fig. 7.38. The molecular structure of $[\text{Cu}(\text{BPB})_2]$ (**16**) along with the atom numbering scheme.

The packing of the complex is shown in Fig. 7.39. In the unit cell the molecules are packed in the lattice in an ordered manner along the a axis. The π - π , C-H \cdots π and hydrogen bonding interactions (Table 7.6) contribute to the stability in the unit cell packing. The six membered ring Cg(6) {N(6), C(28), C(29), C(30), C(31), C(32)} is involved in π - π interaction with Cg(6) of the neighboring unit at a distance of 3.807(4) Å. In addition to the π - π stacking, significant C-H \cdots π interactions of the phenyl hydrogens with metal chelate rings of the neighboring molecules contributes to the stability of the unit cell packing. Two weak hydrogen bonding interactions are observed between C(15)-H(15) and N(1) and between C(30)-H(30) and O(1) with an angle of 136 and 124° respectively. No classic hydrogen bonds are found in this complex. Ring puckering analysis shows that the five membered ring, Cg(1) {Cu1-O1-C7-N1-N2} is puckered and adopts an envelope conformation with N2 forming the flap of the envelope { $Q = 0.100(4)$ Å; $\varphi = 146(3)^\circ$ } [52].

Table 7.6. H-bonding, π - π and C-H $\cdots\pi$ interaction parameters of [Cu(BPB)₂] (**16**).

H-bonding				
Donor-H \cdots A (Å)	D-H	H \cdots A	D \cdots A	D-H \cdots A
C15-H(15) \cdots N(1) ^a	0.93	2.60	3.3318	136
C30-H(30) \cdots O(1) ^b	0.93	2.55	3.1618	124
π - π interactions				
Cg(I) \cdots Cg(J)	Cg-Cg (Å)	α (°)	β (°)	
Cg(6) \cdots Cg(6) ^c	3.8074	21.44	21.44	
C-H $\cdots\pi$ interaction				
X-H(I) \cdots Cg(J)	H \cdots Cg (Å)	X-H \cdots Cg (°)	X \cdots Cg (Å)	
C(16)-H(16) \cdots Cg(1) ^d	2.76	142	3.5348	
Equivalent position codes				
a = 1-x, -y, -z, b = -x, 1-y, -z, c = -x, 1-y, -z, d = 1-x, -y, -z				
Cg(6) = N(6), C(28), C(29), C(30), C(31), C(32); Cg(1) = Cu (1), O(1), C(7), N(1), N(2)				

D, donor; A, acceptor; Cg, centroid; α , dihedral angles between planes I and J; β , angle Cg(I) – Cg(J) vector normal to plane I

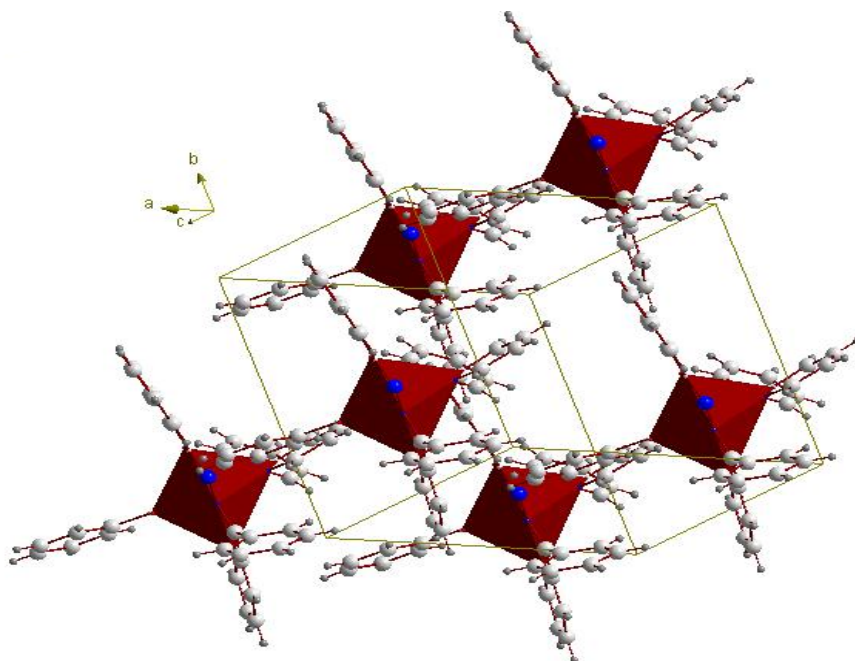


Fig. 7.39. Packing diagram of complex **16** with octahedral polyhedra around the Cu(II) centers.

The crystal structure of $[\text{Cu}(\text{DKN})_2]$ is similar to that of $[\text{Cu}(\text{BPB})_2]$. The Cu(II) ion is in an N_4O_2 coordination sphere in which each of the two meridionally spanning ligands coordinates the metal ion *via* the pyridine-N, imine-N and deprotonated amide-O atoms forming two five membered chelate rings (Fig. 7.40). A distinguishing feature of Cu(II) structure is its asymmetry. In similar complexes reported containing Mn(II), Ni(II) and Zn(II) divalent metal ions, the pairs of corresponding coordinate bond lengths to the two ligands are more or less the same, but here the two ligands bonded to copper are distinct. One ligand forms Cu–N and Cu–O bond lengths that are consistently longer than those of the other ligand. The deviation from perfect octahedron is evident from the bond distances and angles given in Table 7.5. For *eg.* the ideally linear trans angle N2–Cu1–N7 is $\sim 171.7(3)^\circ$ and the interligand angle N1–Cu1–O1 is $\sim 150.9(8)^\circ$, which gives clear evidence for the deviation from perfect octahedron [53]. Least square analyses shows that planes containing O1, N2, N1, Cu1 and N7 (plane 1) and O2, N7, N6, Cu1 and N2 (plane 2) shows a maximum deviation from the mean plane of $-1.3274(5) \text{ \AA}$ for N1 and $1.1553(4) \text{ \AA}$ for N6 and the dihedral angle formed by the two planes is $49.07(1)^\circ$.

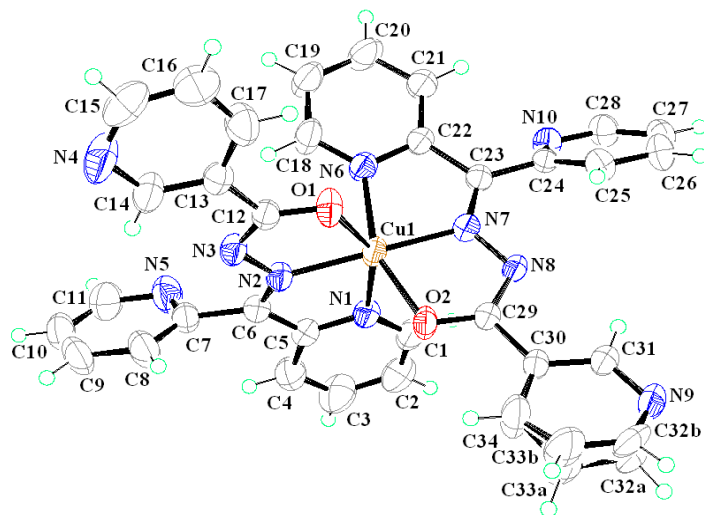


Fig. 7.40. The molecular structure of $[\text{Cu}(\text{DKN})_2] \cdot \text{H}_2\text{O}$ (19) along with the atom numbering scheme (Water molecule is not included for clarity).

There is one lattice water per molecule. C1–H(1) is involved in hydrogen bonding with nicotinoyl nitrogen (N9) of adjacent molecule. C10–H(10) is involved in hydrogen bonding with O2 of adjacent molecule and C20–H(20) is involved in hydrogen bonding with nicotinoyl nitrogen (N9) of yet another molecule. Thus adjacent molecules are linked into chains by these interactions as shown in Fig. 7.41. The metal chelate ring Cg(8) {N6, C18, C19, C20, C21, C22} is stacked *via* π - π interactions with Cg(9) {N9, C30, C31, C32A, C33A, C34} of the neighboring unit with a centroid to centroid distance of 3.708(5) Å [54]. In addition to the π - π stacking, significant C–H \cdots π interactions of the pyridyl hydrogens with metal chelate rings of the neighboring molecules adds the stability of the unit cell packing (Table 7.7). Ring puckering analyses shows that two five membered rings Cg(1) {Cu1–O1–C12–N3–N2}, Cg(2) {Cu1–O2–C29–N8–N7} are puckered and adopts an envelope conformation on Cu1 (Q(2) = 0.145(2) Å, Phi(2) = 360.0(11)°) and twisted conformation on N7 (Q(2) = 0.1042(19) Å, Phi(2) = 350.0(14)°) respectively [52].

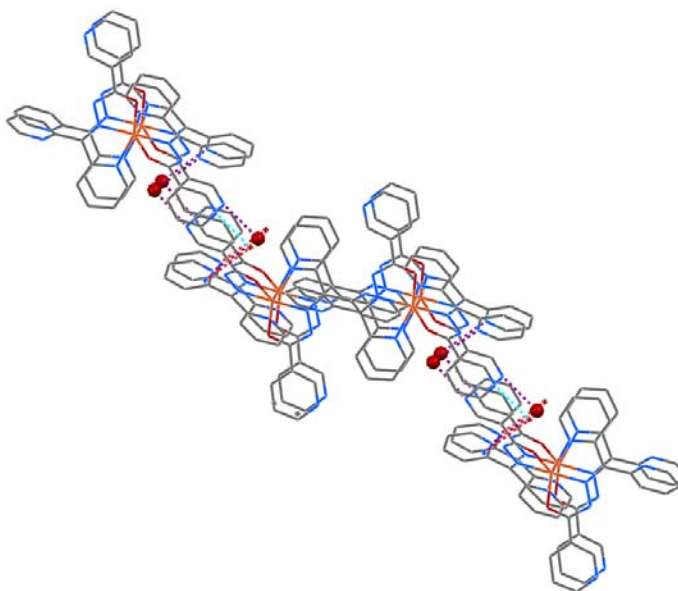


Fig. 7.41. Packing diagram of [Cu(DKN)₂] \cdot H₂O along 'b' axis.

Table 7.7. H-bonding, π - π and C-H $\cdots\pi$ interaction parameters of [Cu(DKN)₂] \cdot H₂O (19)

H-bonding				
D \cdots H \cdots A (Å)	D-H	H \cdots A	D \cdots A	D-H \cdots A
C1-H(1) \cdots N(9) ^a	0.93	2.62	3.371(4)	138
C10-H(10) \cdots O(2) ^b	0.93	2.50	3.221(4)	135
C20-H(20) \cdots N(9) ^c	0.93	2.58	3.389(5)	145
π - π interactions				
Cg(I) \cdots Cg(J)	Cg-Cg (Å)	α (°)	β (°)	
Cg(8) \cdots Cg(9) ^d	3.708(5)	5.6(4)	24.77	
Cg(9) \cdots Cg(8) ^e	3.708(5)	5.6(4)	19.33	
C-H $\cdots\pi$ interaction				
X-H \cdots Cg(J)	H \cdots Cg (Å)	X-H \cdots Cg (°)	X \cdots Cg (Å)	
C(28)-H(28) \cdots Cg(2) ^f	2.64	150	3.482(3)	
Equivalent position codes				
a = 2-x, 1/2+y, 1-z, b 1-x, 1/2+y, -z, c = 1-x, 1/2+y, 1-z, d = -1+x, y, z, e = 1+x, y, z, f = 1-x, 1/2+y, 1-z				
Cg(8) = N(6), C(18), C(19), C(20), C(21), C(22) ; Cg(2) = Cu (1), O(2), C(29), N(8), N(7); Cg(9) = N(9), C(30), C(31), C(32A), C(33A), C(34)				

D, donor; A, acceptor; Cg, centroid; α , dihedral angles between planes I and J; β , angle Cg(I) – Cg(J) vector normal to plane I

References

- [1] T. Miura, A. Hori-i, H. Mototani, H. Takeuchi, *Biochem.* 38 (2009) 11560.
- [2] C. Fernandes, G.L. Parrilha, J.A. Lessa, L.J.M. Santiago, M.M. Kanashiro, F.S. Boniolo, A.J. Bortoluzzi, N.J. Vugman, M.H. Herbst, A. Jr. Horn, *Inorg. Chim. Acta* 359 (2006) 3167.

- [3] V. Rajendiran, R. Karthik, M. Palaniandavar, H.S. Evans, V.S. Periasamay, M.A. Akbarsha, B.S. Srinag, H. Krishnamurthy, *Inorg. Chem.* 46 (2007) 8208.
- [4] P. Mukherjee, M.G.B. Drew, C.J.G. Garcia, A. Ghos, *Inorg. Chem.* 48 (2009) 5848.
- [5] Y. Song, S. Ohkoshi, Y. Arimoto, H. Seino, Y. Mizobe, K. Hashimoto, *Inorg. Chem.* 42 (2003) 1848.
- [6] O. Khan, S. Sikorav, J. Gouteron, S. Jeannin, Y. Jeannin, *Inorg. Chem.* 22 (1983) 2877.
- [7] P. Manikandan, R. Muthukumaran, K.R.J. Thomas, B. Varghese, G.V.R. Chandramouli, P.T. Manoharan, *Inorg. Chem.* 40 (2001) 2378.
- [8] S. Banerjee, A. Ray, S. Sen, S. Mitra, D.L. Hughes, R.J. Butcher, S.R. Batten, D.R. Turner, *Inorg. Chim. Acta* 361 (2008) 2692.
- [9] A. Ray, S. Banerjee, R.J. Butcher, C. Desplanches, S. Mitra, *Polyhedron* 27 (2008) 2409.
- [10] J. Luo, X.-G. Zhou, S. Gao, L.-H. Weng, Z.-H. Shao, C.-M. Zhang, Y.-R. Li, J. Zhang, R.-F. Cai, *Polyhedron* 23 (2004) 1243.
- [11] S. Sen, S. Mitra, D.L. Hughes, G. Rosair, C. Desplanches, *Polyhedron* 26 (2007) 1740.
- [12] S.K. Dey, N. Mondal, M.S. El Fallah, R. Vicente, A. Escuer, X. Solans, M. Font-Bardia, T. Matsushita, V. Gramlich, S. Mitra, *Inorg. Chem.* 43 (2004) 2427.
- [13] J. Ribas, M. Monfort, X. Solans, M. Drillon, *Inorg. Chem.* 33 (1994) 742.
- [14] P. Talukder, A. Datta, S. Mitra, G. Rosair, M.S. El Fallah, J. Ribas, *Dalton Trans.* (2004) 4161.

- [15] W.J. Geary, *Coord. Chem. Rev.* 7 (1971) 109.
- [16] N. Filipovic, H. Borrmann, T. Todorovic, M. Borna, V. Spasojevic, D. Sladic, I. Novakovic, K. Andjelkovic, *Inorg. Chim. Acta* 362 (2009) 2000.
- [17] T. Ghosh, *Trans. Met. Chem.* 31 (2006) 560.
- [18] M.F. Iskander, T.E. Khalil, R. Werer, W. Haase, I. Svoboda, H. Fuess, *Polyhedron* 19 (2000) 949.
- [19] R.C. Maurya, S. Rajput, *J. Mol. Struct.* 833 (2007) 133.
- [20] P. Noblia, E.J. Baran, L. Otero, P. Draper, H. Cerecetto, M. Gonzalez, O.E. Piro, E.E. Castellano, T. Inohara, Y. Adachi, H. Sakurai, D. Gambino, *Eur. J. Inorg. Chem.* (2004) 322.
- [21] H. Yin, *Acta Cryst. C* 64 (2008) 324.
- [22] R.C. Maurya, S. Rajput, *J. Mol. Struct.* 833 (2007) 133.
- [23] N.A. Mangalam, M.R.P. Kurup, *Spectrochim. Acta Part A* 71 (2009) 2040.
- [24] J. Chakraborty, S. Thakurta, G. Pilet, D. Luneau, S. Mitra, *Polyhedron* 28 (2009) 819.
- [25] P.F. Raphael, E. Manoj, M.R.P. Kurup, *Polyhedron* 26 (2007) 5088.
- [26] K. Nakamoto, *Infrared and Raman spectra of Inorganic and Coordination compounds*, 5th ed., Wiley, New York, 1997.
- [27] C. Basu, S. Biswas, A.P. Chattopadhyay, H.S. Evans, S. Mukherjee, *Eur. J. Inorg. Chem.* 31 (2008) 4927.
- [28] A. Ray, C. Rizzoli, G. Pilet, C. Desplanches, E. Garribba, E. Rentschler, S. Mitra, *Eur. J. Inorg. Chem.* (2009) 2915.
- [29] S. Koner, S. Saha, T. Mallah, K.-I. Okamoto, *Inorg. Chem.* 43 (2004) 840.

- [30] S.C. Chan, L.L. Koh, P.-H. Leung, J.D. Ranford, K.Y. Sim, *Inorg. Chim. Acta* 236 (1995) 101.
- [31] M. Morshedi, M. Amirnasr, A.M.Z. Slawin, J.D. Woollins, A.D. Khalaji, *Polyhedron* 28 (2009) 167.
- [32] M. Singh, V. Aggarwal, U.P. Singh, N.K. Singh, *Polyhedron* 28 (2009) 195.
- [33] A.B.P. Lever, *Inorganic Electronic Spectroscopy*, 2nd edition, Elsevier, Amsterdam, 1984.
- [34] R. Li, B. Moubaraki, K.S. Murray, S. Brooker, *Dalton Trans.* (2008) 6014.
- [35] G. Swarnabala, M.V. Rajasekharan, *Inorg. Chem.* 28 (1989) 662.
- [36] S. Thakurta, P. Roy, G. Rosair, C.J.G. -Garcia, E. Garribba, S. Mitra, *Polyhedron* 28 (2009) 695.
- [37] V.P. Singh, *Spectrochim. Acta Part A* 71 (2008) 17.
- [38] I.M. Procter, F.S. Stephens, *J. Chem. Soc. A* (1969) 1248.
- [39] E. Manoj, M.R.P. Kurup, *Spectrochim. Acta Part A* 72 (2009) 474.
- [40] B.J. Hathaway, G. Wilkinson, R.D. Gillard, J.A. McCleverty (Eds.), *Comprehensive Coordination Chemistry*, vol. 5. Pergamon, Oxford, (1987) 533.
- [41] I.M. Procter, B.J. Hathaway, P. Nicholls, *J. Chem. Soc. A* (1968) 1678.
- [42] M. Antosik, N.M.D. Brown, A.A. McConnell, A.L. Porte, *J. Chem. Soc. A* (1969) 545.
- [43] U.L. Kala, S. Suma, S. Krishnan, M.R.P. Kurup, R.P. John, *Polyhedron* 26 (2007) 1427.
- [44] G.M. Sheldrick, *Acta Crystallogr. A* 64 (2008) 211.

- [45] K. Brandenburg, Diamond Version 3.1f, Crystal Impact GbR, Bonn, Germany, 2008.
- [46] L.J. Farrugia, J. Appl. Crystallogr. 30 (1997) 565.
- [47] C.F. Macrac, P.R. Edington, P. McCabe, E. Pidcock, G.P. Shields, R. Taylor, M. Towler, J. Van de Streek, J. Appl. Cryst. 39 (2006) 453.
- [48] V. Suni, M.R.P. Kurup, M. Nethaji, Polyhedron 26 (2007) 3097.
- [49] A.S. -Pedrares, N. Camina, J. Romero, M.L. Duran, J.A. G. -Vazquez, A. Sousa, Polyhedron 27 (2008) 3391.
- [50] E. Manoj, M.R.P. Kurup, Polyhedron 27 (2008) 275.
- [51] A. Sreekanth, H. -K. Fun, M.R.P. Kurup, J. Mol. Struct. 737 (2005) 61.
- [52] D. Cremer, J.A. Pople, J. Amer. Chem. Soc. 97 (1975) 1354.
- [53] A.R. Stefankiewicz, M.W.-Chorab, H.B. Szczesniak, V. Patroniak, M. Kubicki, Z. Hnatejko, J. Harrowfield, Polyhedron 29 (2010) 178.
- [54] M. Kuriakose, M.R.P. Kurup, Struct. Chem. 18 (2007) 579.

Chapter 8

Syntheses, spectral and structural characterization of zinc/cadmium(II) complexes incorporating tridentate acylhydrazones

Contents

- 8.1 Introduction
- 8.2 Experimental
- 8.3 Results and discussion
- Reference

8.1. Introduction

Complexes of d^{10} metal ions, such as Zn(II) and Cd(II) are also of interest since they are involved in many biological processes [1,2]. The chemical similarity of Zn(II) and Cd(II) suggests that the latter may displace the former from the active site in enzyme containing Zn(II). Although Cd has been known as a toxic metal and is often associated with mercury and lead as one of the biologically harmful metal ions, the Cd(II) ion has recently been found to serve as the catalytic centre in a newly discovered carbonic anhydrase [3]. Recent studies by Perez *et al.* on Zn(II) and Cd(II) complexes of thiosemicarbazones have shown that these complexes might overcome cisplatin resistance in murine keratinocytes overexpressing the H-ras oncogene [4].

In addition to their importance in biology, Zn(II) and Cd(II) complexes of mixed diimine ligands have also been shown to display interesting type of ligand-to-ligand charge transfer transition without the involvement of the metal ion. The complexes of Zn(II) and Cd(II) show intense luminescence at room temperature and thus have potential applications as photoactive materials [5-7]. Recently Ray *et al.* have reported that acylhydrazones show intense emission bands when excited with light of suitable wavelength. It was found that these band intensities were reduced many fold and blue shifted on complexation. Quenching of fluorescence of ligands is a rather common phenomenon and since the emission intensities get reduced in the complexes, the fluorescence character is mainly due to the ligand [8].

8.2. Experimental

8.2.1. Materials

Di-2-pyridylketone (Aldrich), 2-benzoylpyridine (Aldrich), benzhydrazide (Aldrich), and nicotinic hydrazide (Aldrich), cadmium(II) acetate dihydrate (E-Merck), cadmium(II) chloride·2¹/₂H₂O (Aldrich), cadmium(II) bromide tetrahydrate (Aldrich), zinc(II) acetate dihydrate (Aldrich) and potassium thiocyanate (Merck) were used as received. Solvents were purified by standard procedures before use.

8.2.2. Syntheses of the acylhydrazones

The syntheses of hydrazones HBPB and HDKN are discussed already in Chapter 2.

8.2.3. Syntheses of the complexes

8.2.3.1. Synthesis of $[Cd(BPB)_2]$ (23)

The complex was obtained according to a general procedure: the hydrazone HBPB (0.301 g, 1 mmol) was dissolved in methanol, this was followed by the addition of $Cd(CH_3COO)_2 \cdot 2H_2O$ (0.266 g, 1 mmol) in methanol and the reaction mixture was refluxed for 3 h. The precipitated solid was then filtered, washed with methanol and ether and dried over P_4O_{10} *in vacuo*.

$[Cd(BPB)_2]$ (23): Yield: 79%, λ_m (DMF): $3 \text{ ohm}^{-1}\text{cm}^2 \text{ mol}^{-1}$, Elemental Anal. Found (Calcd.) (%): C: 64.05 (64.01), H: 3.84 (3.96), N: 11.72 (11.79).

8.2.3.2. Synthesis of $[Cd(BPB)Cl]$ (24)

To a methanolic solution of HBPB (0.301 g, 1 mmol), aqueous solution of $CdCl_2 \cdot 2\frac{1}{2}H_2O$ (0.228 g, 1 mmol) was added slowly. The reaction mixture was kept under reflux for 3 h. Light cream colored crystalline product formed was filtered, washed with methanol and ether and dried over P_4O_{10} *in vacuo*.

$[Cd(BPB)Cl]$ (24): Yield: 83%, λ_m (DMF): $15 \text{ ohm}^{-1}\text{cm}^2 \text{ mol}^{-1}$, Elemental Anal. Found (Calcd.) (%): C: 50.72 (50.92), H: 2.84 (3.15), N: 9.36 (9.38).

8.2.3.3. Synthesis of $[Cd(HBPB)Br_2]$ (25)

An aqueous solution of $CdBr_2 \cdot 4H_2O$ (0.344 g, 1 mmol) was added gradually to a solution of HBPB (0.301 g, 1 mmol) in methanol. The reaction mixture was heated to reflux for 3 h. A cream colored crystalline solid was obtained on hot and obtained after cooling, then filtered off, washed several times with methanol, ether and dried over P_4O_{10} *in vacuo*.

$[Cd(HBPB)Br_2]$ (25): Yield: 71%, λ_m (DMF): $18 \text{ ohm}^{-1}\text{cm}^2 \text{ mol}^{-1}$, Elemental Anal. Found (Calcd.) (%): C: 39.90 (39.79), H: 2.62 (2.64), N: 7.34 (7.33).

8.2.3.4. Synthesis of [Zn(DKN)NCS] (26)

To a solution of HDKN (0.312 g, 1 mmol) in methanol, potassium thiocyanate (0.097 g, 1 mmol) dissolved in minimum volume of water was added and stirred for half an hour. To this mixture, Zn(CH₃COO)₂·2H₂O (0.219 g, 1 mmol) in methanol was added and refluxed for 3 h. Yellow solid obtained soon after refluxing was filtered, washed with methanol, ether and dried over P₄O₁₀ *in vacuo*.

[Zn(DKN)NCS] (26): Yield: 63%, λ_m (DMF): 15 ohm⁻¹cm² mol⁻¹, Elemental Anal. Found (Calcd.) (%): C: 50.59 (50.77), H: 2.66 (2.84), N: 19.33 (19.74).

8.2.3.5. Synthesis of [Cd(DKN)OAc]·H₂O (27)

Complex 27 was synthesized by refluxing equimolar solutions of HDKN (0.312 g, 1 mmol) and Cd(CH₃COO)₂·2H₂O (0.266 g, 1 mmol) in methanol for 3 h. Light yellow colored product obtained was filtered, washed with methanol, ether and dried over P₄O₁₀ *in vacuo*.

[Cd(DKN)OAc]·H₂O (27): Yield: 59%, λ_m (DMF): 11 ohm⁻¹cm² mol⁻¹, Elemental Anal. Found (Calcd.) (%): C: 45.78 (46.21), H: 3.64 (3.88), N: 13.91 (14.18).

8.2.3.6. Synthesis of [Cd(HDKN)Cl₂] (28)

The hydrazone HDKN (0.312 g, 1 mmol) was dissolved in methanol and to this solution CdCl₂·2½H₂O (0.228 g, 1 mmol) in minimum volume of water was added dropwise with stirring. The mixture was further refluxed for 3 h. and the resulting product was filtered, washed with methanol, ether and dried over P₄O₁₀ *in vacuo*.

[Cd(HDKN)Cl₂] (28): Yield: 66%, λ_m (DMF): 13 ohm⁻¹cm² mol⁻¹, Elemental Anal. Found (Calcd.) (%): C: 41.48 (41.96), H: 2.58 (2.69), N: 13.98 (14.39).

8.3. Results and discussion

8.3.1. Elemental analyses and molar conductivity studies

The elemental analyses data agree well with the proposed formulae for the complexes. The molar conductance values of the complexes (10^{-3} M DMF) lie in the range $11\text{--}18\text{ ohm}^{-1}\text{cm}^2\text{ mol}^{-1}$. These low values indicate their non-electrolytic nature as expected [9].

8.3.2. Infrared spectra

Infrared spectral techniques are proved to be useful in identifying the potentially active sites of the hydrazones and the characteristic bands of the hydrazones and complexes are summarized in Table 8.1. The stretching frequency of the azomethine (C=N) group in HBPB observed near 1571 cm^{-1} is shifted to lower frequency values upon complexation with the metal by $20\text{--}40\text{ cm}^{-1}$, suggesting coordination *via* the azomethine group in its complexes [10]. Characteristic band of the hydrazone due to $\nu(\text{N--N})$ stretching has undergone shift to higher wavenumber in complexes due to the increase in the double bond character of N–N, offsetting the loss of electron density *via* donation to the metal ion which gives further evidence of coordination of the ligand through the imine nitrogen atom. Also the complexes **23** and **24** exhibit a strong absorption at 1589 and 1585 cm^{-1} respectively which was absent in the free ligand, and this can be assigned due to the conjugated C=N--N=C--O^- moiety [11]. The disappearance of characteristic spectral band of $\nu(\text{NH})$ and $\nu(\text{C=O})$ of HBPB in **23** (Fig. 8.1) and **24** (Fig. 8.2) complexes suggest the coordination *via* enolate form instead of amido form by the deprotonation of N–H proton during the tautomerisation process [12]. The low energy pyridine ring-in-plane and out-of-plane vibrations are shifted to higher frequencies when compared with the corresponding bands in HBPB, which is a good indication of the coordination of the heterocyclic nitrogen atom [13].

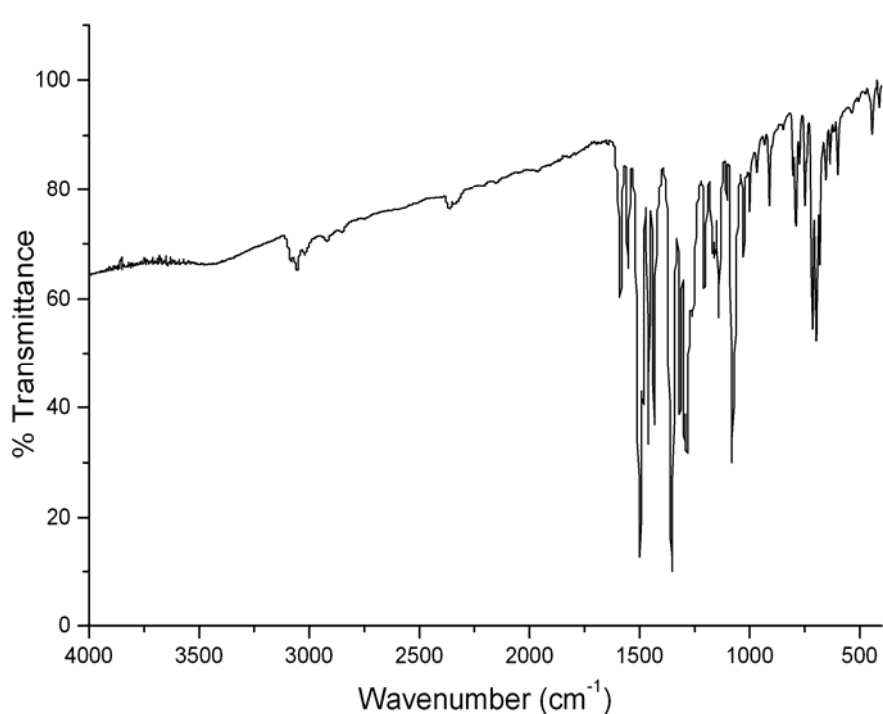


Fig. 8.1. IR spectrum of $[\text{Cd}(\text{BPB})_2]$ (23).

On comparison of the IR spectra of the hydrazone HBPB with the metal complex **24**, $\nu(\text{C}=\text{N})$ has undergone a shift to lower wavenumber (1553 cm^{-1}) suggesting the involvement of azomethine nitrogen with the metal ion. Also the absence of $\nu(\text{NH})$ and $\nu(\text{C}=\text{O})$ bands at 3063 and 1678 cm^{-1} clearly give an evidence of establishing amido-iminol tautomeric system in which the hydrazones has undergone enolization and got deprotonated and has coordinated to the metal centre through this enolate oxygen.

The $\nu(\text{C}=\text{O})$ stretching frequency band in HBPB at 1678 cm^{-1} has undergone only a slight shift to lower wavenumber (Fig. 8.2). This suggests that the ligand has not undergone enolization and has coordinated in neutral form [14]. Coordination of carbonyl oxygen to the metal atom reduces the electron density in the $\text{C}=\text{O}$ bond causing a shift in the $\nu(\text{C}=\text{O})$ band.

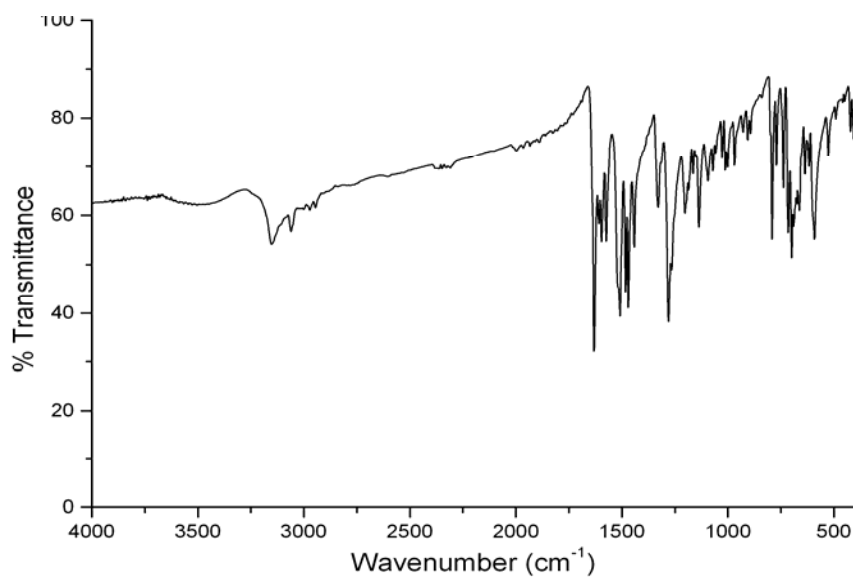


Fig. 8.2. IR spectrum of $[\text{Cd}(\text{HBPB})\text{Br}_2]$ (25).

The spectrum of the thiocyanate complex displayed an intense band at 2081 cm^{-1} (Fig. 8.3) indicating that the thiocyanate group acts as monodentate ligand coordinating through the nitrogen atom [15,16].

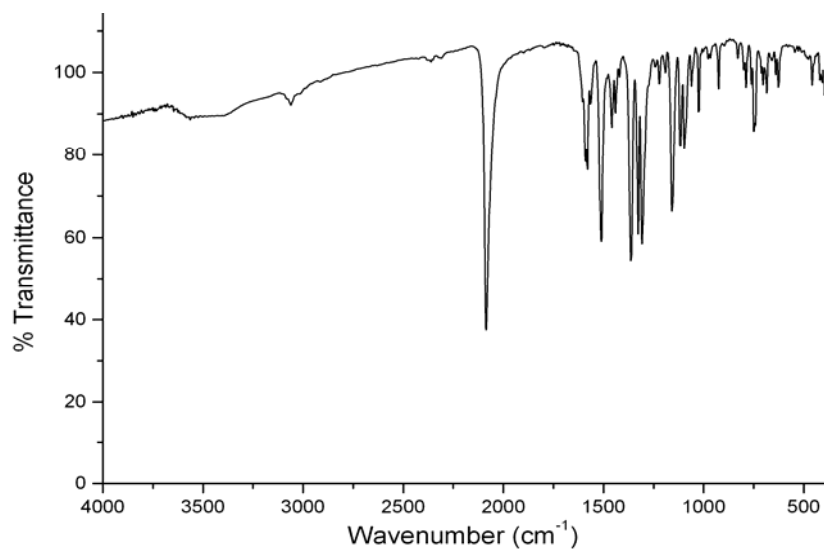


Fig. 8.3. IR spectrum of $[\text{Zn}(\text{DKN})\text{NCS}]$ (26).

The free acetate ion CH_3COO^- exhibits the $\nu_{\text{as}}(\text{COO})$ and $\nu_{\text{s}}(\text{COO})$ at 1578 and 1414 cm^{-1} respectively. It is reported that if it is covalently bonded to a metal as a unidentate ligand the ν_{as} and ν_{s} are shifted to higher and lower frequencies respectively [15]. The present acetato complex shows a peak near 1629 cm^{-1} possibly due to the ν_{as} stretch of the unidentate acetate group [17] (Fig. 8.4). Also the complex displayed a band at 1336 cm^{-1} which was seen in other complexes also. But when compared to the corresponding peak in other complexes, this was found to be significantly stronger. Thus it may be likely due to the ν_{s} stretch of acetate ion. The broad band in the region *ca.* 3130 cm^{-1} is assigned to the stretching frequency of water molecule associate with the complex which was also confirmed by the thermal analysis.

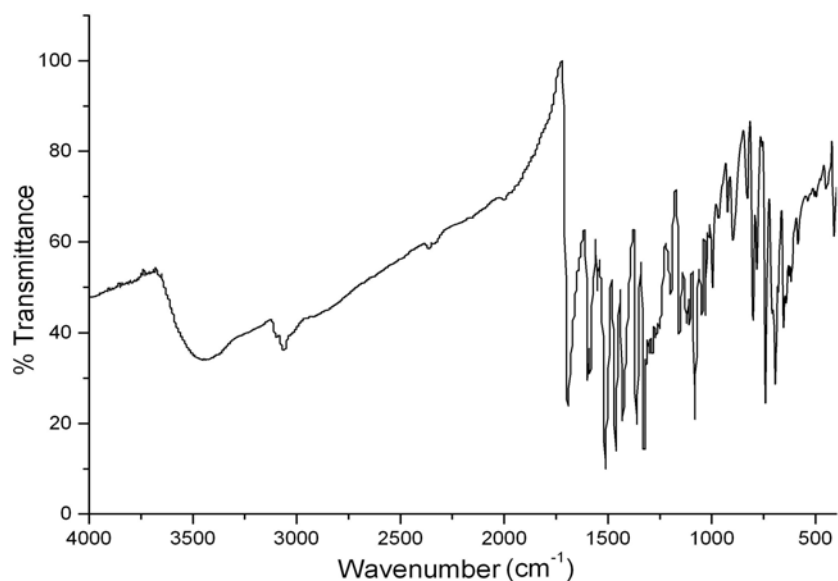


Fig. 8.4. IR spectrum of $[\text{Cd}(\text{DKN})\text{OAc}] \cdot \text{H}_2\text{O}$ (**27**).

In the case of complex **28**, HDKN is coordinated in neutral form as the decrease in $\nu(\text{C}=\text{O})$ stretching is less (1686 cm^{-1}) when compared to the corresponding band (1689 cm^{-1}) in ligand (Fig. 8.5).

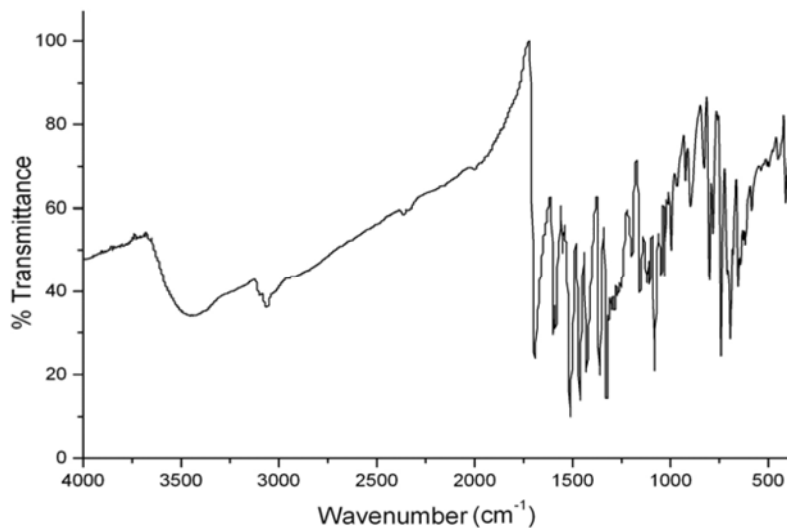


Fig. 8.5. IR spectrum of [Cd(HDKN)Cl₂] (**28**).

Table 8.1. Infrared spectral data (cm⁻¹) of Zn/Cd(II) complexes.

Compound	$\nu(\text{N-H})$	$\frac{\nu(\text{C=O})}{\nu(\text{C-O})}$	$\nu(\text{C=N})$	$\nu(\text{C=N})^a$	$\nu(\text{Cd/Zn-O})$	$\nu(\text{Cd/Zn-N})$
HBPB	3063	1678	1571
[Cd(BPB) ₂] (23)	...	1353	1554	1589	530	443
[Cd(BPB)Cl] (24)	...	1353	1553	1585	520	437
[Cd(HBPB)Br ₂] (25)	...	1626	1570	...	528	430
HDKN	2928	1689	1579
[Zn(DKN)NCS] (26)	...	1364	1517	1587	549	459
[Cd(DKN)OAc]·H ₂ O (27)	...	1336	1576	1590	530	451
[Cd(HDKN)Cl ₂] (28)	...	1686	1520	...	539	447

^aNewly formed C=N

8.3.3. Electronic spectra

The electronic spectra of the complexes were recorded in acetonitrile solution and spectral data are summarized in Table 8.2. The bands in the range 41410 – 33050 cm^{-1} in the electronic spectra of hydrazones are assigned to be the $\pi-\pi^*$ of azomethine, carbonyl group and pyridyl rings. The absorption maximum value of these bands suffered a bathochromic shift; this might greatly be due to the donation of lone pair of electrons to the metal and also due to the conjugation formed on complexation. In addition to this, a new band in the range 25690 – 26570 cm^{-1} is observed in the spectra of complexes and this can be assigned to the metal to ligand (M(II) \rightarrow O_{enolate}) charge transfer transitions (Fig. 8.6) [18].

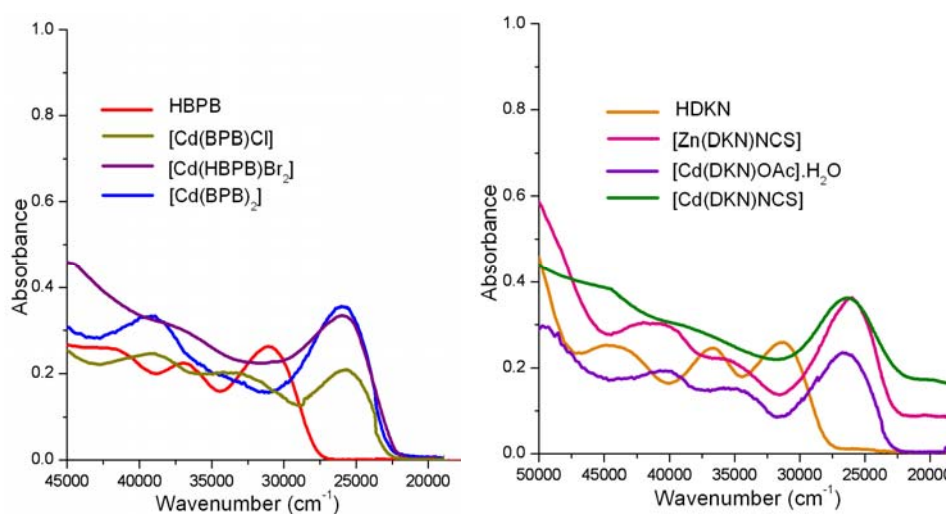


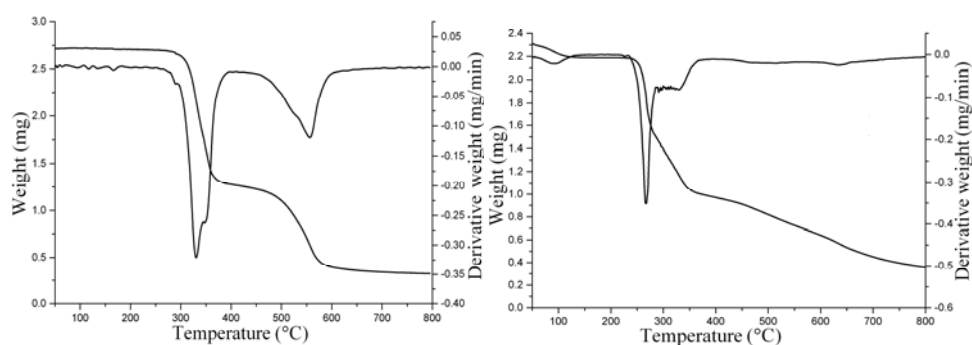
Fig. 8.6. Electronic spectra of the Zn/Cd(II) complexes.

Table 8.2. Electronic spectral data of the Zn/Cd(II) complexes.

Compound	UV absorption bands (cm ⁻¹)
[Cd(BPB) ₂] (23)	39140, 34320, 25940
[Cd(BPB)Cl] (24)	39150, 33050, 25690
[Cd(HBPB)Br ₂] (25)	39270, 33180, 25690
[Zn(DKN)NCS] (26)	41410, 35560, 25990
[Cd(DKN)OAc]·H ₂ O (27)	40420, 34840, 26570
[Cd(HDKN)Cl ₂] (28)	40270, 35980, 26130

8.3.5. Thermal analyses

The presence of solvent in the hydrated complex was confirmed from thermogravimetric analyses. TGA studies were carried out in the 50-800 °C range in nitrogen atmosphere at a heating rate of 10 °C/min. TG-DTG curves of the complexes were very similar and selected TG-DTG curves are shown in Fig. 8.7. For [Cd(DKN)OAc]·H₂O, mainly two stages in the decomposition process. The first stage decomposition temperature is in the range of 55-110 °C, with a mass loss of 3.90 (Calcd. 3.64%) which corresponds to the loss of a water molecule.

**Fig. 8.7.** TG-DTG curves of [Cd(BPB)Cl] (24) (left) and [Cd(DKN)OAc]·H₂O (27) (right).

References

- [1] M.J. Hendrick, M.T. May, M.J. Plishka, K.D. Robinson, *Metals in Biological Systems*, Ellis Horwood, Chichester, 1992.
- [2] Q. Li, H. Tang, Y. Li, M. Wang, L. Wang, C. Xia, *J. Inorg. Biochem.* 78 (2000) 167.
- [3] T.W. Lane, F.M.M. Morel, *Proc. Natl. Acad. Sci., USA* 97 (2000) 4627.
- [4] J.M. Perez, A.I. Matesanz, A. Martin-Ambite, P. Navarro, C. Alonson, P. Souza, *Inorg. Biochem.* 75 (1999) 255.
- [5] X. Chen, Q. Zhou, Y. Cheng, Y. Geng, D. Ma, Z. Xie, L. Wang, *J. Lumin.* 126 (2007) 81.
- [6] H. Wang, P. Zhao, D. Shao, J. Zhang, Y. Zhu, *Struct. Chem.* 20 (2009) 995.
- [7] C.-Yuan Niu, X.-Sheng Wan, X.-Fu Zheng, L.-Yan Meng, H.-Yun Zhang, R. Yang, H.-Wei Hou, *Synth. React. Inorg. Met. Org. Nano Met. Chem.* 37 (2007) 97.
- [8] A. Ray, S. Banerjee, S. Sen, R.J. Butcher, G.M. Rosair, M.T. Garland, S. Mitra, *Struct. Chem.* 19 (2008) 209.
- [9] W.J. Geary, *Coord. Chem. Rev.* 7 (1971) 109.
- [10] V.K. Sharma, S. Srivastava, A. Srivastava, *J. Coord. Chem.* 59 (2006) 321.
- [11] M.R. Maurya, S. Agarwal, M. Abid, A. Azam, C. Bader, M. Ebel, D. Redher, *Dalton Trans.* (2006) 937.
- [12] S.N. Rao, K.N. Munshi, N.N. Rao, M.M. Bhadbhade, E. Suresh, *Polyhedron* 18 (1999) 2491.
- [13] P.F. Rapheal, E. Manoj, M.R.P. Kurup, *Polyhedron* 26 (2007) 607.

- [14] N.B. Raj, M.R.P. Kurup, E. Suresh, *Spectrochim. Acta Part A* 71 (2008) 1253.
- [15] K. Nakamoto, *Infrared and Raman spectra of Inorganic and Coordination compounds*, 5th ed., Wiley, New York, 1997.
- [16] S. Sen, P. Talukder, S.K. Dey, S. Mitra, G. Rosair, D.L. Hughes, G.P.A. Yap, G. Pilet, V. Gramlich, T. Matsushita, *Dalton Trans.* (2006) 1758.
- [17] N.R. Sangeetha, S. Pal, *Polyhedron* 19 (2000) 1593.
- [18] E.B. Seenaa, M.R.P. Kurup, *Spectrochim. Acta Part A* 69 (2008) 726.

Summary and Conclusion

A great deal of work has been carried out on the synthesis and characterization of transition metal compounds, mainly due to their applications in various fields. However, the ability of the metal ion to participate in bonding to all possible coordination sites depends in part on its preferences for the donor atoms of the coordinated ligand, the flexibility and conformational adaptability of the ligand used, as well as on the competition from other Lewis acids and different entities capable of occupying a coordination pocket. The architectural beauty of coordination complexes arises due to the interesting ligand systems containing different donor sites in heterocyclic rings eg: NNO or NNS. Among the ligand systems, hydrazide and hydrazone have attracted much attention due to their use in biological systems and analytical chemistry.

Amide oxygen and azomethine nitrogen are the available donor sites in hydrazone compounds. Further, the number of coordination sites can be increased by suitable substitution on the hydrazone framework. These compounds contain an amide function and consequently exhibit amido-iminol tautomerism. In solid state they predominantly exist in amido form, whereas in solution iminol form predominates. The existence of tautomerism makes it possible to obtain coordination compounds containing either neutral form or deprotonated form. Stereochemistry of the hydrazone is much decided by the steric effects of the various substituents in the hydrazone moiety and also favored by additional interactions such as intramolecular hydrogen bonding. It is observed that the *cis* nature of the bond usually transforms to *trans* geometry when coordinated to metal ions.

The current work deals with the synthesis and characterization of metal complexes derived from 2-benzoylpyridine benzoyl hydrazone and di-2-pyridyl ketone nicotinoylhydrazone. The hydrazones under investigation were characterized by IR, UV, NMR spectral studies and the molecular structure of one of the hydrazones was solved by single crystal XRD studies. In the present work dioxovanadium(V), manganese(II), cobalt(II/III), nickel(II), copper(II), zinc(II) and cadmium(II) complexes were synthesized and characterized by various spectroscopic techniques, molar conductance measurements, magnetic susceptibility measurements and cyclic voltammetry. Single crystals of some of the complexes were isolated and characterized by single crystal X-ray diffraction studies.

The thesis is divided into eight chapters.

Chapter 1 entitled ‘A brief outline on acylhydrazones’ gives an introduction on hydrazones, diversity in their chelating behavior and their application in various fields. This chapter also describes different analytical techniques employed for the characterization of hydrazones and their metal complexes.

Chapter 2 includes the synthesis and characterization of two substituted acylhydrazones. This chapter also discusses how the coordination behavior of hydrazones under investigation is interesting. The ligand systems of our interest include

- 1) 2-Benzoylpyridine benzhydrazone (HBPB)
- 2) Di-2-pyridyl ketone nicotinoylhydrazone (HDKN)

They were characterized by ^1H NMR, IR and electronic spectral studies. We could successfully isolate the single crystals of one of the hydrazone, HBPB. Molecular structure of HBPB reveals that the hydrazone exists in the amido form and the amide proton is involved in intramolecular hydrogen bonding with the pyridine nitrogen. The key feature of the crystal packing is the formation of a supramolecular chain along 'b' direction.

Chapter 3 deals with the synthesis and characterization of two dioxygen bridged vanadium complexes of hydrazones under investigation. Both of them were characterized using molar conductivity studies, IR, electronic spectral studies and single crystal X-ray diffraction studies. They were found to be diamagnetic and EPR silent since vanadium is in +5 oxidation state. From the crystal structure it was observed that these binuclear complexes are centrosymmetric, being disposed about a crystallographic centre of inversion. Each VO_2^+ is coordinated by the tridentate hydrazone anion *via* the pyridyl, azomethine-N and enolic-O atoms. The final position in the hexacoordinated geometry is completed by a bridging oxo-O atom and the bridging is found to be asymmetric. The intervention of solvent molecule in the crystal structure of one of the complex leads to a supramolecular chain in which the molecules are connected through this water molecule.

Chapter 4 describes the synthesis and characterization of two Mn(II) complexes using IR, electronic, EPR spectral studies and cyclic voltammetry. The magnetic moments of the complexes are indicative of a high spin d^5 system. In DMF at 77 K, both of the compounds showed a hyperfine sextet with a pair of low intensity lines between the main hyperfine lines. The crystal structure of both of the complexes has been determined by single crystal X-ray diffraction. In these two

complexes, Mn(II) ion is in a distorted octahedral geometry in which the hydrazones act a monoanionic NNO chelating agent.

Chapter 5 explains the synthesis of five Co(II/III) complexes along with their characterization using various physicochemical techniques including IR spectroscopy, electronic spectral studies and cyclic voltammetry. Magnetic susceptibility measurements indicate that one of the complexes is diamagnetic while others are found to be paramagnetic. In all the complexes, hydrazones are coordinated to the metal in the enolate form which was well supported by IR spectral data. One of the complex was crystallized and the Co(II) center is coordinated in an N₄O₂ meridional manner giving rise to a distorted octahedral geometry.

Chapter 6 describes the synthesis and characterization of four Ni(II) complexes using magnetic susceptibility measurements, IR and electronic spectral studies. All the complexes were found to be paramagnetic excluding the possibility of square planar geometry. In one of the complex it was found that one ligand moiety is coordinated in the enolate form while the other is in the neutral form and was explained by its IR spectra. One of the complex was crystallized and Ni(II) ion is found to be in a distorted octahedral geometry and the disposition of the two ligand moieties is in such a way that the meridional isomer is obtained. The presence of water molecule in the crystal structure is involved in hydrogen bonding with one of the pyridyl nitrogen of one molecule and nicotinic nitrogen of other molecule.

Chapter 7 includes the synthesis of nine Cu(II) compounds followed by their characterization using various spectral techniques including IR, electronic and EPR. The molar conductivity values indicate that the

perchlorate complex was found to be a 1:1 electrolyte. All of them were found to be paramagnetic and in some cases magnetic moments were low indicating their dimeric nature. The IR spectral data indicate that both of the hydrazones coordinate through the pyridyl and azomethine nitrogen and enolate oxygen. Unlike in other complexes, in the chloride complex, hydrazone is coordinated in the neutral form which was well supported by its IR spectrum. EPR spectra of Cu(II) complexes were recorded in polycrystalline state at 298 K and in frozen DMF at 77 K. Some of the spectra in DMF at 77 K were found to be axial with hyperfine lines in the parallel region and seven superhyperfine splittings were observed which gives the evidence for the coordination of pyridyl and azomethine nitrogen to the metal center. In one of the complex an axial spectrum was observed in DMF at 298 K, however when recorded in DMF at 77 K it showed a reverse axial spectrum, indicating the change in geometry which may be due to the coordination of the solvent. Some of the complexes were found to be dimeric and was evident from the half field signal and in the sulfate complex half field signal with seven hyperfine splittings were observed due to the coupling of the electron spin with nuclear spin of two copper atoms. Two complexes were crystallized and Cu(II) is found to be in a distorted octahedral geometry.

Chapter 8 discusses the synthesis and characterization of six Cd/Zn(II) compounds using IR and electronic spectral studies. All of them were found to be non-electrolytic in nature and except in the acetato complex hydrazone is coordinated in the enolate form. In acetate complex hydrazone is coordinated in the neutral form.

****୧୦୨****

Resume

NEEMA ANI MANGALAM

Mangalath Nirmal

Erumakuzhi

Nooranad (P.O)

Alappuzha

Kerala-690504

E-mail: neemaani@gmail.com

neema07_ani@yahoo.co.in

Ph.No.: 04792386925 (Res.)

Areas of Interest

Teaching and Research

Academic Profile

- **Pursuing Ph.D. (Inorganic Chemistry)**
(2007 – present)
Topic of work:
Supervising Guide: Dr. M.R. Prathapachandra Kurup,
Professor of Inorganic Chemistry,
Department of Applied Chemistry, Cochin University of
Science & Technology, Kochi.
- **M. Phil. Chemistry (68%)**
(2006-2007)
Department of Applied Chemistry, Cochin University of
Science & Technology, Kochi.
- **B. Ed. Physical Science (66.83%)**
(2005-2006)
Mar Thoma Training College, Ranni, affiliated to Mahatma
Gandhi University, Kottayam.

- **Master of Science (Pure Chemistry) (69.2%)**
(2002- 2004)
Mar Thoma College, Tiruvalla, affiliated to Mahatma Gandhi University, Kottayam.
- **Bachelor of Science (Chemistry) (75.6%)**
(1999-2002)
N. S. S. College, Pandalam, affiliated to Kerala University, Thiruvananthapuram.
- **Pre-Degree (65.6%)**
(1997-1999)
Bishop Moore College, Mavelikkara, affiliated to Kerala University, Thiruvananthapuram.
- **S. S. L. C. (80%)**
(1997)
Holy Angels' English Medium High School, Adoor.

Achievements

- Qualified the NET exam conducted in June 2009

Professional Skills

- Familiar with MS Office (Excel, PowerPoint and Word), Adobe Photo Shop.
- Familiar with chemistry software packages like Chemsketch, Chem Draw, Microcal Origin, Simulation, MATLAB, crystallographic softwares like DIAMOND 3.0, MERCURY, ORTEP, PLATON FOR etc.
- Experienced in using instruments like UV-VIS spectrophotometer, IR spectrometer, Thermo Gravimetric Analyser, Atomic Absorption Spectrometer, Gouy Balance etc.
- Experienced in using crystallographic softwares for solving (SHELXTL) and in interpreting single crystal X-ray data.

Research papers published in International journals

1. Versatile binding properties of a di-2-pyridyl ketone nicotinoylhydrazone ligand: Crystal structure of a Cu(II) complex, **Neema Ani Mangalam**, M.R. Prathapachandra Kurup, Spectrochim. Acta Part A, doi:10.1016/j.saa.2010.11.032, in press.
2. Mn(II) complexes of some acylhydrazones with NNO donor sites: Syntheses, a spectroscopic view on their coordination possibilities and crystal structures, **Neema Ani Mangalam**, S.R. Sheeja, M.R. Prathapachandra Kurup, Polyhedron 29 (2010) 3318.
3. FT-IR and computational study of Di-2-pyridyl ketone nicotinoylhydrazone, **Neema Ani Mangalam**, C. Yohannan Panicker, S.R. Sheeja, M.R.P. Kurup, Y. Sheena Mary, K. Raju, Hema Tresa Varghese, V. Manikandan Nair, Int. J. Ind. Chem. 1 (2010) 17.
4. Vibrational spectroscopic studies and computational study of quinoline-2-carbaldehyde benzoyl hydrazone, S.R. Sheeja, **Neema Ani Mangalam**, M.R.P. Kurup, Y. Sheena Mary, K. Raju, Hema Tresa Varghese, C. Yohannan Panicker, J. Mol. Struct. 973 (2010) 36.
5. Design and characterization of Cu(II) complexes from 2-benzoylpyridine benzhydrazone: Crystallographic evidence for coordination versatility, **Neema Ani Mangalam**, Sarika Sivakumar, M.R.P. Kurup, E. Suresh, Spectrochim. Acta Part A 75 (2010) 686.
6. Chemistry of molecular and supramolecular structures of vanadium(IV) and dioxygen-bridged V(V) complexes incorporating tridentate hydrazone ligands, **Neema Ani Mangalam**, Sarika Sivakumar, S.R. Sheeja, M.R. Prathapachandra Kurup, Edward R.T. Tiekink, Inorg. Chim. Acta 362 (2009) 4191.
7. Synthesis and spectral investigations of Vanadium(IV/V) complexes derived from an ONS donor thiosemicarbazone ligand,

Neema Ani Mangalam, M.R. Prathapachandra Kurup, Spectrochim. Acta Part A 71 (2009) 2040.

Papers presented in conferences

- Structural and Spectral Properties of Vanadium Complexes of an ONS donor Ligand. (Oral Presentation), **Neema Ani Mangalam**, M.R. Prathapachandra Kurup, National Seminar on Current Trends in Chemistry, January 18-19, 2008, Department of Applied Chemistry, Cochin University of Science & Technology, Kochi-22.
- Spectral and crystal structure of Cu(II) complexes of an NNO donor aroylhydrazone (Poster Presentation), **Neema Ani Mangalam**, M.R. Prathapachandra Kurup, International Conference on Coordination and Organometallic Chemistry, March 19-20, 2009, Bharathiyar University, Coimbatore.
- Spectral and crystal structure of Ni(II) complexes of NNO donor aroyl hydrazones (Poster Presentation), **Neema Ani Mangalam**, M.R. Prathapachandra Kurup, International Conference on Material for the New Millennium, January 1-13, 2010, Department of Applied Chemistry, Cochin University of Science & Technology, Kochi-22.

Personal details

Father's Name	M.G. Aniyankunju
Date of Birth	07-12-1981
Sex & Marital Status	Female, Single
Nationality	Indian
Permanent Address	Mangalath Nirmal, Erumakuzhi, Nooranad P.O, Alappuzha (Dist.), Pin-690504.